The Dissertation Committee for Brian Keith Long Certifies that this is the approved version of the following dissertation:

Design, Synthesis, and Application of Lithographic Resists and Nonlinear Optical Materials

Committee:

C. Grant Willson, Supervisor

Christopher W. Bielawski

Brent L. Iverson

Alan Campion

Benny Freeman

Design, Synthesis, and Application of Lithographic Resists and Nonlinear Optical Materials

by

Brian Keith Long, B.S.

Dissertation

Presented to the Faculty of the Graduate School of

The University of Texas at Austin

in Partial Fulfillment

of the Requirements

for the Degree of

Doctor of Philosophy

The University of Texas at Austin

May 2009

Dedication

To my family, for their love and support.

Acknowledgements

I believe there are few choices one will make in his or her life that truly dictate their future. Selection of a graduate advisor is such a decision and I feel extremely fortunate that Professor Willson chose to allow me to work in his group. Early in my career Dr. Willson told me that his job was to produce students, not papers and patents. In my opinion, he has more than exceeded this statement as he has challenged me to be the best I can inside and outside of the lab. I have learned more from him than I will ever be able to express gratitude for, and I will forever be indebted to him.

I would like to thank the members of the Willson research group who have not only added to my knowledge of chemistry, but to my quality of life as a graduate student. Of those members, I would like to specifically thank Professor Scott Grayson who took me under his vigilance from my first day in the Willson laboratory and has continued to not only be a mentor but a close friend. Also, special thanks to Kathleen Sparks, who through her tireless efforts has managed to keep our group functioning and has become a great friend.

Although I am unsure if it appears on any official documentation, Professor Christopher Bielawski has served as co-advisor to me during my career at UT. Even though my research endeavors have centered mainly in the Willson labratories, I have learned a tremendous amount from our interactions and discussions.

Design, Synthesis, and Application of Lithographic Resists and Nonlinear Optical Materials

Publication No._____

Brian Keith Long, Ph.D.

The University of Texas at Austin, 2009

Supervisor: C. Grant Willson

Fluorinated norbornene monomers exhibit the requisite properties for inclusion in 157 nm photoresists, but traditional addition and radical polymerizations with these monomers have failed. Norbornanediols provide an alternate route to these materials via condensation polymerization, and methods have been developed for the efficient synthesis of the *exo*-2-*syn*-7- and *endo*-2-*exo*-3-dihydroxynorbornanes. Synthesis of the fluorinated analogues is complicated by steric and electronic effects; however, a high-yielding synthesis of *endo*-2-*exo*-3-dihydroxynorbornane bearing a 5-*endo*-[2,2-bis(trifluoromethyl)hydroxyethyl] substituent as well as its corresponding polymer are reported.

As an alternative to 157 nm and other optical lithographies, Step and Flash Imprint Lithography, or S-FIL®, was introduced in 1999 by The University of Texas at Austin. It has proven to be a cost effective, high resolution alternative to traditional optical lithography. Often in the S-FIL process, residual resist may become imbedded within the template features resulting in device defects due to the imprint and repeat

nature of S-FIL. The high silicon and cross-linking content of the resist formulations are extremely difficult, if not impossible to remove from quartz imprint mold without template degradation. Our approach to this problem was the synthesis of a family of thermally reversible, cross-linkable monomers that will facilitate resist removal while maintaining template integrity. Our monomers utilize classic Diels-Alder chemistry to provide thermal reversibility, while pendant acrylate functionalities facilitate cross-linking. Herein we report the synthesis of several Diels-Alder compounds, incorporate them into resist formulations, and test their efficacy for resist removal.

In an effort to develop unique patternable materials, our laboratory is currently engaged in the design and development of photonic crystals comprised of organic elements with highly stable electro-optic activity. Fabrication of these devices requires polymers that can be patterned at high resolution, have large second order nonlinear optical (NLO) coefficients, and that are thermally stable after poling. Our route to these materials involves the synthesis of a prepolymer that can be spin coated, poled, and then fixed by a photochemical cross-linking reaction. We now describe an efficient synthetic route to a new class of biscross-linkable monomers and the characteristics of their corresponding nonlinear optical polymers.

Table of Contents

List of Tables

List of Figures

xviii

xx

List of Schemes

Chapter 1: Introduction to Photolithography

Throughout history, few inventions have had such a pervasive impact that life before their inception is difficult to imagine. The printing press, automobile, incandescent light bulb, vaccines, and antibiotics have all had such effects on the world and have changed how we view the dissemination of knowledge, distance and time, darkness, and even sickness and death.[1] The inventions of the transistor, integrated circuit, and personal computer have had a similarly profound influence on the world.

The invention of the transistor and its incorporation into integrated circuits (ICs) has enabled the manufacture of the compact and powerful computers known today. Early computers were massive, unreliable, and fragile collections of vacuum tubes and other antiquated parts that were soldered together by hand. These goliath machines consumed large amounts of energy, produced copious amounts of heat, could fill entire warehouses, and were so expensive to build and run that only major research institutions could afford them. ENIAC, one of the first such computers (Figure 1.1), was unveiled in 1946. It inhabited close to 1,000 square feet of space and could perform a meager 5,000 operations per second.[2] Conversely, today's microprocessors consisting of ICs, are approximately the size of the average adult thumbnail, and possess more computing power than the computers NASA had available when Neil Armstrong and Edwin 'Buzz' Aldrin first landed on the moon in 1969. The evolution of computers from ENIAC to modern laptops and desktops has catalyzed an information revolution comparable to that achieved by Johann Guttenberg's printing press which was developed in 1439.
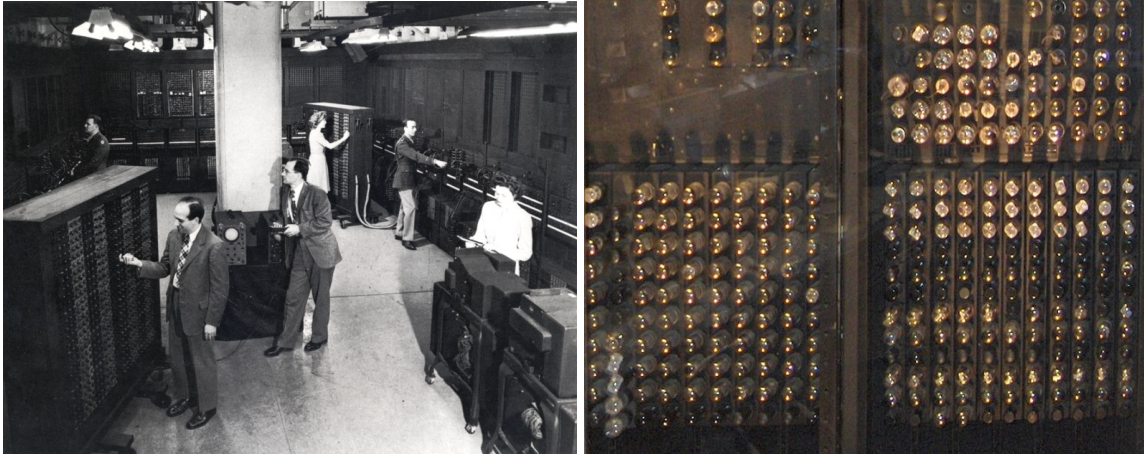
Figure 1.1: Photograph of ENIAC (left)[3] and a small portion of ENIAC's almost 18,000 vacuum tubes (right).[4]

DEVELOPMENT OF THE MODERN COMPUTER

The Transistor

The first step toward the computers of today came when William Shockley, a scientist at Bell laboratories, invented the transistor in 1947 (Figure 1.2).[5] Shockley's transistor was simply an electronic "valve" which was smaller, more robust, and more efficient than classical vacuum tubes.[6] His transistor consisted of a source and drain wire as well as a middle "gate" electrode connected to a triangular piece of germanium. The germanium crystal served as a semiconductor material that did not allow current to flow in its native state, but when a small voltage was applied to the gate electrode it became a much better conductor therefore closing the circuit and allowing current to flow from the source to the drain.[7,8] Shockley, along with co-inventors John Bardeen and Walter Houser Brattain won the 1956 Nobel Prize in Physics "for their research on semiconductors and their discovery of the transistor effect".[9]
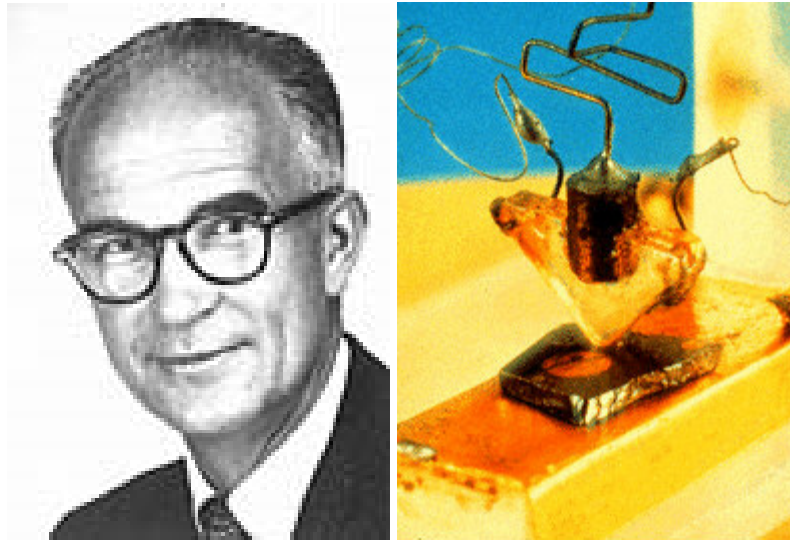
Figure 1.2: William Shockley and his germanium transistor.[10]

The Integrated Circuit

Although the transistor was a drastic improvement over vacuum tube technology it still required the use of numerous capacitors and resistors that were soldered together onto large circuit boards. This process was costly and produced devices much larger than modern day computers. In 1958, Jack Kilby of Texas Instruments and Robert Noyce of Fairchild Semiconductor both independently invented the integrated circuit (IC) in which the resistors and capacitors were made *in situ* from the same material as the transistors (Figure 1.3).[11] Noyce received a patent for his invention, which solved several practical problems found in Kilby's IC, namely the problem of interconnecting the components. Kilby received the 2000 Nobel Prize in Physics "for his part in the invention of the integrated circuit".[9]
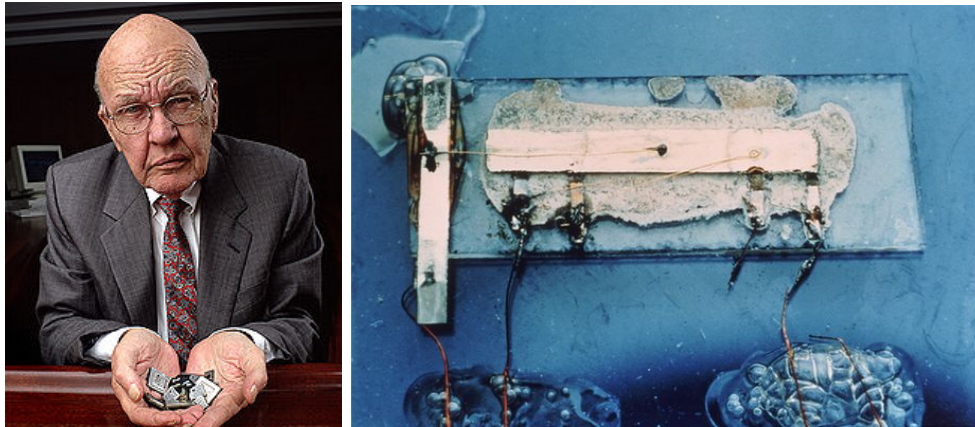
Figure 1.3: Jack Kilby and his first ICs. *Images Courtesy of Texas Instruments*[.12]

The IC compiled all of the requisite components for a processor onto a single semiconducting substrate allowing engineers to pack more components into a given area.[13] This miniaturization proved to be advantageous for many reasons, monetary savings and processor speed improvements leading the list. As one might assume, the smaller components could be produced more quickly while using fewer raw materials giving a dramatic economic savings. The speed was greatly increased for two reasons: first, the smaller capacitors could be charged and discharged more quickly and second, the devices could be located in closer proximity to one another thereby decreasing signal propagation time.[14] The first complete microprocessor, the Intel 4004, was released in 1971.
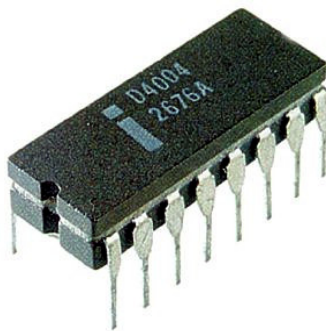
Figure 1.4: The Intel 4004 processor.[15]

Moore's Law

      The drive toward miniaturization of IC devices continues today as scientists make improvements in materials and processes that enable the manufacturing of smaller, faster, and cheaper microelectronic devices. In 1965, Gordon Moore, then an employee of Fairchild Semiconductor, observed that the number of transistors placed on a single integrated circuit doubled approximately every year.[16] This observation, which encompassed five data points (1959-1964), came to be known as "Moore's Law".[17] At an IEEE meeting in 1975, Moore, now a co-founder of Intel, noted that "circuit and device cleverness" had allowed his projection to be realized and that with current data he projected the rate to slow to a doubling of transistors every two years rather than every year. His prediction has become a self-fulfilling prophecy and a primary driving force behind the semiconductor industry (Figure 1.4).
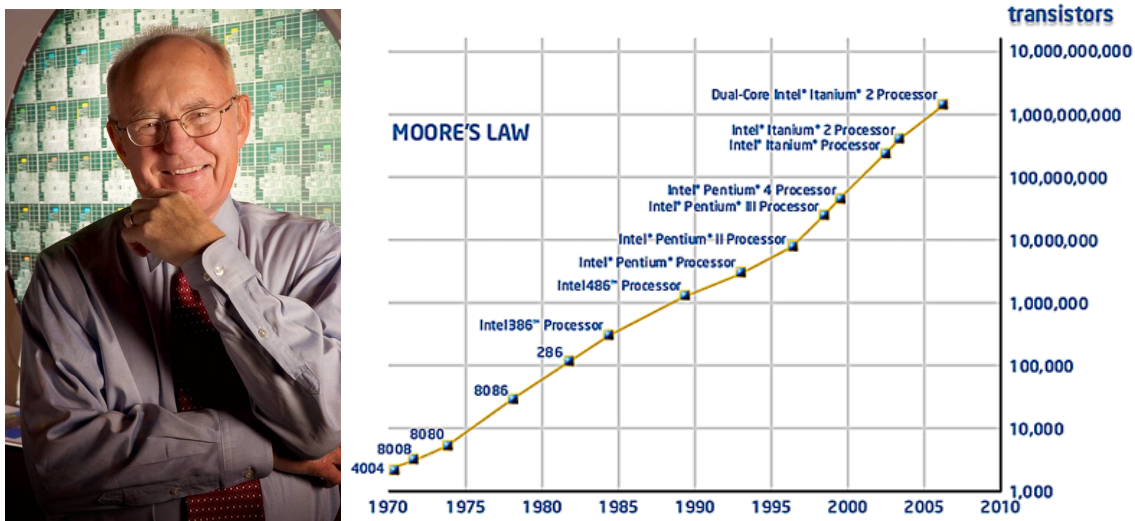
Figure 1.5: Gordon Moore and a representation of Moore's Law.[18]

MICROPROCESSOR MANUFACTURING

Transistor Design

Semiconductor devices today are produced on silicon substrates and their design has become increasingly cleaver. Below is a representation of a metal oxide semiconductor field effect transistor (MOSFET) (Figure 1.6). Its complex geometries are produced via a process known as photolithography, or more specifically microlithography, which is the name given to photolithography when used to produce microelectronic devices (Figure 1.7).[13,19] In the scheme below, the source and drain are connected to areas of n-type doped silicon and are separated by a region of p-type doped silicon. This n-p-n junction does not allow current to flow because electrons from the electron rich n-type silicon rapidly combine with the excess holes in the p-type silicon preventing electron flow. When a positive voltage is applied to the gate electrode, the build up of positive charge repels the positive charges in the p-type silicon while electrons are attracted creating what is labeled as an "n-channel" allowing current to flow from source to drain. When the potential is removed from the gate electrode, the temporary n-channel is reverted once again to p-type silicon, stopping all current flow. By varying potentials, dopant types, and device structure, it is possible to form integrated circuits capable of performing complex logic operations.[19]
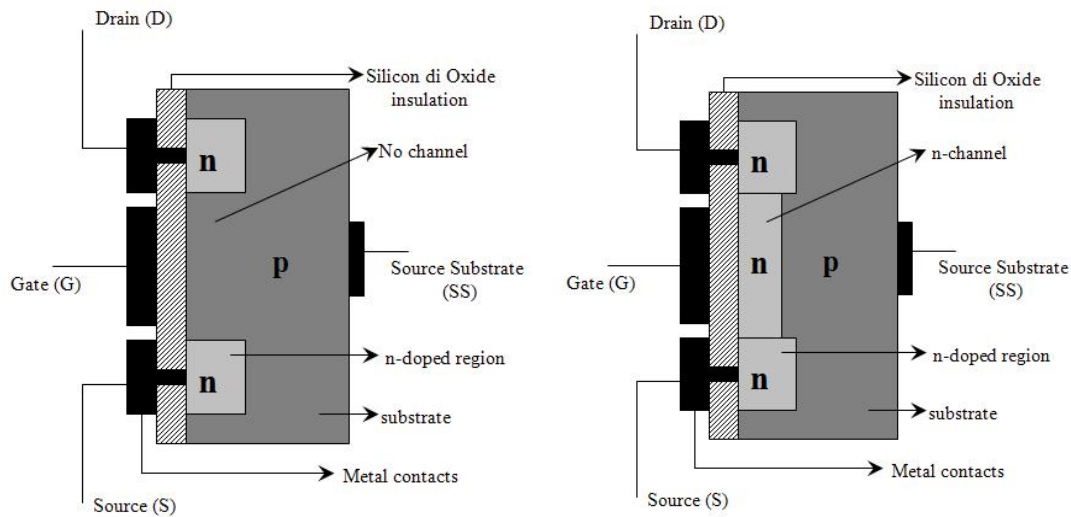
Figure 1.6: Schematic of a MOSFET in the off state (left) and in the on state where a potential is applied to the gate electrode (right).[20]
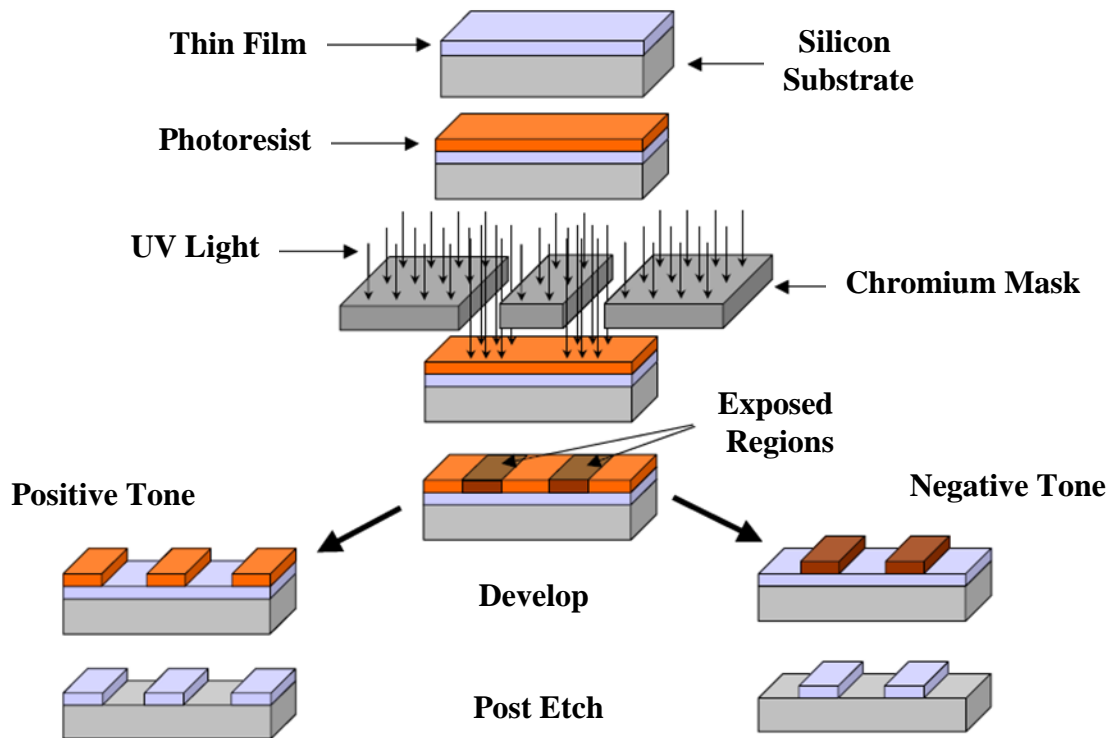
Figure 1.7: Representation of the photolithographic process.

Photolithography and Microlithography

       The process of photolithography (Figure 1.7) begins with highly pure, single crystal silicon wafers that are cut from precisely grown silicon ingots.[21] An insulator or conductor is then deposited onto the wafer depending on the function of the desired feature. Next, a layer of a polymeric material known as "photoresist" is deposited on top of the insulator/conductor layer via spin coating. Photoresists are organic solutions of polymeric resins, photoactive compounds, and other additives that upon irradiation undergo a chemical change resulting in decreased or increased solubility depending on the function of the polymeric resin and developer chosen.

       After application of the photoresist, the wafer is typically baked for a short period of time known as a post-application bake (PAB) to remove excess solvent from the thin polymer film. After returning to ambient temperature, the wafer is exposed through a chromium coated quartz mask and lens stack that projects the desired pattern and focuses the light onto the photoresist (Figure 1.8). The wafer is then baked for another short period of time known as a post-exposure bake (PEB) in which the chemical transformation is driven to completion in the exposed areas. The final image is ultimately developed using either an aqueous base (typically 2.6 N solution of tetramethylammonium hydroxide) or organic developing solution. This relief image can then be transferred into the underlying substrate using anisotropic etching and the remaining resist stripped from the substrate exposing the newly patterned substrate layer.
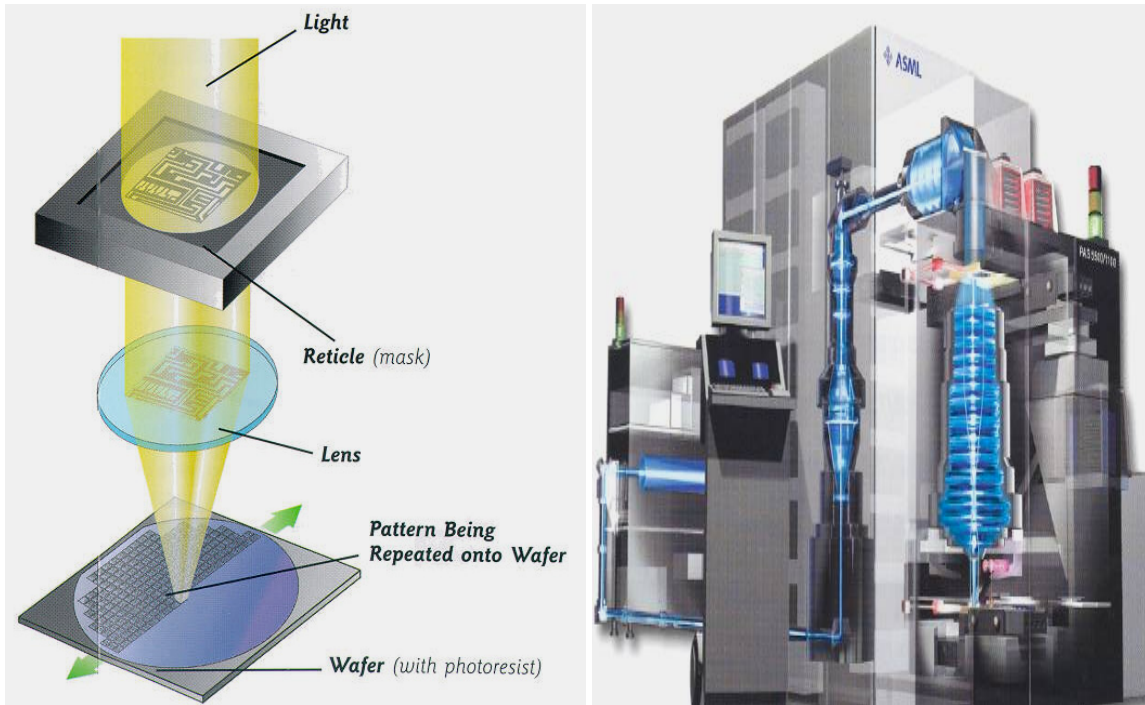
Figure 1.8: Graphical representation of a wafer exposure (left) and a complete exposure tool (a.k.a. "stepper").[22]

The Rayleigh Equation

The minimum feature size that can be printed by projection lithography is governed by physics and can be best estimated by the Rayleigh Equation (Eq. 1.1). In this equation, R is the minimum feature size that can be resolved, k is a constant associated with the tool, resist, and mask used, λ is the wavelength of light, and NA is the numerical aperture of the lens. A typical example is as follows: if k = 0.4, λ = 365 nm, and NA = 0.6 an image as small as R = 243 nm can be produced. In order to fulfill Moore's Law, current volume production requires the production of much smaller features, as small as 65 and 45 nm, which cannot be achieved using the previous conditions. The three ways industry has pushed toward these nano-scale features is by either decreasing the wavelength of light used (λ), which is directly proportional to the resolution limit (R), by

9

increasing the NA, which is inversely proportional to R, or by decreasing k, which is directly proportional to R. While increasing NA improves resolution, it has a detrimental power of two influence on depth of focus.[13] Hence, industry has chosen to steadily decrease the wavelength of light to keep pace with Moore's Law. Next generation exposure sources are chosen according to the commercial availability of highly intense light sources. For example, 365 nm lithography uses the I-line of a mercury arc lamp, 248 nm lithography employs a KrF laser, 193 nm utilizes an ArF laser, and 157 nm lithography uses a F_2 excimer laser. With each new light source, a new set of chemical and engineering requirements must be met; the most prominent being the photoresist's absorbance at the wavelength of light used.

$$ \mathbf{R = k \frac{\lambda}{NA}} \qquad (1.1) $$

Photoresist transparency is of utmost importance to the lithographic process; so much that even slightly absorbing resists can have detrimental effects to feature formation. Figure 1.9 shows an actual demonstration of this constraint. In this figure, the resist on the left is transparent to the irradiation source used and ultimately produces images that are developed completely to the underlying substrate. On the right hand side of Figure 1.9, a resist that is highly absorbing was used and incomplete development is observed. To overcome this and other obstacles, ingenuity is required of both the chemists who design and synthesize the photoresists and the engineers who process them. The evolution of these "ingenious" photoresist materials will be presented in the following sections.
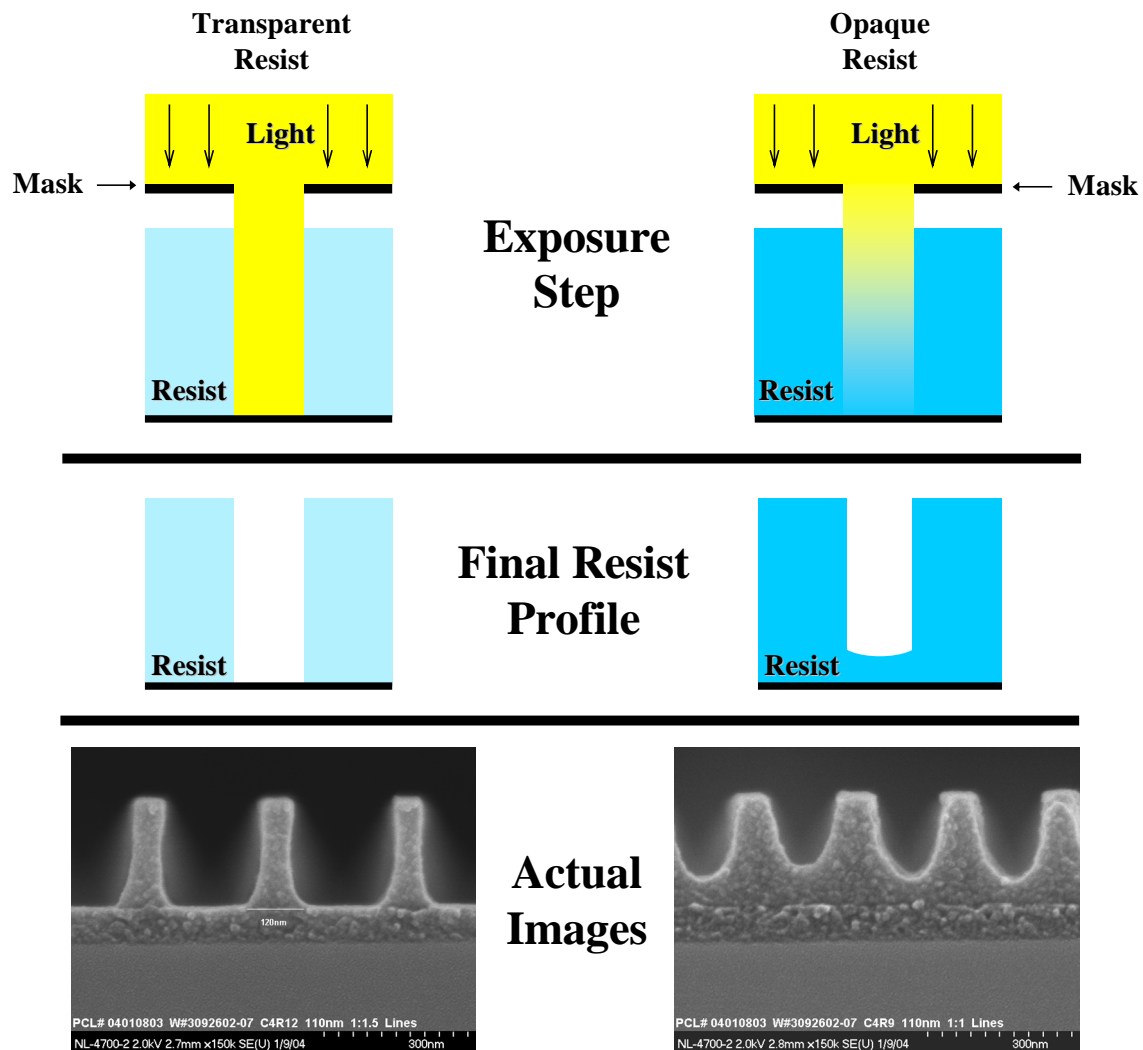
Figure 1.9: An example of a transparent photoresist (left) and a strongly absorbing one (right).[23]

HISTORY OF PHOTORESIST MATERIALS

Photoresist development actually originated many years before the invention of the transistor when in 1826, a Frenchman, Joseph Nicéphore Niépce captured what is known as the first "permanent image of nature" (Figure 1.10).[24] To make this first photograph, Niépce used a tar that has been recovered in chunks from the Dead Sea since early written history called Bitumen of Judea. Niépce discovered the substance had

different solubility characteristics after baking in the sun, it could be dissolved in lavender oil, and that uniform coatings could be formed from solutions of the tar.[25] He coated the tar onto a polished pewter plate and exposed it using a simple camera which overlooked a courtyard outside a window in his home. As can be seen in the image, both faces of the surrounding buildings are illuminated depicting the fact that the exposure took eight hours to complete.[26] Once finished, Niépce developed the plate in a mixture of oils and white petroleum to produce the gray scale relief image which was titled "Point de vue du Gras" (Figure 1.10). The image is not as crisp as one might hope but was an amazing first example of a gray-scale recording in a digital medium. The image was produced via projection printing. More intricate detail could be imaged using contact printing, as seen in Niépce's reproduction of a vellum drawing of French Roman Catholic Cardinal Georges d'Amboise (Figure 1.10).[13] Niépce's permanent photograph of nature was presented to the royal society in 1827 and was sent on tour until 1898 when it was lost, not to be found until 1950 by Helmut and Alison Gernsheim.[27] Both images now reside in the Gernsheim collection at The University of Texas at Austin.
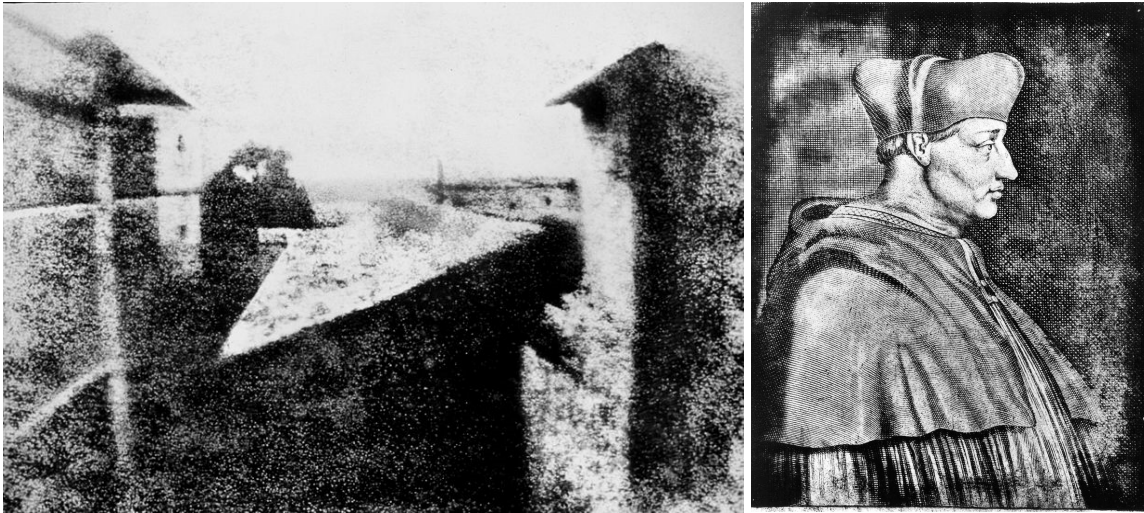
Figure 1.10: Niépce's photograph "Point de vue du Gras" (left)[28] and reproduction of a vellum drawing of Cardinal Georges d'Amboise (right).[29]

Bitumen of Judea was used for several years until 1839 when Mungo Ponton first discovered that a mix of protein and potassium dichromate, called dichromated gelatin, had high sensitivity to light. In 1840, Becquerel first used this dichromated gelatin to produce relief images and was eventually given credit for coining the term "resist".[30] It wasn't until the late 1840s when the first practical resist based on dichromated gelatin was developed by William Henry Fox Talbot (Figure 1.11) who was later awarded the patent in 1852.[26] Talbot's resist required orders of magnitude less exposure than bitumen, spawned the lithography industry, and was the medium of choice for the transfer of images to printing plates for over 100 years.[31]

Figure 1.11: William H. F. Talbot (left)[32] and a picture take by Talbot in 1853 (right).[33]

Dichromated gelatin was the logical choice for William Shockley and his Bell Laboratories team when they set out to develop the first transistor almost 100 years later. Shockley soon found that it had adequate resolution but had little etch resistance to hydrofluoric acid, which was needed to etch the silicon dioxide substrates. Dichromated gelatin also had poor shelf life as a "dark reaction" (cross-linking in the absence of light) took place upon storage of the material resulting in inconsistent results. The Bell Labs team then contacted Eastman Kodak director Dr. Kenneth Mees who turned to researcher Louis Minsk for help solving this difficult problem. Minsk was soon able to develop a photoactive polymeric material based on the dimerization of cinnamic acid.[34] Minsk's poly(vinylcinnamate) cross-linked efficiently upon exposure to radiation from a mercury arc lamp to produce highly insoluble material (Figure 1.12). The cinnamate resist had no "dark reaction", produced sharp images with clean edges, and even resisted hydrofluoric acid etches. Bell Labs began pilot scale manufacturing of semiconductor devices utilizing Minsk's negative tone resist, but soon realized the polymers adhesion to the polished

surface of oxidized wafers was inadequate. Despite many attempts to improve the adhesion of poly(vinylcinnamate) it became clear that a new material was needed.
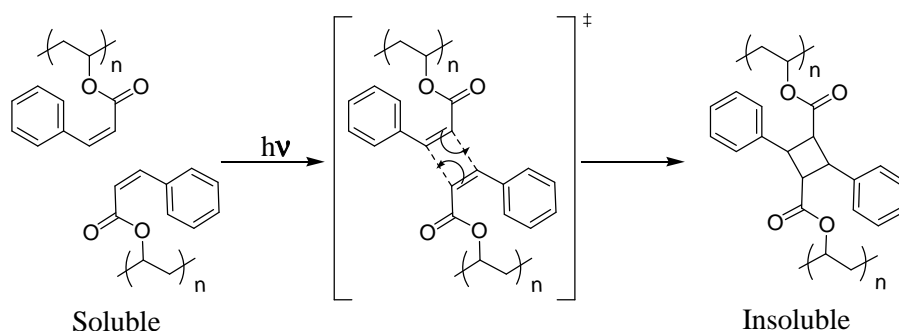
Figure 1.12: Louis Minsk's cross-linkable poly(vinylcinnamate) resist.

With a need for a new photoresist, Dr. Kenneth Mees then turned to Martin Hepher, the head of the Graphic Arts Department at Kodak Ltd. Hepher decided that a light sensitive rubber adhesive was the answer, and over lunch with Hans Wagner, an organic chemist, designed a system they believed would solve the problem. The negative tone resist designed by Hepher and Wagner consisted of bis(arylazides) and low molecular weight rubber. They found that the resist formed sharp images and had ideal adhesion to glassy surfaces such as oxidized silicon wafers. The low molecular weight rubber was eventually replaced by well defined and cyclized poly(*cis*-isoprene), which increased shelf life and lowered the intrinsic viscosity of the resist solution allowing coatings with higher solids content.[26] Their resist (Figure 1.13) was marketed by Kodak as "Kodak Thin Film Resist" (KTFR) and was the workhorse of the semiconductor industry until 1972.
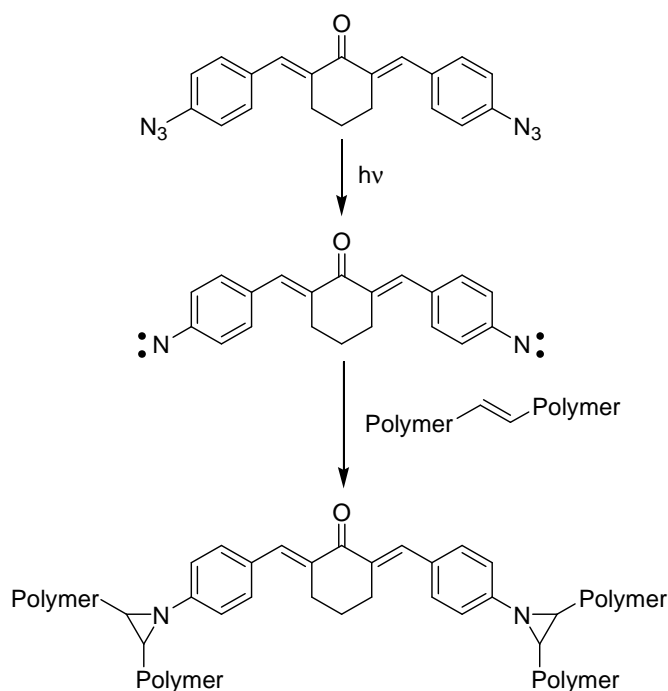
Figure 1.13: Martin Hepher and Hans Wagner's KTFR.

In 1972, device features reached approximately two micrometers, as predicted by Moore's Law, and the resolution limits of KTFR. Devices two micrometers and smaller formed using Kodak's negative tone resist were found to swell upon development in typical organic developers (Figure 1.14), and a quest for a high resolution replacement for KTRF began.[35] The answer eventually was found to lie with Kalle Corporation (later Hoescht AG) and work originally done in the early 1900s by a German monk named Gustav Kögel. Kögel's work, along with that of Kalle Corporation, led to the development and utilization of diazonium salt chemistry to produce what is still used today for engineering and architectural blueprints.[26]
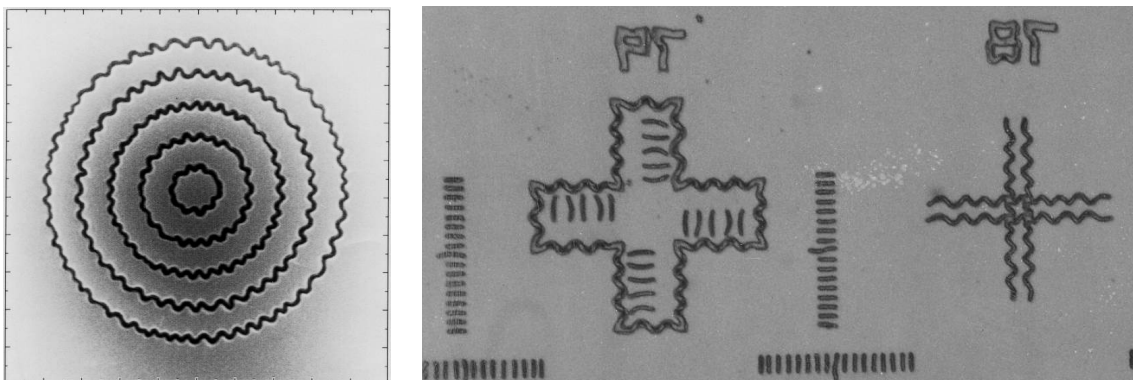
Figure 1.14: Images of swollen negative tone resist.

Under the direction of Oskar Süss, Kalle chemists synthesized numerous "diazo" compounds in the 1930s and 1940s. In what has been assumed to be an attempt to make a single component blueprinting material, Süss synthesized a class of compounds known as diazonaphthoquinones (DNQs). Even though these materials were not effective as blueprint materials, it was discovered that when incorporated into novolac resins, an experimental binder used by Kalle chemists, that it drastically inhibited solubility of the typically highly soluble novolac in basic aqueous solutions compared to that of the exposed samples. Süss speculated that the change between exposed and unexposed samples was due to a chemical reaction known as the Wolff rearrangement which was known to occur in diazoketones.[36,37] He was able to confirm this (Figure 1.15) and his resist was commercialized in 1950 under the Ozatec® tradename for positive tone printing plates.[38]
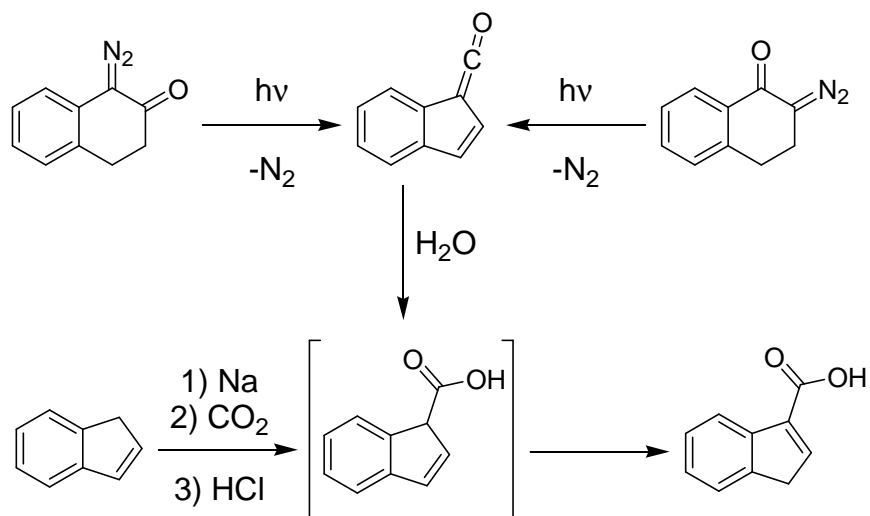
Figure 1.15: Süss's proof of the Wolff rearrangement.

Historic lore tells us that the novolac/DNQ resist system was brought to the microlithographic industry by a father and son. The father worked at Bell laboratories and his son just across the street at Azoplate, the US supplier of Ozatec®. The story tells us that the father, one day after complaining about difficulties with KTRF to his son, took a bottle of the Azoplate novolac/DNQ resist to work with him at Bell Laboratories. The resist was given to him by his son who bragged of its desirable properties, and hence the novolac/DNQ age began.[39] These resists were marketed by Azoplate under the tradename "AZ Photoresists" and quickly replaced KTRF as the industry workhorse.[40] Between 1972 and 1990, novolac/DNQ resists accounted for 90% of the photoresist world market and were not replaced until the lithographic industry demanded another reduction in wavelength to achieve yet smaller devices.[26]

Novolac/DNQ resists operate by taking base soluble novolac polymer and adding a small amount of a photoactive dissolution inhibitor, diazonaphthoquinone (Figure 1.16). Adding DNQ causes the dissolution rate of the resist in aqueous base to decrease by several orders of magnitude. Upon exposure to 365 nm light, the DNQ is converted to

18

an indene carboxylic acid photoproduct via the Wolff rearrangement. The photoproduct is now soluble in aqueous basic developers and removed along with the now uninhibited novolac. This exposed resist has a higher dissolution rate than the novolac alone resulting in a resist image with a nearly vertical sidewall profile. Even though its resolution limits have been exceeded, novolac/DNQ resists are still widely used today in the manufacturing of back-end-of-the-line (BEOL) device structures, or upper level wiring, which are significantly larger than transistor gate level features.
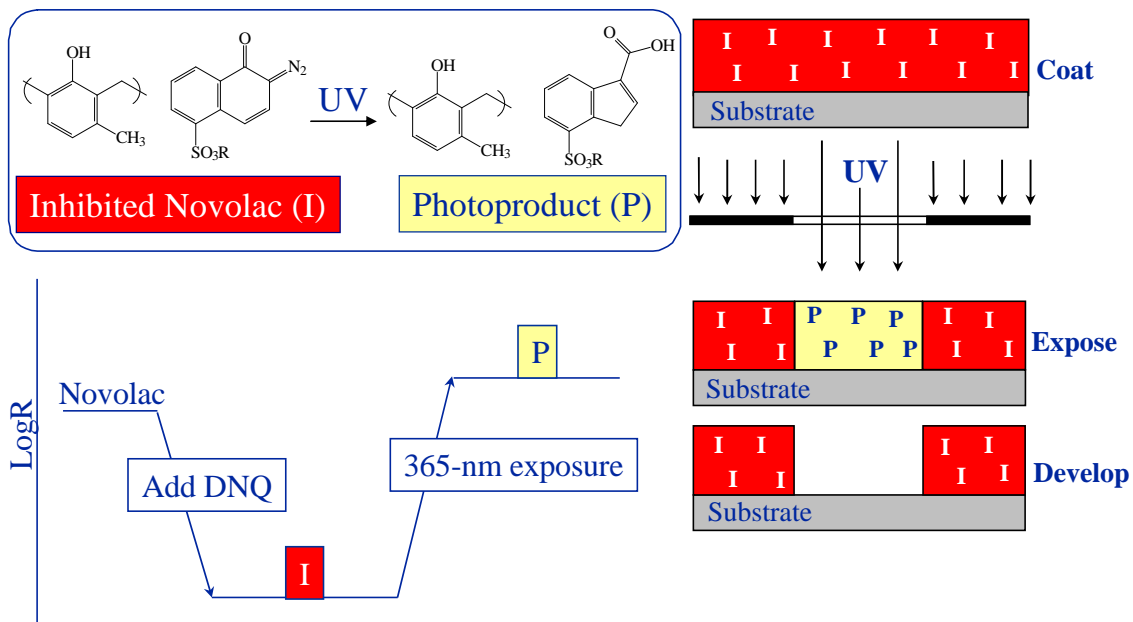
Figure 1.16: Novolac/Diazonaphthoquinone resist chemistry.

Chemically Amplified Resists

As with KTRF, novolac/DNQ resists eventually reached their resolution limits in the late 1980s and industry found itself once again with the necessity to decrease the wavelength of light. As can be seen in the mercury arc lamp spectra (Figure 1.17), the next available wavelength was in the deep UV at approximately 254 nm. This emission

has less than 10% as much power as that generated at 365 nm, hinting that a minimum of an order of magnitude increase in sensitivity must be achieved. The first attempts at deep UV resists were reported as early as 1970,[41] and the first commercial resist was released by Tokyo Okah Kogyo under the tradename ODUR 10XX.[26] These resists were not very useful given the low lamp intensity in the deep UV.

DNQs only have quantum efficiencies on the order of ~0.3. This meant that improvements in DNQ efficiency could only give a factor of three improvement, in theory, not the one to two orders of magnitude needed. This convinced researchers that a new resist was needed and eventually led them to the concept of "chemical amplification".[42,43]
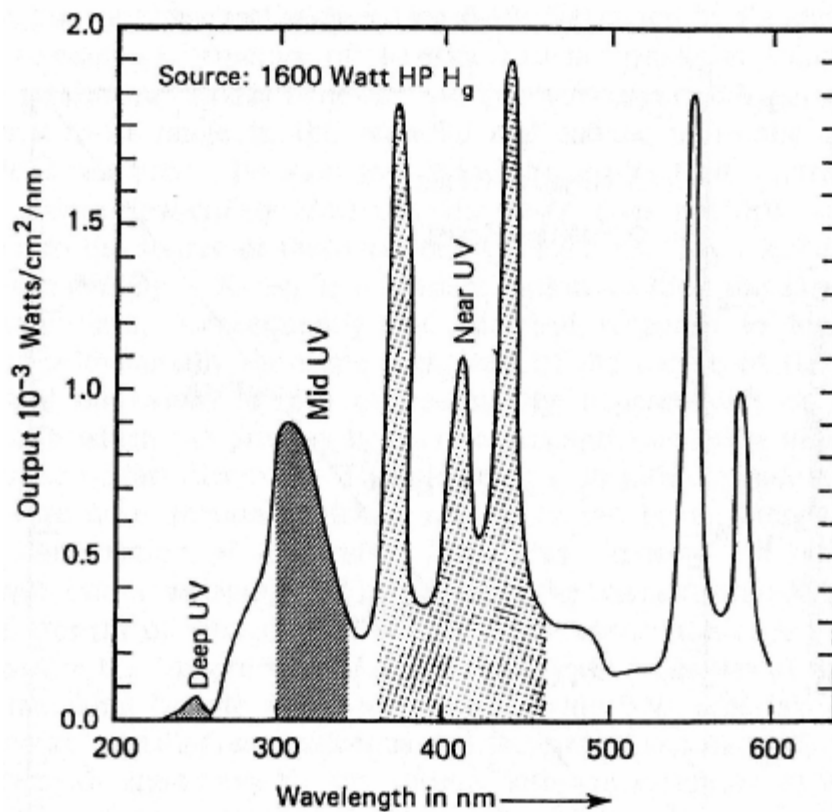
Figure 1.17: Emission spectra for a mercury arc lamp.[44]

20

In traditional novolac/DNQ like systems a single photon may at best cause a single photochemical reaction, but in chemical amplification, a single photon may produce a single active species or catalyst that may perform numerous chemical transformations in the surrounding polymer matrix. The first systems to incorporate chemical amplification were developed by G. H. Smith of the 3M Company. Smith's patent describes using the tetrahydropyranyl ether of novolac and a photoacid generator to achieve chemical amplification.[45] His work was never exploited by 3M and was essentially lost in patent literature.

248 nm Resist Development

Throughout the late 1970s and early 1980s the team of Willson, Fréchet, and Ito worked on the development of chemically amplified resists at the IBM Almaden Research Center. Their initial studies began using poly(phthalaldehyde) polymers that could "unzip" after photo-cleavage of the *o*-nitrobenzaldehyde unit which was incorporated as a co-monomer. Later renditions of this system incorporated photoacid generators (PAGs) that were developed by Crivello at General Electric in place of the photolabile *o*-nitrobenzaldehyde units.[42,43,46] These systems showed two orders of magnitude increase in sensitivity over novolac/DNQ systems, but were not useful photoresists as they "did not resist much of anything", especially under typical dry etch conditions.[26]

Willson's team developed the first practical system in 1983 which utilized poly(*t*-bocstyrene) (PBOCST), a phenolic polymer they were studying as a novolac replacement.[47] This PBOCST system had two orders of magnitude improvement in sensitivity, could be developed in both positive and negative tones, was etch resistant, and had remarkable resolution.[48] The only major problem with PBOCST was not

encountered until it reached full scale manufacturing where dramatic inconsistencies were found when the delay between the PAB and exposure steps was varied. This phenomenon was called "aging" and was ultimately discovered to be associated with the uptake of basic, airborne contaminants into the resist film.[49] The problem was solved by the implementation of carbon filtered air in the production areas, as well as slight modifications of the resist to decrease contaminant uptake.[49,50,51]

Figure 1.18 shows a general example of how PBOCST resists work. In this system, irradiation using a KrF laser (248 nm) causes the production of strong acid. This acid catalyzes the removal of the *t*-boc protecting group from the poly(hydroxystyrene) (PHOST) releasing isobutylene gas. The acid molecule is regenerated after deprotection is complete allowing it to react with a second monomeric unit which can then react with a third and so on. This amplification or "gain" allows the system to work at lower doses of irradiation and has been so revolutionary that almost all resists designed after its inception have incorporated the concept of chemical amplification. PBOCST systems were used for transistor gate level manufacturing until the turn of the century and as with novolac/DNQ resists, they continue to be used in BEOL manufacturing processes today.
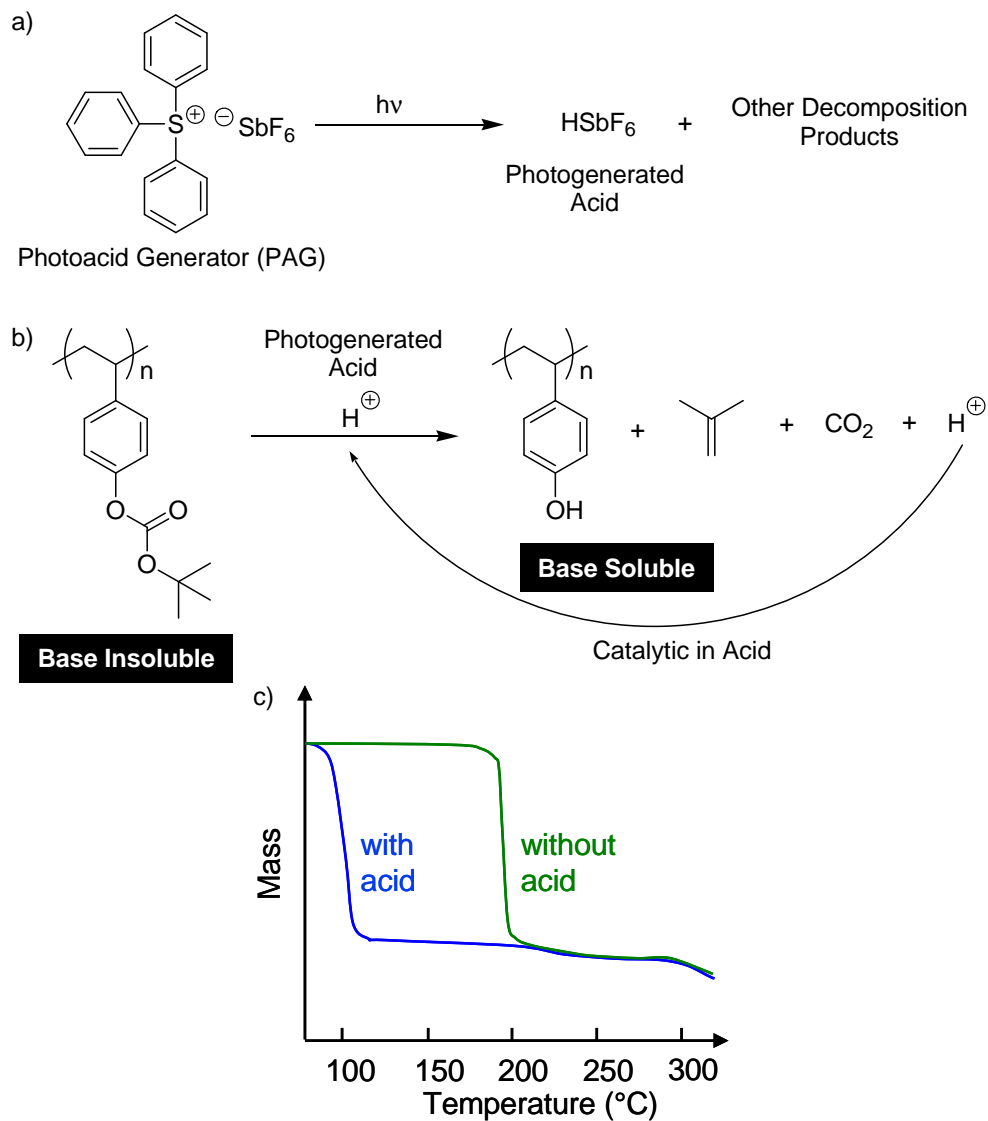
Figure 1.18: Photoacid generation (a), PBOCST deprotection (b), and a TGA showing catalyzed versus uncatalyzed mass loss (c).

193 nm Resist Development

Around the turn of the millennium, it was evident the resolution limits of 248 nm lithography were rapidly being approached. The next wavelength chosen by the lithographic industry as a successor to 248 nm lithography was 193 nm produced via ArF

laser emission. At 193 nm, most all aromatic structures are expected to absorb strongly therefore prohibiting PBOCST type resists. Poly(methacrylates) were known to be highly transparent at 193 nm, but researchers were unsure where to go as most poly(methacrylates) were not resistant to classical dry etching conditions.[52] The first publications reporting the use of 193 nm chemically amplified resists appeared in 1992 by researchers at Fujitsu Limited and IBM.[53,54,55] They found that the incorporation of alicyclic pendant groups drastically increased the dry etch resistance of methacrylate polymers making them useful as photoresist materials.[53,54,56,57] This observation was further elaborated on in a detailed study by Kunz and coworkers in which they empirically derived a relationship, called the "ring parameter", that predicts the etch rate of various alicyclic methacrylate polymers.[58]

This enhanced dry etch resistance also prompted researchers to incorporate alicyclic ring structures directly into the polymer backbone. Of major interest was the norbornene family of structures that were found to be highly etch resistant, but their polymerization via radical processes was prohibitively sluggish. Norbornene did undergo radical copolymerization with maleic anhydride to form an alternating copolymer, but its high lipophilicity prohibited its development in aqueous base. In response, researchers soon found that if acrylic acid was incorporated at 5-20% in the feed, it could act as a "defect" providing base solubility.[53,54,59] Poly(norbornenes) were also synthesized utilizing transition-metal mediated vinyl-addition polymerization catalysts developed by BF Goodrich Company.[60,61,62]

Figure 1.19 shows an example of a chemically amplified 193 nm photoresist. The highly absorbing aromatic rings associated with novolac/DNQ and PBOCST resists have been replaced with alicyclic ring structures such as norbornane, which provide etch resistance while maintaining high transparency at 193 nm. The *t*-boc protected phenolic

24

moieties have been replaced by *t*-boc protected carboxylic acids which impart similar solubility switching functionality. As with PBOCST resists, the *t*-boc removal is catalyzed by photogenerated acid that releases isobutylene gas and regenerates an acid molecule which can catalyze further deprotections. The resultant pendant carboxylic acids render the polymer soluble in basic developers while protected moieties remain insoluble. Today, 193 nm lithography continues to be used for transistor gate level manufacturing, and its resolution limits are being rapidly approached.
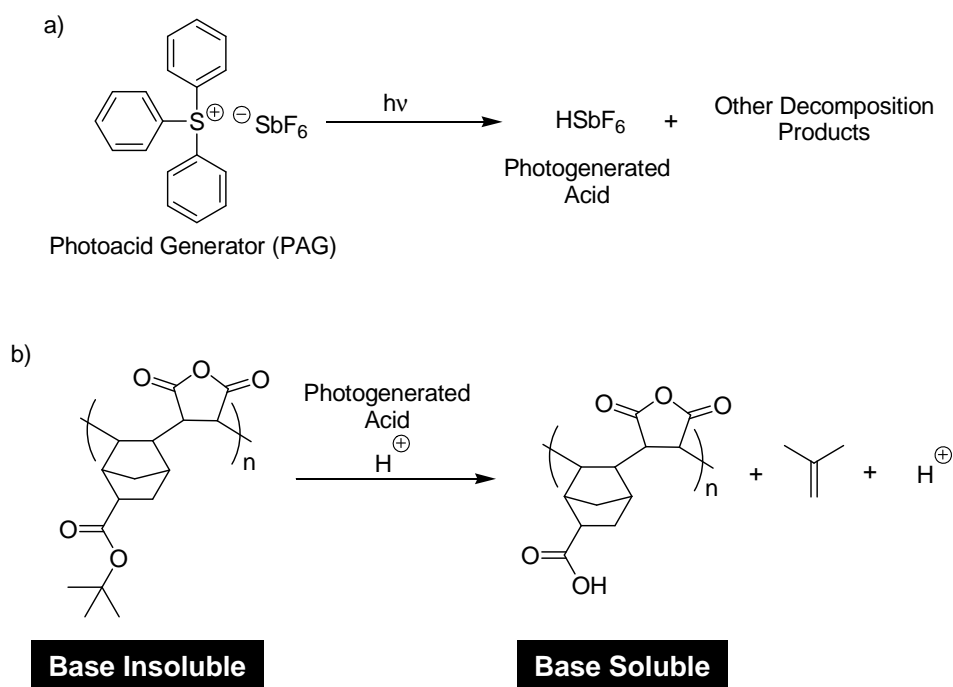
Figure 1.19: Photoacid generation (a) and an example of a 193 nm photoresist (b).

WHERE DO WE GO NEXT?

The lithographic industry has worked for many years as a well oiled machine. When one system fails or its limits are reached, a new system is ready to replace it. These

changes have often met synthetic, engineering, and monetary challenges, but so far, all such challenges have been met, and the drive toward miniaturization has continued (Figure 1.20). Current fabrication using 193 nm lithography is swiftly approaching its limits and sadly the next solution does not seem to be as clear as in years past. Many systems have been proposed to replace 193 nm lithography, but industry leaders have yet to make a unanimous decision as to a unified direction.

Year	Milestone
1826	Niépce makes first photograph called "Point de vue du Gras"
1839	Ponton first uses dichromated gelatin
1840	Bacquerel uses dichromated gelatin to produce relief images, coins term "resist"
1852	British patent awarded to Talbot who made the first practical resist from dichromated gelatin, spawns lithographic industry
1898	"Point de vue du Gras" was lost and remained missing until 1950
1910	Novolac polymer is first produced
1935	Minsk at Eastman Kodak develops the first synthetic photopolymer
1940	Süss develops the first novolac/DNQ resist
1946	The first general-purpose digital computer, "ENIAC," was unveiled
1947	Shockley invents the first transistor
1950	The first commercial novolac/DNQ resist was released as "Ozatec®" by Kalle Co.
1957	Hepher and Wagner develop Kodak's KTFR resist
1958	Kilby of Texas Instruments and Noyce of Fairchild Semiconductor both independently invent the integrated circuit
1965	Intel co-founder Moore develops Moore's Law
1970	The first deep UV (248 nm) resists were made using a methacrylate backbone
1971	The first microprocessor, the Intel 4004, is released
1972	Critical dimensions reach 2 μm and the resolution limits of Kodak's KTFR
1972	Novolac/DNQ resists replace KTRF as the industrial workhorse
1973	Smith of 3M developed the first acid catalyzed resist but never exploited their findings and his work was lost in the patent literature
1978	TOK produces the first commercial deep UV resist named ODUR 10XX
1978	Willson and Fréchet develop first "chemically amplified resist" based on poly(phthalaldehyde)
1979	Crivello develops iodonium and sulfonium photoacid generators at GE
1982	Ito, Fréchet, and Willson improve poly(phthalaldehyde) using a photoacid generator achieving unprecedented sensitivity
1983	Poly(*t*-bocstyrene), a revolutionary chemically amplified resist, was developed.
1988	The first commercial wide-field stepper for 248 nm lithography is produced
1990	Eastman Kodak scaled up production of poly(*t*-bocstyrene) and was used in the negative tone to print IBM's 1 megabit DRAM
1992	The first publications for 193 nm lithography emerge
1993	Carbon filtration systems fix poly(*t*-bocstyrene)'s poor positive-tone performance
1997	Deep UV 248 nm lithography is placed on the SIA roadmap as the standard for 250 nm device fabrication
1997	Kunz publishes first paper detailing the use of 157 nm lithography
1998	The first commercial wide-field stepper for 193 nm lithography is produced
2000	Kilby receives the Nobel Prize in Physics "for his part in the invention of the integrated circuit"
2001	193 nm lithography is placed on the SIA roadmap as the standard for 130 nm device fabrication
2003	Intel drops 157 nm lithography from its roadmap and others soon follow suit

Figure 1.20: A historic timeline of significant events.

The lithographic industry is populated with scientists and business men who are, for a lack of better terms, "frightened" of a departure from traditional optical projection lithography. These lithographic "conservatives" have pushed for the development of 157 nm lithography and 193 nm immersion lithography, while more "daring" researchers have pushed for new technologies such as extreme ultraviolet (EUV), X-ray, e-beam, and imprint lithographies. These radical departures from traditional optical lithography have been termed disruptive technologies and have been met with a great deal of resistance from industry. Chapter two of this dissertation will cover our approach toward the development of a fluorinated 157 nm resist materials, while chapters three and four will focus heavily on the development of materials for Step-and-Flash Imprint Lithography S-FIL[®], a so-called disruptive technology.

Chapter 2: Norbornane Diol Isomers and Their Fluorinated Analogues for 157 nm Imaging Materials [63]

INTRODUCTION

The continued drive to miniaturize microelectronic devices has been accomplished by printing the circuit elements with ever decreasing wavelengths of light.[64] Leading edge manufacturing is now done with 193 nm light and many have pursued the technology required to expose at 157 nm, in the vacuum ultraviolet. Polynorbornenes are of particular interest as the basis for the design of due to their unique set of desirable properties including: high glass transition temperatures, high resistance to reactive ion etching, low UV absorbance, and relative ease of synthesis via metal catalyzed addition polymerizations.[65,66,67,68,69] However, at 157 nm even aliphatic hydrocarbons such as polynorbornene absorb strongly.[70] Fortunately, introduction of fluorinated substituents onto the norbornane skeleton provides materials with sufficient transparency to be used at this wavelength,[71,72] but the most transparent of the fluorine-substituted norbornene monomers resists addition polymerization initiated by classical nickel and palladium catalyst.[2] Therefore an alternate route to fluorinated norbornene polymers by condensation polymerization was sought. Norbornane diols offer a number of attractive opportunities for the preparation of such polymers, for example, via condensation with phosgene to yield polycarbonates.

Although synthetic routes from norbornene to the 2,3-dihydroxy[73] and 2,7-dihydroxy[74,75,76,77,78,79] norbornane have been reported, much of this chemistry is not viable for fluorine substituted norbornane systems as the synthetic methods do not provide sufficient yields or purity of the monomers. While the purity of the monomer is crucial for the production of high molecular weight condensation polymers, the isolation of pure enantiomers was not necessary; therefore an alternate synthetic procedure was developed to yield racemic products. The preparation of fluorinated norbornane compounds most easily proceeds through the Diels-Alder reaction of cyclopentadiene with a fluorinated alkene to yield a substituted norbornene, and many such reactions have been investigated.[4] In this study norbornene was used as a model to develop routes to the corresponding diols. After the synthesis was optimized for norbornene, these routes were investigated with the incorporation of fluorinated substituents. It was soon discovered that in most cases, the hydrocarbon norbornene was a not an appropriate model for the fluorinated monomers. Finally, the diol monomers were incorporated into polycarbonate polymers and their transparency measured using a vacuum-ultraviolet variable angle spectroscopic ellipsometer (VUV-VASE).

RESULTS AND DISCUSSION

Oxidative Dihydroxylation

The most straightforward route from norbornene, **2.1**, to a norbornane diol is oxidative dihydroxylation. The *cis* diol can be obtained by oxidation with either permagnate[6] or osmium tetraoxide. As reported for a range of reactions with the alkene functionality of norbornene,[80] the higher steric hindrance on the *endo* face leads to a strong preference for the *exo*-diol isomer, **2.2**. While the synthetic route to the monomer

is a single step, all attempts to prepare a poly-carbonate by condensation with phosgene yielded exclusively the cyclic carbonate, **2.3**. Attempts to carry out the ring opening polymerization of **2.3** using either acid or Sn(Oct)$_2$ catalysts also failed,[81,82,83] therefore efforts shifted towards the synthesis of a norbornene diol with regiochemistry that precluded the formation of the cyclic carbonates, specifically, the *trans*-2,3-norbornanediol (Scheme 2.1).
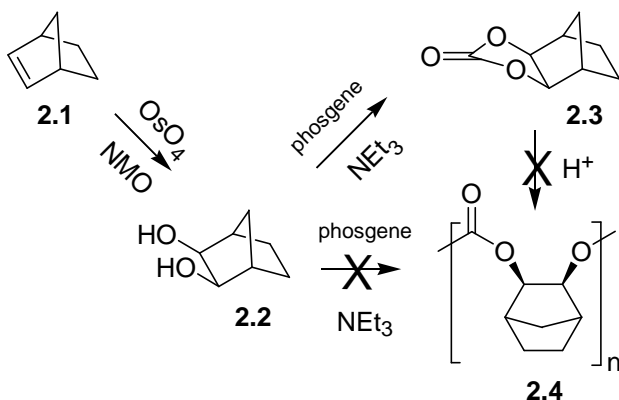
Scheme 2.1: Synthesis and phosgene condensation of 2-exo-3-exo-norbornanediol.

Previously reported techniques for the synthesis of *trans*-2,3-dihydroxynorbornane are limited to the Raney Nickel isomerization of the *cis*-2,3-dihydroxynorbornanes (**2.2**).[5] Our attempts to repeat this work invariably gave mixtures regardless of the source of the catalyst, and the isomerization failed on the fluorinated norbornanes, so an alternative procedure was sought.

Epoxynorbornane Ring Opening

exo-2-*exo*-3-Epoxynorbornane is readily accessible by oxidation of norbornene but attempts to ring-opening the unsubstituted epoxynorbornane, **2.5a**, under acidic aqueous conditions have been demonstrated to yield a mixture of products due to

norbornyl cation rearrangements (Scheme 2.2).[7] The 0.5M HCl catalyzed epoxide ring opening was monitored by GC-MS to determine the time-dependant product distribution and was found initially to yield a complex mixture of dihydroxy- and chlorohydroxy-norbornanes[84] (see Figure 2.1), the chief constituents being, the *exo*-2-*syn*-7-dihydroxynorbornane (**2.6**), *exo*-2-chloro-*syn*-7-hydroxynorbornane (**2.7**), as well as the desired *trans*-2,3-diol (**2.8**). Each of these products was isolated by column chromatography, and the structures were confirmed by x-ray crystallography. Separation of the isomers required difficult, tedious chromatography; but increasing the reaction time to one day led to isomerization to the thermodynamically favored *exo*-2-*syn*-7-dihydroxynorbornane (**2.6**). Because the primary impurities after one day were norbornyl ether oligomers, the product (**2.6**) could be purified easily by sublimation. Confirmation of the regiochemistry of **2.6** was verified by reaction with phosgene which yielded the cyclic carbonate at temperatures above 0 ℃. Although this diol was successfully condensed with phosgene at low temperatures to yield a polycarbonate polymer, attempts to ring-open fluorinated epoxynorbornanes under these and other acidic conditions led to a complex mixture of inseparable isomers.
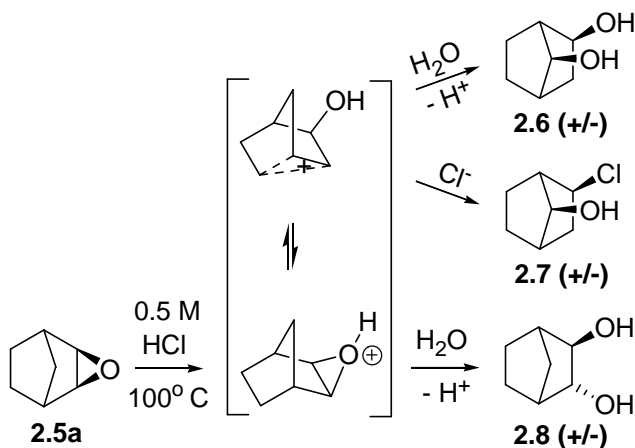
Scheme 2.2. Acid-catalyzed 2-exo-3-exo-epoxynorbornane ring opening products.

32
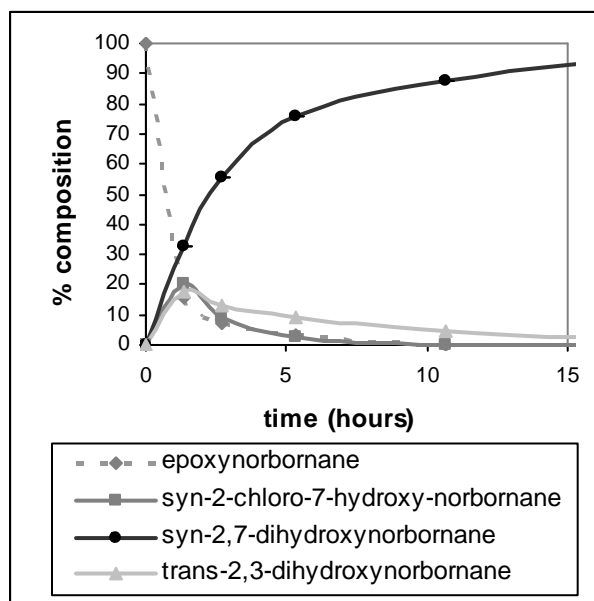
Figure 2.1: Product distribution of acid catalyzed epoxynorbornane ring opening.

The ring opening of 2-*exo*-3-*exo*-epoxynorbornanes under basic conditions should preclude the problems associated with norbornyl carbocation rearrangements, but this reaction is complicated instead by steric hindrance inhibiting nucleophilic attack from the *endo*-face. A range of basic aqueous conditions were investigated using hydroxide ion as the nucleophile with a number of different counterions, crown ethers, and phase transfer catalysts at a range of temperatures but these reactions yielded only starting material. Nucleophilic attack of the unsubstituted epoxide, **2.5a**, could only be achieved using potassium benzyloxide, generated in situ by reaction between benzyl alcohol and potassium metal, which afforded a 30% yield of **2.9** after 10 days at 150 ˚C. Reaction with potassium benzyloxide at temperatures below 130 ˚C yielded only starting material, while temperatures above 160 ˚C led to degradation of the material. The benzyl group of **2.9** was readily removed by palladium catalyzed hydrogenolysis to afford a racemic mixture of the *trans*-2,3-norbornanediol, **2.8** (Scheme 2.3). The structure was verified by

33

obtaining the crystal structure of the di(phenylcarbamate) after reaction of the diol with phenylisocyanate. Condensation with phosgene yielded the corresponding polycarbonate without formation of the cyclic carbonate, making the trans-diol the most attractive route to production of fluorinated norbornane condensation polymers. The details of the polymerizations will be discussed later.

Unfortunately, attempts to open the fluorinated norbornene epoxides **2.5b** and **2.5c** with potassium benzyloxide at 150 ˚C failed, and increasing the temperature led to decomposition of the starting material (Scheme 2.3). The reduced reactivity of the substituted epoxynorbonanes is presumably the result of the increased steric blockage by the bulky fluorinated substituent on the already hindered *endo* face.
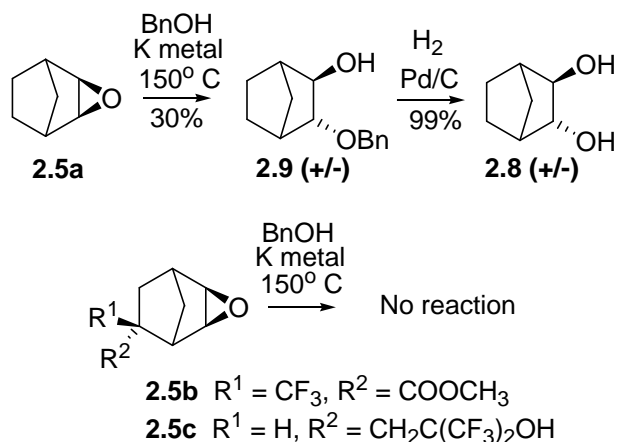
Scheme 2.3: Base catalyzed 2-exo-3-exo-epoxynorbornane ring opening products.

Multistep Synthesis

A revised synthetic approach was developed, taking into consideration the sensitivity of norbornanes to strongly acidic conditions, and the steric blockage of the *endo* face. As the 2-*exo*-3-*exo*-norbornane diol was readily accessible in high yields through osmium tetroxide dihydroxylation, a synthetic route was devised by which one of

the hydroxyls would be protected while the stereochemistry of the other was inverted. This was achieved by protecting the *cis exo* diol via a *p*-toluenesulfonic acid catalyzed condensation with benzaldehyde dimethyl acetal. When this reaction was carried out in an ice bath under reduced pressure, the *exo*-isomer **2.10** was formed exclusively. A single hydroxyl group was deprotected by reaction with a 10 fold excess of DIBAL[85,86] and oxidation of the product **2.11** with PCC afforded 2-*exo*-benzyloxynorbornan-3-one, **2.12**. Reduction of *exo*-benzyloxynorbornanone with sodium borohydride afforded 61% of the *trans* isomer **2.13**, but regenerated 39% of the cis isomer **2.11**. The stereoselectivity for this reaction is reduced significantly when compared to the reduction of unsubstituted norbornanone, as a result of the bulky benzyl ether on the *exo* face; however, reduction with the more stereoselective superhydride afforded the desired isomer, **2.13**, in a 90% yield. The benzyl protecting group was quantitatively removed by hydrogenolysis to afford the target model compound, 2,3-*trans*-norbornanediol, **2.8** in excellent overall yield (Scheme 2.4).
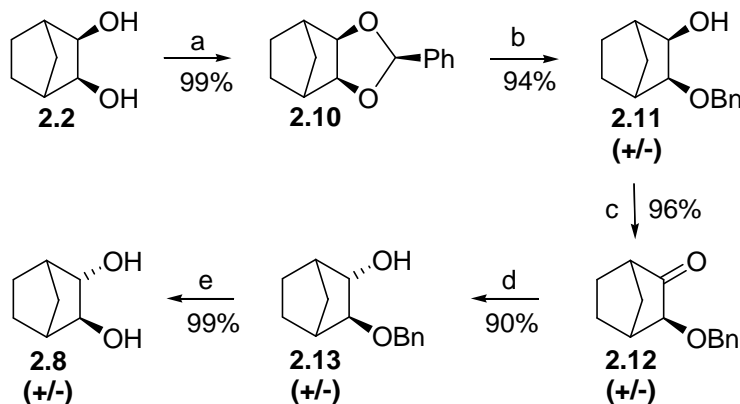
Scheme 2.4: Alternative synthesis of 2,3-trans-norbornanediol. Key: (a) PhCH(OCH$_3$)$_2$, PhCH$_3$, 0 °C, 10 Torr; (b) DIBAL, PhCH$_3$; (c) PCC, CH$_2$Cl$_2$; (d) superhydride, THF 0 °C; (e) Pd/C, H$_2$, EtOH/EtOAc

Fluorinated analogs

The 2,2-bis(trifluoromethyl)hydroxyethyl substituent was the primary fluorinated substituent investigated because it incorporates sufficient fluorine into the structure to improve transparency for 157 nm lithography while also providing an aqueous base soluble functional group. This alcohol has a pKa similar to that of phenol, and is a base soluble group that has been used in previous generations of commercial resists. The *endo* alkene **2.14** was oxidized with osmium tetroxide and precipitated into dichloromethane to afford *cis*-diol **2.15**. The large steric bulk of the fluorinated substituent assured solely *exo* dihydroxylation. Benzylidene protection was carried out with *p*-toluenesulfonic acid as the acid catalyst, and as before, if carried out at ~0 °C under reduced pressure the *exo*-benzylidene protected diol **2.16** was solely isolated in nearly quantitative yields (Scheme 2.5). The structure was verified by X-ray crystallography.
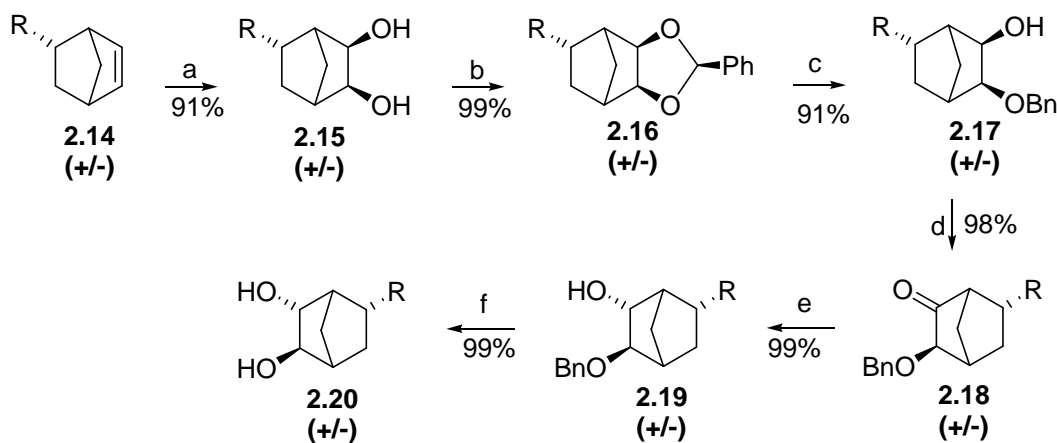
Scheme 2.5: Preparation of fluorinated norbornane monomer. Key: R = CH$_2$C(CF$_3$)$_2$OH (a) OsO$_4$, NMO, THF; (b) PhCH(OCH$_3$)$_2$, PhCH$_3$, 0 °C, 10 Torr; (c) DIBAL, PhCH$_3$ (d) PCC, CH$_2$Cl$_2$; (e) superhydride, THF 0 °C; (f) Pd/C, H$_2$, EtOH/EtOAc.

A single hydroxyl group on **2.16** was deprotected by reaction with 6 equivalents of DIBAL, and although two regioisomers from this reaction were observed by GC,

carrying this reaction out under high dilution (5 μM in substrate) provided a 91% yield of a single racemate after flash chromatography. X-ray crystallography verified that the deprotection occurred at the hydroxyl β, rather than γ, to the HFA substituent, yielding **2.17**. It is proposed that cleavage occurs in the observed position because of anchimeric assistance from the free hydroxyl group of the fluorinated substituent (Scheme 2.6). The first equivalent of DIBAL acts to deprotonate this acidic hydroxyl, and provides a tethered Lewis acid which preferentially activates the β-ether towards cleavage by a second hydride. Such assistance by free hydroxyls during the DIBAL deprotection of benzylidene groups has been reported previously for threitol systems.[87] Additional support for this mechanism was obtained by protecting the hydroxyl group with a benzyl ether which resulted in greatly reduced regioselectivity. (Figure 2.2)
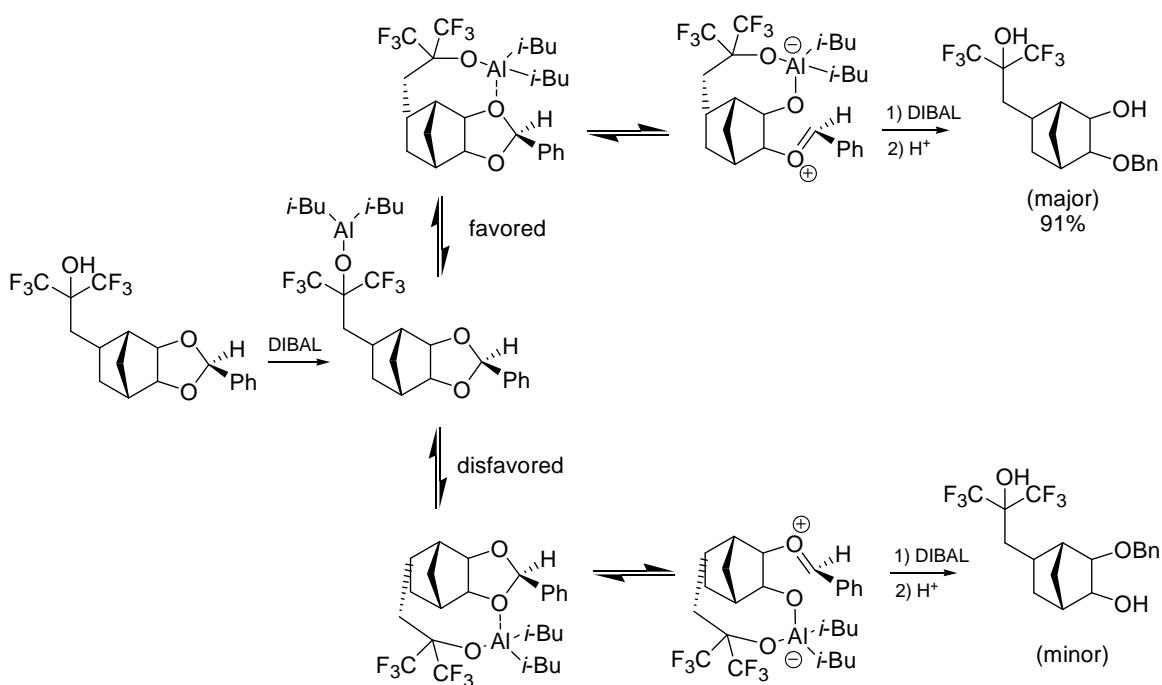
Scheme 2.6: Proposed mechanism for regioselective deprotection of **2.16**.

37
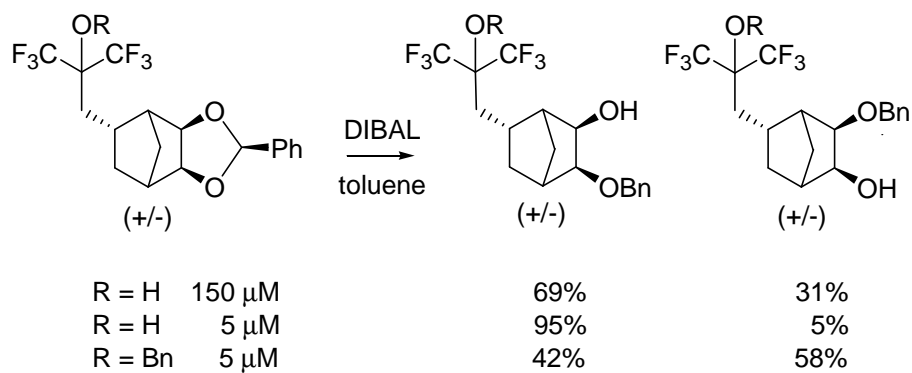
Figure 2.2: Ratio as determined by GC of DIBAL deprotection products.

Oxidation using PCC afforded a nearly quantitative yield of the norbornanone **2.18**, which was converted to the *endo* alcohol **2.19** by reduction with superhydride. This reduction was significantly more stereoselective than that of the unsubstituted ketone (**2.12**) because of the presence of the bulky hexafluoroisopropanol group on the *endo* face. Finally, catalytic hydrogenolysis of the benzyl protecting group afforded the target compound, **2.20**. The relative stereochemistry of the three substituents was confirmed by X-ray crystallography.

Figure 2.3: ORTEP diagrams of a) the bisphenylcarbamate of compound **2.8**, b) compound **2.16**, c) compound **2.17**, d) compound **2.19**, and e) compound **2.20**.

Polycarbonate Formation

Bischloroformates **2.21** and **2.23** were synthesized using phosgene and pyridine from *trans*-diol compounds **2.8** and **2.20** respectively. These reactions proceeded at room

temperature and however stable enough to be purified via silica gel chromatography, were not isolated in the preparation of polymers **2.22** and **2.24**. The conversion to bischloroformates was monitored by GC-MS and once completed were subjected to further reaction with a second equivalent of their respective diol and refluxed for 24 hrs (Scheme 2.7). The polymers obtained were of low molecular weight (≤10 kDa) but were able to be spin coated from propyleneglycol monomethylether acetate (PGMEA) solution onto silicon wafers. The absorbance of polymer **2.22** was found to be 5.37 μm^{-1} while polymer **2.24** showed an absorbance of 2.79 μm^{-1} at 157 nm.

The low molecular weights obtained are likely an artifact of a slight stochiometric imbalance of bischloroformate and second equivalent of diol added. Fluorinated polymer **2.24** showed a dramatic improvement in transparency over its nonfluorinated analogue **2.22.** However, its absorbance was too high to be useful as a functional 157 nm photoresist. This high absorbance was surprising due to the high transparency of hydrogenated monomer **2.14**[88]. Most speculation attributes this absorbance to the effect that carbonates have at this low wavelength.
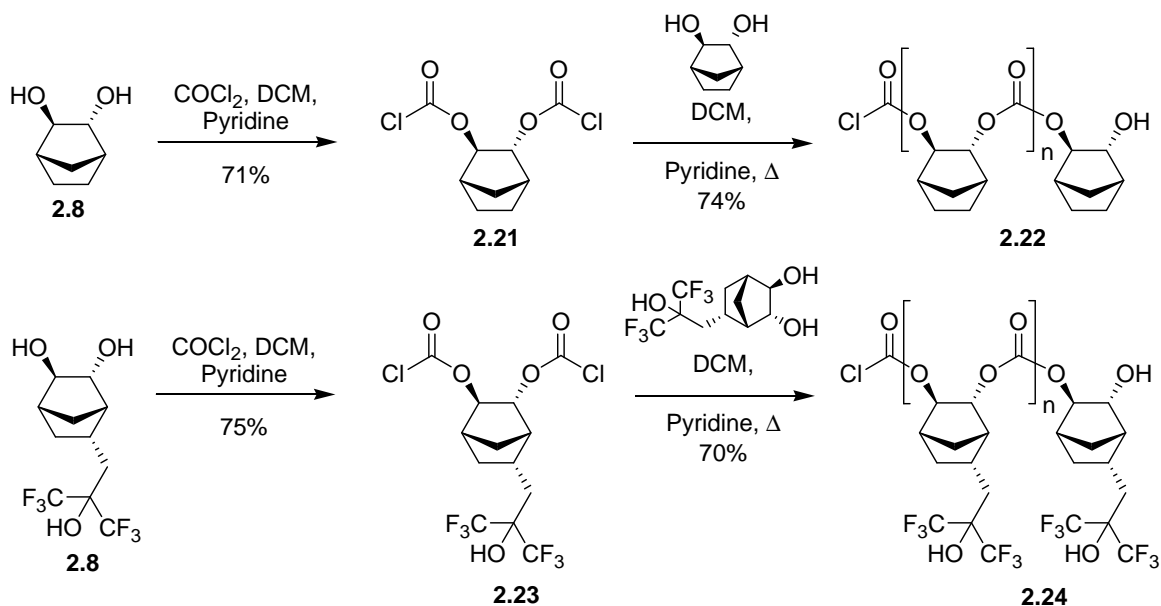
Scheme 2.7: Synthesis of *trans*-diol poly(norbornene carbonate).

CONCLUSION

Due to the steric and electronic effects of fluorine incorporation into the norbornene ring structure, previously reported techniques for the synthesis of many norbornene diols failed to provide an effective route to fluorinated analogues. A high yielding, multistep route has been developed to provide synthetic access to the fluorinated norbornane diol, **2.20**, in a 79% overall yield, and with minimal chromatographic purification. The unfluorinated and fluorinated *trans*-2-endo-3-exo-norbornanediols readily condense with phosgene to afford poly(norbornene carbonates), however their slight absorbance precludes their implementation as 157 nm photo resists.

Chapter 3: Materials for Step and Flash Imprint Lithography (S-FIL®)[89]

INTRODUCTION

The lithographic industry is driven to produce ever smaller, faster, and cheaper microelectronic devices. As feature size steadily decreases, drastic changes in materials and tools are periodically necessary to meet consumer needs and standards outlined by the ITRS. Industry has pushed photolithography to exposure at 193 nm (immersion), 157 nm, and extreme ultra-violet (11 nm) wavelengths of light in attempts to meet these requirements. Each change, however, is accompanied by ever increasing costs associated with tool replacement and materials development. This economic stress has resulted in the exploration of disruptive lithographic techniques that might provide high resolution imaging at significantly lower cost.

Nanoimprint lithography (NIL) has emerged as a viable alternative to traditional optical lithography.[90] Thermal nanoimprint lithography, first described by Chou *et al.*,[91] uses a patterned template and high pressures to transfer an image into a heated thermoplastic material. This process, sometimes referred to as "hot embossing," has shown impressive resolution down to 5 nm.[92,93,94] Although this demonstration of resolution is attractive and the process is valuable for making some nanostructures, thermal imprint is not favorable for multi-layer device fabrication due to the repeated heat and cool cycles associated with its process. This cycling of temperature can lead to

decreased throughput and improper overlay of device layers and features due to differences in resist, substrate, and template coefficients of thermal expansion.[95]

To circumvent these disadvantages, Step and Flash Imprint Lithography, or S-FIL®, was introduced in the late 1990's as a room temperature, low pressure NIL process applicable to multi-level device fabrication.[96] S-FIL uses a low viscosity prepolymer (monomer) solution which is dispensed onto a substrate and imprinted using a quartz template. Once the template features have filled with monomer solution via capillary action, the sample is irradiated to initiate photopolymerization of the prepolymer solution. After irradiation, the template is separated from the substrate leaving behind an exact inverse replica of the template pattern (Figure 3.1). The samples are irradiated with an inexpensive mercury arc lamp through simple optics making this a cost effective alternative to optical lithography.
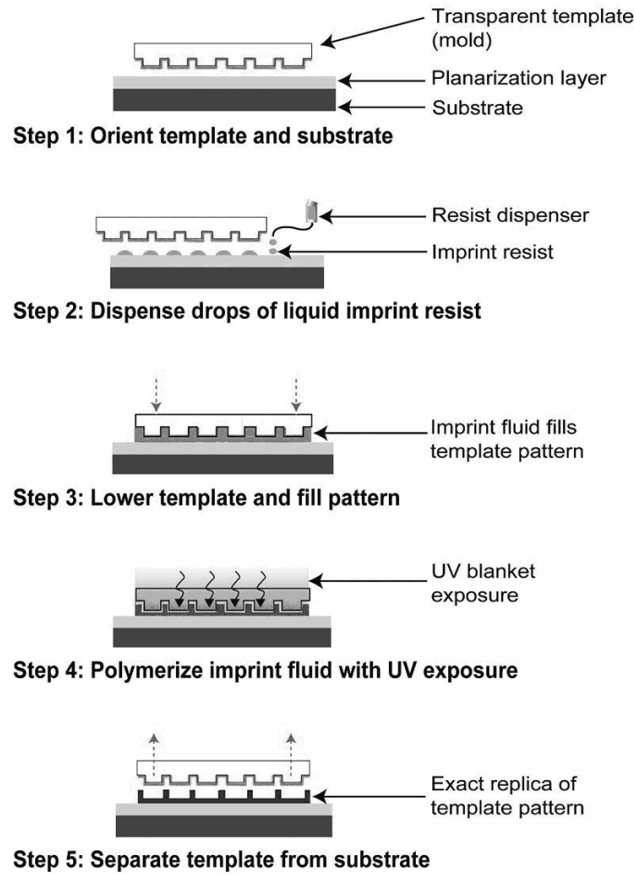
Figure 3.1: Overview of the S-FIL process.

While traditional optical lithography has struggled to reliably produce sub 45 nm features, S-FIL has repeatedly shown resolution capabilities of 20 nm and below.[95] S-FIL's versatility and remarkable resolution potential were highlighted further when Rogers *et al*. used a variation of S-FIL to successfully imprint a mold of a single walled carbon nanotube into a polyurethane prepolymer solution producing a 2.4 nm wide feature.[97] Such demonstrations of high resolution have only helped to cement NIL's incorporation into the ITRS roadmap as a potential candidate for the production of high resolution 32 nm device features.[98] Examples of high resolution imprints with various architectures are shown in Figure 3.2. The following sections will give an overview of the

types of S-FIL materials being investigated to produce such features while maximizing throughput and minimizing cost.
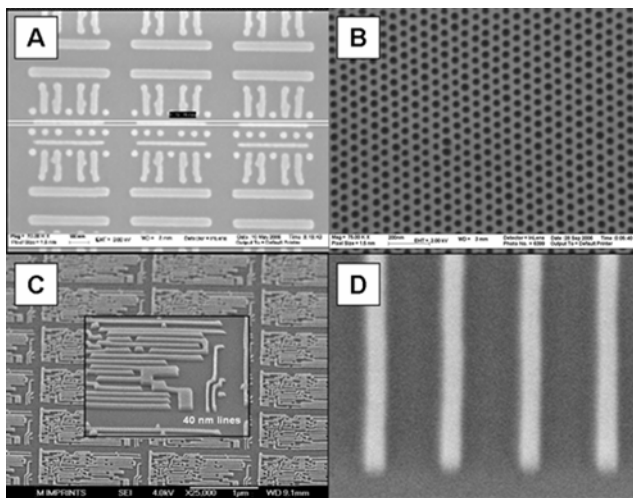
Figure 3.2: Images produced using S-FIL: a) 22 nm logic before etch, b) staggered 25 nm contact via holes with aspect ratio of approximately 3, c) 40 nm logic before etch, and d) 20 nm lines with aspect ratio of 2.5 and residual layer etched. Aspect ratios are height/width. *All images courtesy of Molecular Imprints Inc.*

MATERIALS FOR S-FIL

An imprint resist is typically a mixture of various polymerizable components, each adding desired characteristics to the final polymeric material. There are four main components to any S-FIL resist. The first is a bulk polymerizable monomer, which constitutes a large portion of the repeat units (30-50%) in each of the polymer chains. The second is a silicon or siloxane containing monomer, which provides the oxygen etch resistance needed to transfer the pattern onto the underlying substrate. The third is a difunctional cross-linker that is used to provide mechanical strength, and finally a photoinitiator is required to initiate polymerization.[99]

Several factors must be considered when selecting components for an imprintable S-FIL resist material. First, the prepolymer formulation must have low enough viscosity to be dispensed by an automated dispense system and its composition must not change significantly due to evaporation. Second, it must photopolymerize rapidly to maintain high throughput and shrinkage due to polymerization must be minimal. Third, it must adhere to the substrate, be able to release from the imprint template, and still have sufficient mechanical properties and integrity to avoid feature collapse. Finally, it must be thermally stable to common temperatures associated with reactive ion etching and must possess the high etch selectivity required to produce high aspect ratio device features.[100] The following paragraphs will describe the two predominant S-FIL formulations which have been found to meet the above requirements.

Acrylate formulations

Acrylates are the most widely studied monomers for S-FIL.[90,95,96,100,101,102] They provide a low viscosity prepolymer solution that can easily be dispensed while maintaining low volatility. They cure quickly upon photoinitiated radical polymerization, and a variety of silicon containing monomers are readily available from various commercial sources avoiding time consuming and ultimately expensive syntheses. An example of a widely used S-FIL formulation is given in Figure 3.3. The bulk polymerizable monomer of the formulation is t-butyl acrylate (37.5%), or other aliphatic acrylic monomer, while the remainder is composed of Darocur 1173 (product of Ciba Geigy) for photoinitiation, a siloxane monomer for etch resistance and ethylene glycol diacrylate which provides cross-links for mechanical strength and feature integrity.
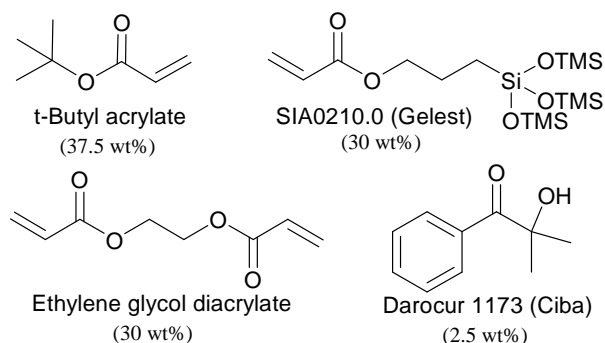
Figure 3.3: Example of standard imprint resist formulation.

Despite the many advantages of acrylates, there are several limitations inherent to radical based photopolymerizations. The primary limitation is inhibition due to the presence of molecular oxygen in the imprint formulation and the surrounding atmosphere. Oxygen readily forms stable peroxy radicals during radical polymerizations[103] which cause an induction period at the onset of irradiation and often produce a band of unpolymerized material at the periphery of the template.[101,102] This requires extended exposure times and ultimately decreases wafer throughput.

Vinyl ether formulations

Vinyl ethers, which polymerize via a cationic pathway, are an attractive alternative to acrylates.[104,105,106] Cationic polymerization is accomplished by the incorporation of a photoacid generator (PAG) in place of the photo-induced radical initiators found in typical acrylate formulations. The omission of a radical mechanism avoids inhibition of polymerization due to atmospheric oxygen and hence, polymerization takes place with little to no induction period. Another advantage of vinyl ethers is that they are generally of lower viscosity (approximately 1 cP) than acrylate

based systems (commonly used acrylates are 3-4 cPs), facilitating dispense and spreading processes while maintaining adequate material properties[99].

Although vinyl ethers offer certain advantages over acrylate formulations, they are not without limitations. In general vinyl ethers have higher vapor pressures than acrylates, which can result in a change of prepolymer composition and ultimately affect resist performance and stability. They also produce a separation force approximately twice that of acrylates which can lead to template fouling, a topic that will be discussed in detail later[99]. Finally, the limited selection of commercially available monomers, cross-linkers, and silicon containing monomers has handicapped the incorporation of vinyl ethers into standard SFIL resists.

FUNCTIONAL MATERIALS FOR S-FIL AND S-FIL/R

Many of today's microprocessors contain multiple ($\geq$ 8) levels of wiring that are interconnected through vias between wiring levels. To avoid certain limitations associated with the lack of effective plasma etch processes for copper, researchers have instituted the use of a dual-layer patterning process referred to as "Dual Damascene." This process, when performed using traditional optical lithography, can take as many as 20 steps per wiring layer. S-FIL has been shown to reduce that number by more than half through the use of multi-tiered templates, which are imprinted just as described in Fig. 1, producing both a via and a wiring level in a single step.[107] A further improvement can be made if the imprinted material is a functional dielectric. These dielectric materials have to meet 5 key requirements to be implemented in the S-FIL process: they must 1) be thermally stable to 400 °C, 2) be liquids at room temperature, 3) be photocurable, 4) have

48

a low dielectric constant, and 5) embody sufficient mechanical properties after curing to maintain feature stability.[107,108]

A material that is being extensively studied for "Dual Damascene" is based on functionalized polyhedral oligomeric silsesquioxanes (POSS) (Figure 3.4). These materials have been used for dielectric materials in other semiconductor manufacturing processes[109,110] and provide an attractive basis for S-FIL as well.[111] It was determined that a mixture of functionalities is integral to achieving sufficient mechanical and thermal properties. This POSS material typically incorporates three methacrylate functionalities and five pendant benzocyclobutane (BCB) groups. The methacrylate groups efficiently cure via free radical polymerization to provide initial feature integrity while the BCB groups are cured through a thermal process, further improving mechanical properties and thermal stability with minimal shrinkage due to polymerization. The material has a dielectric constant of 2.89 which meets the requirement for upper level wiring (<3) and has a Young's modulus of 1.8 Gpa which is appropriate for S-FIL.[108]
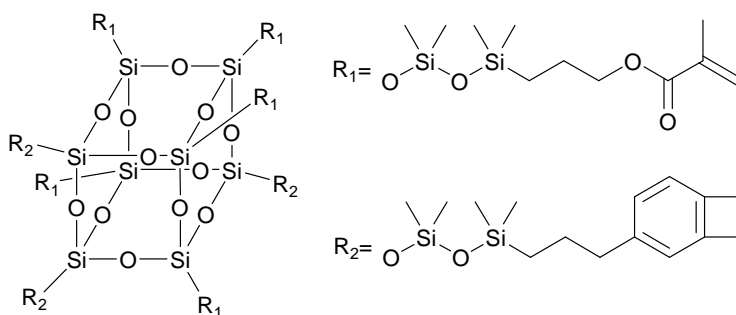
Figure 3.4: POSS structure.

These POSS materials, just as with typical acrylate and vinyl ether formulations, have a drawback concerning their high silicon content. If the material becomes imbedded within the template features, the material can become difficult if not impossible to clean

49

or remove without template degradation. Approaches that may help circumvent this template fouling will be discussed in the following sections.

REVERSIBLE MATERIALS TO PREVENT TEMPLATE FOULING

Template fouling is one of the more significant challenges facing S-FIL. Fouling occurs when portions of the polymerized, silicon containing resist adhere and/or become lodged within the features of the imprint template. S-FIL requires that the template be a 1:1 scale, inverse mold of the features to be patterned due to its direct imprinting nature. Small feature sizes along with high silicon content and a large degree of cross-linking make any residual imprint polymer left on the mold almost impossible to remove from the template without damaging the expensive quartz template. The high cross-linker loading is needed to provide mechanical properties for the desired high aspect ratio features, but results in a material that is insoluble in any aqueous or organic solvent. Similarly, high silicon content is needed for etch resistance, but gives the material a quartz like property when exposed to typical oxygen plasma or other oxidative cleaning processes, making removal of this material from a quartz template virtually impossible.

A number of solutions have captured the interest of researchers including the use of fluorinated self assembled monolayers (FSAMs) as template release layers and the inclusion of reversible or degradable cross-linkers in place of ethylene glycol diacrylate or its divinyl ether analogue. Although surface treatments such as FSAMs are attractive solutions, preliminary research has shown that currently available surface treatments cannot exclusively prevent template fouling. Therefore, many researchers have chosen to focus their efforts toward the use of degradable and reversible cross-linkers instead. Theory suggests that the highly cross-linked, insoluble resist may become soluble in

common organic solvents if the cross-links were to be broken, resulting in lower molecular weight linear polymer.[112] Thermally reversible cross-linking materials and acid labile cross-linking materials provide two attractive routes through which this theory could be tested.

Thermally reversible cross-linked resists

The first class of thermally reversible cross-linkers studied is based upon the reversible linkage referred to as a blocked isocyanate[113] (Scheme 3.1). Cross-linker **3.1** is readily synthesized by the formation of aromatic oximes which are further reacted with diisocyanates. This diol structure can be functionalized with acrylates, methacrylates, or vinyl ethers to provide the cross-linking structure. Compound **3.1** was found to revert back to its constituent oximes and diisocyanate at temperatures greater than 100 °C, making it a likely candidate for incorporation into S-FIL formulations. The reversible nature of this linkage was confirmed by solid state IR spectroscopic analysis and solution state NMR spectroscopy. Unfortunately difficulties were encountered due to the low solubility of **3.1** in standard S-FIL formulations that prevented further studies.[114]
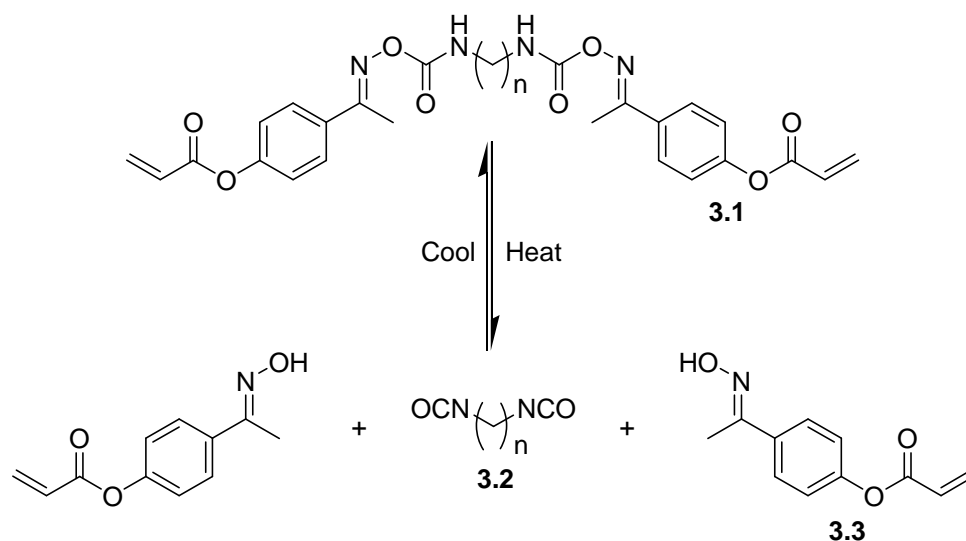
Scheme 3.1: Blocked isocyanate cross-linker reversibility.

A second class of thermally reversible cross-linkers is based on the reversible linkage formed from the Diels-Alder reaction between substituted furans and maleimides. This reversible linkage was popularized by Wudl *et al.*[115,116] and has been extensively studied.[117,118,119,120,121] The reversible cross-linker **3.4** (Scheme 3.2) was synthesized via a Diels-alder reaction between furfuryl alcohol and a hydroxyethyl functionalized maleimide, which was then further functionalized with pendant acrylates or methacrylates providing the cross-linking structure. Model studies showed that the cycloreversion of these Diels-Alder adducts occurs at temperatures above 80 °C in solution making them excellent candidates for S-FIL. The Diels-Alder adduct **3.4** was easily incorporated into S-FIL formulations and provided adequate mechanical properties for feature integrity. Solid state ^{13}C-NMR data of poly(methyl methacrylate) cross-linked with compound **3.4** showed conclusively that upon heating, the equilibrium is shifted toward the cycloreversed product. Despite this evidence, the polymer films could never be removed from silica substrates through immersion into hot organic solvents such as DMSO, NMP, toluene, DMF, etc. Research continues within our group to understand this

surprising observation. The detailed synthesis, characterization, and discussion of these and other Diels-Alder compounds will be discussed in chapter 4.
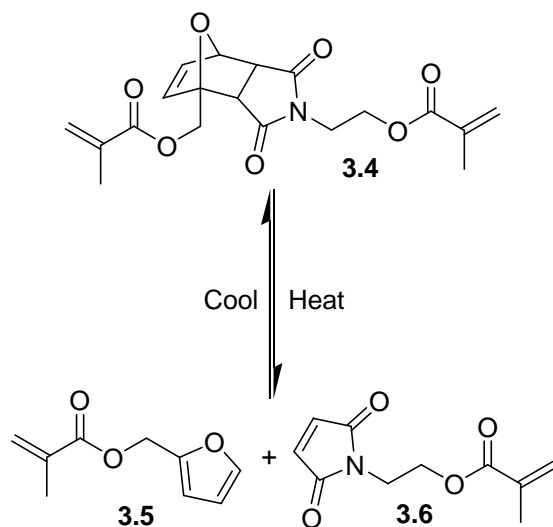
Scheme 3.2: Diels-Alder cross-linker reversibility.

Acid labile cross-linked resists

The first class of acid labile cross-linkers studied were *t*-butyl ester cross-linkers that have been reported for various other applications.[122,123,124] Cross-linker **3.7** (Scheme 3.3) is known to readily decompose, upon exposure to acid and mild heat, to products **3.8** and **3.9**. This allows the system to be decross-linked, rendering the remaining linear polymer soluble in the warm, acidic, organic media. Cross-linker **3.7** is readily soluble in common acrylate formulations and upon photocuring, provides mechanical properties suitable for the S-FIL process. Imprints containing compound **3.7** have been successfully stripped from their respective substrates upon immersion in warm acidic organic solvent demonstrating the utility of these reversible compounds. This demonstration gives promise that these *t*-butyl esters may be successfully incorporated into commercial prepolymer resists in the future.[114]
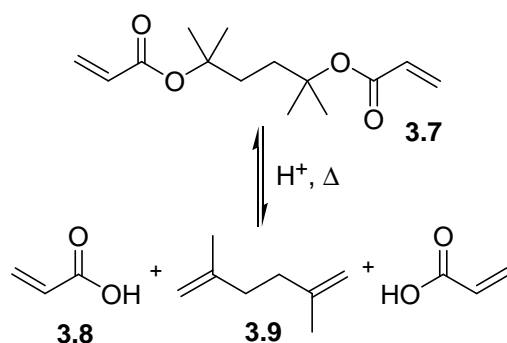
Scheme 3.3: *t*-Butyl ester cross-linker reversibility.

A second class of cross-linkers derived from acetal and/or ketal linkages have been investigated. Acetals and ketals are known to readily hydrolyze to their corresponding ketone and hydroxyl compounds upon treatment with wet, acidic, organic solvent.[125,126,127,128,129] Compound **3.10** was synthesized and has been successfully incorporated into S-FIL formulations and imprinted. The imprints were successfully decross-linked (Scheme 3.4) and dissolved away after introduction into room temperature acidic organic media. One drawback of these ketal type materials is they require a higher concentration in the prepolymer solution to obtain satisfactory mechanical properties,[114] but they do not require heat to reverse the linkages.
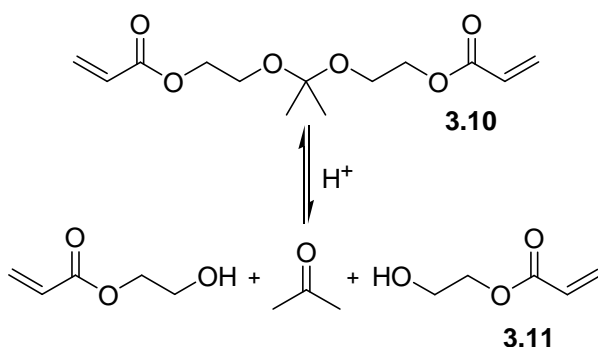
Scheme 3.4: Ketal cross-linker reversibility.

CONCLUSIONS

Many challenges remain before S-FIL will be fully ready for commercialization. One problem is the need for improved template release chemistry. The improvement of this release chemistry may avoid many of the problems associated with template fouling and the higher separation forces encountered when using vinyl ether formulations. There is also an urgent need to develop new dielectric and sacrificial imprint materials[130] (SIM) that may be patterned via imprint lithography. The development of these materials, specifically for the "Dual Damascene" process, offers an opportunity to reduce the cost of advanced devices and may aid the acceptance and implementation of S-FIL as an effective alternative lithography.

A relatively unexplored area of S-FIL is the use of "fugitive" materials. These are materials that may be patterned via imprint and remain as part of the device until all metal layers have been deposited. Once all levels of metal deposition are complete, the "fugitive" material is removed to leave free standing metal structures separated by air. These so called air bridges take advantage of the extremely low dielectric constant of air, thereby providing further advances in the miniaturization of microelectronic device features.

From the time of its inception at The University of Texas at Austin in the late 1990's, Step and Flash Imprint Lithography has come from a demonstration of resolution, to having been placed on the ITRS roadmap as a viable alternative lithography.[98] S-FIL has shown that it provides a low cost alternative to traditional optical lithography with overlay and resolution capabilities that meet or exceed those required for 32 nm device fabrication and beyond.

Chapter 4: Thermally Reversible Materials for Step and Flash Imprint Lithography (S-FIL®)

INTRODUCTION

Template fouling is one of the most significant challenges facing S-FIL®. Fouling occurs when portions of the polymerized, silicon containing resist adhere and/or become lodged within the features of the imprint template. Small feature sizes along with high silicon content and a large degree of cross-linking make any residual imprint polymer almost impossible to remove without damaging the expensive quartz template. The high cross-linker loading is needed to provide mechanical properties for the desired high aspect ratio features but results in a material that is insoluble in any aqueous or organic solvent. Similarly, high silicon content is needed for etch resistance but gives the material a quartz like property when exposed to typical oxygen plasma, or other oxidative cleaning processes, making removal of this material from a quartz template virtually impossible.[131,132] We have chosen to focus our efforts toward the incorporation of reversible cross-linkers instead. Theory suggests that the highly cross-linked, insoluble resist may become soluble in common organic solvents if the cross-links are broken, resulting in lower molecular weight linear polymer.[133] Cross-linking materials capitalizing on the thermal reversibility of the classic Diels-Alder reaction will be discussed herein.

RESULTS AND DISCUSSION

Cross-linker Design

Since its discovery by Otto Diels and Kurt Alder in 1927,[134] the Diels-Alder reaction has become widely adopted as a useful carbon-carbon bond forming reaction. It has found utility in the synthesis of numerous organic compounds ranging from small molecules to complex natural products. Despite this popularity, it wasn't until the turn of the century that the reversibility of common Diels-Alder products was popularized as a framework for reversible materials.[135,136,137,138,139,140,141] In experiments by Wudl *et al.*, monoliths were formed that could be cracked and healed via the application of heat. They attribute this "remendability" to the cleavage and reformation of the Diels-Alder network upon slow cooling (Figure 4.1).
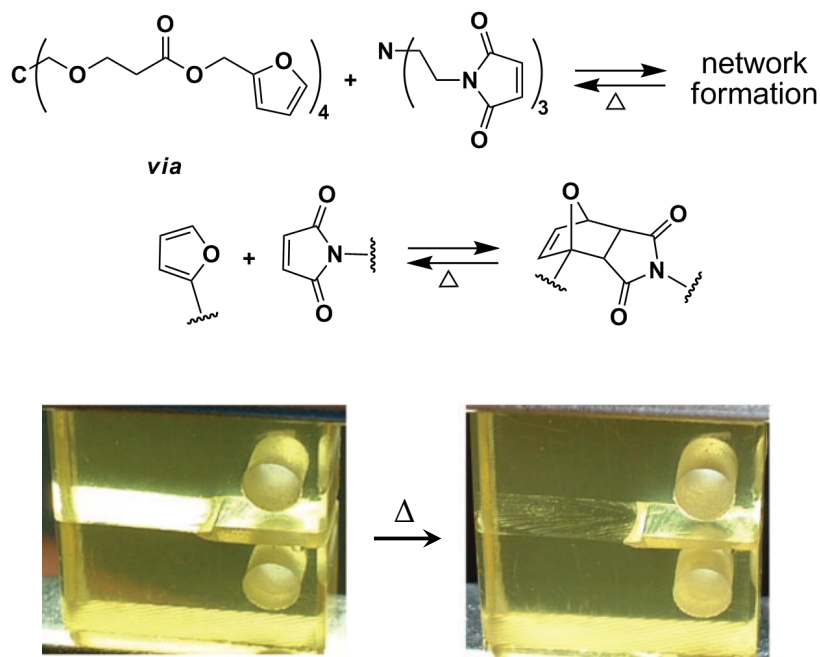
Figure 4.1: Wudl's remendable materials (Monoliths are 14 mm tall). From Chen, X; Dam, M. A.; Ono, K.; Mal, A.; Shen, H.; Nutt, S. R.; Sheran, K.; Wudl, F. *Science* **2002**, *295*, 1698. Reprinted with permission from AAAS.[135]

We envisioned that an S-FIL resist containing Diels-Alder adducts could be decross-linked in a similar manner via a low to moderate temperature thermal process. To provide this thermally reversible cross-link we also chose to utilize classic furan-maleimide Diels-Alder adducts which are known to have low reversal temperatures.[135,136] These adducts should provide sufficient mechanical strength through cross-linking, yet upon introduction of the material into a hot solvent such as DMF, DMSO, or NMP, can be rendered soluble as the Diels-Alder adducts are cycloreversed yielding linear polymeric material (Figure 4.2).
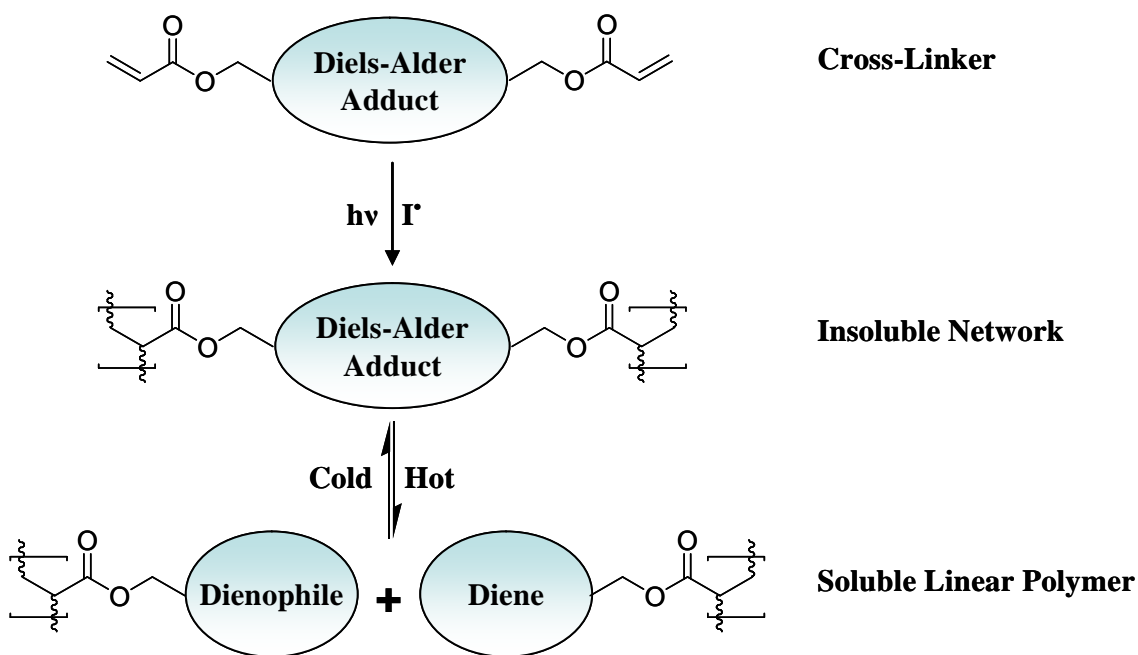
Figure 4.2: Resist Processing.

Our synthetic approach to target compound **4.8a** could arise from three distinct pathways (Figure 4.3). The first of which (route A) would alkylate the substituted furan-maleimide Diels-Alder adduct **4.4a**, the second (route B) would functionalize the maleimide dienophile prior to Diels-Alder adduct formation, and the third (route C)

would utilize amine insertion into compound **4.6** followed by deprotection. All three routes were explored in the laboratory and will be discussed in the following sections.
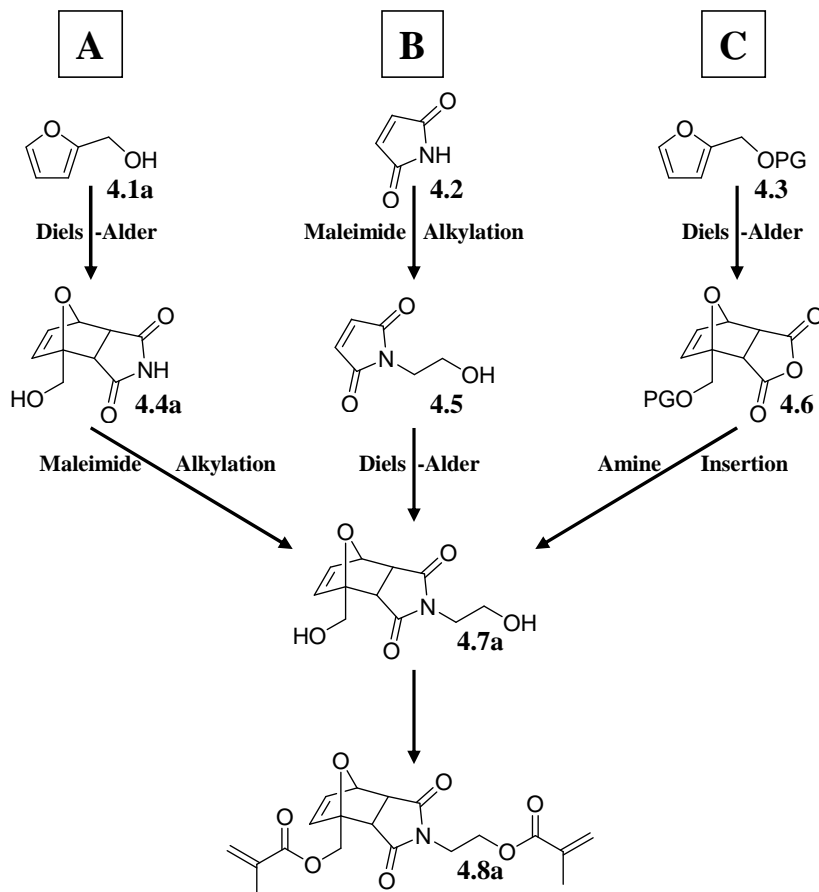
Figure 4.3: Routes to target compound **4.8**.

Synthesis

Route A yielded compounds **4.4a** and **4.4b** in excellent yields via Diels–Alder reaction in an ethyl acetate/ether solvent mixture. This reaction proceeded quickly and was found to yield a mixture of *endo* and *exo* diastereomers. Conversion of the mixture to 100% *exo* (as determined by NMR) stereochemistry was afforded through extended reflux in benzene (Scheme 4.1). Alkylation was found to be somewhat problematic for

compound **4.4b** yielding no product under standard Sn2 conditions. Compound **4.4a** was able to be alkylated in low yields, but the high cost of three substituted furans made this a less attractive approach. Despite this unforeseen obstacle, compounds **4.4a-b** were used as model compounds and valuable information was obtained via variable temperature NMR (VT-NMR) studies. The VT-NMR data showed that simply switching from furan substituted at the three position (**4.1b**) to furan substituted at the two position (**4.1a**) drastically decreased the cycloreversion temperature giving compound **4.4a** approximately 91% dissociated at 110 °C while compound **4.4b** is only 30% dissociated at the same temperature. Conducting the same experiment at 130 °C produced compound **4.4a** approximately 96% dissociated at 130 °C while compound **4.4b** is only 56% dissociated at the same temperature (Figures 4.4 and 4.5). This lower cycloreversion temperature may broaden the window of organic solvents that could be used in subsequent stripping experiments.
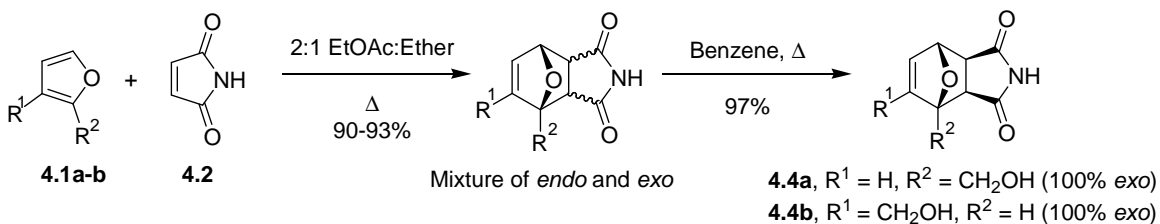
Scheme 4.1: Synthesis of Diels-Alder adducts **4.4a** and **4.4b**.
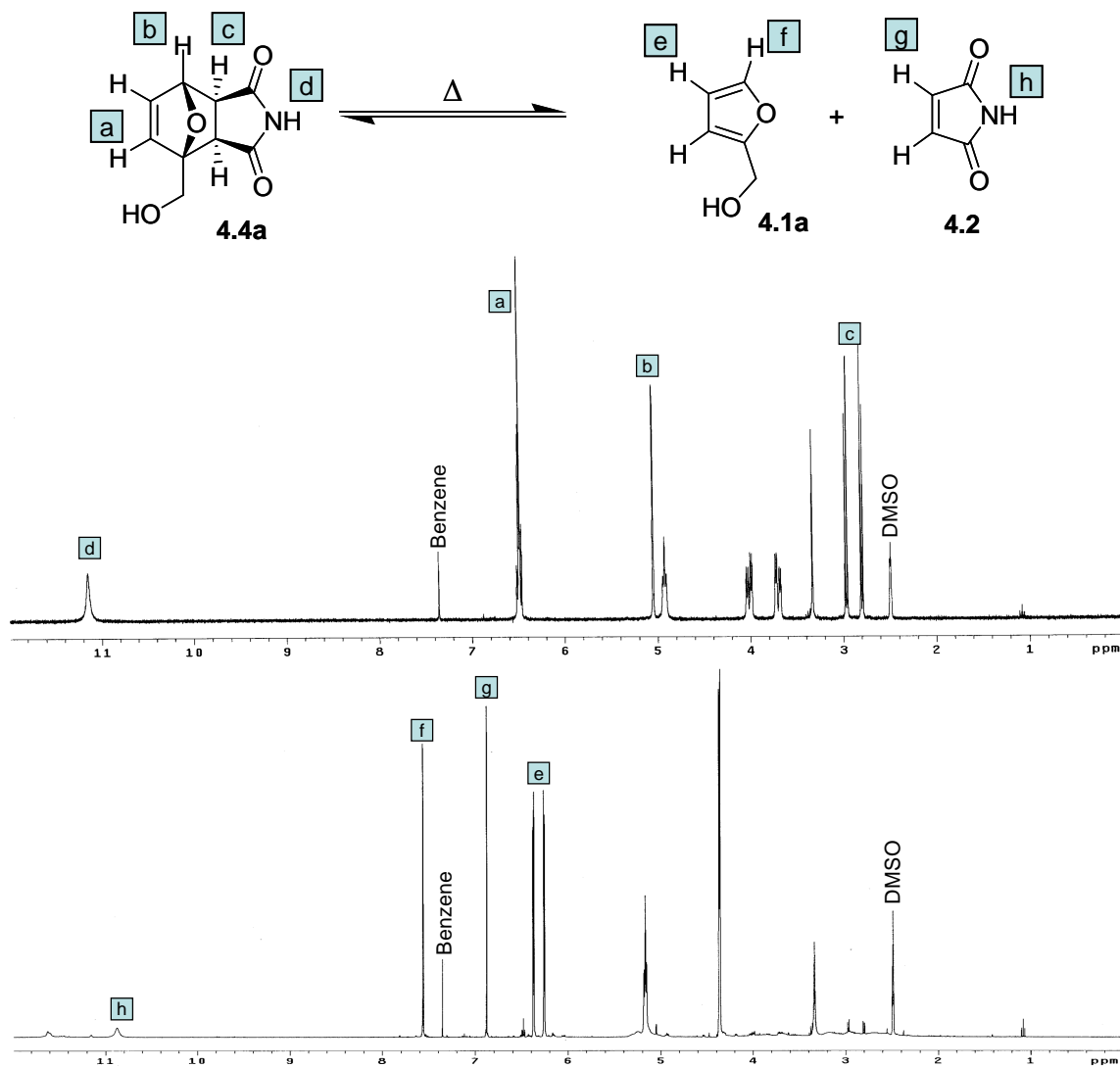
Figure 4.4: Solution state reversibility of model compound **4.4a** before heating (top) and after heating for 2 hours at 130 °C (96% dissociated) (bottom).

61
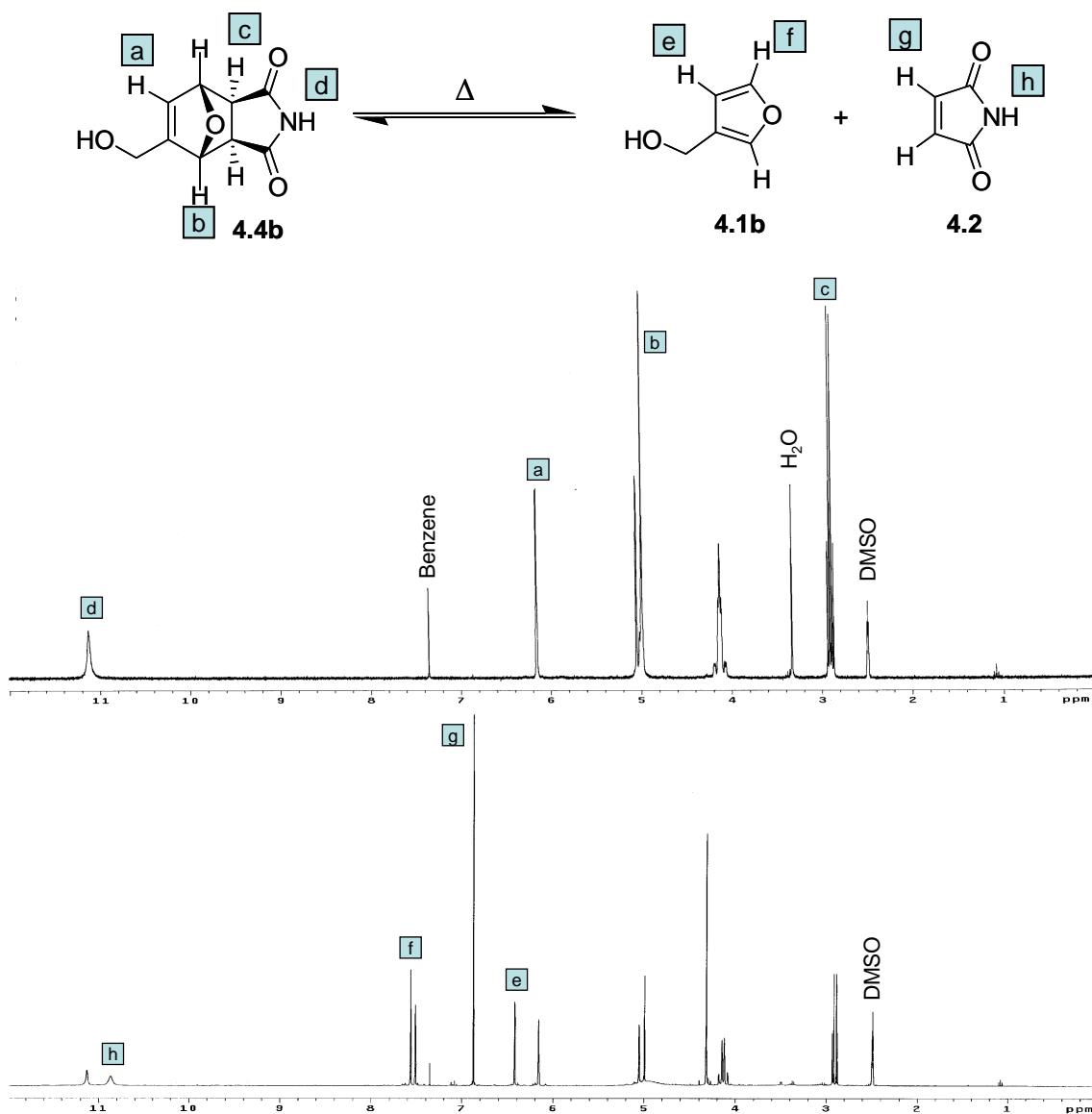
Figure 4.5: Solution state reversibility of model compound **4.4b** before heating (top) and after heating for 72 hours at 130 °C (56% dissociated) (bottom).

Initial studies with route C were promising early on yielding the acetate protected Diels-Alder adduct **4.6** in good yields.[142] Reaction of **4.6** with various amino-alcohols afforded the ring open amide-acid as expected, but the ring closure proved problematic at temperatures low enough to avoid Diels-Alder cycloreversion. This was somewhat

expected as many amide-acid cyclizations proceed only at elevated temperatures and the route was abandoned.[143]

While routes A and C were met with difficulties early on, route B proceeded smoothly and was deemed the appropriate route for the synthesis of our target molecule. Functionalized maleimides were prepared via three distinct routes outlined by SCHEME 4.2 in moderate to good yields. Substituted maleimide **4.9** was synthesized by base catalyzed addition of maleimide to formaldehyde in water yielding the somewhat sensitive hemiaminal.[144] The unstable hemiaminal compound **4.9** decomposed at the temperatures required for Diels-Alder reactions and further attempts were abandoned. Compound **4.12** was synthesized via the activation of maleimide through reaction with methylchloroformate to produce compound **4.11**. Amine insertion in water using K_2CO_3 as a base ultimately yielded hydroxypentyl maleimide **4.12**.[145,146] Compound **4.5** was synthesized by first reacting furan with maleic anhydride to produce adduct **4.15**. Amine insertion followed by deprotection in refluxing toluene afforded crystalline compound **4.5** in good overall yield.[147,148]
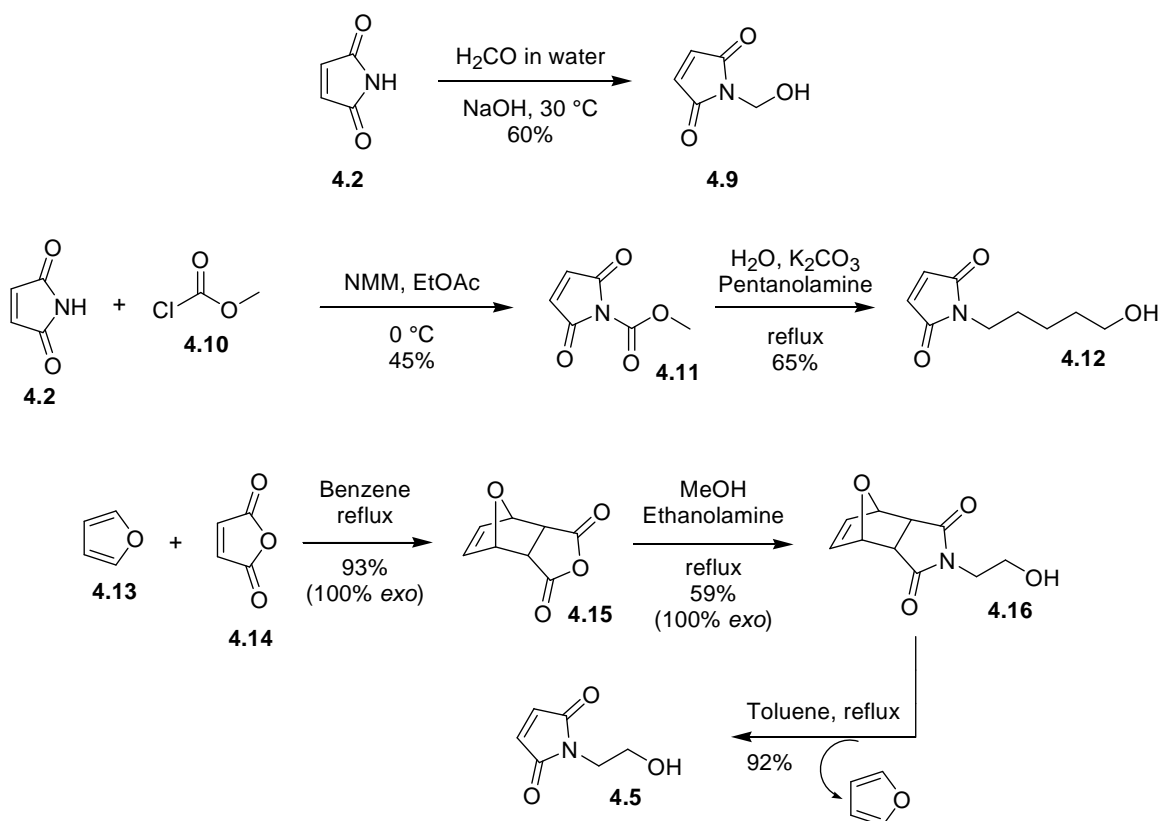
Scheme 4.2: Synthesis of substituted maleimides **4.9**, **4.12**, and **4.5**.

A second set of maleimides was synthesized which facilitate the formation of cross-linkers containing two Diels-Alder linkages. Bismaleimides **4.17a-c** were synthesized by a modified literature procedure in which an α,ω-diamine was reacted with two equivalents of maleic anhydride in DMF. This produced the ring opened amide-acid which was then ring closed via the addition of Ni(OAc)$_2$, triethylamine, and acetic anhydride to afford the bismaleimides **4.17a-c** in overall good yields (Scheme 4.3).[136] Bisfuran **4.18** was synthesized by reacting furfuryl alcohol with diisocyanatohexane in refluxing THF (Scheme 4.4). It was believed the incorporation of more than one Diels-

Alder moiety could in theory have an advantage over single Diels-Alder compounds in that they are statistically twice as likely to undergo cycloreversion and hence decross-link. This could also be advantageous in that if both Diels-Alder adducts are reversed then the bismaleimide or bisfuran may be dissolved away yielding an "irreversible" reaction.
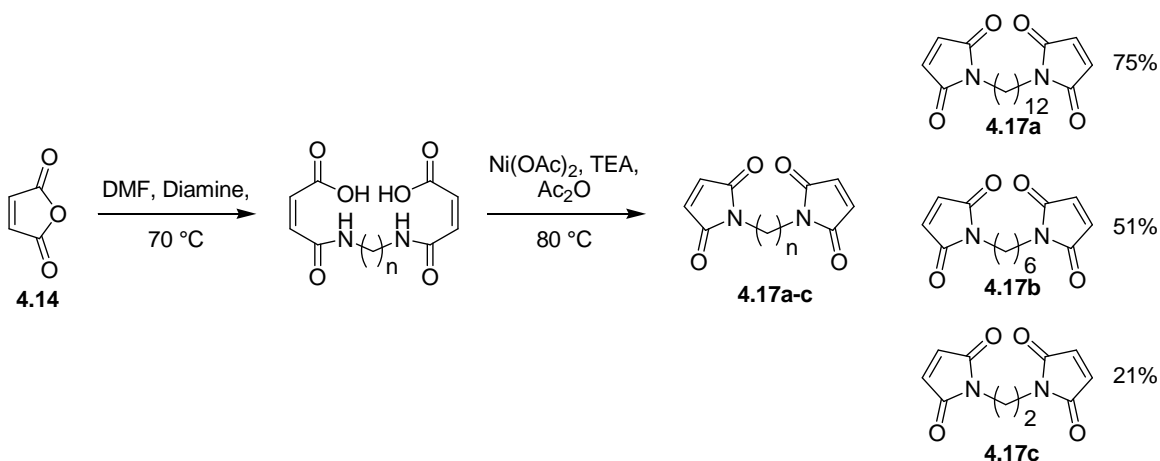
Scheme 4.3: Synthesis of bimaleimides **4.17a-c**.
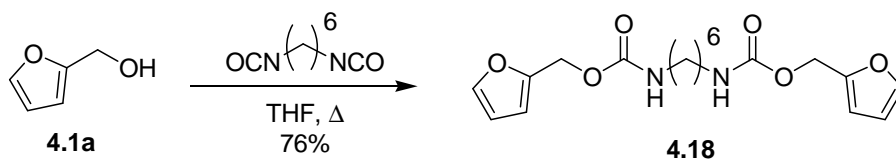
Scheme 4.4: Synthesis of bisfuran compound **4.18**.

Efforts then turned toward the synthesis of the corresponding Diels-Alder adducts of the above compounds. All compounds in Scheme 4.5 were synthesized in good yield by refluxing in benzene with the appropriately substituted furan. Scale up often proved difficult producing an inseparable mixture of *endo* and *exo* isomers. This product mixture could be avoided by utilizing extended reaction times. It is important to point out that for

the end application stereospecificity is not required but makes the characterization of these and other Diels-Alder adducts more facile. Compounds **4.7a-b** and **4.20b** precipitated out of solution upon cooling and were collected via vacuum filtration as pure white solids. Compounds **4.19** and **4.20a** were purified via column chromatography also yielding white solids.
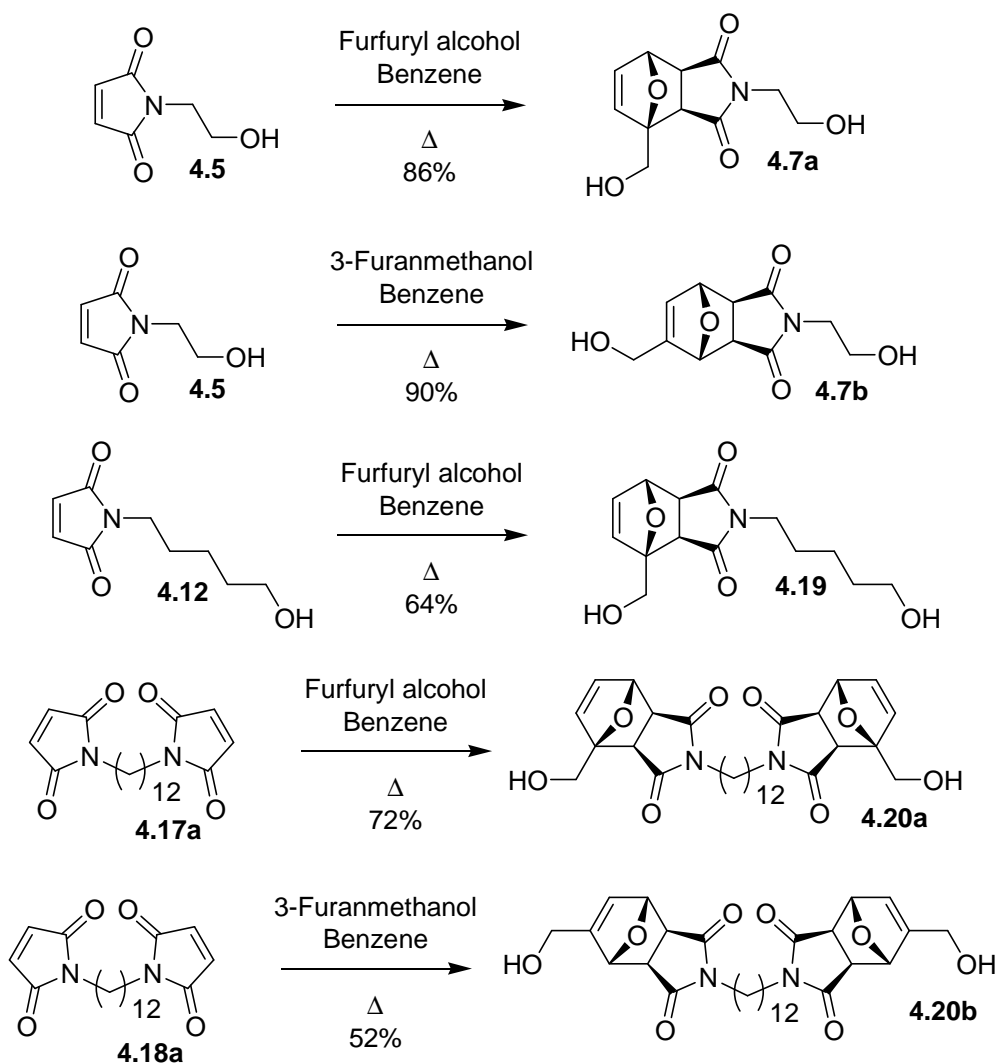
Scheme 4.5: Synthesis of Diels-Alder compounds **4.7a-b**, **4.19**, and **4.20a-b**.

As expected from study of model compounds **4.4a-b**, the Diels-Alder adducts constructed using furans substituted at the two position cycloreversed at milder temperatures and to a much greater extent than their analogues substituted in the three position. For the resist to dissolve into solution, the number of cross-links remaining must be extremely small. Hence, only compounds **4.7a** and **4.20a** were carried to the next reaction and studied in stripping experiments. Single Diels-Alder adduct compound **4.7a** was acrylated under classical conditions using methacryloyl chloride and pyridine to yield cross-linker **4.21a** in 80% yield. Likewise, cross-linker **4.22a** was synthesized in 60% yield from diol **4.20a** (Scheme 4.6). Both cross-linkers were incorporated into S-FIL resist formulations and the results are presented below.
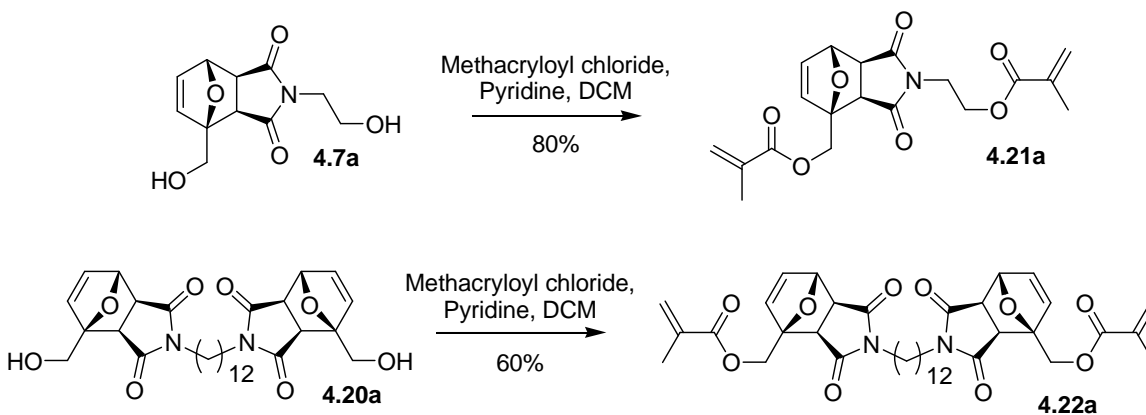
Scheme 4.6: Synthesis of bismethacrylates **4.21a** and **4.22a**.

Resist Formulations

The resist formulations consisted of a combination of either cross-linker **4.20a** or **4.22a**, methyl acrylate, and 5 wt% photoinitiator (Daracure 1173). The silicon containing monomers, which typically provide etch resistance, were omitted for simplicity. The resist formulations were imprinted by hand using an FSAM pretreated imprint template, and images of two such imprint attempts can be seen in Figure 4.1. From these

experiments, it was established that a minimum of 20 mol% cross-linker was needed to maintain acceptable mechanical stability and this formulation was used for all further experiments.
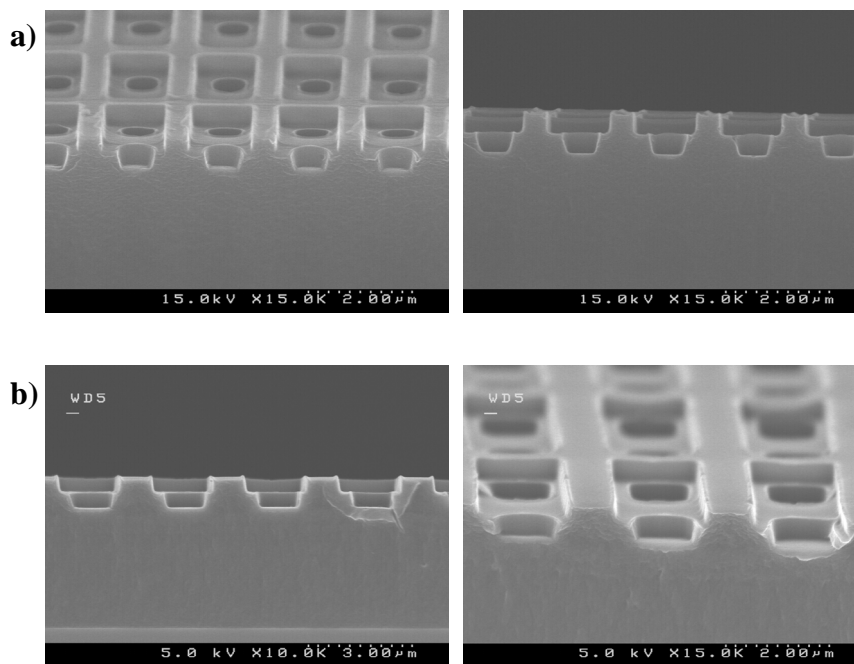
Figure 4.6: Scanning electron micrographs of resist images created using a) 20 wt% and b) 10 wt% cross-linker concentrations.

Stripping Experiments

Stripping experiments were carried out by submerging wafers with imprinted images into heated solvents at various temperatures. Dimethyl sulfoxide (DMSO), N-methyl pyrrolidone (NMP), and dimethylformamide (DMF) were chosen as they are good solvents for most acrylate polymers and boil at temperatures greater than 100 °C. As can be seen in Table 4.1, no conditions attempted were found to either strip or swell the resist layer.[149]

Solvent	Temp (°C)	Swell?	Strip?
DMSO	120	No	No
NMP	120	No	No
DMF	120	No	No
DMSO	150	No	No
NMP	150	No	No
DMF	150	No	No
DMSO	180	No	No
NMP	180	No	No
DMF	180	No	No

Table 4.1: Stripping experiments.

This observation led us to the literature in which several examples were discovered where retro-Diels-Alder reactions were driven by the addition of a competitive diene or dienophile.[150] Cyclopentadiene was chosen as a competitive diene, and diethyl acetylenedicarboxylate as a competitive dienophile (Scheme 4.7). Here, as the original Diels-Alder cross-linking adducts are broken they can react with the added diene or dienophile competitor forming new adducts that are known to be irreversible at the same temperatures. This approach should in theory utilize LeChatlier's principle to drive the decross-linking reaction forward rendering our polymeric material soluble. Despite numerous attempts, this approach failed as no conditions were found that could swell or strip the resist material (Table 4.2).
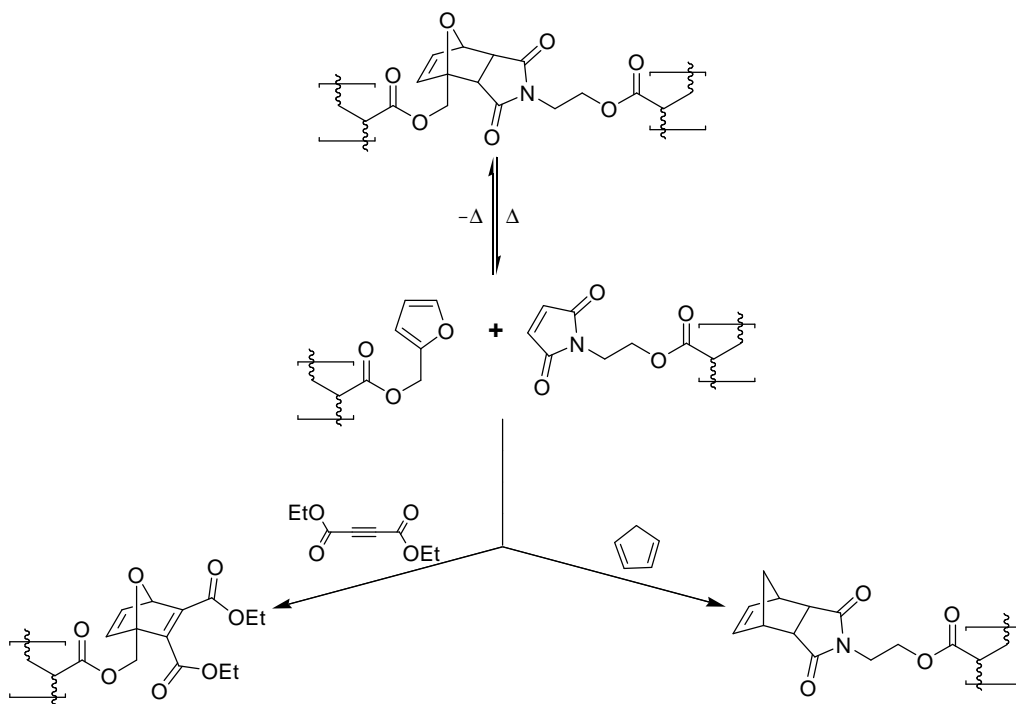
Scheme 4.7: Proposed function of added competitive diene or dienophile.

Solvent	Temp. (°C)	Additive	Swell?	Strip?
DMSO	130	Dienophile	No	No
NMP	130	Dienophile	No	No
DMSO/NMP	130	Dienophile	No	No
Toluene	110	Dienophile	No	No
DMSO	170	Diene	No	No
DMSO	200	Diene	No	No
NMP	170	Diene	No	No
DMF	150	Diene	No	No

Table 4.2: Stripping experiments with a competitive diene or dienophile. Experiments using cyclopentadiene were run in a Parr pressure reactor.

In an attempt to better understand these results, gel-point calculations were performed by Frank Palmieri (Willson Group member).[151] He discovered that the inability to strip Diels-Alder containing resists may lie in the analysis of the calculations which are plotted in Figure 4.7. His calculations suggested that a resist polymerized to 85% conversion consisting of 20 mol% cross-linker would be above its gel-point if greater than 0.02% of its cross-linkers remain intact. This in turn means that $\geq$ 99.98% of all Diels-Alder linkages must be reversed to fall below its gel-point and become soluble (Figure 4.7).
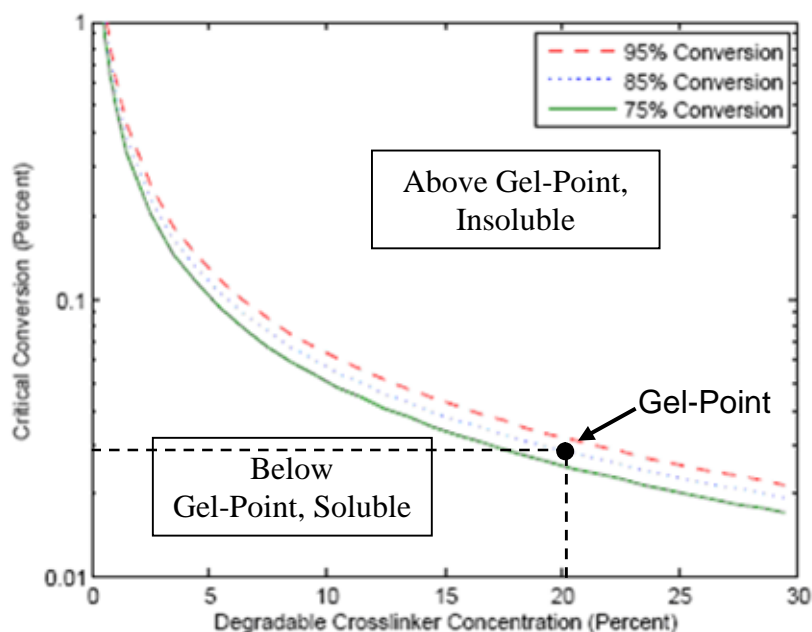
Figure 4.7: Critical conversion at the gel-point versus cross-linker concentration.

Given the extremely high cycloreversion requirements predicted from gel-point calculations, the reversibility of these Diels-Alder compounds in the solid state was investigated. It was known from model studies of compound **4.4a** that cycloreversion

occurred to a large extent in solution, but its conversion in the solid state had not been studied. Compound **4.8a** was chosen to study solution state versus solid state cycloreversion extent as it was most similar to cross-linker **4.22a**. Solution state VT-NMR data showed the excellent reversibility of Diels-Alder adduct **4.8a** as it was heated form 25 °C to 140 °C and then cooled to 25 °C. It can be seen that although the cycloreversion occurs quickly, the recombination to form compound **4.8a** occurs more slowly (Figure 4.8). Figure 4.9 shows that compound **4.8a** reached an equilibrium concentration of 80% cycloreversed product at 120 °C in solution, while heating the same compound in the solid state, followed by quenching in liquid nitrogen, showed an equilibrium concentration of only 28% cycloreversed product present at the same temperature (Figure 4.10).
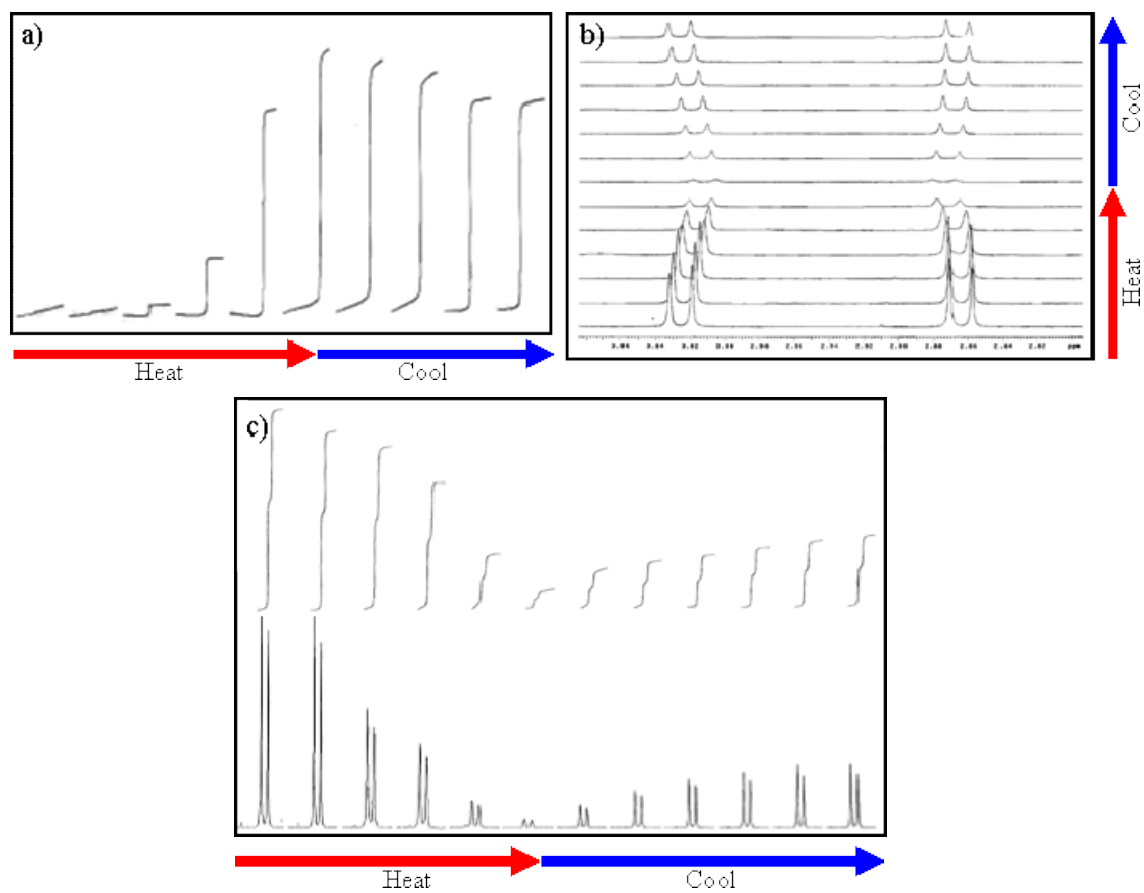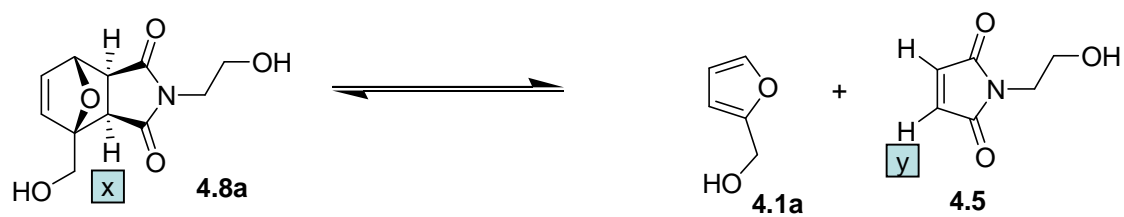
Figure 4.8: Solution state VT-NMR of compound **4.8a**. a) Integral of proton y, b)^{1}H-NMR signal of proton x, and c) signal and integral of proton x.
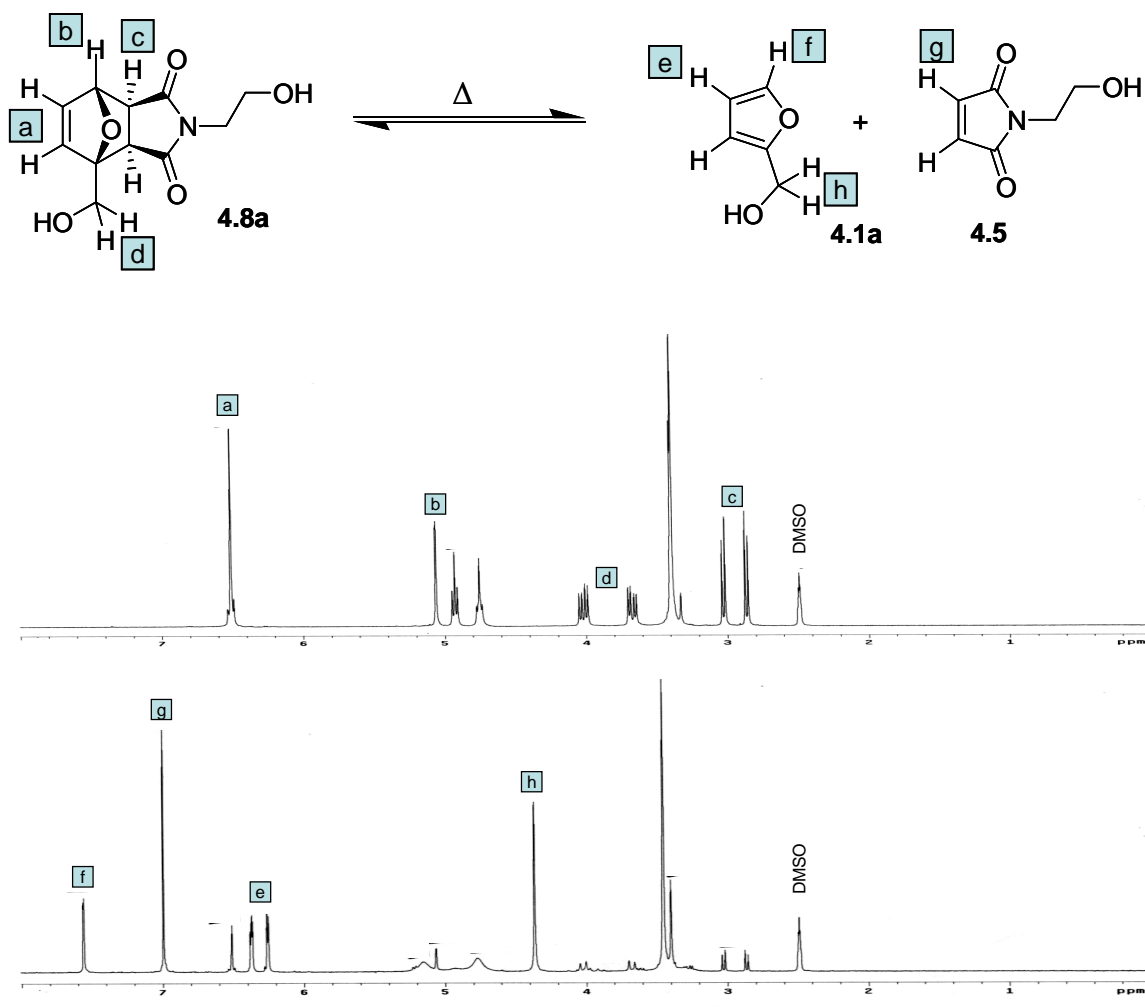
Figure 4.9: Solution state NMR of compound **4.8a** before (top) and after heating to 120 °C (80% dissociated) (bottom).
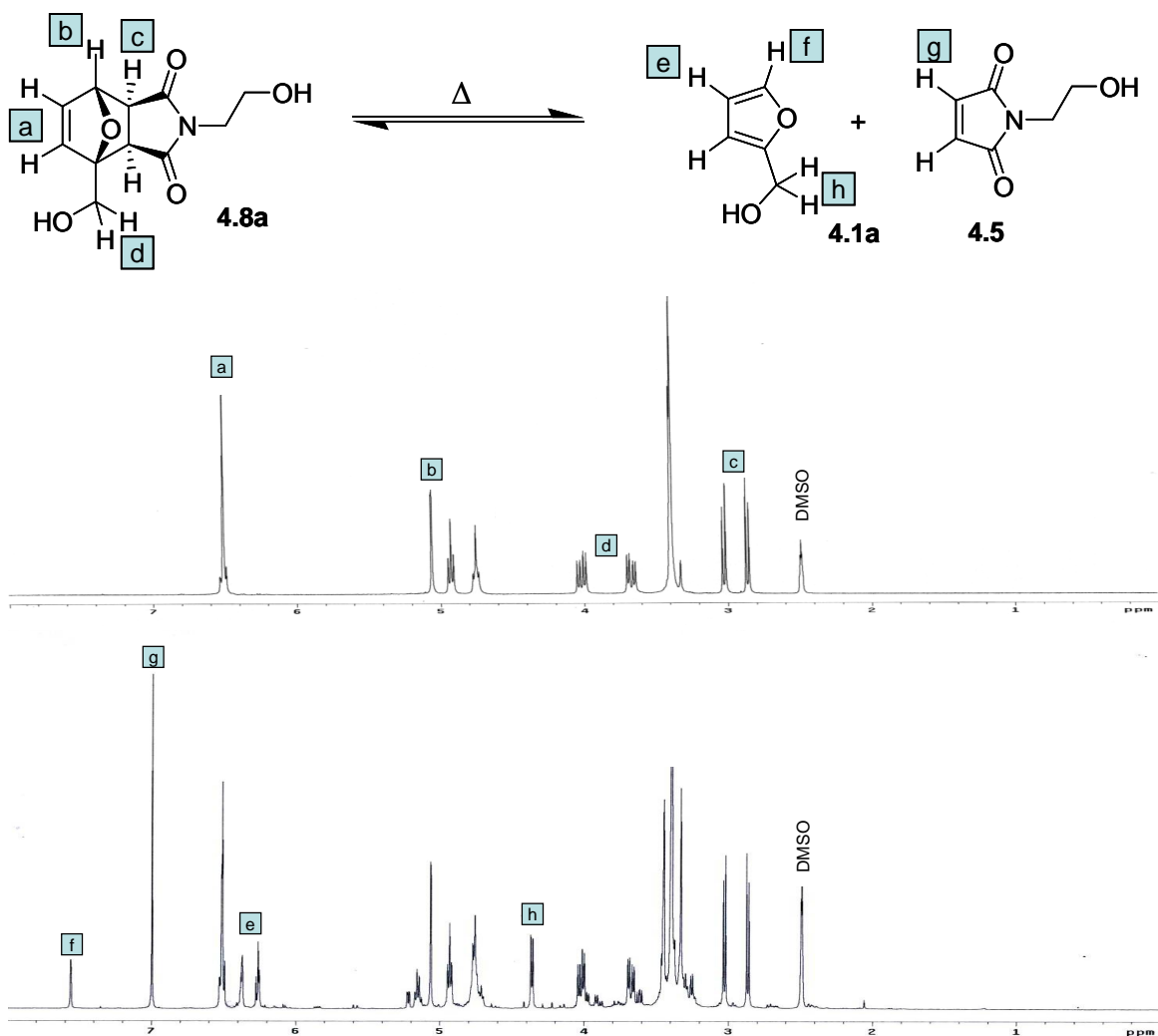
Figure 4.10: NMR of compound **4.8a** before (top) and after heating to 120 °C (bottom) in the solid state (28% dissociated).

To conclude the NMR studies, the reversibility of cross-linker **4.21a** in a polymer matrix was examined via solid-state NMR. Cross-linked polymer samples were formed via radical copolymerization of methyl methacrylate and compound **4.21a**. The resultant insoluble polymeric material was analyzed using both $^{1}H \rightarrow {}^{13}C$ cross-polarization/magic-angle spinning and quantitative ^{13}C Bloch decay/magic-angle spinning NMR spectroscopies (experiments performed at Oklahoma State University

with the help of Professor Jeffrey White and Matthew Truitt) . In both cases a spectrum was recorded prior to and after heating at 130 °C.[148] As can be seen in Figure 4.11, the retro-Diels-Alder reaction does occur, but a significant amount of cross-linker remains intact in the polymeric system. Key peaks in the Bloch decay spectra, which are indicative of the reverse Diels-Alder chemistry, are labeled with arrows that point up (171.3, 150, 144.3, and 111.5 ppm) or down (177.3, 138, 90, and 82 ppm) if the thermal treatment increases or decreases their signal intensities, respectively.[148] This data agrees well with the solid-state spectral data obtained by Wudl.[135,136] It was hypothesized that although cycloreversion of the Diels-Alder adduct was being realized in the solid state, the incomplete conversion was due to the increased rate of Diels-Alder adduct formation in its condensed state. This lead us to believe that in the stripping experiments the thermodynamically favored Diels-Alder adduct reformed faster than solvation, preventing material removal.
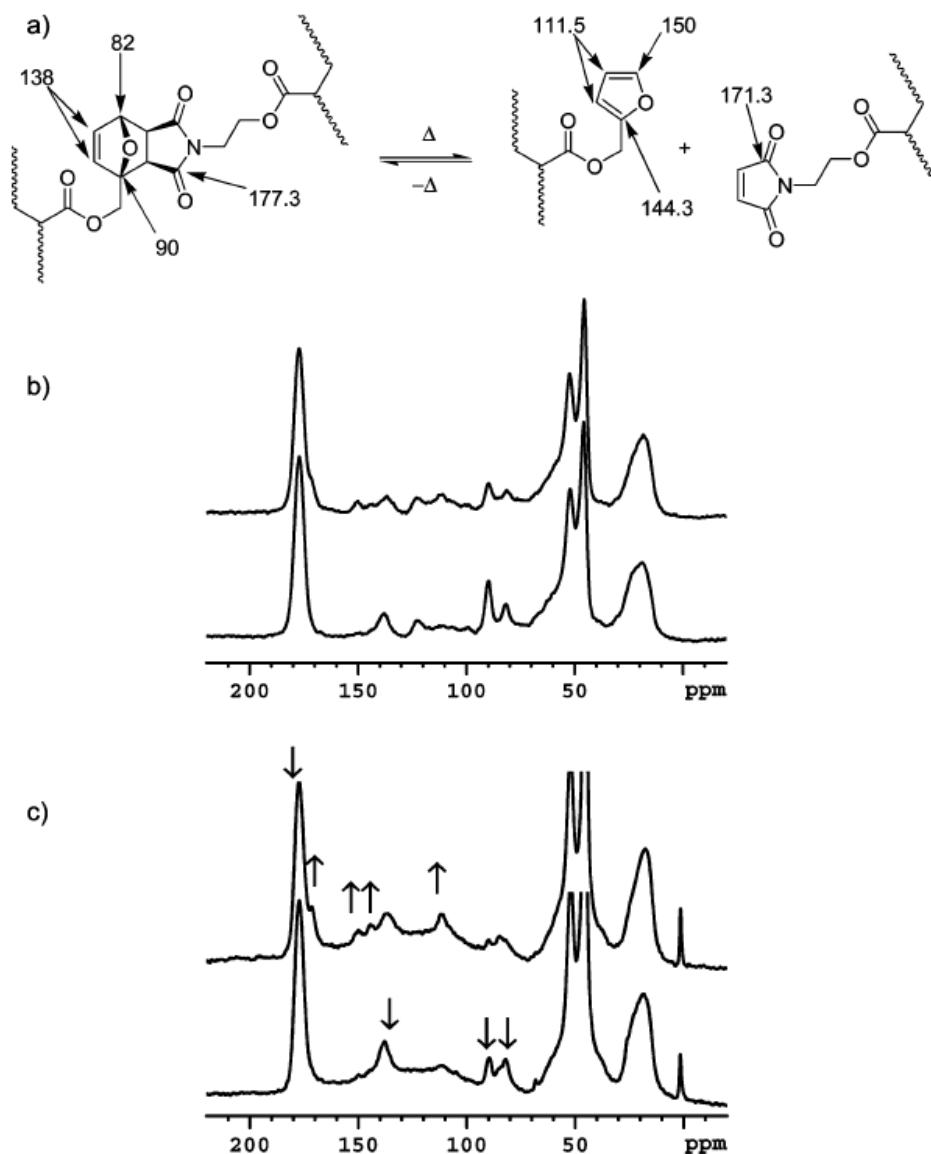
Figure 4.11: Solid-state NMR of the cross-linked polymeric system. a) Forward and reverse Diels-Alder reactions with ^{13}C NMR signal assignments in ppm. b) [1]H → [13]C cross-polarization/magic-angle spinning spectra, with sideband suppression via TOSS, for species 4.21a before (bottom trace) and after (top trace) heating at 130 °C. c) Quantitative [13]C Bloch decay/magic-angle spinning spectra for species 4.21a before (bottom trace) and after (top trace) heating at 130 °C. Key peaks in the Bloch decay spectra, which are indicative of the reverse Diels-Alder chemistry, are labeled with arrows that point up (171.3, 150, 144.3, and 111.5 ppm) or down (177.3, 138, 90, and 82 ppm) if the thermal treatment increases or decreases their signal intensities, respectively.148

77

CONCLUSIONS

Efficient routes to various Diels-Alder containing, thermally reversible, cross-linkable monomers have been developed. The material was patterned via S-FIL and shown to have mechanical properties meeting those required by the S-FIL process. To date, all attempts to strip the imprinted material from its substrate have failed, and hence, the cycloreversion of these compounds was extensively investigated via solution and solid state VT-NMR. VT-NMR results suggest the reversion behavior of Diels-Alder compounds greatly differ depending upon their concentration. Gel-point calculations suggest that conversions as high as 99.98% may need to be reached before polymer dissolution is realized. To date, conversions this high have not been observed in our studies. Attempts to trap the reactive diene and dienophile of the reversed cross-linkers using a competitive Diels-Alder partner have failed and remain a mystery.

Chapter 5: Introduction to Organic Second-Order Nonlinear Optical Polymers

INTRODUCTION

The field of nonlinear optics has flourished since the invention of the laser by Theodore Maiman in 1960.[152] High intensity laser light made it possible to detect many nonlinear optical phenomena which were theorized but previously unobservable. In 1961, Franken and coworkers were the first to demonstrate second–harmonic generation (SHG) (also known as frequency doubling) using a quartz sample and ruby laser (694 nm) (Figure 5.1).[153] After passing through the quartz substrate, the light was sent through a spectrometer and recorded on photographic paper. Historic lore tells us the copy-editor for *Physical Review Letters* mistook the faint spot at 347 nm as a speck of dirt and initially removed it prior to publication. Obviously if true, the errant editing was corrected and this single event marked what many regard as the first milestone in the area of nonlinear optics research. SHG was first observed in organic crystals in 1965, and then in organic polymeric materials in 1982.[152,154,155] Since then, the area of organic second-order nonlinear optical polymers has exploded giving promise as future candidates for electro-optic (EO) switches, frequency doublers, optical storage devices, and EO modulators, many of which have been developed in the past ten years (Figure 5.2).[156,157,158,159,160,161]

Ruby Laser = 694 nm ω · NLO Material · **Output = 347 nm** 2ω
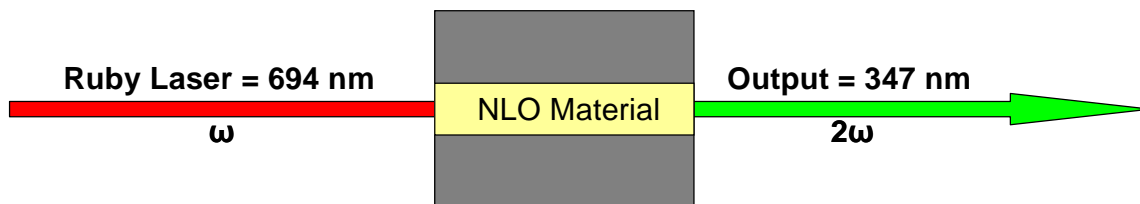
Figure 5.1: Second harmonic generation (SHG) (frequency doubling).
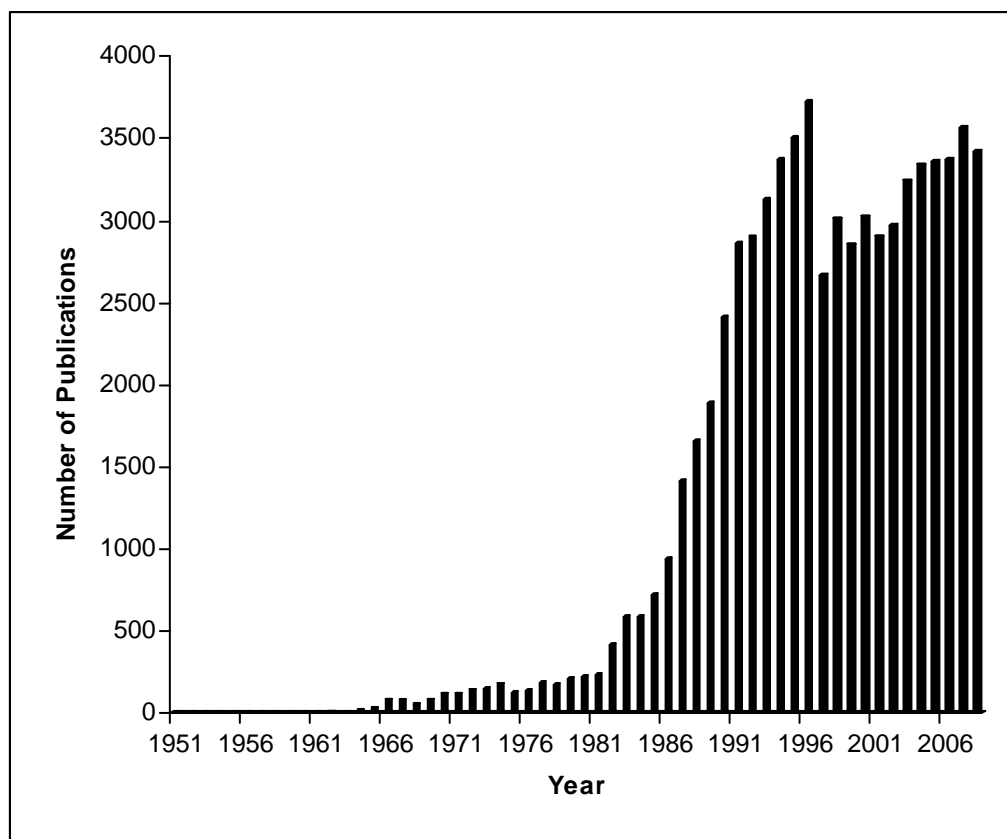
Figure 5.2: Publications by year containing the topic of nonlinear optics (data obtained from Scifinder®).

ORIGINS OF SECOND-ORDER NONLINEARITY

Microscopic versus Macroscopic Nonlinearity

Nonlinear optical (NLO) phenomena arise due to the interaction of light with dielectric media producing electromagnetic fields altered in amplitude, frequency, and phase.[152] The origins of these phenomena are complex but can be directly linked to the optical nonlinearity of the materials constituent molecules. Production of second-order NLO effects, such as SHG or the EO effect, require that the molecules possess noncentrosymmetric molecular symmetry, meaning they have a net dipole moment (this

80

will be discussed in greater detail in the following sections). As light passes through the dielectric medium, an oscillating displacement of charge density occurs in the molecules which is proportional to the amplitude of the incident electric field. Under small intensities of incident light, this molecular polarization is linear and can be described as follows:

$$p = p_0 + \alpha_{ij} E_j \tag{5.1}$$

Here p is the microscopic polarization response, p_0 is the molecular dipole moment, α_{ij} is the microscopic linear susceptibility, and E_j is the applied electric field vector.[152] This may be expanded to describe the bulk material as follows:

$$P = P_0 + \chi_{ij}^{(1)} E_j \tag{5.2}$$

where $\chi_{ij}^{(1)}$ is the macroscopic linear susceptibility.[152] When strong intensities of incident irradiation are used, specifically lasers, this relationship must be modified to include nonlinear terms to describe the induced polarization. The new microscopic nonlinear expression is as follows:

$$p = p_i^0 + \alpha_{ij} E_j + \beta_{ijk} E_j E_k + \gamma_{ijkl} E_j E_k E_l + \cdots \tag{5.3}$$

where $i,j,k,$ and l refer to the molecular coordinate system and E_j, E_k, and E_l refer to the vector components of the applied electric field. p_i^0 is the molecular dipole moment and α_{ij}, β_{ijk}, and γ_{ijkl} refer to the linear polarizability, first hyperpolarizability, and second hyperpolarizability respectfully.[152] Second-order NLO properties are described by the

81

second term of this power series expansion (β_{ijk}) and in the bulk can be described similarly as follows:

$$P = P_0 + \chi_{IJ}^{(1)}E_J + \chi_{IJK}^{(2)}E_J E_K + \chi_{IJKL}^{(3)}E_J E_K E_L + \cdots \qquad (5.4)$$

P_0 is the bulk dipole moment and $\chi^{(n)}$ are susceptibility components.[152] Due to spatial-symmetry restrictions, the second-order term (Eq. 5.4) has a requirement that noncentrosymmetry is present in both the microscopic and macroscopic regimes for second-order, and all other even-order susceptibilities to be nonzero.

Material Properties

The need for noncentrosymmetry is best illustrated in Figure 5.3. As an oscillating electric field passes through a symmetric molecule such as benzene, one observes a linear polarization response (solid line), but if that same field is passed through an asymmetric molecule such as 4-nitroaniline, the presence of the electron rich donor and the electron deficient acceptor group causes a nonlinear polarization response (dashed line). Fourier analysis of this nonlinear response predicts multiple modulations of phase and frequency with second-order processes such as SHG, or frequency doubling, and the related EO effect being most important to this discussion. SHG can be defined as the use of monochromatic coherent optical waves at frequency ω to induce a new emission at frequency 2ω in a second-order active medium (Figure 5.1).[162] SHG is directly proportional to the EO effect, which is described as control of the refractive index of a material via application of a DC or AC voltage. As electric potential is varied across a NLO medium, further changes in charge distribution arise producing variation in

refractive index proportional to the applied voltage, and hence the speed at which light propagates through that material.[152]
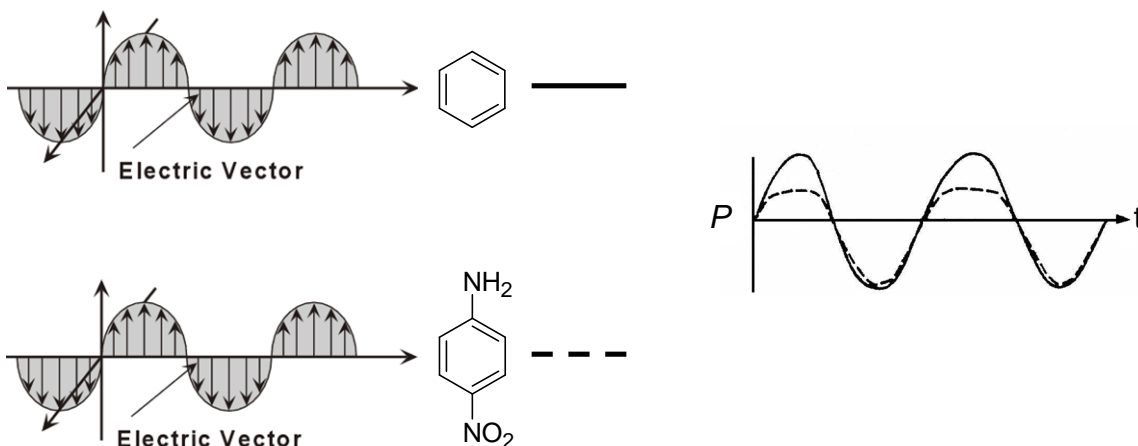
Figure 5.3: Linear polarization response (*P*) of benzene (solid line) and the nonlinear response of 4-nitroaniline (dashed line) as a function of time (t).

Molecules possessing the molecular ground state charge distribution (noncentrosymmetry) required to produce SHG and EO effects are easily designed through the incorporation of various electron donating groups, π-conjugated bridges, and electron accepting groups. Conversion of these microscopic dipolar molecules into bulk materials exhibiting macroscopic dipolar ordering is much more challenging and will be discussed in the following section. The degree of dipolar ordering and its stability, known as temporal stability, on the macroscopic level is one of the attributes that dictates a materials usefulness as a second-order NLO device.

Poling

While macroscopic dipolar order can be achieved through the utilization of liquid crystalline materials,[156] Langmuir-Blodgett-film formation,[163] and self-assembly,[156] the most common and successful technique is that of electric field poling.[164] Electric field

poling is generally performed using one of two different techniques: electrode contact poling or corona poling.[165] Both techniques require the polymer films to be heated close to their glass transition temperature (T_g) where segmental chain motions begin to occur and the NLO chromophores can efficiently reorient themselves according to the direction of the applied electric field. It is important to note that the T_g observed by differential scanning calorimetry (DSC) is not always exactly the same as the transition temperature in the thin film.[166] After poling, the films are cooled and the electric field removed assuming that below the T_g the chromophores are locked in their dipolar aligned state.[167]

The experimental setup for electrode contact poling can be seen in Figure 5.4 where an indium-tin oxide (ITO) coated glass slide is used as a bottom electrode upon which a NLO film is spin-coated. A top electrode (typically gold) is deposited, wires are attached using silver paste, and the material is poled via the application of a potential between the conductive ITO and the upper electrode. The entire device is usually contained within a nitrogen or argon purged environment that is capable of heating to the temperatures required for poling.[164] However convenient, electrode poling requires that high quality defect free films be fabricated to prevent dielectric breakdown across the film.[152]
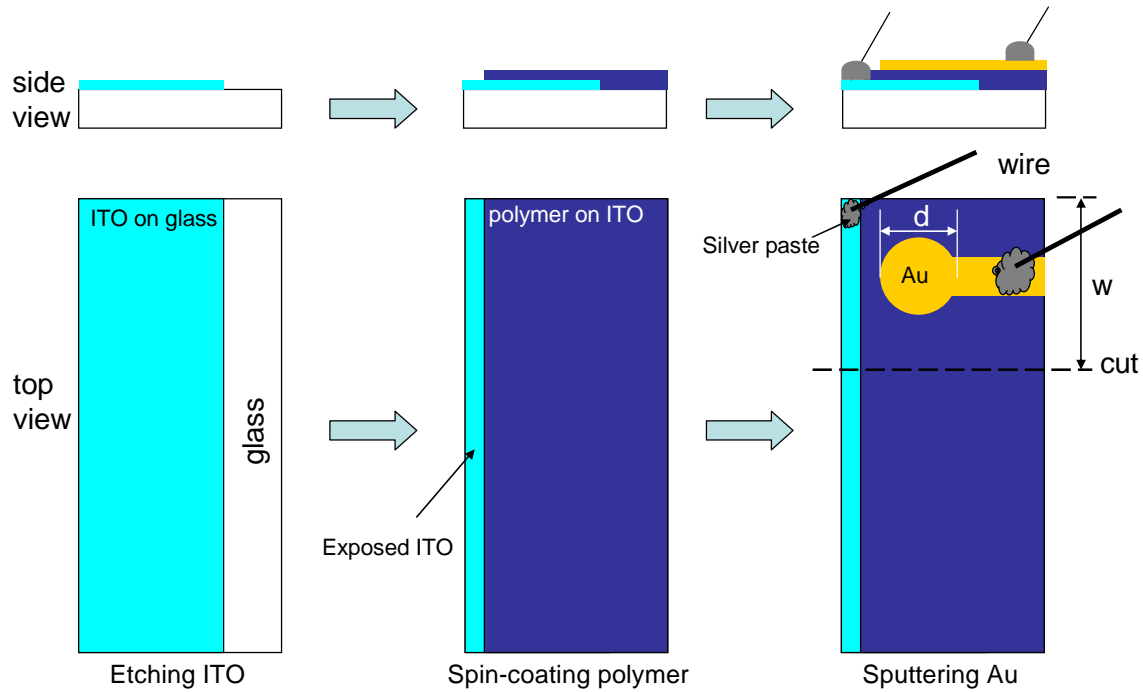
Figure 5.4: Experimental setup for electrode poling.

Corona poling is the second type of electrode poling commonly used. It is performed by coating a NLO material on a bottom electrode, then applying a large potential between the bottom electrode and a suspended wire referred to as a "corona-needle" (Figure 5.5).[165] As with electrode poling, corona poling is often performed in an inert atmosphere, and as the increasing electric potential reaches the dielectric breakdown point of the surrounding atmosphere, charged particles are formed and evenly disperse atop the insulating polymer film.[164] Corona poling is advantageous in that lower quality films may be used as well as very large corona fields, but is disadvantageous in that the magnitude of the corona field is difficult to control and to measure.[152]
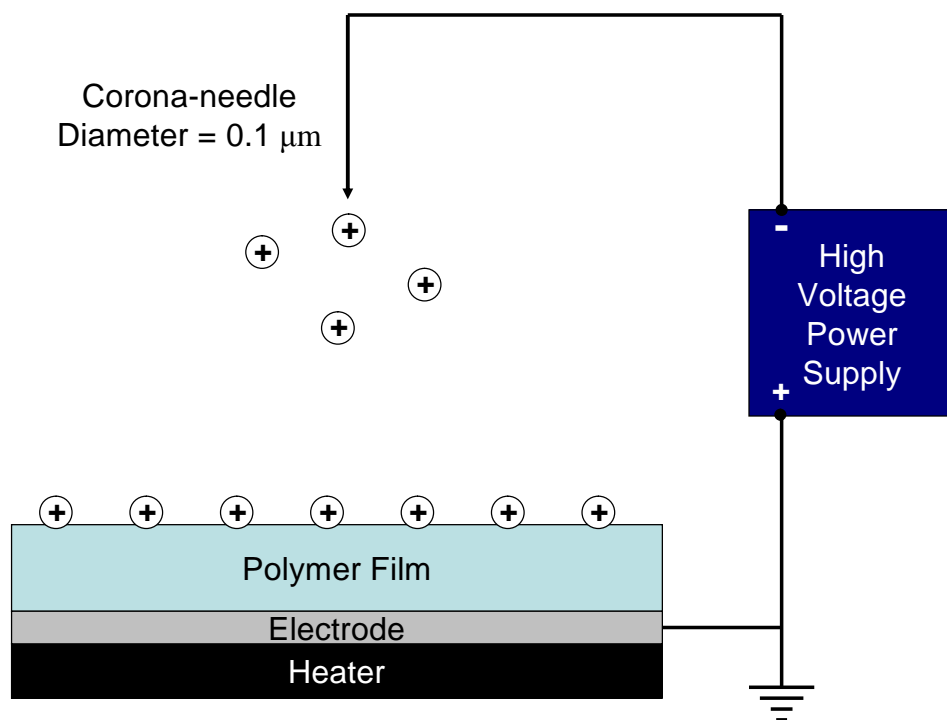
Figure 5.5: Corona poling experimental setup.

Characterization

Organic NLO materials are characterized by typical characterization techniques such as NMR, IR, UV-Vis, and mass spectrometry, but are also studied by several methods designed to extract their NLO properties and coefficients. On the microscopic level, the chromophore dipole moment (μ) and first hyperpolarizability (β) are often the values of most interest. Dipole moments (μ) are typically calculated using modeling software while β is experimentally measured by one of three different techniques, hyper-Rayleigh scattering (HRS), electric field induced second-harmonic generation (EFISH), and solvatochromism. Only the first two techniques will be discussed as solvatochromism is a crude method that only gives approximate β values while HRS measures β directly and EFISH measures the product of μ and β at a particular fundamental wavelength.[168]

HRS does not require field induced dipolar order but generates second-harmonic signal from variations in chromophore orientation in solution.[169,170] Since no alignment is required, the signal observed is typically weak and often impeded by processes such as multi-photon-induced fluorescence.[171,172] This problem has been circumvented through the development of time-resolved HRS.[173] Conversely, EFISH uses an electric field applied across a sample cell to stimulate dipolar order of chromophores in solution. This temporary alignment gives rise to strong SHG, which is easily distinguishable from other processes that hinder HRS. A chromophore's $\mu\beta$ product is referred to as its "molecular figure of merit" for poled polymer films and care should be taken when comparing those values as first hyperpolarizability (β) values are wavelength dependent.[174,175,176,177]

Macroscopic second-order NLO effects can be measured in a variety of ways such as Maker-fringe for SHG[178] and attenuated total reflection (ATR),[179,180,181] Teng-Mann (ellipsometry),[182,183,184,185] and two-slit interference modulation[186,187] to measure EO coefficients. Maker-fringe is performed by passing polarized laser light through a thin film sample of poled NLO material. The p-polarized second-harmonic light emanating from the film is measured as a function of angle as the sample is rotated relative to the incident beam. The recorded data is compared to that of quartz and its pattern analyzed to determine second-order susceptibility.[178] The methods of measuring EO coefficients are often much more complicated and will be omitted here for brevity, but if further information is required, please see the above references. Below is a comparison of typical values encountered for second-order NLO polymers relative to their major inorganic competitors, gallium arsenide and lithium niobate (Table 5.1).

Property	Gallium Arsenide	Lithium Niobate	EO Polymers
EO Coefficient (pm/v at 1.3 μm)	1.5	31	>70
Dielectric Const. (ε)	10-12	28	2.5-4
Refractive Index (n)	3.5	2.2	1.6-1.7
Bandwidth-Length Product (GHz/cm)	>100	10	>100
Voltage-Length Product (V/cm)	1-5	5	1-2
Figure of Merit ($\mu\beta$)	6	10	100
Optical Loss (dB/cm at 1.3 μm)	2	0.2	0.2-1.1

Table 5.1: Comparison of organic polymeric materials to gallium arsenide and lithium niobate.[217]

CHROMOPHORE DESIGN

NLO chromophores all contain a design motif consisting of electron rich donating groups and an electron deficient withdrawing groups joined via a π-conjugated bridge. Molecular modeling and quantum mechanical calculations have proven to be valuable tools for the design process, aiding in the maximization of dipole moments and molecular hyperpolarizability.[152] Although the calculations guide synthetic chemists as they pursue new NLO chromophores and materials, they can not always predict performance factors such as stability. Modeling often suggests that increasing the length of the π-conjugated

bridge will increase the chromophore's hyperpolarizability. Experiments confirm this prediction, but also show that as the length of the π-conjugated bridge is increased, the stability of the compound often decreases depending on the π-bridging units used. This extension also frequently results in dramatic red-shifts in absorption maxima which can have detrimental effects on device usefulness and longevity. Below is a brief description of research efforts, both theoretical and experimental, focused toward the synthesis of improved second-order NLO chromophores. Table 5.2 gives an overview of some known second-order NLO chromophores and their $\mu\beta$ values.
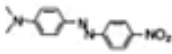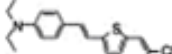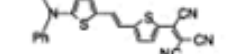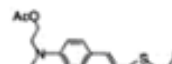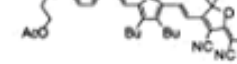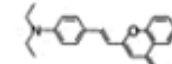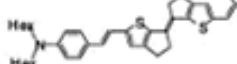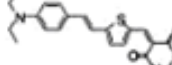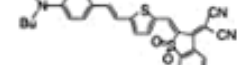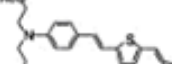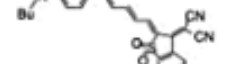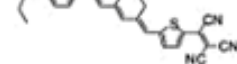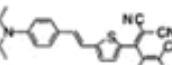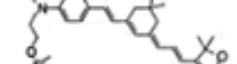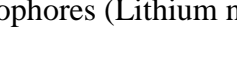
Chromophore	μβ (10^{-48} esu) @ 1907 nm	μβ/M_w	Chromophore	μβ (10^{-48} esu) @ 1907 nm	μβ/M_w
(chromophore structure)	580 r_{33} = 13 pm/V at 1330 nm (30 wt% in PMMA)	2.1	*(chromophore structure)*	10600	19.8
(chromophore structure)	1300	3.9	*(chromophore structure)*	10200	22.1
(chromophore structure)	2000	4.1	*(chromophore structure)*	9800	25.5
(chromophore structure)	3300	4.3	*(chromophore structure)*	18000	25.9
(chromophore structure)	1720	4.7	*(chromophore structure)*	19400	26.4
(chromophore structure)	2400	5.1	*(chromophore structure)*	15000	27.1
(chromophore structure)	6100	9.7	*(chromophore structure)*	13500 r_{33} = 55 pm/V at 1330 nm (20 wt% in PC)	27.1
(chromophore structure)	10400	14.1	*(chromophore structure)*	13000	27.2
(chromophore structure)	r_{33} = 36 pm/V at 1330 nm (25 wt% in PQ-100)		*(chromophore structure)*	r_{33} = 65 pm/V at 1330 nm (20 wt% in PMMA)	
(chromophore structure)	6200	17.3	*(chromophore structure)*	35000 r_{33} > 60 pm/V at 1330 nm (30 wt% in PMMA) $V\pi$ = 0.8 V	45.7

Table 5.2: $\mu\beta$ values for common NLO chromophores (Lithium niobate $\mu\beta = 10$).[188]

Donors

The most widely used and accepted donors today are alkyl or aryl amines (Figure 5.6). While many other structures have been investigated, the commercial availability of this class of compounds makes them attractive to researchers in both academia and industry.[152] Dialkyl anilines are by far the most common as their unfunctionalized and monofunctionalized starting materials can be easily derivatized. Diaryl anilines such as those seen in Figure 5.6b are also readily available but after extensive investigation were found to produce lower SHG efficiencies and EO coefficients.[189] This decrease in NLO activity is attributed to the delocalization of the nitrogen lone pair into the π-systems of the aryl substituent moieties. More complex dialkoxyphenyl-anilines were found to alleviate this problem, but the difficult synthesis of such compounds has limited their widespread acceptance.[190,191] Carbazole derivatives (Figure 5.6d) have also been utilized to produce Y-shaped, orientationally constrained chromophores but these display only moderate optical activities.[192]
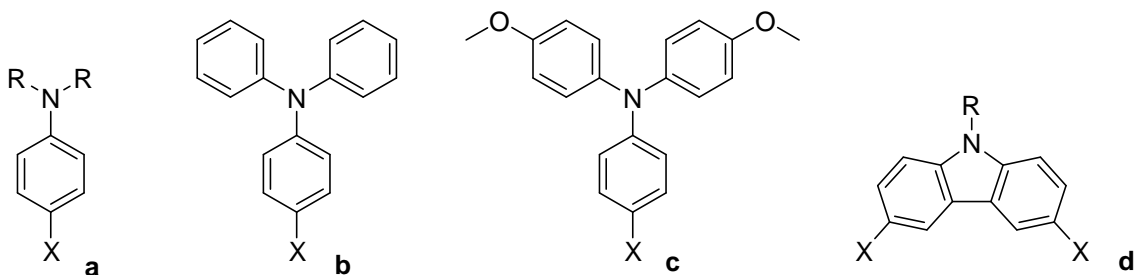
Figure 5.6: Commonly utilized NLO donors.

Bridges

It is of utmost importance to maximize the conjugation length and communication efficacy of the π-bridge. Increasing the length of the π-bridge does increase the $\mu\beta$ product of most chromophores, but along with this enhancement often come drastic

bathochromic shifts as well as decreased thermal and photochemical stability as seen in compounds where the donor and acceptor are separated by simple polyene bridges (Figure 5.7d).[193,194,195] To circumvent this, the use of aromatic rings in the π-bridge has been extensively investigated (Figure 5.6a-c) and has shown greatly enhanced thermal and photochemical stability but suffers from lower $\mu\beta$ values. This decrease in NLO activity is attributed to the energy threshold associated with aromatic disruption.[196]
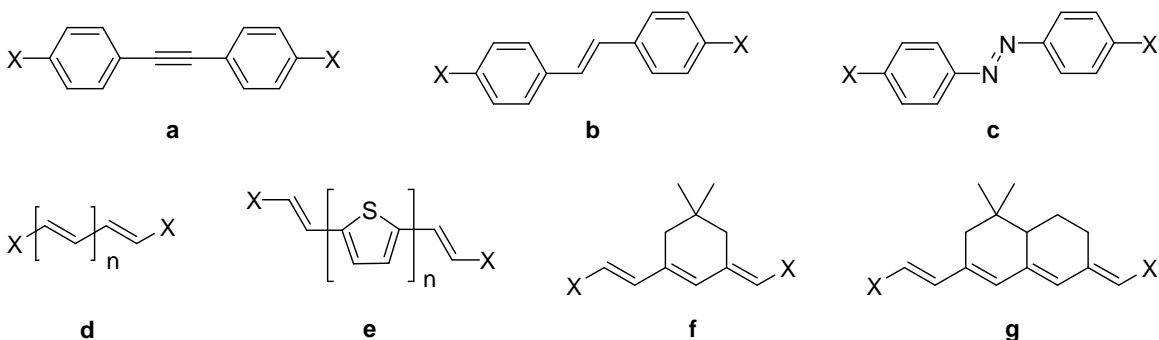
Figure 5.7: Commonly utilized NLO π-chromophore bridges.

Researchers desiring the large $\mu\beta$ values observed with polyenes but also the stabilities observed when using aromatic bridged structures, soon turned to the incorporation of ring-locked polyenes and thiophene containing moieties (Figure 5.7f-g).[197] Ring-locked polyenes were found to have increased stability over their non-ring-locked counterparts while exhibiting similar EO coefficients.[198,199,200,201] Even further improvement in thermal stability was found when thiophene moieties were incorporated into the bridge structures as seen in Figure 5.7e. Despite also being aromatic, thiophene incorporation was found to have a smaller detrimental effect on $\mu\beta$ values while providing thermal stability similar to compounds bearing phenyl moieties. This discovery has prompted a tremendous amount of interest in thiophene containing chromophores and has been at the center of much of the current research.[202,203,204,205]

Acceptors

Of the three main design components of NLO chromophores, the acceptor has by far been the most extensively studied and varied (Figure 5.8). Classic NLO chromophores first utilized nitro, nitrile, dicyanovinyl, tricyanovinyl, and sulfone acceptors. These moieties, while being synthetically convenient and well understood, have largely been replaced by much more complicated acceptor structures, most of which were adopted from the textile dye industry.[152] Two such complex structures are those of isoxazolones (Figure 5.8j) and tricyanofurans (TCFs) (Figure 5.8m).[188]
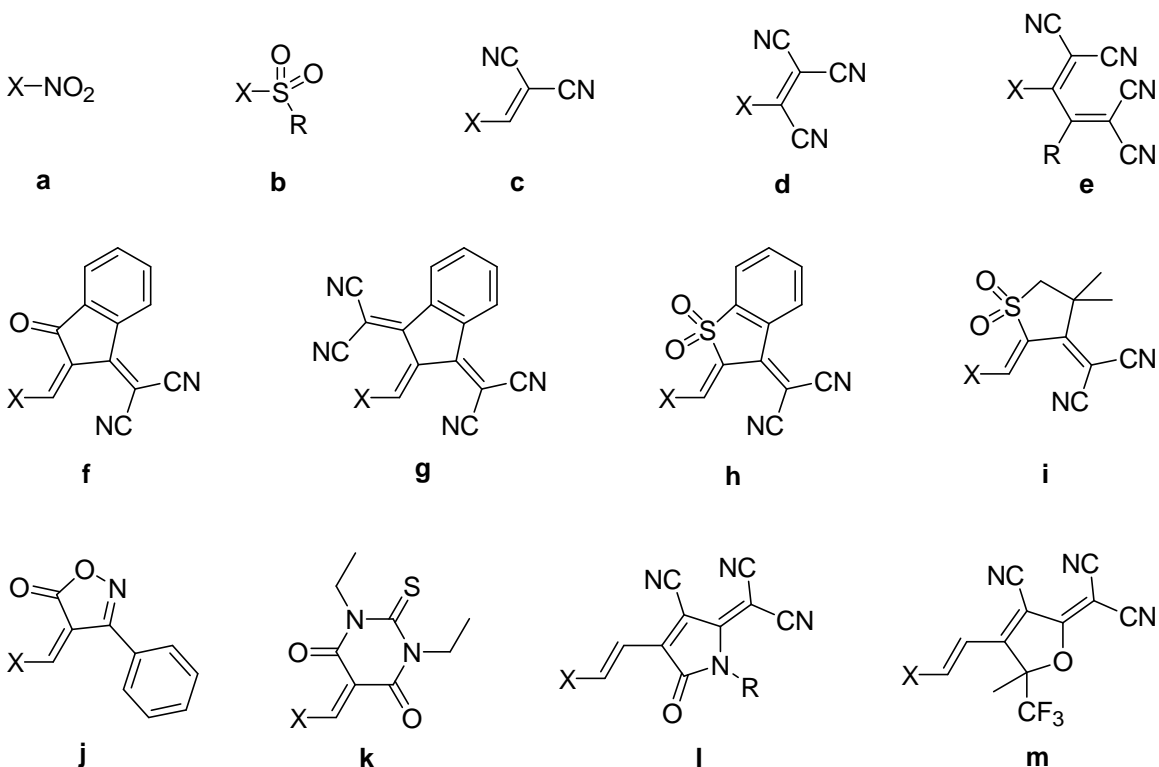
Figure 5.8: Commonly utilized NLO acceptors.

Isoxazolones were first discovered in 1965 and were used to make merocyanine dyes.[206] Upon their incorporation into NLO chromophores, they were found to produce

modest $\mu\beta$ values, moderate EO coefficients, but were more stable than unprotected dicyano- and tricyanovinyl groups.[152] Despite their increased stability, researchers once again turned to the extreme electron-withdrawing properties of multi-cyano acceptors to produce the $\mu\beta$ values required to surpass that of lithium niobate.[207] Chromophores containing dicyanovinyl and tricyanovinyl acceptors were known to produce large $\mu\beta$ values but were prone to decomposition. In an effort to produce stable multi-cyano acceptors, researchers soon developed TCFs (Figure 5.8m), which have widely been recognized as the leading acceptor, producing chromophores showing thermal stabilities of ~300 °C, $\mu\beta$ values greater than 10,000 x 10^{-48} esu, and EO coefficients (r_{33} values) in excess of 60 pm/v.[152] Perhaps the one drawback of TCF acceptors has been their low synthetic yield making their industrial use and acceptance less likely.[208,209,210,211] These synthetic problems have been somewhat alleviated via the use of focused microwave irradiation (Figure 5.9).[212]
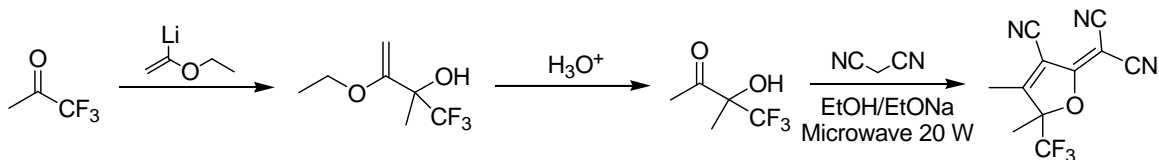
Figure 5.9: Synthesis of TCF acceptors.

Two more classes of recently reported acceptors are those of the tricyanopyrroline (TCP) and heterocyclic sulfonyl families. TCP acceptors (Figure 5.7*l*) were discovered in the 1960s and used for textile dyes as they bear structural similarities to TCF compounds.[213] They have shown similar electron-withdrawing characteristics to TCF and tout the advantage that the amide nitrogen is easily functionalized. Heterocyclic sulfonyls (Figure 5.7h-i) have also been investigated with aryl sulfonyls (Figure 5.7h) proving to be the most efficient, exhibiting EO coefficients of ~55 pm/v.[214,215] Work continues within

this field to improve the synthesis of existing acceptors, optimize their structure, and to discover new thermally stable, extremely powerful electron-withdrawing groups.

POLYMER DESIGN

The conversion of microscopic nonlinearity to macroscopic nonlinearity and the temporal stability of that macroscopic poling induced order are of utmost importance. Early research focused on polymeric systems based on guest-host incorporation motifs, but as work progressed, it quickly became evident that a system imparting greater temporal stability was required. Many different solutions to this problem will be discussed in the following sections and are summarized by Figure 5.10. It is important to keep in mind when reading the following sections that there is a continual balancing act being performed which is often referred to as the "nonlinearity-stability trade-off".[152] This trade-off is simply defined by the fact that systems which can be poled easily, meaning the chromophores rotate easily, typically decay quickly, and those which are difficult to pole, meaning the chromophores are more orientationally restricted, decay more slowly and to a lesser extent.
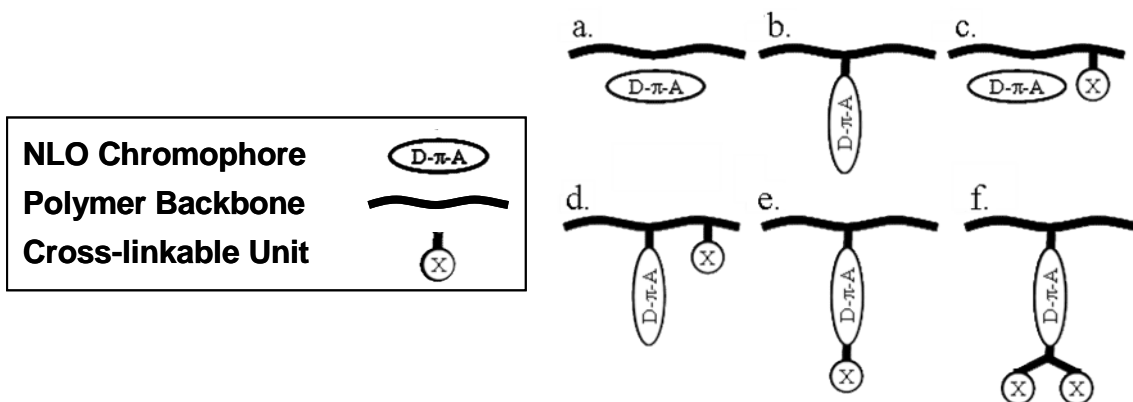
Figure 5.10: Motifs for the incorporation of NLO chromophores into organic polymeric systems.

95

Guest-Host Polymers

The incorporation of NLO chromophores into linear polymeric systems in a guest-host type motif is perhaps the earliest and most widely studied for NLO device fabrication (Figure 5.10a).[216,156] No lattice hardening or cross-linking processes occur in these systems, and their usefulness was eventually found to be dictated by the T_g of the host polymer which is often lowered due to plasticization effects of chromophore incorporation.[165,217,218] It was quickly found that the stabilities of such systems, often based on poly(methyl methacrylate) (PMMA), were insufficient and studies were conducted to improve temporal stability of guest-host systems. Studies suggested higher T_g polymers should be used with ideal T_g being around 150 °C, and for high operating temperature applications, T_gs on the order of 200-250 °C were desirable.[217] In response, researchers found polymers such as amorphous polycarbonates, polyurethanes, poly(amic acids), and polyimides provided drastically enhanced poled order stabilities. The drawback to these systems is that polymers such as polyimide are highly insoluble in common spin-casting solvents and chromophore phase separation often occurred.[217] Attention then turned to the optimization of the guest chromophores. NLO chromophores with larger molecular volumes were found to temporally decay slower as were those containing functionalities which could hydrogen-bond with the polymer matrix.[219,220,221,222] Despite these discoveries and the experimental ease of using guest-host type systems, there is great doubt they will ever be industrial useful due to their low temporal stability.

Side-Chain Polymers

Side-chain NLO polymers are those in which NLO chromophores have been covalently bound to the polymer chain as pendant groups (Figure 5.10b). This covalent

attachment can be realized via the polymerization of monomeric units bearing chromophores or by the post-polymerization modification of linear polymers with reactive side-groups.[152,223,224] Both methods allow greater chromophore density loadings and usually do not suffer from the crystallization and plasticization problems encountered in most guest-host materials.[164] Using post-polymerization modification it can be difficult to quantify covalent attachment and often reproducibility issues and chromophore concentration gradients are encountered. This method is attractive in that chromophore mixtures may be introduced which impart unique properties not possible with single chromophore systems.[224] The covalent attachment of one end of the NLO chromophore greatly increases stability over guest-host systems owing largely to removal of a degree of freedom from the chromophore (Figure 5.11).[217] This observation has led many researchers to explore systems in which more degrees of freedom are removed from the chromophore, a topic that will be discussed in the following sections.
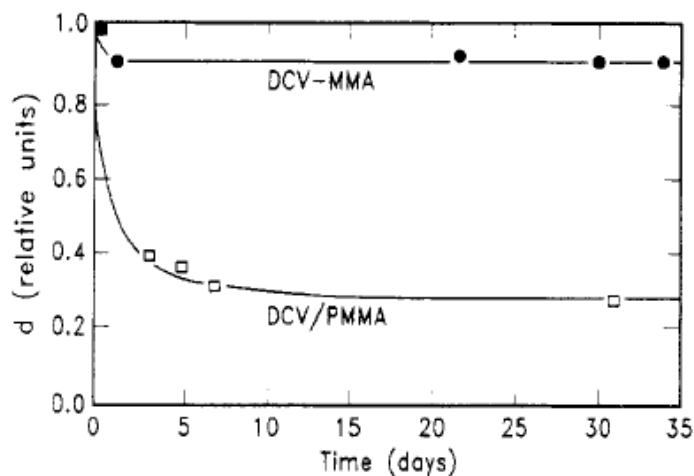
Figure 5.11: Comparison of the 4-(dicyanovinyl)-4'-(dialkylamino)azobenzene chromophore incorporated into a guest-host matrix of PMMA (DCV/PMMA), and as a side-chain (DCV-MMA).[225] Reprinted with permission from Singer, K.; Kuzyk, M.; Holland, W.; Sohn, J.; Lalama, S.; Comizzoli, R.; Katz, H.; Schilling, M., *Appl. Phys. Lett*., **1988**, *53*, 1800. Copyright 1988, American Institute of Physics.

Main-Chain Polymers

Main-chain NLO polymers are those in which the push-pull chromophores are incorporated in a head-to-head, or more commonly head-to-tail type arrangement in the polymer chain. These systems were sought following studies such as the one shown in Figure 5.11, since a further degree of freedom has been removed from the chromophore by physically binding it at both ends.[164] Main-chain systems do show enhanced stabilities but greatly suffer in that they are extremely difficult to pole, producing drastically lower SHG and EO coefficients compared to side-chain and guest-host motifs. This reduction in poling efficiency is attributed to the necessity for large segmental chain motions to occur in order for the polymer chain to reorient itself in the poling field rather than the simple rotations required for pendant groups and guest chromophores.[152] Main-chain systems have been shown to produce enhanced mechanical properties[226] but have been less widely studied because of their low poling efficiencies.[152]

Cross-Linked Polymers

NLO polymers that can cross-link are extremely attractive targets for the fabrication of highly active and stable devices, and a tremendous amount of literature has been generated on this topic. Most researchers agree that the number, nature, and position of the cross-linking units are directly related to temporal stability.[164] Due to the insolubility of most cross-linked polymer networks and the high immobility of chromophores contained within, the cross-linking process must occur during or after the film forming and poling steps of device fabrication.[217] The cross-links may be formed via thermal or photochemical processes and can be formed in a single step from multifunctional monomeric components (thermosetting prepolymers) or may result from reaction of cross-linkable moieties pendant to linear polymer in an additional step. Linear

polymers which can be cross-linked in subsequent steps are called double-end cross-linkable (DEC) materials (Figure 5.10e) and if a third functionality exists are referred to as trilinking chromophores (Figure 5.10f). In almost all cases, enhanced temporal stability is observed relative to their uncross-linked analogues (Figure 5.).[217]
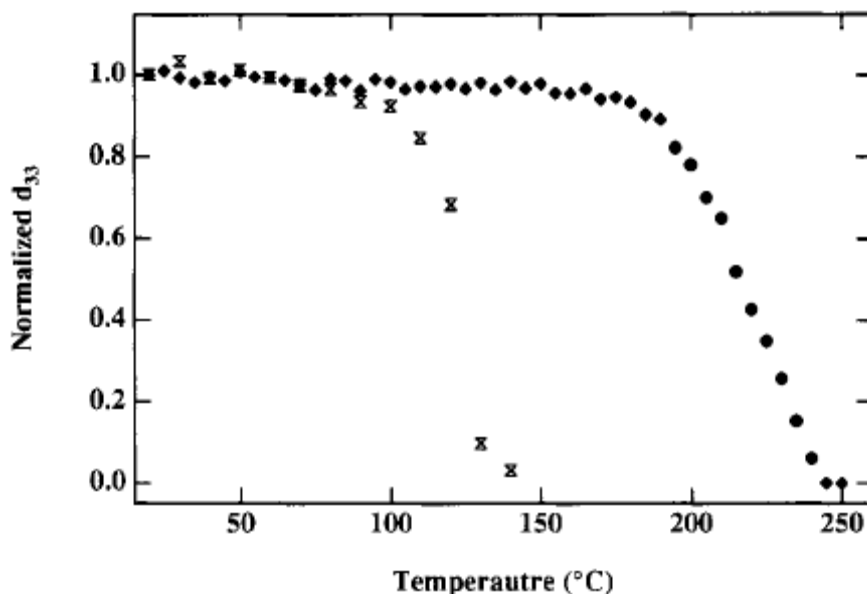
Figure 5.12: Cross-linking (dots) versus noncross-linking (crosses) temporal stability.[227] Reprinted with permission from Becker, M.; Sapochak, L.; Ghosen, R.; Xu, C.; Dalton, L.; Shi, Y.; Steier, W.; Jen, A., *Chem. Mater*., **1994**, *6*, 104. Copyright 1994, American Chemical Society.

Thermal Cross-Linking

Perhaps the most widely studied thermosetting prepolymers for this purpose are epoxy resins whose wide selection and commercial availability make them attractive for the fabrication of NLO devices in research labs and for commercial applications.[228,229,230] Since NLO chromophores typically containing one or more amine functionalities, they can be combined with multifunctional epoxides or vice versa. The two compounds react slowly at room temperature, but the rate is greatly accelerated at elevated temperatures

where the material cross-links via epoxide ring opening and becomes a thermoset resin with an extremely high T_g. The use of a single primary amine can inherently react with a bis-epoxide creating a linear polymer network, while the use of a chromophore with more than one amine or a multifunctional epoxy can quickly lead to cross-linked material formation.[231,232] An example of a cross-linked epoxy resin is shown in Figure 5.13. The disadvantages of such systems are that they are often limited to low chromophore loadings, dictated by solubilities and phase separation, and the fact that the reaction of amines with epoxides is a thermal process and begins as soon as the two components are mixed. This creates a race between alignment and cross-linking that ultimately limits their maximum poling abilities.[164]

Cross-Linked Network
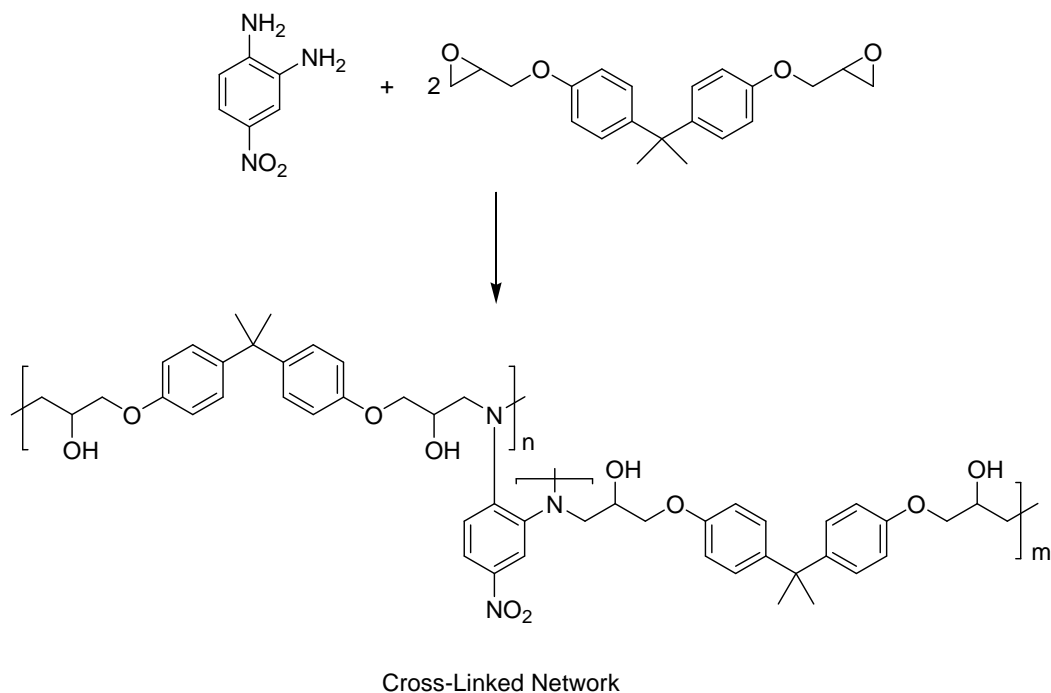
Figure 5.13: Epoxy network formation.[233]

The thermal cross-linking motif has been expanded to polyurethanes,[234,235,236] polyamides,[237,238] and polyimides[239] through the incorporation of multifunctional reactive

monomers and chromophores. Of these, the use of polyurethanes has been the most extensively studied and involves the incorporation of multifunctional alcohols and isocyanates; a beautiful synthetic example of which can be seen in Figure 5.14. As with epoxy resins, the reaction between an alcohol and an isocyanate is a thermal process, which begins to slowly react as soon as the two are mixed. This immediate reaction, albeit slow, ultimately limits the degree of poling-induced dipolar order observed as well as its potential as an industrial product due to limited material shelf life. To circumvent this problem Jen *et al*. developed a unique lattice hardening approach that capitalized on the thermal reversibility of the Diels-Alder reaction (Figure 5.15).[241] His system incorporated furan-protected maleimide pendant groups which upon heating would cycloreverse producing an unprotected maleimide. This pendant maleimide could then react with pendant anthracene moieties in a [4+2] cycloaddition reaction producing cross-links. This essentially eliminated network formation upon mixing at room temperature, but remains a thermal process which can proceed at the elevated temperatures required for poling.

Cross-Linked Network
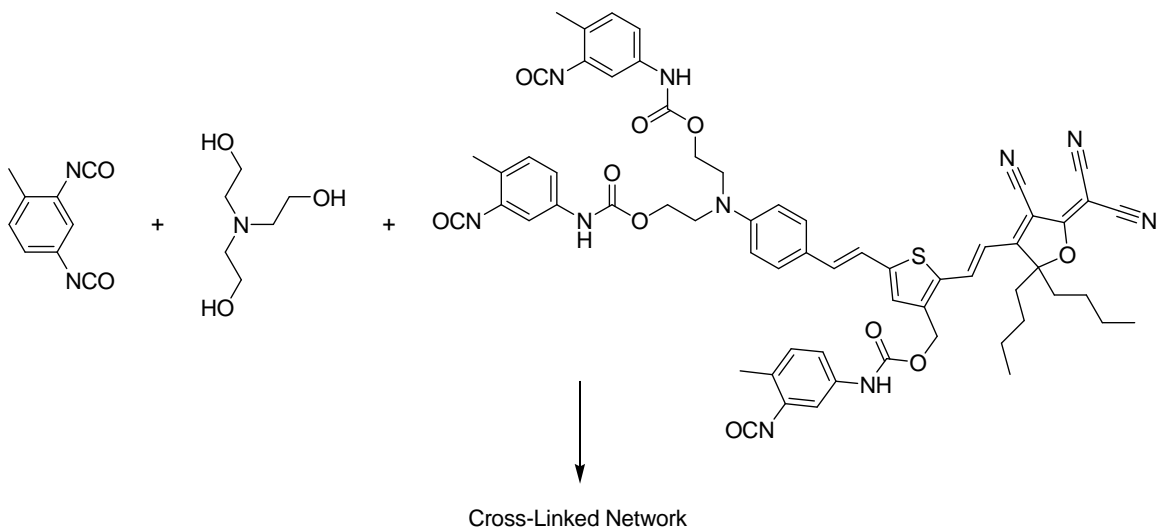
Figure 5.14: Polyurethane network formation.[240]
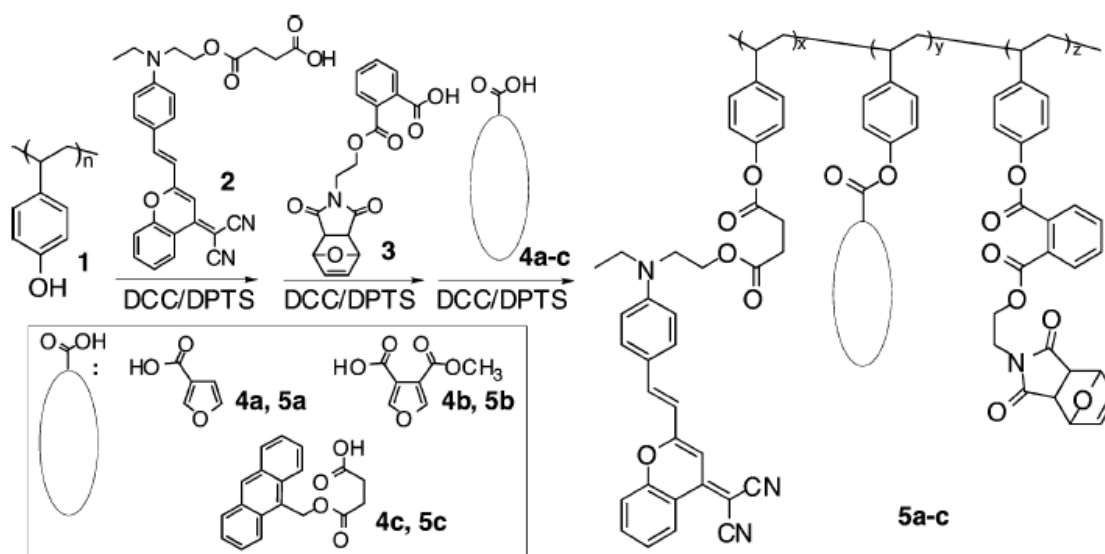
Figure 5.15: Lattice hardening via Diels-Alder reactions.[241] Reprinted with permission from Haller, M.; Luo, J.; Li, H.; Kim, T.; Liao, Y.; Robinson, B.; Dalton, L.; Jen, A., *Macromolecules*, **2004**, *37*, 688. Copyright 2004, American Chemical Society.

Photochemical Cross-Linking

In contrast to thermal cross-linking, photochemical cross-linking to produce lattice hardened thermosets has not been extensively studied. Studies by Robello and co-workers utilized trifunctional acrylates to cross-link with methacrylated chromophores (Figure 5.16). They found the absorption of the chromophores often limited the photoinitiation event and cross-linking efficiency.[242] They also discovered that many NLO chromophores suffered from low solubility in the formulation resulting in low chromophore densities and low optical activities. Other attempts to produce photocross-linkable NLO materials have utilized nitrene generation from azides[243] as well as the incorporation of vinylcinnamate moieties, which undergo a well-known photochemical [2+2] cycloaddition reaction.[244] DEC type photocross-linkable chromophores have been

alluded to in the literature, but to the author's knowledge no successful reports have ever been published.[245,246,247] Despite its many difficulties, photochemical cross-linking is still an active area of research as it provides a means to totally separate the lattice hardening step from the thermal poling step.
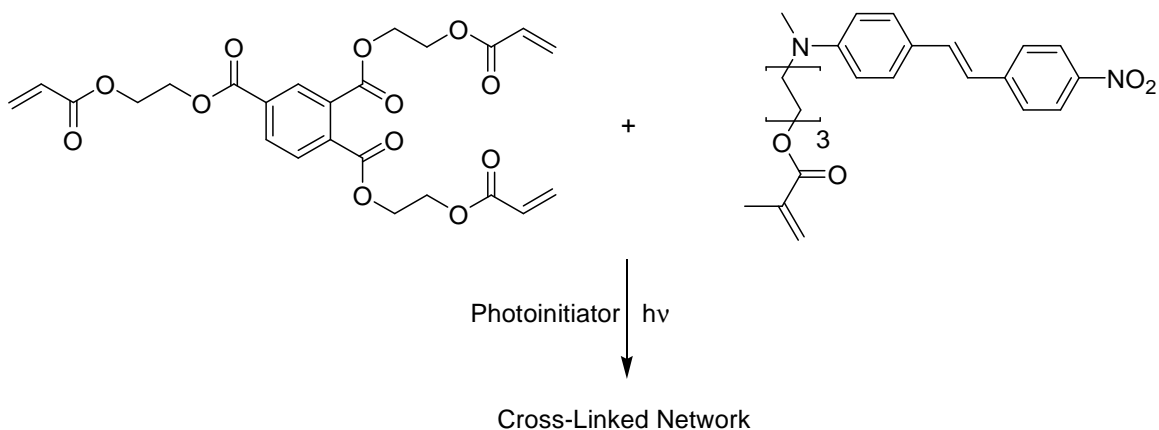
Figure 5.16: Photochemical network formation of acrylates and methacrylates.[242]

CONCLUSIONS

Organic nonlinear optical polymers are promising candidates for optical switching, optical data storage, EO modulators, and optical fiber-based devices. Tremendous amounts of effort have been exhausted in the development of optimized chromophores, mostly centering on the development of the TCF and TCP type acceptor moieties. Side-chain materials have overcome many of the issues encountered with guest-host type systems while still having optical performance exceeding that of the inorganic benchmark compound, lithium niobate. With side-chain polymers, the most significant hurdles remaining are those of temporal, thermal, and photochemical stabilities. Cross-linking materials are attractive solutions to some of these problems (Figure 5.17), but to date most all cross-linking reactions are thermal processes giving rise to difficulties in

separating the poling process from the thermosetting process (the "nonlinearity-stability trade-off"). Photochemical cross-linking has proven extremely difficult owing primarily to chromophore absorbance and photostability at the initiation wavelength. Presently, no organic NLO materials are suited for applications requiring sub 1 μm wavelengths. Devices such as flat panel and virtual reality displays would benefit from low drive voltage EO modulators which are capable of operating in the visible wavelengths. Researchers hope to solve these problems and eventually realize commercialization of polymeric NLO materials.
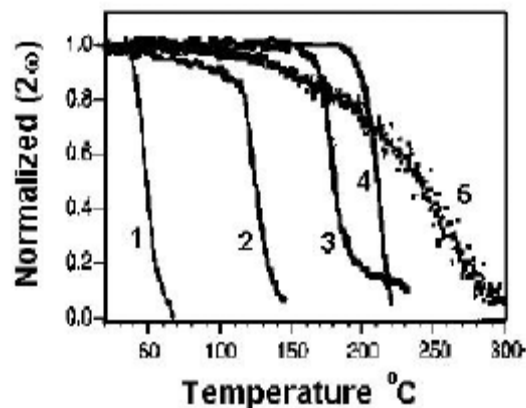
Figure 5.17: Dynamic thermal stability of Disperse Red type chromophores in (1) guest-host matrix of PMMA, (2) attached as a side-chain, (3) DEC chromophore attached at both ends, (4) side-chain in polyimide, and (5) DEC type covalently attached at both ends in a sol-gel type material.[217] Reproduced from Dalton, L., *Nonlinear Optical Polymeric Materials: From Chromophore Design to Commercial Applications*, Springer-Verlag, Berlin/Heidelberg, **2002**. With kind permission from Springer Science + Business Media.

Chapter 6: Progress toward the Design, Synthesis, and Cross-Linking of Highly Stable, Nonlinear Optical Materials for Electro-Optic Applications

INTRODUCTION

Our laboratory is currently engaged in the design and development of photonic crystals comprised of organic chromophores with highly stable electro-optic (EO) activity. Fabrication of such devices requires polymers that can be easily processed, have large second order nonlinear optical (NLO) coefficients, can be patterned at high resolution, and are thermally, photochemically, and temporally stable after poling. Solutions to most of these requirements have been developed including the adoption of side-chain type NLO polymers, the synthesis of many complex acceptors, and the use of aromatic groups in the chromophore bridge. Perhaps the only remaining hurdle is that of loss of poling-induced dipolar (temporal) order. This is of utmost importance to the field of nonlinear optics, and despite recent advances, most materials currently available are incapable of producing stable devices at the elevated operating temperatures often encountered in EO devices (90-125 °C).[248,249]

To address this problem, researchers have turned to cross-linkable polymeric systems to produce lattice-hardened materials. A number of cross-linking methodologies have been explored in literature including those of thermosetting prepolymers, guest-host systems where the polymer backbone may be cross-linked (Figure 6.1c), side-chain polymers where the NLO chromophore and cross-linking groups are both covalently attached to the polymer backbone (Figure 6.1d), and finally, side-chain systems where the cross-linking sites are tethered to the covalently attached chromophore (Figure 6.1e). Thermosetting prepolymers, such as the ones described in chapter 5 (Figures 5.13 and

5.14), have been shown to provide materials with enhanced temporal stability but are classically hindered by solubility limitations and phase separation issues. Systems in which linear side-chain polymer is initially formed and then thermally cross-linked (Figure 6.1c-d) have also been shown to exhibit further enhanced stabilities while avoiding solubility and phase separation issues, however, still remain short of the stabilities required for most EO applications.[249] These systems cross-link via thermal processes, which are accelerated upon heating during the poling process, resulting in material that is cross-linked prior to full chromophore alignment. This premature cross-linking orientationally locks the chromophores, prohibiting maximum dipolar alignment efficiencies and ultimately limiting NLO activity.
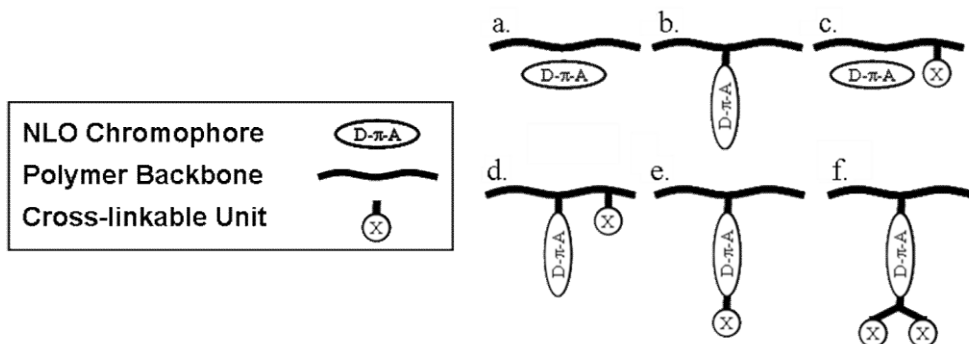
Figure 6.1: Motifs for the incorporation of NLO chromophores into a polymeric system.

The ability to photochemically cross-link side-chain NLO materials should preclude network formation during poling and therefore allow for maximum poling efficiencies and enhanced temporal stabilities. Systems resembling Figure 6.1e, which may be photochemically cross-linked, have been attempted, but to the author's knowledge no successful reports have been published.[250,251] From studies of cross-linked prepolymers such as the one in Figure 5.16, it is known that photochemical cross-linking is difficult owing in part to high chromophore absorbance which increases chromophore

photo-degradation, impedes photoinitiation, and leads to temporal device decay. Our assumption is that the observed device decay in many cross-linked systems is the direct result of a majority of intrachain rather than interchain cross-linking as well as poor cross-linking conversion in the polymer film. This problem should be improved if lower absorbing chromophores are used and the cross-linking density is increased. We now describe an efficient synthetic route to a new class of photochemically biscross-linkable monomers (Figure 6.1f) with low absorption in the visible spectrum. The characteristics of their corresponding linear and cross-linked polymers as well as preliminary lithographic patterning and characterization of their nonlinearity will be discussed. The patterning and NLO characterization are ongoing projects within the Willson research group.[251]

DESIGN

Our design (Figure 6.1f) calls for the use of a trifunctional monomer in which one of the three functionalities can be selectively polymerized in the presence of the other two. This allows for the formation of linear polymeric material that can be heavily cross-linked via irradiation following poling. Norbornene moieties provide an attractive functionality as they are known to readily undergo ring opening metathesis polymerization (ROMP)[252,253,254,255] yielding polyolefins that often possess low glass transition temperatures (T_gs) (< 100 °C). A low T_g is advantageous in that poling may be achieved at mild temperatures prior to cross-linking via subsequently applied external stimuli. ROMP also provides functional group tolerance to acrylates, methacrylates, and epoxides that are logical choices for cross-linkable groups. Methacrylates were chosen because their polymerization can be selectively carried out via photolysis of an incorporated photo-radical initiator following poling. To compliment our polymerizable

107

groups, tolanes were chosen as the π-conjugated system with a sulfone as the acceptor and an amine as the donor. All three of these functionalities have been shown to be effective in NLO materials, should provide a chromophore with low visible absorption, and are virtually inert to ROMP and radical cross-linking conditions.[256,257,258,259,260,261,262]

RESULTS AND DISCUSSION

Synthesis

Synthesis of compound **6.4** was accomplished via the alkylation of commercially available 4-bromothiophenol with 3-bromo-1-propanol. Hydrogen peroxide oxidation in acetic acid produced a mixture of the desired compound **6.3** and its acetate functionalized analogue. Subsequent saponification of the mixture using basic methanol produced hydroxyl compound **6.3**. Esterification using 5-norbornene-2-carboxylic acid chloride and triethylamine (TEA) yielded the sulfone acceptor **6.4** in good overall yield (Scheme 6.1). This provided our first polymerizable functionality, and its electron deficient aryl bromide made it an ideal handle for Sonogashira coupling with an electron rich alkyne.
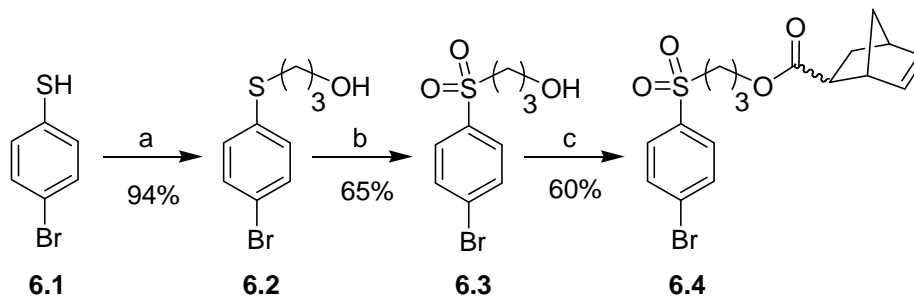
Scheme 6.1: Synthesis of polymerizable sulfone acceptor **6.4**. Conditions: (a) (i) NaH, THF; (ii) Bromopropanol, THF. (b) (i) HOAc, 30% H$_2$O$_2$, reflux; (ii) NaOH, MeOH, 90 °C. (c) DCM, TEA, 5-norbornene-2-carboxylic acid chloride.

108

The donor alkyne **6.8** was synthesized via the selective *p*-iodination of commercially available substituted aniline **6.5** using ICl in an aqueous HCl solution. After the excess ICl was quenched with sodium thiosulfate (Na$_2$S$_2$O$_3$), the solution was added drop wise to a saturated solution of sodium bicarbonate to precipitate compound **6.6** as an off-white solid. Sonogashira coupling of the iodo compound **6.6** with trimethylsilylacetylene (TMSA) and TEA afforded the protected alkyne **6.7**. Deprotected alkyne **6.8** was readily obtained by desilylation using potassium carbonate and methanol (Scheme 6.2). The diol functionality of compound **6.8** provided the functionality to which methacrylate groups were added.
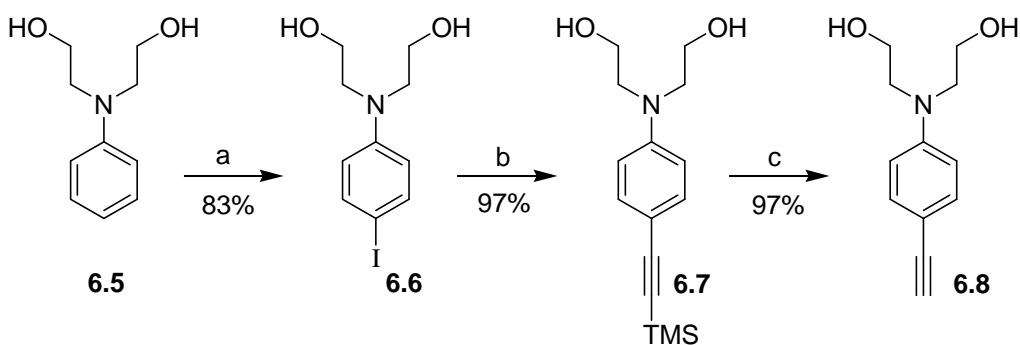
Scheme 6.2: Synthesis of donor **6.8**. Conditions: (a) (i) ICl, HCl, H$_2$O; (ii) NaHCO$_3$, H$_2$O. (b) THF, TEA, CuI, Pd(PPh$_3$)$_2$Cl$_2$, TMSA, 60 °C. (c) MeOH, K$_2$CO$_3$.

In order to facilitate a systematic study of cross-linker density on temporal stability, donors bearing a single cross-linkable group and no cross-linkable groups were needed. After repeated attempts to iodinate compound **6.9** in a manner similar to dihydroxyl compound **6.5**, it was found that selective *p*-iodination could be realized using I$_2$ in a 1:1 mixture of pyridine and dioxane (Scheme 6.3). Sonogashira coupling of **6.10** with TMSA and using diisopropylamine (DIPA) as a base afforded the TMS protected compound **6.11** in excellent yields. Deprotection of compound **6.11** using K$_2$CO$_3$ in

methanol produced a 1:1 mixture of the desired free alkyne and the zwitterionic carbamate salt resulting from amine addition to CO_2 (Scheme 6.4). These could be separated via column chromatography, but at greatly decreased yields. The use of tetrabutylammonium fluoride (TBAF) in THF precluded salt formation yielding the free alkyne **6.12** in excellent yields (Scheme 6.3).
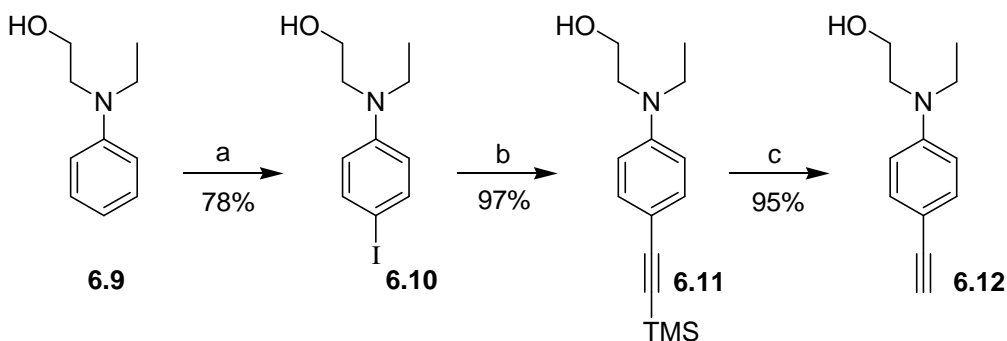
Scheme 6.3: Synthesis of donor **6.12**. Conditions: (a) I_2, pyridine/dioxane (1:1). (b) THF, DIPA, CuI, Pd(PPh$_3$)$_2$Cl$_2$, TMSA, 60 °C. (c) TBAF, THF.
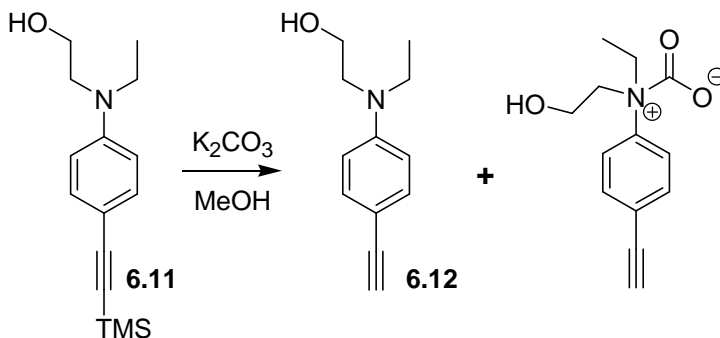
Scheme 6.4: Observed carbamate salt formation.

To produce the noncross-linkable chromophore analogue, bisacetate protected compound **6.13** was synthesized using acetic anhydride and pyridine with a catalytic amount of 4-(dimethylamino)pyridine (DMAP). The acetate group was used as it most closely mimics acrylates. The Sonogashira reaction of **6.13** with TMSA and TEA yielded

the TMS protected alkyne **6.14**. Deprotection using TBAF in THF yielded the desired donor compound **6.15** in satisfactory overall yields (Scheme 6.5).
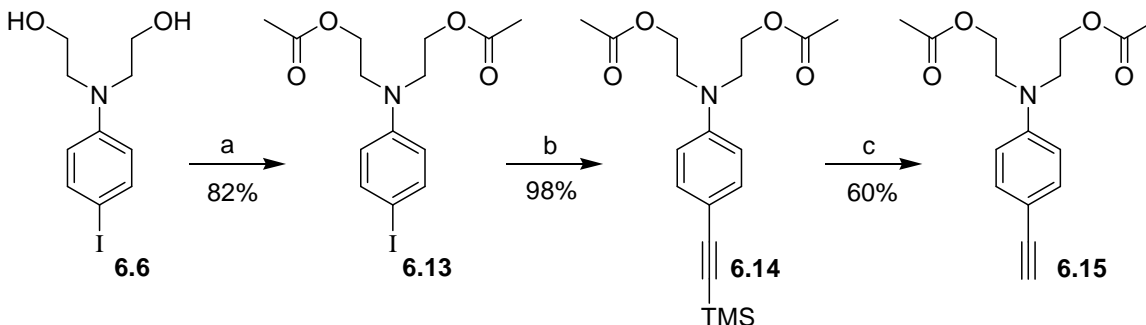
Scheme 6.5: Synthesis of donor **6.15**. Conditions: (a) Ac$_2$O, pyridine, DMAP (cat.). (b) THF, TEA, CuI, Pd(PPh$_3$)$_2$Cl$_2$, TMSA, 60 °C. (c) TBAF, THF.

Donor compounds **6.8, 6.12,** and **6.15** and acceptor **6.4** were then coupled via the Sonogashira reaction using DIPA to yield the donor-acceptor tolanes **6.16-6.18** in good overall yields (Scheme 6.6). Tolane **6.16** was recovered in 64% overall yield from the commercially available diol **6.5** as a yellow crystalline solid, and its structure was confirmed by X-ray crystallographic analysis (Figure 6.2). UV-visible analysis showed that as the chromophore was lengthened, a dramatic red-shift occurred suggesting that good electronic communication was established between the donor and acceptor (Figure 6.3). Compounds **6.16-6.17** were then reacted with methacryloyl chloride in the presence of triethylamine to produce the biscross-linkable and monocross-linkable monomers **6.19-6.20** (Scheme 6.7).

111
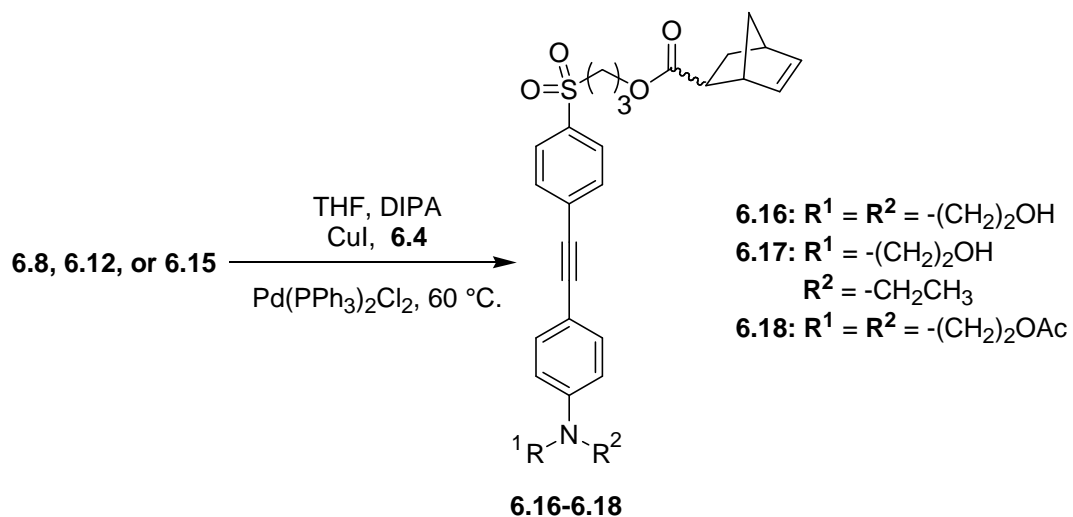
Scheme 6.6: Synthesis of donor-acceptor tolane compounds **6.16-6.18**.
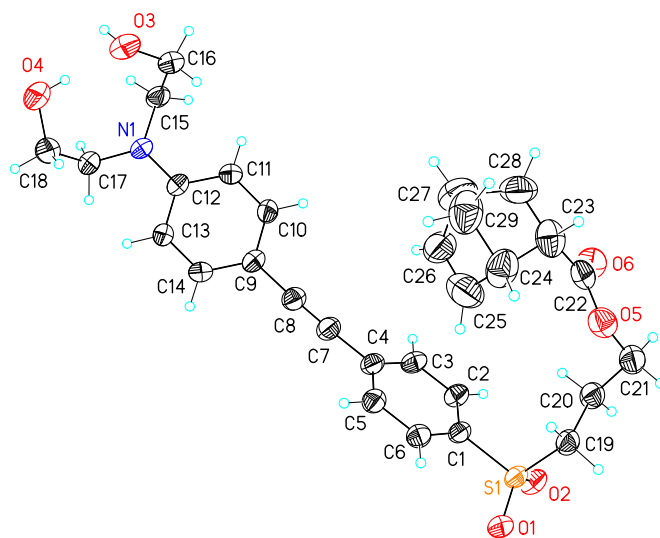
Figure 6.2: Crystal structure of *endo*-norbornyl tolane **6.16**.
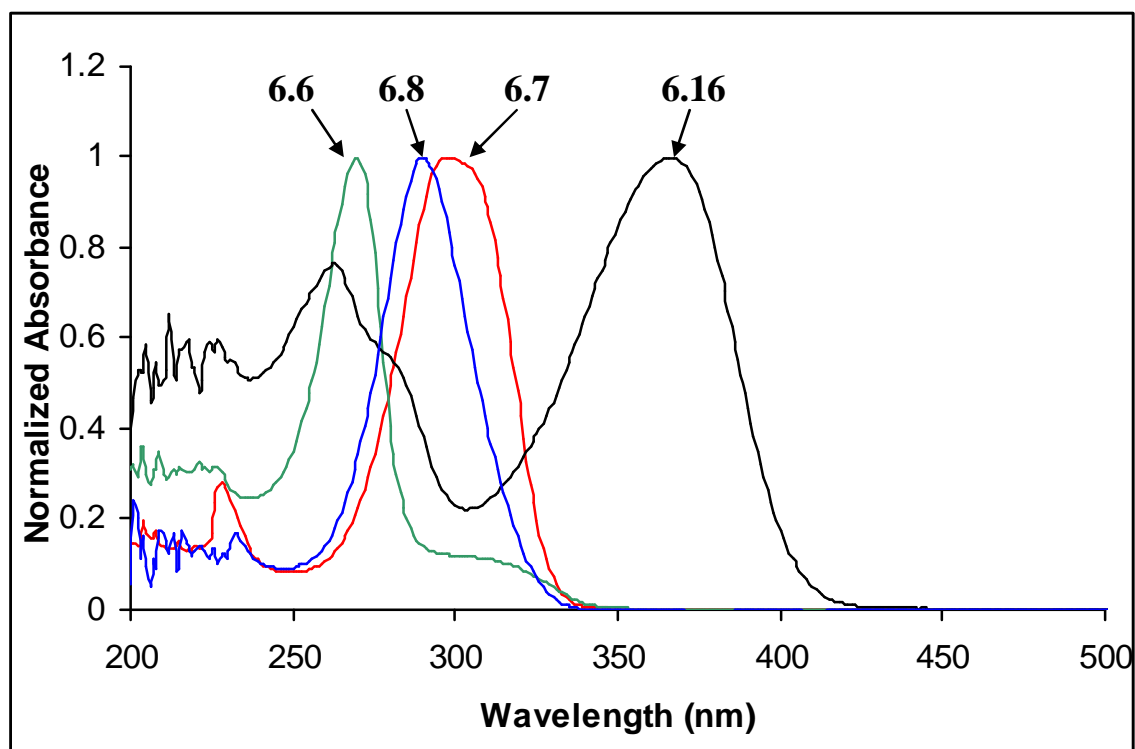
Figure 6.3: UV-visible spectra of compounds 6.6, 6.7, 6.8, and 6.16.
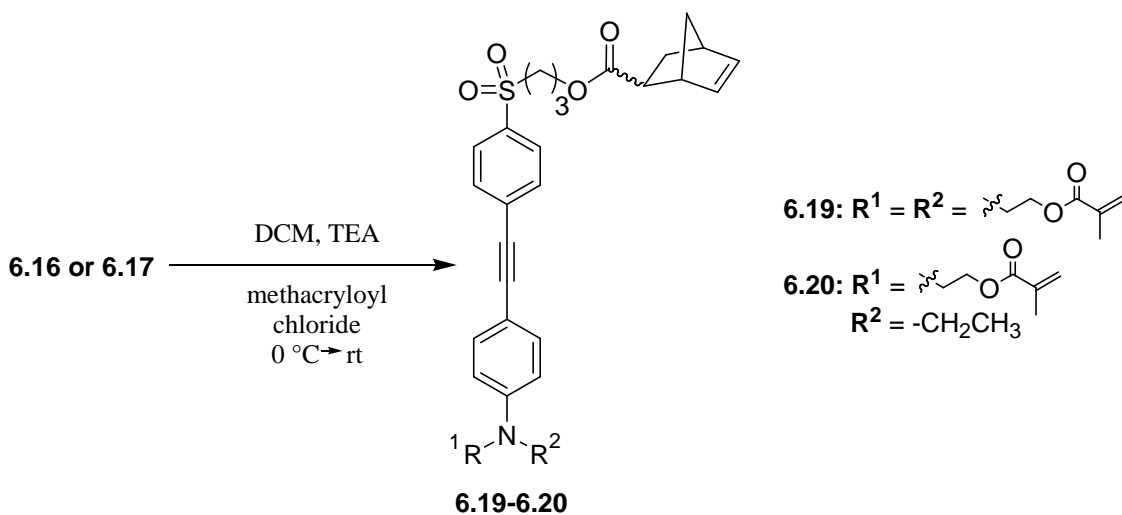
Scheme 6.7: Synthesis of cross-linkable tolane compounds **6.19-6.20**.

Initial attempts to polymerize the tolane chromophore **6.16** using Grubbs 1st generation catalyst (Grubbs I) (Figure 6.4) failed to produce any polymer (Table 6.1 entries 1-2) and the monomer was recovered by column chromatography. Grubbs 2nd generation catalyst (Grubbs II) produced a significant amount of a dark colored precipitate in the reaction mixture, which was found to be highly insoluble in most common solvents (Table 6.1 entries 3-4). In attempt to better control the polymerization, two additives were chosen that are known to facilitate polymerization, triphenylphosphine and trifluoroacetic acid (TFA). Triphenylphosphine is known to compete with olefin coordination thereby slowing polymerization rates and increasing initiation efficiencies.[263] The addition of TFA is speculated to protonate amine functionalities that may coordinate with the ruthenium complex.[264] In this case, it is important to note that compounds such as diethanolamine are known to coordinate to Grubbs type catalysts lowering metathesis activity.[265] The addition of both additives (Table 6.1 entries 5-6) produced the same insoluble precipitate observed in prior runs. The bis(3-bromopyridine) complex (Grubbs III) was also utilized but yielded no polymer. It was then decided that attention should be focused on the polymerization of bisacetate chromophore **6.18**. Reaction with Schrock's catalyst provided no product (Table 6.1 entry 8), but use of Grubbs II was found to provide polymer with good control of molecular weight (Table 6.1 entry 9). In light of these results, chromophores **6.19** and **6.20** were also polymerized under these conditions (Table 6.1 entries 10-11) (Scheme 6.8). No unwanted reaction of the methacrylate groups was confirmed via ^{1}H-NMR.
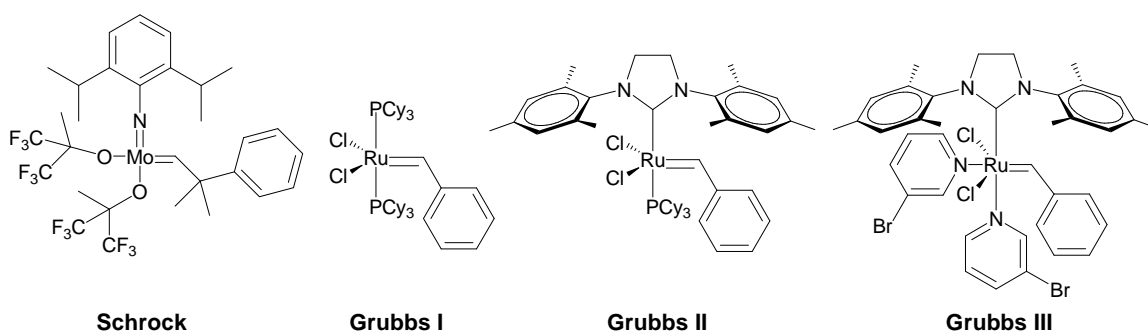
Figure 6.4: Catalysts used for polymerization attempts.

Entry	Tolane	Catalyst	Solvent	Additive	Result	M_n	PDI
1	**6.16**	Grubbs I	DCM	-	No Polymer	-	-
2	**6.16**	Grubbs I	THF	-	No Polymer	-	-
3	**6.16**	Grubbs II	DCM	-	Insoluble PPT	-	-
4	**6.16**	Grubbs II	THF	-	Insoluble PPT	-	-
5	**6.16**	Grubbs II	THF	PPH$_3$	Insoluble PPT	-	-
6	**6.16**	Grubbs II	DCM	TFA	Insoluble PPT	-	-
7	**6.16**	Grubbs III	THF	-	No Polymer	-	-
8	**6.18**	Schrock	DCM	-	No Polymer	-	-
9	**6.18**	Grubbs II	DCM	-	Polymer	33 kDa	1.59
10	**6.19**	Grubbs II	DCM	-	Polymer	59 kDa	1.90
11	**6.20**	Grubbs II	DCM	-	Polymer	52 kDa	1.62

Table 6.1: Polymerization attempts and conditions .
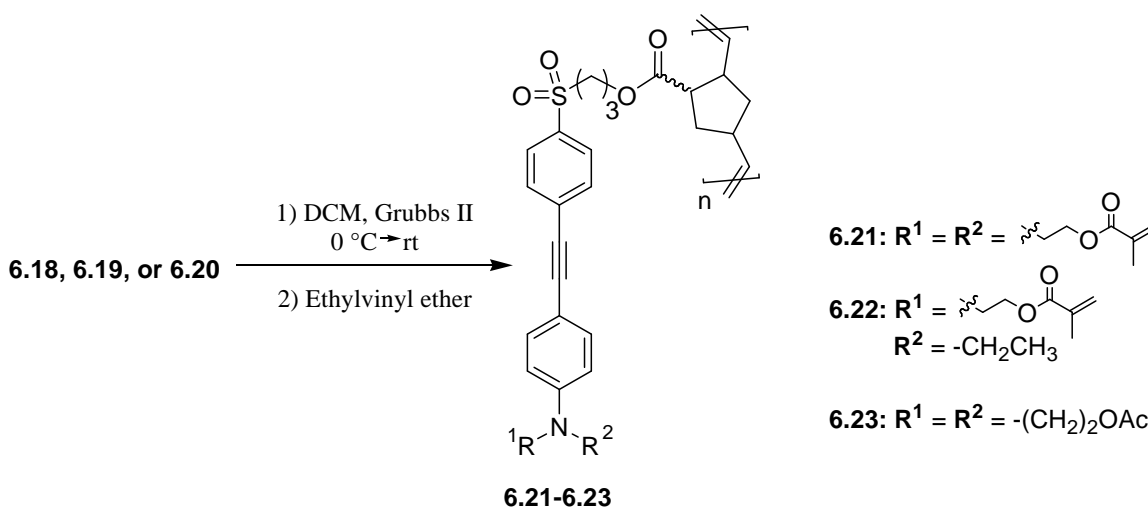
Scheme 6.8: Polymerization of NLO chromophores **6.18-6.20**.

Thermal Analysis and Solution-State Cross-Linking

Thermal gravimetric analysis (TGA) showed that all three polymers exhibit thermal stability up to ~300 °C (Figure 6.5). Differential scanning calorimetry (DSC) analysis revealed all three polymers possess T_gs below 100 °C as expected. To test the solution-state cross-linking of polymer **6.21**, 2,2′-azobis(2-methylpropionitrile) (AIBN) and polymer **6.21** were added to THF and refluxed for 24 hr. Upon completion of cross-linking, the polymer network precipitated out of solution, and its thermal properties were evaluated as evidence for cross-linking. The results can be seen in Figure 6.7 where the T_g, which occurred at approximately 60 °C prior to cross-linking, is no longer present. The absence of an apparent T_g and the extreme insolubility of the polymer in any organic solvent, precluded further GPC and ^{1}H-NMR analysis and is evidentiary of heavily cross-linked material.
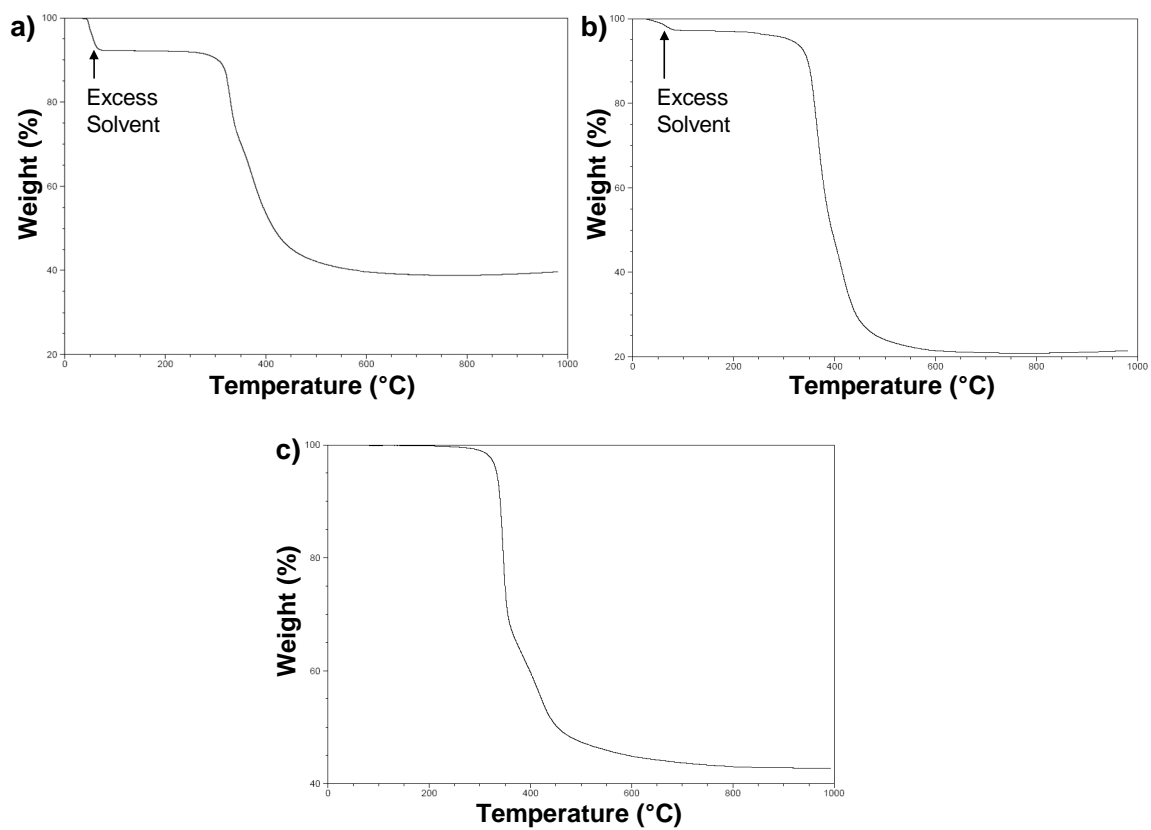
Figure 6.5: TGA analysis of compounds a) **6.21**, b) **6.22**, and c) **6.23**.

117
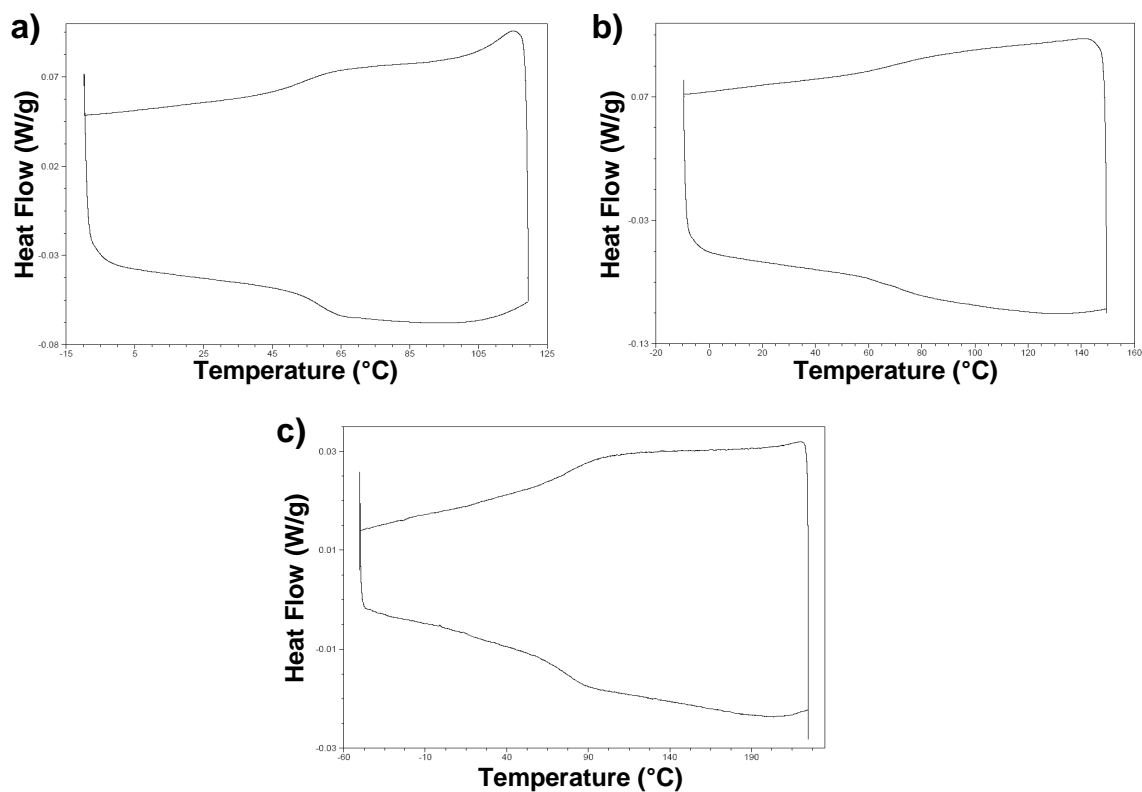
Figure 6.6: DSC traces (exothermic is up) of NLO polymers showing T_gs of (a) 60 °C for **6.21**, (b) 71 °C for **6.22**, and (c) 76 °C for **6.23**.
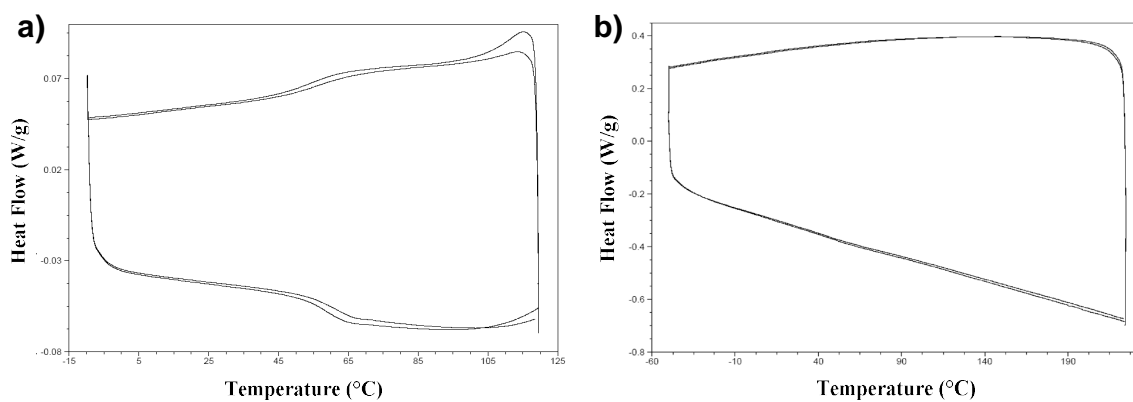
Figure 6.7: DSC trace (exothermic is up) of polymer **6.21** cycled twice before (a) and after (b) chemical cross-linking in solution.

Photochemical Cross-Linking and Patterning

The high absorbance of our material below 410 nm requires initiation in the visible region, which precluds the use of most classical photoinitiators (Figure 6.8). Commercially-available Irgacure 784 (Ciba) and camphorquinone-amine were chosen as initial targets for photoinitiators using visible light. Camphorquinone-amine systems are widely used as visible photoinitiators in dental fillings and their reactivity is well understood.[266,267,268,269,270,271,272] They are obviously nontoxic and both the camphorquinone (CQ) and the amine, typically ethyl-4-(dimethylamino)-benzoate (EDMAB), are readily available from numerous chemical and dental materials suppliers. Typical required loadings are extremely high (often 10-20 wt%) and surpassed the solubility limits in our chosen casting solvent (cyclopentanone). The high loadings are also speculated to dramatically affect chromophore density in the thin film. Irgacure 784 was found to be completely soluble, and the results are summarized in Table 6.2.
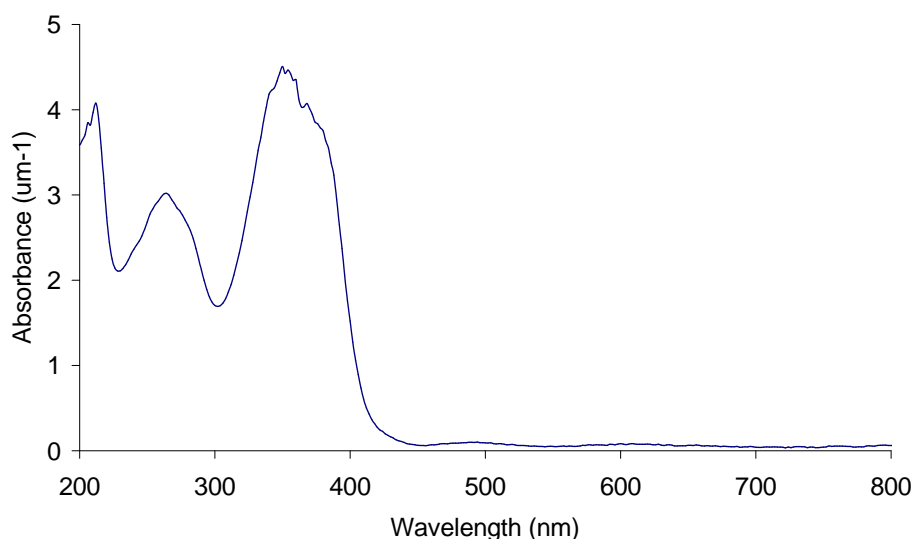
Figure 6.8: UV-Visible absorbance per μm of polymer **6.23**.

119

#	Initial Thickness	Source	Time	Result	Thickness Remaining
1	3.216 μm	No Exposure (with initiator)	-	Dissolved	0 μm
2	3.237 μm	No Exposure (no initiator)	-	Dissolved	0 μm
3	3.216 μm	365 nm	16 min	Dissolved	0 μm
4	3.216 μm	Dental Lamp (470 nm LED)	10 min	Delamination	0 μm
5	3.216 μm	Visible	10 min	Delamination	0 μm
6	3.216 μm	Novacure (w/ 436 nm filter)	2 min	Delamination	0 μm
7	3.216 μm	Novacure (broad band)	1.5 min	Film Remains	3.187 μm
8	3.237 μm	Novacure (no initiator)	1.5 min	Film Remains	3.201 μm

Table 6.2: Exposure conditions attempted to cross-link films of polymer **6.21**. Samples prepared by spin coating on silicon wafers with a post application bake for 1 min at 90 °C and developed in cyclopentanone for 30 sec. All samples contained 2 wt% Irgacure 784 (Ciba) except where noted.

Two control experiments (Table 6.2, entries 1-2) were performed by casting polymer films with and without photoinitiator, and both films dissolved within seconds in cyclopentanone. These controls were necessary to show that the reactive groups did not cross-link during spin casting, post application baking, or due to the incorporation of the Irgacure itself. Next, three visible sources and a 365 nm UV source were tested (Table 6.2 entries 3-6). To our surprise, none of these sources were able to successfully cross-link the films. Observation revealed that as the films were lowered into the developer swelling and delamination from their silicon substrates occurred rather than dissolution. After lift off, the films quickly dissolved suggesting that the films had undergone cross-linking but to a negligible extent. Using the EXFO Novacure® exposure tool with no cutoff filter (broad band) (Table 6.2 entry 7), rendered the film completely insoluble in

the developer solution. A similar film was irradiated under identical conditions but without the incorporation of the Irgacure (Table 6.2 entry 8). This film was also rendered insoluble despite the omission of photoinitiator suggesting that our system could self initiate under high intensities of irradiation. To make sure that this self initiation did not destroy the NLO chromophores, FT-IR studies were used to determine whether any tolane degradation was occurring. Studies utilizing the C-C triple bond stretch showed that even after 2 min of irradiation that 5% of the alkynes were affected, a number we felt was acceptable given that no photoinitiator was needed.
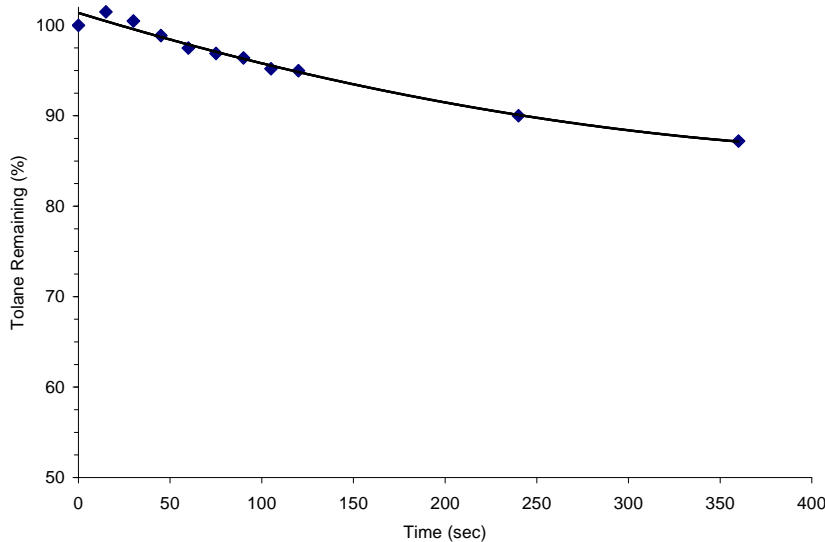
Figure 6.9: Tolane decomposition with increasing exposure time.

After curing conditions were found, we wanted to test if the cross-linkable films could be patterned in a fashion similar to a negative-tone photoresist. Using an optical grating mask, which allows various percentages of irradiation to pass through, and cyclopentanone as a developer, it was found that biscross-linkable film **6.21** could be patterned using the Novacure exposure tool (Figure 6.10), and the film cross-linked

sufficiently at 14% transparency to resist development. Further analysis using an optical microscope showed that even finer image detail was resolved at the higher doses, but swollen by the organic developer. This is a promising discovery, and its usefulness is currently being examined within the Willson Labs.
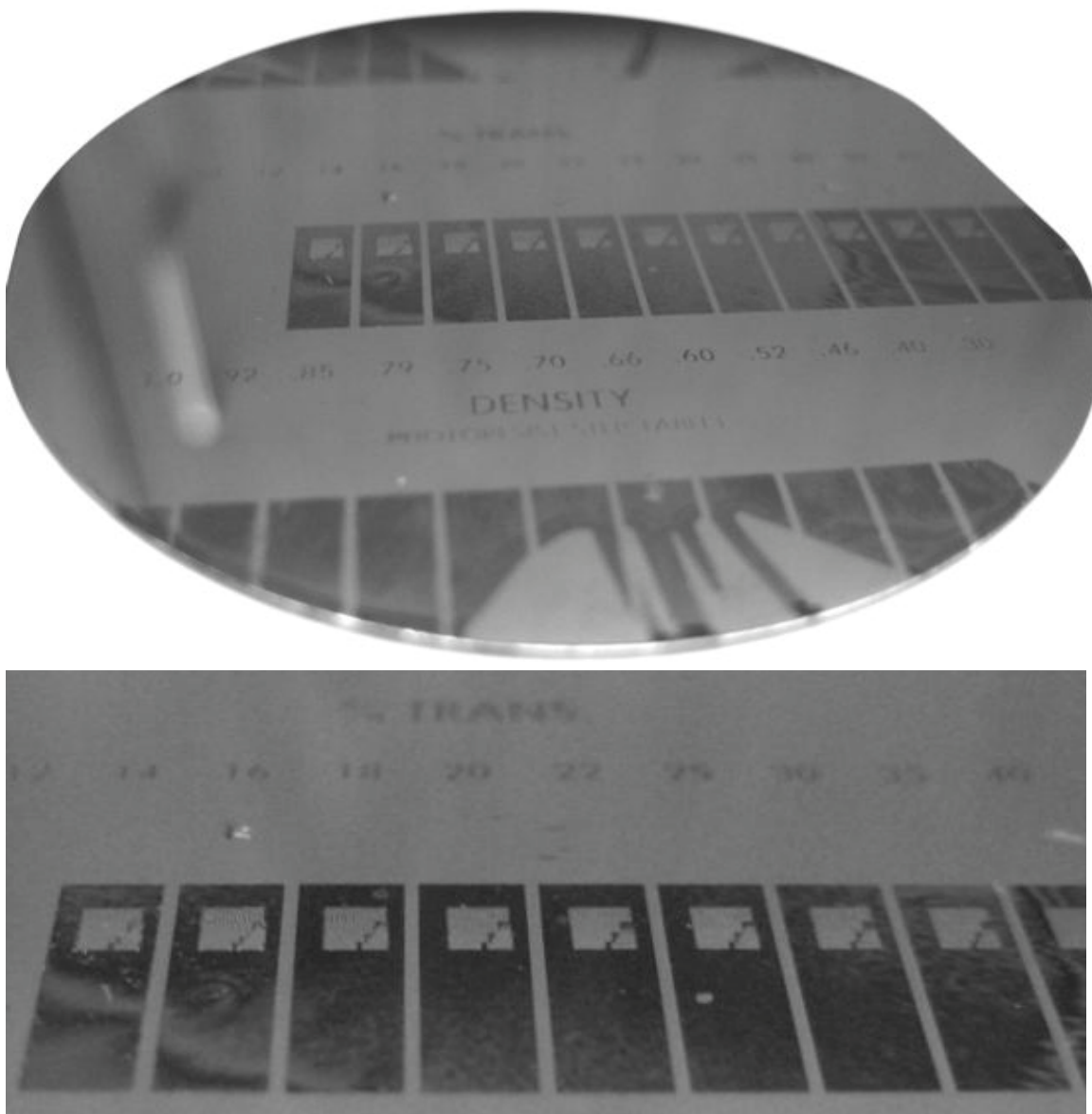
Figure 6.10: Patterning using biscross-linkable polymer **6.21**.

Poling and NLO Activity

Electrode contact poling was chosen for our experiments as it is the most widely utilized and is easily performed without complicated instrumentation. The major drawback to this technique is that extremely high quality films must be produced to prevent short circuiting. The first solvents tested were chloro- and dichlorobenzene. All three polymers showed excellent solubility in these aromatic solvents and on small silicon wafer samples, produced decent films. Further experiments on ITO coated glass slides revealed that the polymer precipitated out of the casting solvent during spin casting causing film defects that produced shorts between the electrodes. Many solvents were then screened ultimately leading to the use of cyclopentanone. Cyclopentanone exhibited even greater polymer solubility than dichlorobenzene, was able to dissolve large amounts of photoinitiator (Irgacure 784) if needed, and produced pristine films on silicon wafers and ITO surfaces.

Poling samples were produced as shown in Figure 6.11 by first etching the ITO back from a slide edge using HCl. This was done to prevent possible short circuits from the ITO edge to the deposited gold keyhole-shaped electrode. Next, polymer films were spin coated from 15 wt% solutions in cyclopentanone at 1500 rpm to produce films 3.2-3.3 μm thick. Gold keyhole shaped electrodes were then deposited via sputter coating using a shadow mask. Finally wires were attached to the gold and ITO electrodes using silver paste after a small section of polymer film was removed by simply scrapping with a razor blade (Figure 6.11). The samples could be used as entire slides or cut into smaller pieces that were easier to work with.
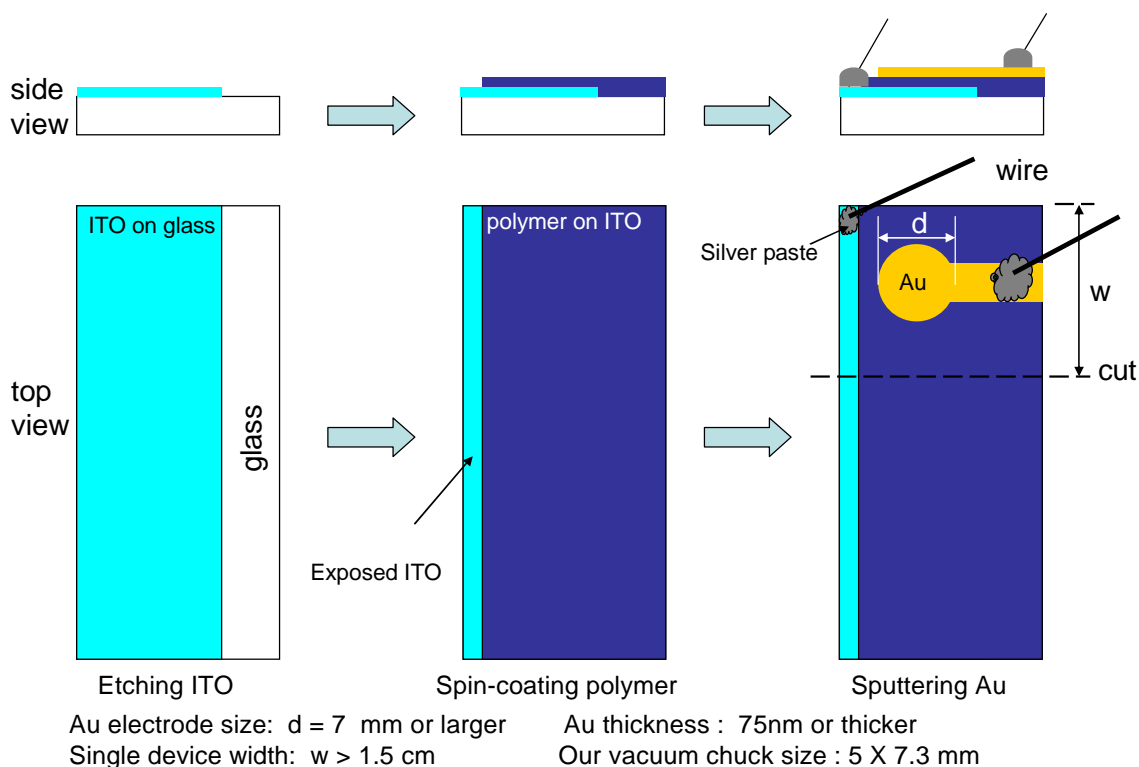
Figure 6.11: Sample preparation for electrode contact poling.

The poling process was performed via a step-wise method as outlined in Figure 6.12. In step one, the voltage was ramped up to 130 V so that as soon as heating began, the chromophores would begin to align. Step two ramped the temperature of the poling apparatus to ~10 °C below the T_g of the polymer film. During step three the voltage was raised to the final poling voltage desired (here 200 V) (typically 50-100 V per µm). Step four consisted of raising the temperature to just below the T_g obtained from DSC analysis. Samples that were photochemically cross-linkable were irradiated through the glass/ITO slide using the Novacure at its maximum power setting for 2 min during stage five. Stage six consisted of maintaining voltage while the temperature was dropped below the T_g. Finally, in stage seven the film was cooled to room temp.

124
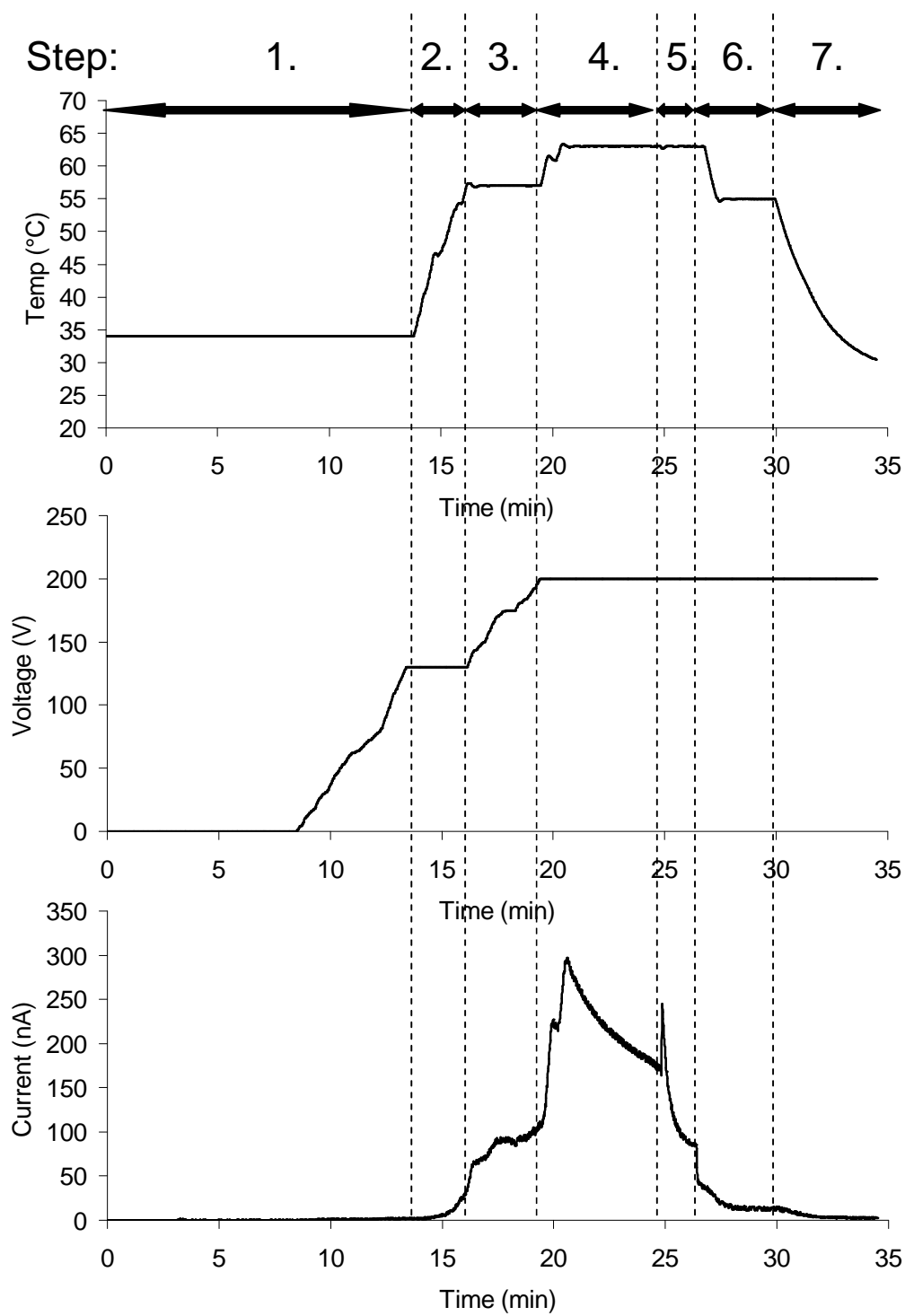
Figure 6.12: Poling conditions including temperature (top), voltage (middle), and current (bottom) for biscross-linkable polymer **6.21**.

125

After poling, the wires were removed from the sample and the gold electrode was washed away by rinsing with a solution of iodine and potassium iodide in water (wt ratio of 1:4:40, I_2:KI:H_2O). The top electrode was removed so the material's SHG coefficient and thermal stability could be determined by the Maker fringe technique (Figure 6.13). To perform Maker fringe experiments, the sample was positioned in the path of a lightly focused, fundamental beam produced by a diode-pumped Q-switched 1.31 μm laser. The pulse width was 14 ns and the repetition rate was 750 Hz. The fundamental beam was p-polarized, and after passing through the sample, the p-polarized component of the Second Harmonic output was detected by a Hamamatsu R928 photomultiplier tube (PMT) in conjunction with a Stanford Research SR250 boxcar averager. To account for laser power fluctuations, the fundamental beam was split off using a cover slip and sent through a potassium dihydrogen phosphate (KDP) crystal to produce a second-harmonic reference signal. The sample was mounted on a computer-controlled Oriel rotation stage that was temperature controlled and data were collected, by computer at 1-2° increments of the angle of incidence.
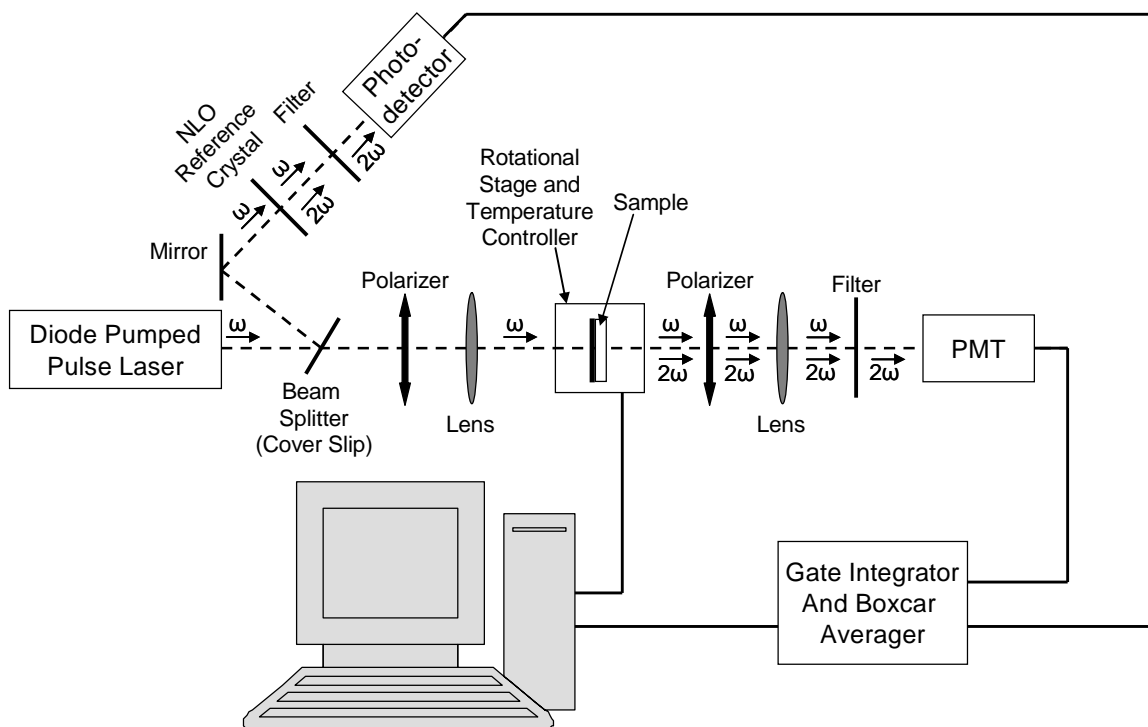
Figure 6.13: Schematic of Maker fringe experimental setup to obtain SHG coefficients (PMT = photomultiplier tube). For the experiments reported herein $\lambda = 1.31$ μm, the laser pulse width is 14 ns at 750 Hz, and the NLO reference crystal is potassium dihydrogen phosphate (KDP).

The data collected from the Maker fringe experiment can be seen in Figure 6.14 along with that from a reference sample of quartz, which is known to exhibit SHG.[273] Due to the tri-layer film stack composed of glass, ITO, and NLO polymer, the data is somewhat complicated due to the presence of multiple reflections arising at the material interfaces. The analysis of these data required subtraction of the reflection effects as outlined by Herman *et al*.[274] It should be noted here that the slight asymmetry of the SHG intensity pattern relative to angle is an artifact of slight misalignment of the sample in the beam path. Efficiencies of 2 pm/v were recorded in our first experiments with polymer **6.21**.
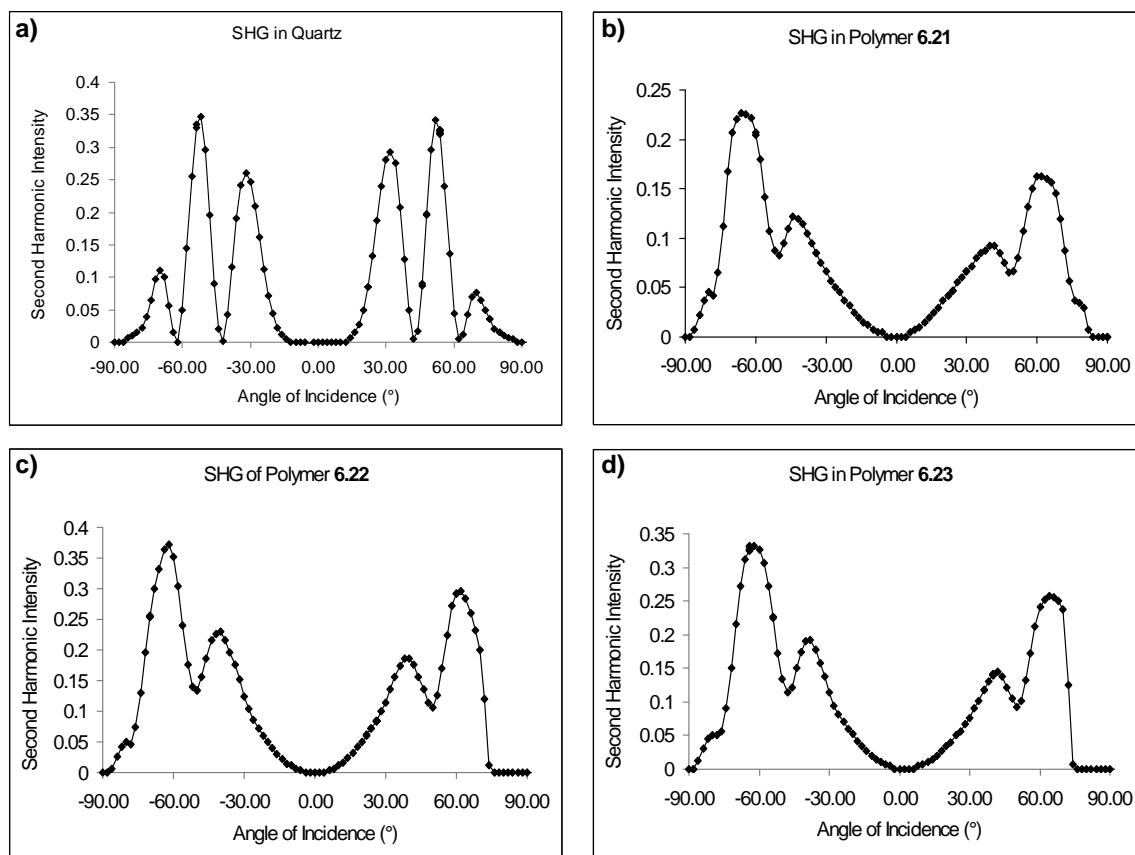
Figure 6.14: SHG in a) quartz and polymers b) **6.21**, c) **6.22**, and d) **6.23**.

Temporal Stability

Maker fringe was used in conjunction with a heated sample stage to study the temporal stability of polymers **6.21**, **6.22**, and **6.23**. By heating a sample on the rotational stage, it was possible to determine stability either by ramping the temperature slowly and plotting SHG intensity versus temperature or by holding it at a constant elevated temperature and plotting SHG intensity versus time. Since the latter can often require weeks or months to complete depending on the temperature chosen, the ramping method was used herein. The sample was aligned in the beam path and rotated to an angle where maximum SHG intensity was observed. In early attempts, the temporal stabilities of all

128

three polymers including "cross-linked" samples of poled polymers **6.21** and **6.22** were obtained (Figure 6.15). Unexposed samples of polymers **6.21**, **6.22**, and **6.23** all decayed rapidly as their T_g was reached. The slight tails in the data for monocross-linkable **6.22** and biscross-linkable **6.21** hint that at elevated temperatures, slight thermally initiated cross-linking may have begun to occur. Exposed samples of bis- and monocross-linkable polymers showed enhanced stability relative to unexposed films.
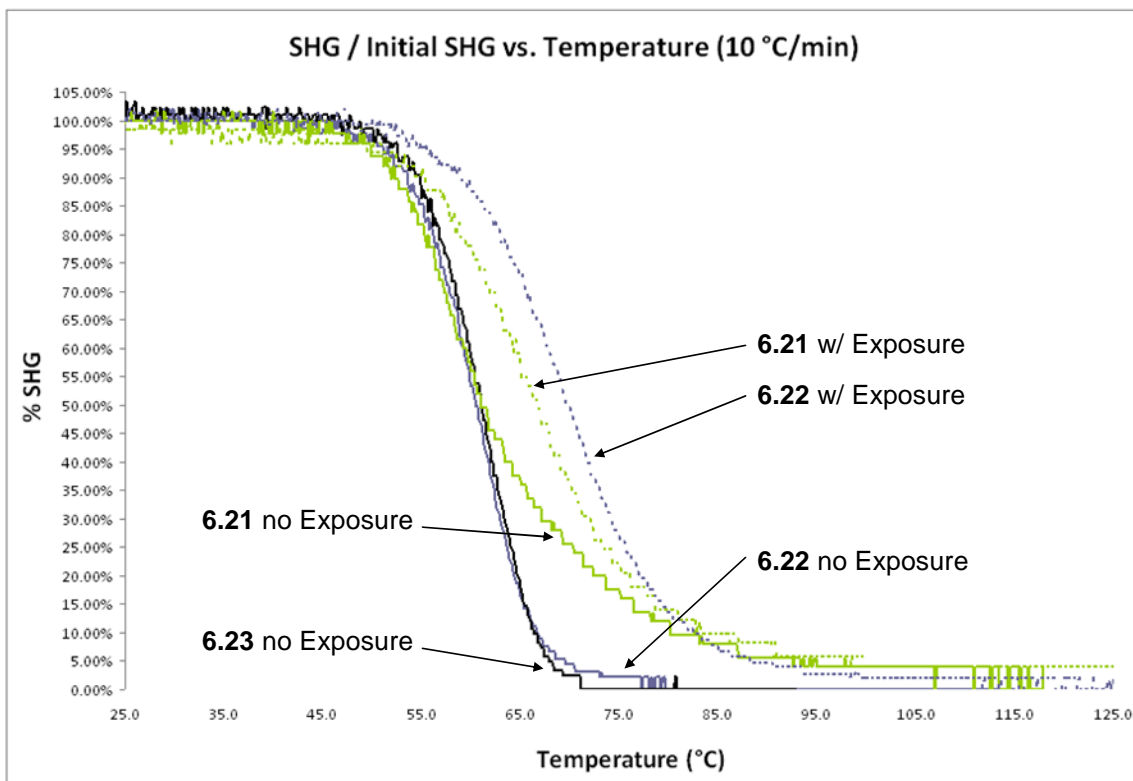
Figure 6.15: Temporal stability of normalized SHG signals versus heating at 10 °C/min.

Although enhanced stabilities were observed in both cross-linked samples (5-10 °C), the results were not as dramatic as had been hoped. Our interpretation of these data suggests that the cross-linking conversions achieved were extremely low. It is expected the conversion may be dramatically increased by increasing the sample temperature,

including a photoinitiator, by adding a reactive additive (chain transfer agent), or some combination of the three.[275,276]

CONCLUSIONS

Three multi-functional monomers and there corresponding linear polymers were successfully synthesized. Spin coating conditions were found that provided the virtually defect free films required for electrode contact poling. The photoinitiation of cross-linkable polymers **6.21** and **6.22** was found to proceed with or without the incorporation of photoinitiator using a Novacure exposure tool (broad band). The samples were photopatterned by irradiation through a photomask. Thin-film samples of all three polymers were successfully coated onto ITO substrates, gold electrodes were deposited, and individual poling procedures were developed. Upon completion of poling, the samples were irradiated through the glass substrate to photochemically cross-link the reactive methacrylate groups. Maker fringe was used to determine SHG coefficients and temporal stabilities. The results suggest that even though some cross-linking did occur, it was to a minor extent and that further improvements in the cross-linking efficiency needs to be made.

Appendix A: Progress toward Functionalized NLO Acceptors

INTRODUCTION

Although many papers may be found concerning donor design, the majority of research has focused on acceptor functionalities. This is partially due to their synthetic ease, but also to the fact that the optimization of their electron-withdrawing capabilities has a greater impact on individual molecular dipole moment. This is attributed to the fact that it is much easier to remove electron density from an already electron rich aryl π-system than it is to donate extra electron density into that same system.

As can be seen in Figure 5.8, a large variety of acceptors have been developed in recent literature. Many have extreme electron-withdrawing properties, but most do not have a functional handle to which a polymerizable group may be attached. This polymerizable group is necessary for our chromophore design and has presented us with an interesting set of synthetic challenges. The four groups of interest are shown in Figure A.1 as they are all known to be strongly electron-withdrawing groups. Tetracyanoindane (TCI) (Figure A.1b), tricyanofuran (TCF) (Figure A.1c), and dicyanoarylsulfone (DCAS) (Figure A.1d) acceptors all require modification of their synthetic routes to accommodate additional functionality, but tricyanopyrroline (TCP) (Figure A.1a) acceptors are attractive as they inherently have a functionalizable amide moiety.[277,278,279] The proposed structures are summarized in Figure A.2 and progress toward their synthesis will be discussed herein.
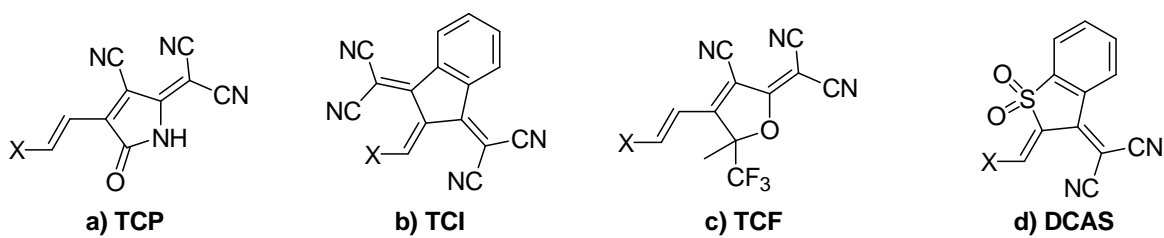
Figure A.1: Acceptors of interest reported in literature.
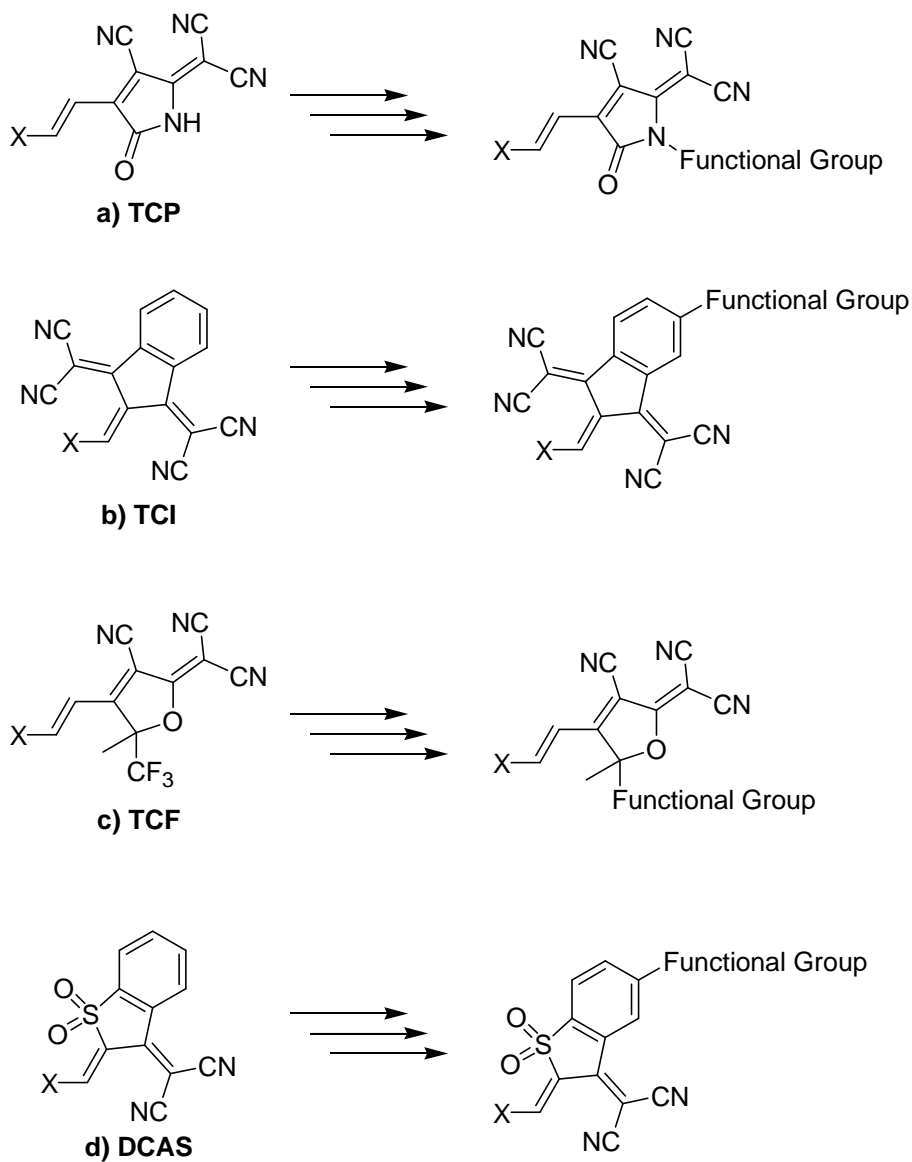
Figure A.2: Envisioned acceptors with pendant functionality.

132

TCP ACCEPTOR

TCP type acceptors were attractive in that the functionalization of the pyrroline nitrogen with strongly electrophilic reagents, such as diethyl sulfate, was established in the literature.[279] Compound **A.3** is known to readily self-condense in solution giving rise to extremely low yields (10%) and are hence usually ran in a one-pot fashion. Following literature procedure, compound **A.3** was formed by refluxing the dimmer of malonitrile (A.1) and ethyl pyruvate (A.2) in ethanol for 1 hr before 4-bromobenzaldehyde was added and refluxed for an additional 3 hr (Scheme A.1). The reaction mixture was reduced *in vacuo* and found to give an extremely complex mixture of products by thin-layer chromatography (TLC). Several products were isolated by column chromatography, but none were the desired compound **A.4**. This route is still being explored and if successful will be reacted with 5-norbornene-2-carboxylic acid to produce polymerizable acceptor **A.5**.
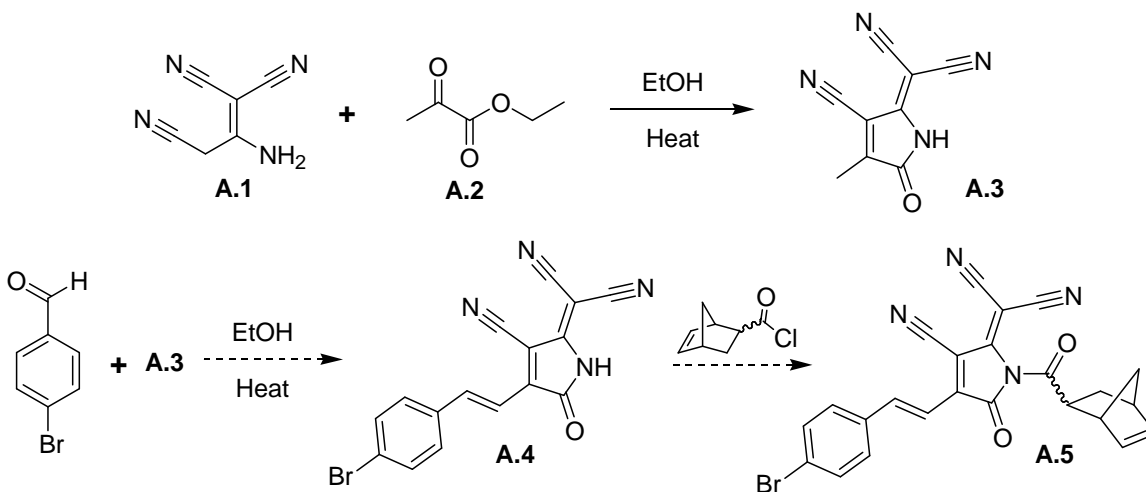
Scheme A.1: Attempted synthesis of TCP type acceptor **A.5**.

TCI ACCEPTOR

TCI type acceptors are well known to the dye industry for their use as methine dyes, and were eventually utilized in the field of nonlinear optics.[280,281] Scheme A.2 shows the known literature procedure to synthesize compounds **A.7** and **A.8**, but unlike TCP acceptors, TCI compounds do not have a functional handle by which a polymerizable group may be attached, therefore requiring a new synthetic route. Phthalic anhydride was brominated using Br_2 and NaOH to yield the monosodium bromophthalic acid salt **A.10** (Scheme A.3).[282] The anhydride was reformed by refluxing in $SOCl_2$ and then transformed into the indanedione derivative **A.12** using ethyl acetoacetate, acetic anhydride, and pyridine.[283] Numerous attempts were made to synthesize **A.13** via double Knoevenagel condensation, but no product was ever isolated. The reason compound **A.13** was unable to be formed is still a mystery.
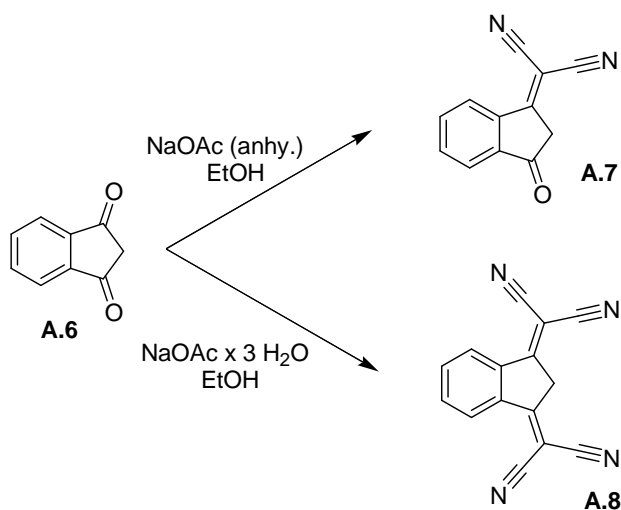
Scheme A.2: Literature methods of making di- and tetracyanoindane derivatives **A.7** and **A.8**.[280]
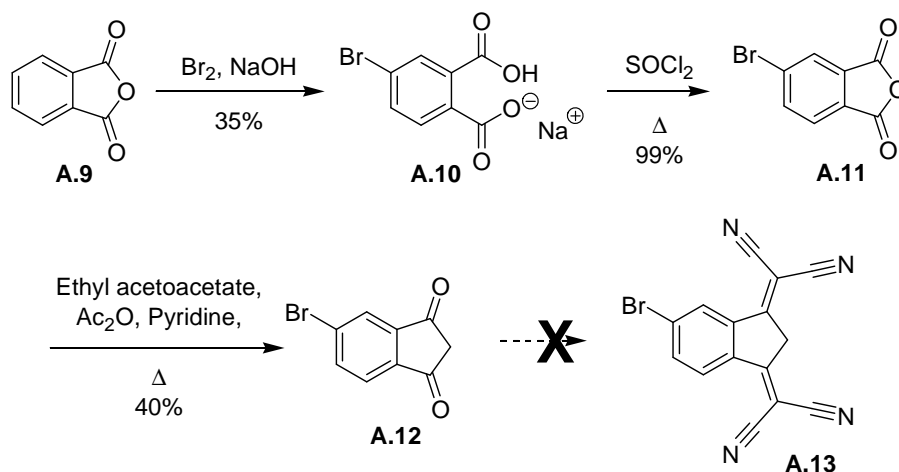
Scheme A.3: Attempted synthesis of the tetracyanoindane acceptor **A.13**.

TCF ACCEPTOR

An alcohol functionalized TCF acceptor such as the one shown in Figure A.2 has been used in the literature, however, its synthesis was not reported.[284,285] TCF type compounds are typically synthesized by the addition of the anion of ethylvinyl ether to methyl ketone compounds.[279] Our attempt to produce compound **A.14** was successful but in a disappointing yield.

An alternate route to alkene functionalized α-hydroxy ketone compounds was reported using indium promoted addition of allyl bromide to 2,3-butanedione.[286,287] When set up as reported, an inseparable mixture of mono- and bis-addition products were produced. To modify the procedure, two equivalents of 2,3-butanedione was used and found to produce greater than 95% of the mono-addition product **A.15** in 90% yield (Scheme A.4). Compound **A.15** was cyclized to form tricyano compound **A.16** in a three-step, one-pot reaction that consisted of a Knoevenagel condensation, intramolecular attack of a nitrile by the formed alkoxide, and finally another Knoevenagel condensation.[279,288] Compound **A.16** was found to readily condense with 4-

bromobenzaldehyde using catalytic glycine and microwave irradiation at 30 W for 30 min. The resultant compound **A.17** crystalized from an ethanol solution, and its structure was confirmed by X-ray crystallographic analysis (Figure A.3). Its highly planar structure is visible in the ball-and-stick model and is indicative of its strong electronic communication.
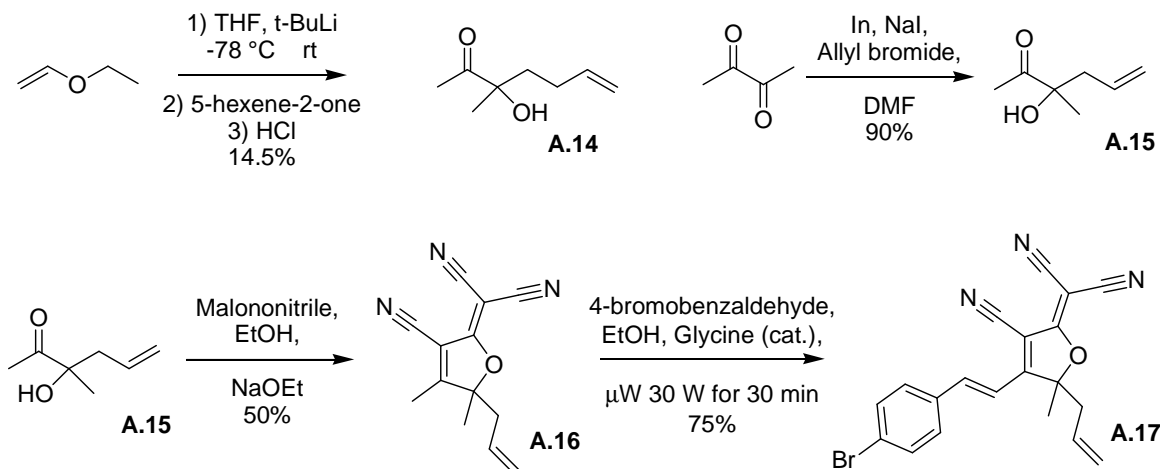
Scheme A.4: Synthesis of alkene substituted TCF acceptor **A.17**.
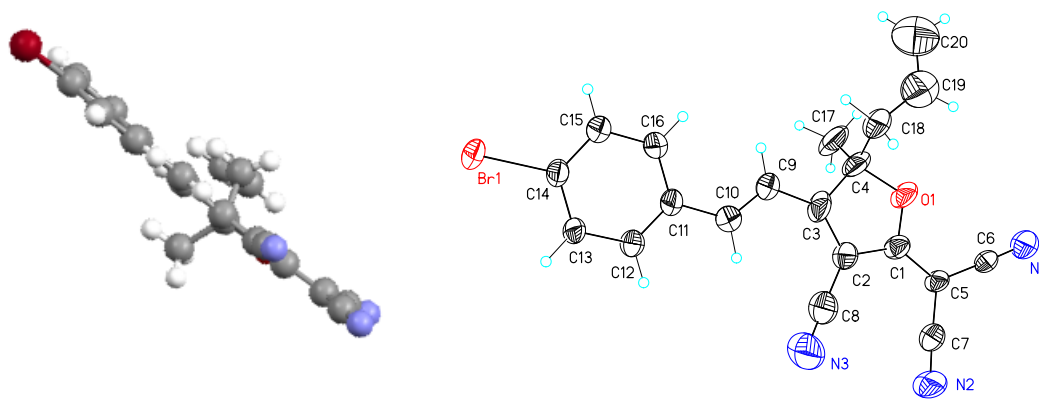
Figure A.3: Crystal structure of TFC type acceptor **A.17**.

The remaining obstacle was the functionalization of the terminal olefin in compounds **A.15** and **A.16**. Hydroboration using dicyclohexyl borane or B_2H_6 and various oxidants yielded complex mixtures of products for **A.16**, and in the case of **A.15**, reduction of the ketone to produce the diol compound **A.18** (Scheme A.5). To avoid the problematic alkene oxidation, the use of cross-metathesis was explored using Grubbs 2nd generation catalyst and 1,4-diacetoxy-2-butene. This led to a complex mixture that consisted mainly of the homo-metathesis product when **A.15** was used, but when compound **A.16** was used, it produced the functionalized TCF compound **A.19** in a disappointing 10% yield. Another route investigated was the use of the thiol-ene reaction. Reaction of compound **A.15** with mercaptoethanol and catalytic benzophenone produced **A.19** in 80% yield. Using similar conditions, reaction with compound **A.16** showed no reaction. Early attempts to cyclize **A.19** have been promising but yields have been quite low.
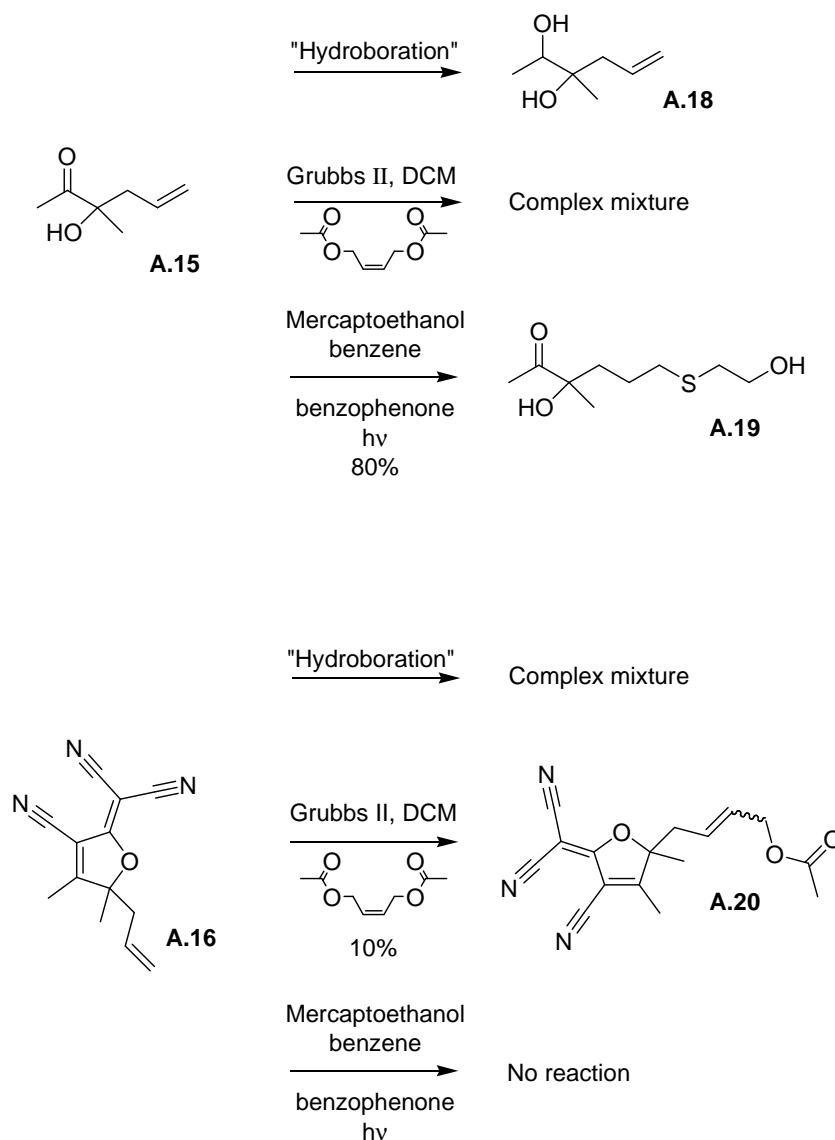
Scheme A.5: Attempts to functionalize the terminal alkene of compounds **A.15** and **A.16**.

To avoid functionalization of the terminal alkenes, an alternate route was designed in which the TBS protected compound **A.22** was reacted with ethynylmagnesium bromide to produce alkynyl compound **A.23** in 58% yield (Scheme A.6). Attempts to produce compound **A.24** through various oxymercuration conditions

138

were unsuccessful. Despite the synthetic hurdles encountered, functionalized TCFs are still an area of great interest to our group and their synthesis is currently being pursued.
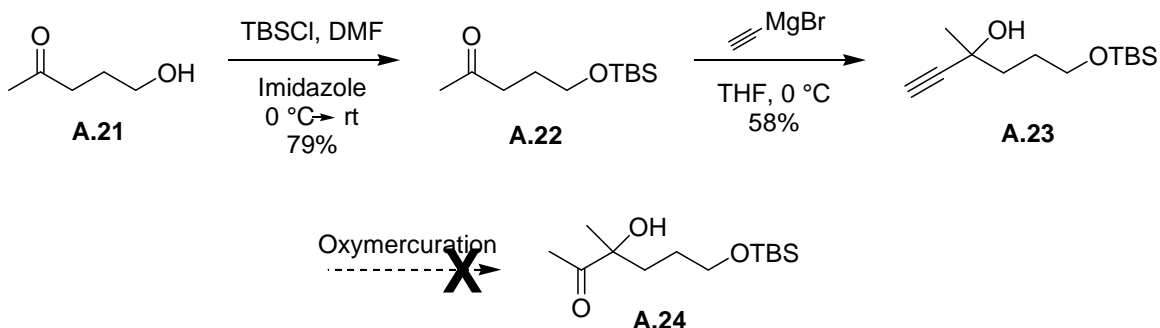
Scheme A.6: Alternate route to α-hydroxy ketones.

DCAS ACCEPTOR

Dicyanoarylsulfones are another attractive target due to their strong electron-withdrawing properties. We designed a synthetic route that centered around the S$_N$Ar reaction of thiols with nitrobenzoates reported by Kondoh *et al.*[289] The commercially available aniline **A.25** was oxidized to the corresponding nitro compound (**A.26**) using *m*-chloroperbenzoic acid (mCPBA) (Scheme A.7). To test the feasibility of nucleophilic aromatic substitution on this compound, 1.2 equivalents of ethanethiol (methanethiol was ordered but not available at this time) was added in the presence of K$_2$CO$_3$ and DMSO. To our surprise, a 60% yield of compound **A.27** was recovered along with 40% starting material. This result suggested that coupling of the bromide should precede substitution in the overall reaction scheme. Propargyl alcohol was protected as its *t*-butyldimethylsilyl (TBS) ether analogue (**A.28**) and was coupled to the aryl bromide compound **A.26** using classic Sonogashira conditions. Nucleophilic aromatic substitution of the nitro group using ethanethiol produced the thioether compound **A.30** in 71% yield. To remove the

unnecessary alkyne functionality, a diimide reduction was utilized to produce **A.31** in good yields. Once methanethiol arrived was obtained, a similar procedure was used to produce the methyl thioether analogue of **A.30**. As methanthiol is gaseous at room temperature, an excess was used and the isolated product was determined to be the double Michael addition product **A.32**. This was unexpected as ethanethiol had added cleanly to **A.29**. To avoid this additional functionalization, diimide reduction of **A.29** produced **A.33** in 62% yield, and S_NAr displacement of the nitro-group using excess methanethiol gas produced **A.34**. This synthetic pathway is currently under investigation within our group.
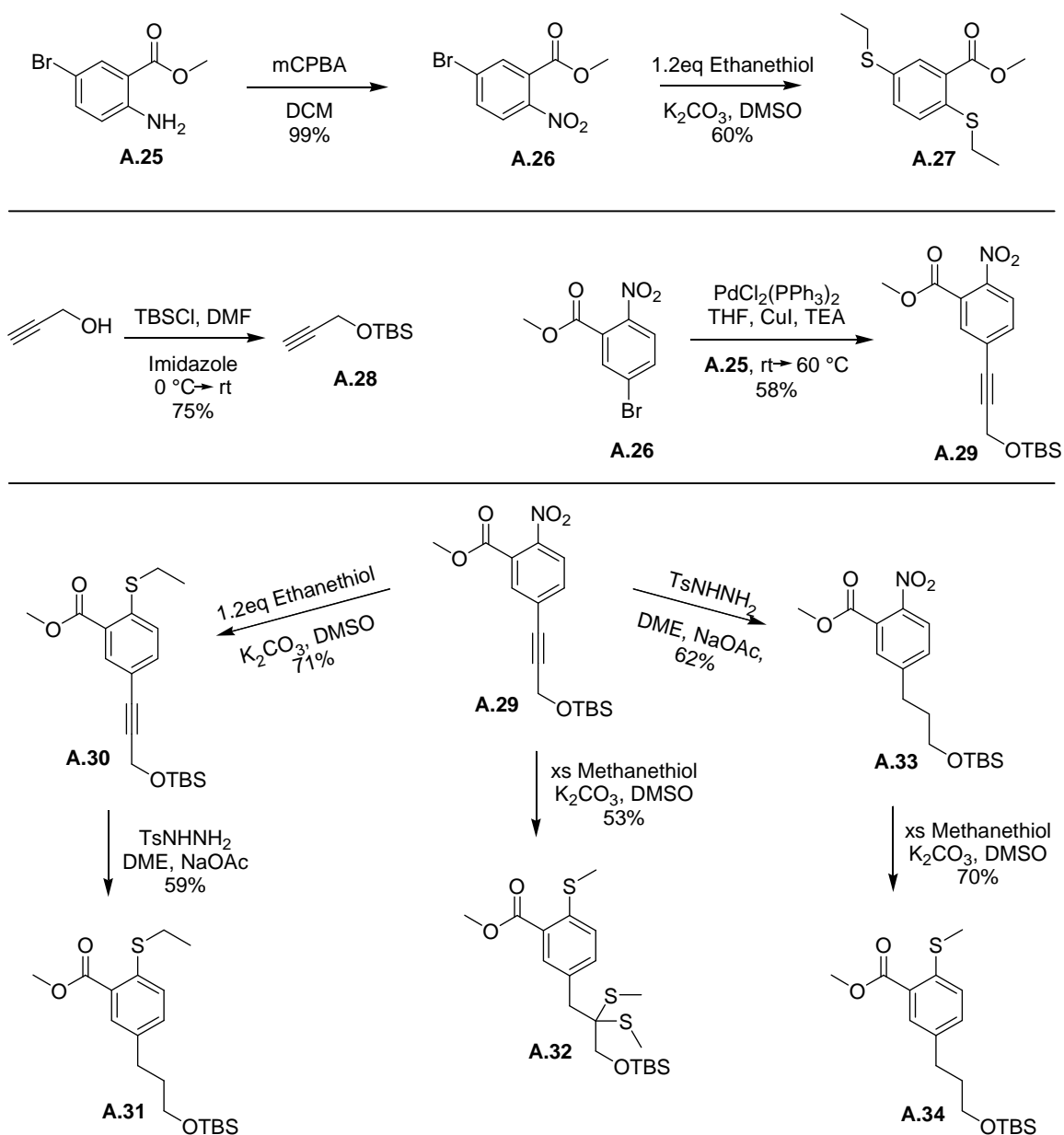
Scheme A.7: Synthesis of DCAS precursor **A.31**.

CONCLUSION

All routes to the described acceptor compounds, with the exception of the TCI derivative, are ongoing projects within our group. The TCI compound is no longer pursued as molecular modeling suggested that the cyano groups are bent out of plane of

the π-system due to steric interactions with the proposed aryl moieties once connected to a NLO chromophore. TCP type acceptors proved difficult to handle as they readily condensed with themselves in solution, while TCF type acceptors are being extensively investigated, focusing mainly on the functionalization of the terminal alkene. Lastly, the DCAS type acceptor has been met with a few synthetic difficulties but have all been circumvented through changing the reaction order.

Appendix B: Crystal Structures

Figure B.1: ORTEP diagram of the bisphenylcarbamate of *trans*-diol **2.8**.
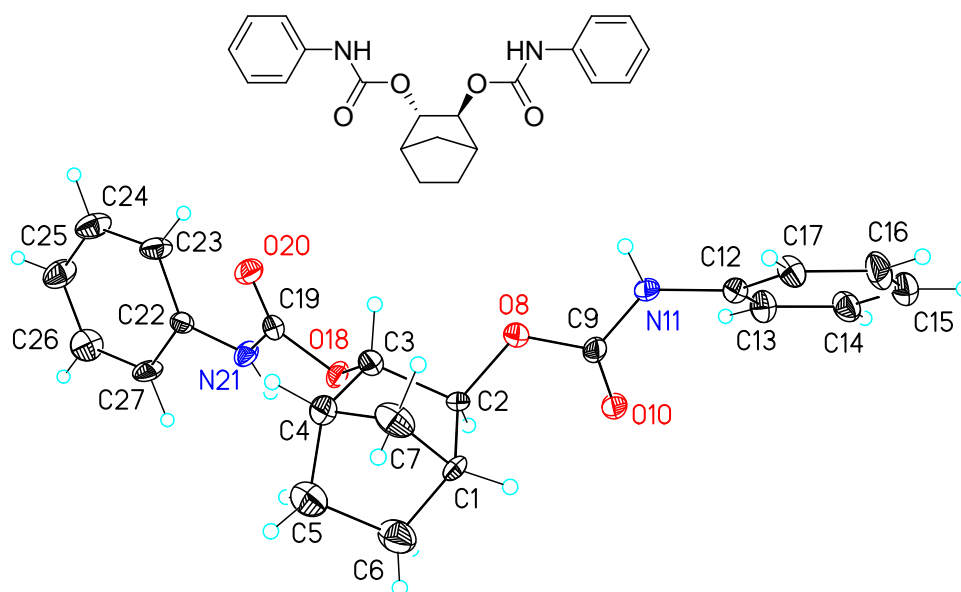
X-ray Experimental for C₂₁H₂₂N₂O₂: Crystals grew as colorless plates by slow evaporation. The data crystal was cut from a larger crystal and had approximate dimensions; 0.52 x 0.21 x 0.04 mm. The data were collected on a Nonius Kappa CCD diffractometer using a graphite monochromator with MoKα radiation ($\lambda = 0.71073$Å). A total of 168 frames of data were collected using ω-scans with a scan range of 1° and a counting time of 75 seconds per frame. The data were collected at 153 K using an Oxford Cryostream low temperature device. Details of crystal data, data collection and structure refinement are listed in Table B.1. Data reduction was performed using DENZO-SMN.[290] The structure was solved by direct methods using SIR97[291] and refined by full-matrix least-squares on F^2 with anisotropic displacement parameters for

the non-H atoms using SHELXL-97.[292] The hydrogen atoms on carbon were calculated in ideal positions with isotropic displacement parameters set to 1.2xUeq of the attached atom (1.5xUeq for methyl hydrogen atoms). The function, $\Sigma w(|F_o|^2 - |F_c|^2)^2$, was minimized, where $w = 1/[(\sigma(F_o))^2 + (0.02*P)^2]$ and $P = (|F_o|^2 + 2|F_c|^2)/3$. $R_w(F^2)$ refined to 0.138, with R(F) equal to 0.0733 and a goodness of fit, S, = 1.09. Definitions used for calculating R(F), $R_w(F^2)$ and the goodness of fit, S, are given below.[293] The data were corrected for secondary extinction effects. The correction takes the form: $F_{corr} = kF_c/[1 + (6.1(7)x10^{-7})* F_c^2 \lambda^3/(sin2\theta)]^{0.25}$ where k is the overall scale factor. Neutral atom scattering factors and values used to calculate the linear absorption coefficient are from the International Tables for X-ray Crystallography (1992).[294] All figures were generated using SHELXTL/PC.[295] Tables of positional and thermal parameters, bond lengths and angles, torsion angles, H-bonding interactions, figures and lists of observed and calculated structure factors are located in Tables B.1 through B.2.

Table B.1: Crystal data and structure refinement for the bisphenylcarbamate of *trans*-diol **2.8**.

Empirical formula	C42 H44 N4 O8
Formula weight	732.81
Temperature	153(2) K
Wavelength	0.71073 Å
Crystal system	Monoclinic
Space group	C2/c
Unit cell dimensions	a = 36.105(2) Å α= 90°.
	b = 9.5750(6) Å β= 118.320(3)°.
	c = 24.620(2) Å γ = 90°.
Volume	7492.6(9) Å^3
Z	8
Density (calculated)	1.299 Mg/m^3

Absorption coefficient	0.091 mm^{-1}	
F(000)	3104	
Crystal size	0.52 x 0.21 x 0.04 mm	
Theta range for data collection	3.10 to 22.48°.	
Index ranges	-38<=h<=38, -10<=k<=9, -26<=l<=26	
Reflections collected	8708	
Independent reflections	4862 [R(int) = 0.1330]	
Completeness to theta = 22.48°	99.2 %	
Absorption correction	None	
Refinement method	Full-matrix least-squares on F^2	
Data / restraints / parameters	4862 / 0 / 488	
Goodness-of-fit on F^2	1.094	
Final R indices [I>2sigma(I)]	R1 = 0.0733, wR2 = 0.1092	
R indices (all data)	R1 = 0.1912, wR2 = 0.1375	
Extinction coefficient	0.00061(7)	
Largest diff. peak and hole	0.283 and -0.286 e.Å^{-3}	

Table B.2: Atomic coordinates (x 104) and equivalent isotropic displacement
parameters (Å2x 103) for the bisphenylcarbamate of compound **2.8**. U(eq)
is defined as one third of the trace of the orthogonalized Uij tensor.

	x	y	z	U(eq)
C1'	1422(2)	-2501(6)	4881(2)	40(2)
C2'	1258(1)	-2870(6)	4196(2)	31(2)
C3'	1584(2)	-2214(6)	4038(2)	32(1)
C4'	1914(2)	-1635(7)	4663(2)	41(2)
C5'	1721(2)	-337(7)	4787(2)	50(2)
C6'	1387(2)	-918(7)	4943(3)	51(2)
C7'	1897(2)	-2683(6)	5122(2)	42(2)
O8'	855(1)	-2254(4)	3787(1)	35(1)

C9'	509(2)	-2813(7)	3784(2)	34(2)
O10'	505(1)	-3900(5)	4028(2)	39(1)
N11'	187(1)	-1904(5)	3490(2)	39(1)
C12'	-233(2)	-2059(6)	3399(3)	34(2)
C13'	-558(2)	-1563(6)	2864(2)	44(2)
C14'	-960(2)	-1631(8)	2768(3)	61(2)
C15'	-1050(2)	-2203(8)	3196(4)	68(2)
C16'	-723(2)	-2702(7)	3746(3)	62(2)
C17'	-308(2)	-2643(6)	3849(3)	45(2)
O18'	1763(1)	-3356(4)	3844(2)	34(1)
C19'	1986(2)	-2954(7)	3556(2)	35(2)
O20'	1992(1)	-1765(4)	3383(2)	34(1)
N21'	2184(1)	-4073(5)	3484(2)	33(1)
C22'	2484(2)	-4043(7)	3263(2)	31(2)
C23'	2769(2)	-5139(7)	3458(2)	42(2)
C24'	3081(2)	-5170(8)	3281(3)	60(2)
C25'	3106(2)	-4135(8)	2908(3)	61(2)
C26'	2815(2)	-3088(8)	2726(3)	59(2)
C27'	2499(2)	-3018(7)	2890(2)	45(2)
C1	1250(2)	3504(7)	2704(2)	44(2)
C2	1350(1)	2880(6)	3339(2)	31(2)
C3	926(1)	2232(6)	3215(2)	35(2)
C4	630(2)	2572(7)	2534(2)	41(2)
C5	544(2)	4116(7)	2472(2)	56(2)
C6	966(2)	4737(7)	2605(3)	61(2)
C7	928(2)	2373(6)	2257(2)	48(2)
O8	1646(1)	1726(4)	3496(1)	35(1)
C9	2057(2)	2099(8)	3795(2)	31(2)
O10	2187(1)	3248(5)	4000(2)	38(1)
N11	2299(1)	984(5)	3830(2)	34(1)
C12	2746(2)	1046(6)	4073(2)	30(2)
C13	2993(2)	1689(7)	4629(2)	39(2)
C14	3426(2)	1725(7)	4850(2)	43(2)

146

C15	3606(2)	1101(7)	4528(3)	48(2)
C16	3353(2)	444(7)	3980(3)	49(2)
C17	2921(2)	414(6)	3747(2)	38(2)
O18	804(1)	2858(4)	3641(1)	32(1)
C19	499(2)	2157(7)	3712(2)	32(2)
O20	371(1)	1011(5)	3499(2)	39(1)
N21	378(1)	2969(5)	4046(2)	32(1)
C22	56(2)	2615(6)	4203(2)	29(2)
C23	-59(2)	1263(7)	4236(2)	42(2)
C24	-385(2)	1027(7)	4375(2)	51(2)
C25	-584(2)	2102(8)	4493(2)	51(2)
C26	-460(2)	3457(8)	4477(2)	52(2)
C27	-137(2)	3733(6)	4334(2)	40(2)

Figure B.2: ORTEP diagram of compound **2.16**.

2.16
(+/-)
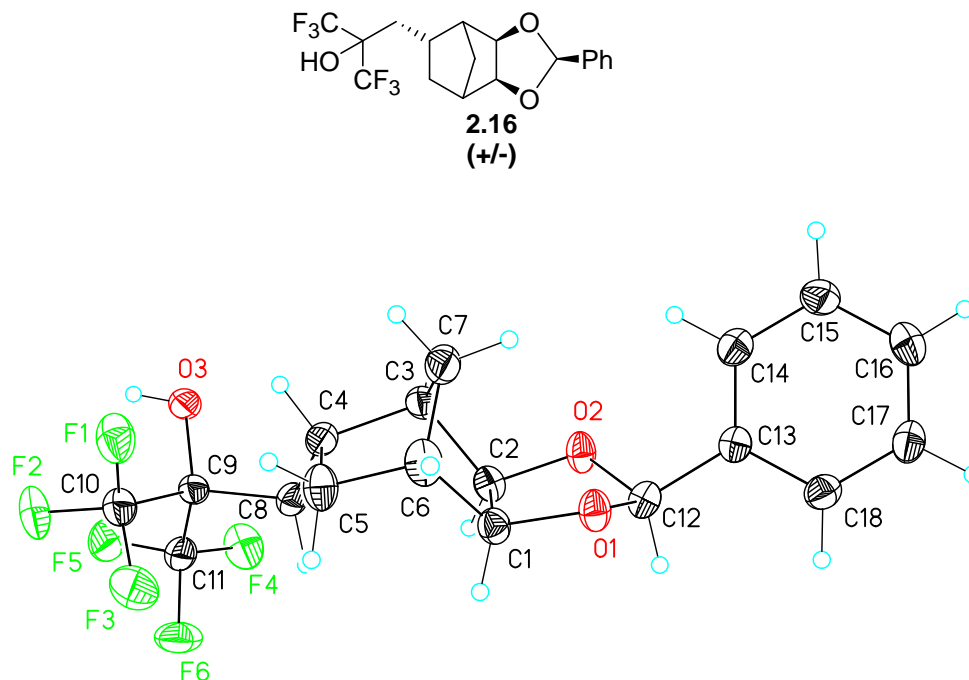
X-ray Experimental for C₁₈H₁₈F₆O₃: Crystals grew colorless prisms by slow evaporation. The data crystal was cut from a larger crystal and had approximate dimensions; 0.34 x 0.27 x 0.13 mm. The data were collected on a Nonius Kappa CCD diffractometer using a graphite monochromator with MoKα radiation (λ = 0.71073Å). A total of 279X frames of data were collected using ω-scans with a scan range of 1° and a counting time of 54 seconds per frame. The data were collected at 153 K using an Oxford Cryostream low temperature device. Details of crystal data, data collection and structure refinement are listed in Table B.3. Data reduction was performed using DENZO-SMN.[290] The structure was solved by direct methods using SIR97[291] and refined by full-matrix least-squares on F² with anisotropic displacement parameters for the non-H atoms using SHELXL-97.[292] The hydrogen atoms were observed in a ΔF map

and refined with isotropic displacement parameters. The function, $\Sigma w(|F_o|^2 - |F_c|^2)^2$, was minimized, where $w = 1/[(\sigma(F_o))^2 + (0.0448*P)^2 + (0.555*P)]$ and $P = (|F_o|^2 + 2|F_c|^2)/3$. $R_w(F^2)$ refined to 0.104, with $R(F)$ equal to 0.0433 and a goodness of fit, S, = 1.01. Definitions used for calculating $R(F)$, $R_w(F^2)$ and the goodness of fit, S, are given below.[293] The data were corrected for secondary extinction effects. The correction takes the form: $F_{corr} = kF_c/[1 + (2.1(3)x10^{-6})* F_c^2 \lambda^3/(sin2\theta)]^{0.25}$ where k is the overall scale factor. Neutral atom scattering factors and values used to calculate the linear absorption coefficient are from the International Tables for X-ray Crystallography (1992).[294] All figures were generated using SHELXTL/PC.[295] Tables of positional and thermal parameters, bond lengths and angles, torsion angles, figures and lists of observed and calculated structure factors are located in Tables B.3 through B.4.

Table B.3: Crystal data and structure refinement for compound **2.16**.

Empirical formula	C18 H18 F6 O3
Formula weight	396.32
Temperature	153(2) K
Wavelength	0.71073 Å
Crystal system	Monoclinic
Space group	C2/c
Unit cell dimensions	a = 27.5075(5) Å α= 90°.
	b = 7.0079(2) Å β= 106.701(2)°.
	c = 18.2798(4) Å γ= 90°.
Volume	3375.15(14) Å^3
Z	8
Density (calculated)	1.560 Mg/m^3
Absorption coefficient	0.148 mm^{-1}
F(000)	1632
Crystal size	0.34 x 0.27 x 0.13 mm
Theta range for data collection	3.01 to 27.48°.

Index ranges	-35<=h<=35, -9<=k<=9, -23<=l<=23			
Reflections collected	6574			
Independent reflections	3798 [R(int) = 0.0382]			
Completeness to theta = 27.48°	98.2 %			
Absorption correction	None			
Refinement method	Full-matrix least-squares on F^2			
Data / restraints / parameters	3798 / 0 / 317			
Goodness-of-fit on F^2	1.008			
Final R indices [I>2sigma(I)]	R1 = 0.0433, wR2 = 0.0864			
R indices (all data)	R1 = 0.0967, wR2 = 0.1035			
Extinction coefficient	$2.1(3) \times 10^{-6}$			
Largest diff. peak and hole	0.210 and -0.266 e.Å^{-3}			

Table B.4: Atomic coordinates (x 10^4) and equivalent isotropic displacement
parameters (Å^2x 10^3) for compound **2.16**. U(eq) is defined as one third of
the trace of the orthogonalized U^{ij} tensor.

	x	y	z	U(eq)
F1	3438(1)	1285(2)	3567(1)	41(1)
F2	2891(1)	1348(2)	4193(1)	44(1)
F3	2690(1)	2349(2)	3033(1)	48(1)
F4	2942(1)	7152(2)	4428(1)	43(1)
F5	2768(1)	4518(2)	4886(1)	43(1)
F6	2375(1)	5296(2)	3731(1)	44(1)
O1	3795(1)	7596(2)	940(1)	26(1)
O2	4065(1)	9255(2)	2040(1)	27(1)
O3	3690(1)	4221(2)	4574(1)	28(1)
C1	3563(1)	6633(3)	1456(1)	24(1)

150

C2	3756(1)	7765(3)	2210(1)	23(1)
C3	4083(1)	6307(3)	2753(1)	26(1)
C4	3737(1)	4805(3)	2967(1)	24(1)
C5	3508(1)	3755(3)	2190(1)	30(1)
C6	3788(1)	4673(3)	1663(1)	29(1)
C7	4305(1)	5148(3)	2214(1)	33(1)
C8	3352(1)	5601(3)	3351(1)	24(1)
C9	3242(1)	4338(3)	3973(1)	23(1)
C10	3064(1)	2328(3)	3692(1)	30(1)
C11	2829(1)	5325(3)	4256(1)	29(1)
C12	3915(1)	9491(3)	1237(1)	24(1)
C13	4338(1)	10365(3)	982(1)	23(1)
C14	4842(1)	10061(3)	1382(1)	29(1)
C15	5224(1)	10946(3)	1159(1)	32(1)
C16	5108(1)	12149(3)	533(1)	32(1)
C17	4607(1)	12458(3)	130(1)	31(1)
C18	4224(1)	11569(3)	350(1)	28(1)

Figure B.3: ORTEP diagram of compound **2.17**.

2.17
(+/-)
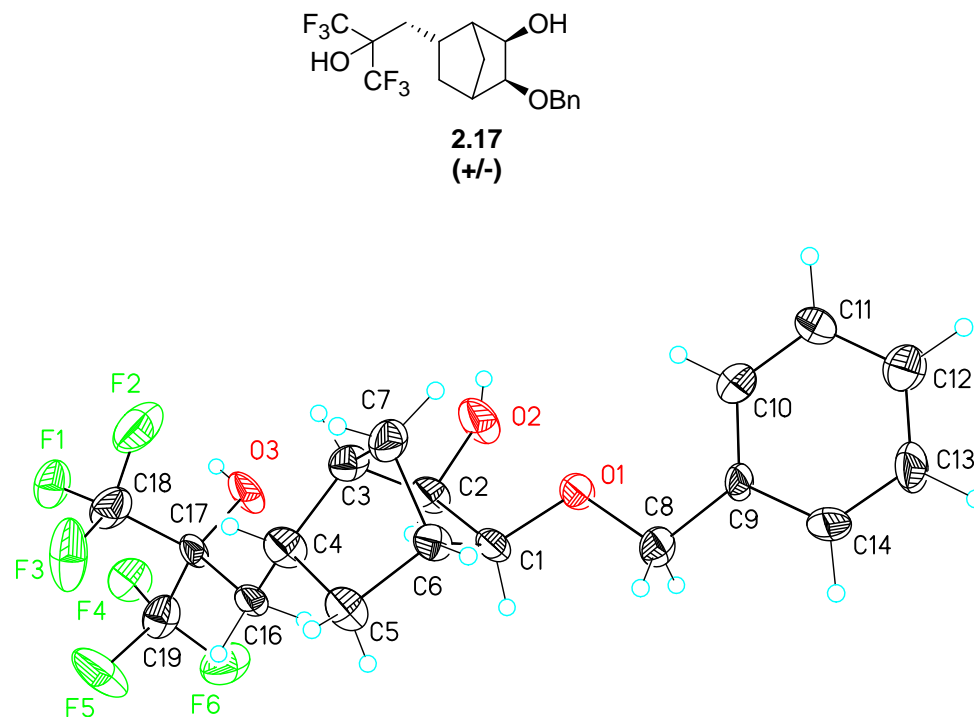
X-ray Experimental for $C_{18}H_{20}F_6O_3$: Crystals grew as colorless needles by slow evaporation. The data crystal was a needle that had approximate dimensions; 0.42 x 0.08 x 0.7 mm. The data were collected on a Nonius Kappa CCD diffractometer using a graphite monochromator with MoKα radiation (λ = 0.71073Å). A total of 320 frames of data were collected using ω-scans with a scan range of 1° and a counting time of 246 seconds per frame. The data were collected at 153 K using an Oxford Cryostream low temperature device. Details of crystal data, data collection and structure refinement are listed in Table B.5. Data reduction was performed using DENZO-SMN.[290] The structure was solved by direct methods using SIR97[291] and refined by full-matrix least-squares on

F^2 with anisotropic displacement parameters for the non-H atoms using SHELXL-97.[292] The hydrogen atoms were calculated in ideal positions with isotropic displacement parameters set to 1.2xUeq of the attached atom (1.5xUeq for methyl hydrogen atoms). The function, $\Sigma w(|F_o|^2 - |F_c|^2)^2$, was minimized, where $w = 1/[(\sigma(F_o))^2 + (0.02*P)^2]$ and $P = (|F_o|^2 + 2|F_c|^2)/3$. $R_w(F^2)$ refined to 0.192, with R(F) equal to 0.0983 and a goodness of fit, S, = 1.14. Definitions used for calculating R(F), $R_w(F^2)$ and the goodness of fit, S, are given below.[293] The data were checked for secondary extinction but no correction was necessary. Neutral atom scattering factors and values used to calculate the linear absorption coefficient are from the International Tables for X-ray Crystallography (1992).[294] All figures were generated using SHELXTL/PC.[295] Tables of positional and thermal parameters, bond lengths and angles, torsion angles, figures and lists of observed and calculated structure factors are located in Tables B.5 through B.6.

Table B.5: Crystal data and structure refinement for compound **2.17**.

Empirical formula	C18 H20 F6 O3
Formula weight	398.34
Temperature	153(2) K
Wavelength	0.71073 Å
Crystal system	Triclinic
Space group	P-1
Unit cell dimensions	a = 6.6091(5) Å α= 87.770(3)°.
	b = 14.7078(11) Å β= 87.230(3)°.
	c = 18.1937(15) Å γ= 87.682(3)°.
Volume	1763.8(2) Å^3
Z	4
Density (calculated)	1.500 Mg/m^3
Absorption coefficient	0.142 mm^{-1}
F(000)	824

Crystal size	0.42 x 0.08 x 0.07 mm
Theta range for data collection	2.95 to 24.99°.
Index ranges	-7<=h<=7, -17<=k<=17, -21<=l<=19
Reflections collected	9826
Independent reflections	6041 [R(int) = 0.1152]
Completeness to theta = 24.99°	97.4 %
Absorption correction	None
Refinement method	Full-matrix least-squares on F^2
Data / restraints / parameters	6041 / 324 / 487
Goodness-of-fit on F^2	1.134
Final R indices [I>2sigma(I)]	R1 = 0.0983, wR2 = 0.1423
R indices (all data)	R1 = 0.3533, wR2 = 0.1925
Largest diff. peak and hole	0.626 and -0.255 e.Å^{-3}

Table B.6: Atomic coordinates (x 10^4) and equivalent isotropic displacement parameters (Å^2x 10^3) for compound **2.17**. U(eq) is defined as one third of the trace of the orthogonalized U^{ij} tensor.

	x	y	z	U(eq)
F1	4993(7)	292(4)	3862(3)	70(2)
F2	5195(7)	1707(5)	4077(3)	103(2)
F3	6438(8)	692(5)	4819(3)	109(2)
F4	7986(7)	-404(4)	3036(3)	73(2)
F5	9113(10)	-533(4)	4144(4)	117(2)
F6	10936(8)	22(4)	3239(3)	95(2)
O1	12153(7)	4743(4)	3545(3)	55(2)
O2	9895(9)	3949(5)	2721(3)	90(2)
O3	7981(8)	1440(4)	3005(3)	75(2)
C1	11973(12)	3816(6)	3814(5)	49(3)

154

C2	10441(12)	3330(6)	3329(5)	53(3)
C3	8659(12)	3177(6)	3861(5)	51(3)
C4	9206(13)	2373(7)	4394(5)	57(3)
C5	10901(12)	2777(6)	4831(5)	56(3)
C6	10887(12)	3785(6)	4564(5)	46(2)
C7	8656(11)	3978(6)	4358(5)	60(3)
C8	14027(11)	5128(6)	3727(4)	50(3)
C9	13894(13)	6149(7)	3604(4)	45(3)
C10	12243(13)	6645(7)	3353(5)	64(3)
C11	12221(13)	7570(7)	3247(5)	64(3)
C12	13916(14)	8026(7)	3381(5)	68(3)
C13	15596(15)	7561(8)	3601(6)	82(4)
C14	15613(13)	6625(8)	3699(5)	77(3)
C16	9803(11)	1460(6)	4106(4)	53(3)
C17	8223(13)	981(7)	3681(5)	49(3)
C18	6238(15)	885(9)	4136(6)	68(3)
C19	9045(15)	13(8)	3534(6)	63(3)
F7	5367(8)	5565(4)	943(3)	94(2)
F8	6483(7)	5382(4)	2043(3)	71(2)
F9	3512(8)	4999(4)	1819(3)	90(2)
F10	9476(6)	4749(4)	1182(3)	67(2)
F11	7982(7)	4394(5)	209(3)	106(2)
F12	9228(7)	3351(4)	922(3)	106(2)
O4	2155(7)	310(4)	1485(3)	56(2)
O5	4651(8)	1019(5)	2291(3)	84(2)
O6	6573(8)	3574(4)	2013(3)	75(2)
C29	4013(12)	1656(6)	1710(4)	51(3)
C30	2414(12)	1228(6)	1225(5)	53(3)
C31	3456(11)	1262(6)	464(5)	54(3)
C32	3487(11)	2292(6)	208(4)	49(2)
C33	5242(13)	2676(6)	630(5)	53(3)
C34	5701(12)	1842(6)	1192(5)	53(3)
C35	5653(11)	1061(6)	675(5)	63(3)

C36	262(11)	-56(6)	1300(5)	58(3)
C37	257(15)	-1061(6)	1403(5)	44(2)
C38	1958(15)	-1567(7)	1283(5)	66(3)
C39	1930(15)	-2531(8)	1340(5)	79(3)
C40	156(19)	-2937(7)	1532(5)	72(3)
C41	-1573(15)	-2401(8)	1660(5)	63(3)
C42	-1508(14)	-1464(8)	1599(5)	70(3)
C43	4655(11)	3574(6)	932(4)	49(3)
C44	6247(11)	4065(6)	1360(5)	40(2)
C45	5328(16)	4982(8)	1546(6)	60(3)
C46	8173(14)	4187(8)	905(6)	65(3)

Figure B.4: ORTEP diagram of compound **2.19**.
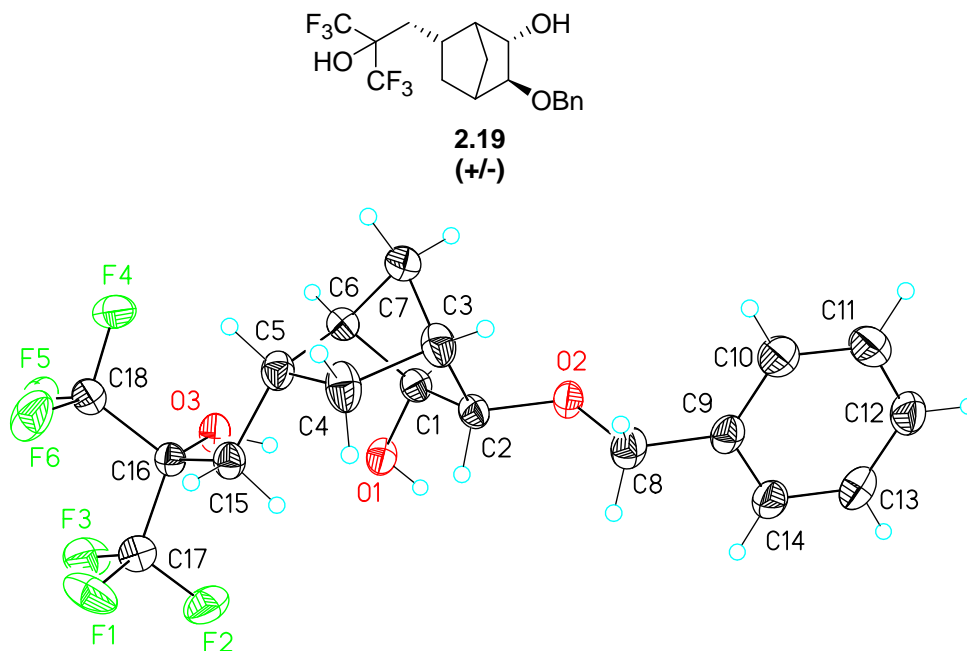
X-ray Experimental for $C_{18}H_{20}F_6O_3$: Crystals grew as colorless plates by slow evaporation from diethyl ether. The data crystal was cut from a cluster of colorless plates and had approximate dimensions; 0.28 x 0.26 x 0.14 mm. The data were collected on a Nonius Kappa CCD diffractometer using a graphite monochromator with MoKα radiation (λ = 0.71073Å). A total of 544 frames of data were collected using ω-scans with a scan range of 1° and a counting time of 94 seconds per frame. The data were collected at 153 K using an Oxford Cryostream low temperature device. Details of crystal data, data collection and structure refinement are listed in Table B.7. Data reduction was performed using DENZO-SMN.[290] The structure was solved by direct methods using SIR97[291] and refined by full-matrix least-squares on F^2 with anisotropic displacement parameters for the non-H atoms using SHELXL-97.[292] The hydrogen atoms on carbon were calculated in ideal positions with isotropic displacement

157

parameters set to 1.2xUeq of the attached atom (1.5xUeq for methyl hydrogen atoms). The hydroxyl group hydrogen atoms were observed in a ΔF map and refined with isotropic displacement parameters. The function, $\Sigma w(|F_o|^2 - |F_c|^2)^2$, was minimized, where $w = 1/[(\sigma(F_o))^2 + (0.0335*P)^2 + (0.7017*P)]$ and $P = (|F_o|^2 + 2|F_c|^2)/3$. $R_w(F^2)$ refined to 0.113, with R(F) equal to 0.0478 and a goodness of fit, S, = 1.10. Definitions used for calculating R(F), $R_w(F^2)$ and the goodness of fit, S, are given below.[293] The data were corrected for secondary extinction effects. The correction takes the form: $F_{corr} = kF_c/[1 + (6.6(9)x10^{-6})* F_c^2 \lambda^3/(sin2\theta)]^{0.25}$ where k is the overall scale factor. Neutral atom scattering factors and values used to calculate the linear absorption coefficient are from the International Tables for X-ray Crystallography (1992).[294] All figures were generated using SHELXTL/PC.[295] Tables of positional and thermal parameters, bond lengths and angles, torsion angles, H-bonding interactions, figures and lists of observed and calculated structure factors are located in Tables B.7 through B.8.

Table B.7: Crystal data and structure refinement for compound **2.19**.

Empirical formula	C18 H20 F6 O3
Formula weight	398.34
Temperature	153(2) K
Wavelength	0.71073 Å
Crystal system	Triclinic
Space group	P-1
Unit cell dimensions	a = 8.6062(1) Å α= 110.104(1)°.
	b = 13.2352(2) Å β= 94.328(1)°.
	c = 17.0519(3) Å γ = 90.126(1)°.
Volume	1817.93(5) Å^3
Z	4
Density (calculated)	1.455 Mg/m^3

Absorption coefficient	0.138 mm^{-1}	
F(000)	824	
Crystal size	0.28 x 0.26 x 0.14 mm	
Theta range for data collection	2.93 to 27.48°.	
Index ranges	-11<=h<=11, -16<=k<=17, -22<=l<=22	
Reflections collected	14492	
Independent reflections	8235 [R(int) = 0.0268]	
Completeness to theta = 27.48°	98.8 %	
Max. and min. transmission	0.9810 and 0.9625	
Refinement method	Full-matrix least-squares on F^2	
Data / restraints / parameters	8235 / 0 / 504	
Goodness-of-fit on F^2	1.099	
Final R indices [I>2sigma(I)]	R1 = 0.0478, wR2 = 0.1003	
R indices (all data)	R1 = 0.0885, wR2 = 0.1132	
Extinction coefficient	6.6(9)x10^{-6}	
Largest diff. peak and hole	0.280 and -0.277 e.Å^{-3}	

Table B.8: Atomic coordinates (x 10^4) and equivalent isotropic displacement parameters (Å^{2}x 10^3) for compound **2.19**. U(eq) is defined as one third of the trace of the orthogonalized U^{ij} tensor.

	x	y	z	U(eq)
F1	3964(2)	9048(1)	5665(1)	50(1)
F2	4455(1)	7370(1)	5238(1)	45(1)
F3	2107(1)	7861(1)	5378(1)	47(1)
F4	1856(1)	8687(1)	3272(1)	45(1)
F5	665(1)	8527(1)	4270(1)	44(1)
F6	2389(2)	9794(1)	4518(1)	49(1)
O1	5450(2)	6023(1)	3180(1)	29(1)
O2	8494(1)	5888(1)	2023(1)	27(1)
O3	2822(2)	6976(1)	3725(1)	29(1)

C1	5877(2)	6309(2)	2490(1)	26(1)
C2	7582(2)	6712(2)	2561(1)	25(1)
C3	7429(2)	7715(2)	2306(1)	32(1)
C4	6924(2)	8630(2)	3068(1)	36(1)
C5	5194(2)	8307(2)	3122(1)	29(1)
C6	4936(2)	7237(2)	2374(1)	28(1)
C7	5910(2)	7465(2)	1729(1)	37(1)
C8	10140(2)	6134(2)	2249(1)	33(1)
C9	11096(2)	5284(2)	1685(1)	28(1)
C10	11433(3)	5314(2)	916(1)	40(1)
C11	12366(3)	4553(2)	410(2)	50(1)
C12	12952(3)	3736(2)	664(1)	42(1)
C13	12618(2)	3691(2)	1427(2)	39(1)
C14	11711(2)	4466(2)	1939(1)	35(1)
C15	4949(2)	8349(2)	4015(1)	26(1)
C16	3342(2)	8025(1)	4209(1)	23(1)
C17	3460(2)	8088(2)	5128(1)	31(1)
C18	2064(2)	8761(2)	4069(1)	29(1)
F1'	10247(1)	2379(1)	-519(1)	45(1)
F2'	8789(2)	1605(1)	-1635(1)	48(1)
F3'	10139(2)	652(1)	-1052(1)	59(1)
F4'	6574(2)	308(1)	-1593(1)	46(1)
F5'	5564(2)	588(1)	-433(1)	51(1)
F6'	7591(2)	-375(1)	-703(1)	56(1)
O1'	7498(2)	3791(1)	1198(1)	28(1)
O2'	7445(1)	4412(1)	3288(1)	28(1)
O3'	7009(2)	2392(1)	-341(1)	30(1)
C1'	6809(2)	3442(2)	1797(1)	25(1)
C2'	7887(2)	3520(2)	2581(1)	26(1)
C3'	7652(2)	2425(2)	2672(1)	33(1)
C4'	8583(3)	1619(2)	2014(1)	36(1)
C5'	7618(2)	1475(2)	1167(1)	27(1)
C6'	6272(2)	2258(2)	1449(1)	27(1)

C7'	5976(2)	2112(2)	2285(1)	35(1)
C8'	8685(3)	4708(2)	3945(1)	44(1)
C9'	8195(2)	5555(2)	4719(1)	29(1)
C10'	8755(2)	6607(2)	4939(1)	36(1)
C11'	8406(3)	7378(2)	5685(2)	43(1)
C12'	7492(2)	7105(2)	6213(1)	45(1)
C13'	6905(2)	6069(2)	5998(1)	41(1)
C14'	7257(2)	5295(2)	5253(1)	35(1)
C15'	8679(2)	1581(2)	517(1)	26(1)
C16'	7941(2)	1525(2)	-349(1)	26(1)
C17'	9279(3)	1533(2)	-897(1)	34(1)
C18'	6926(3)	509(2)	-776(1)	36(1)

_____

Figure B.5: ORTEP diagram of compound **2.20**.
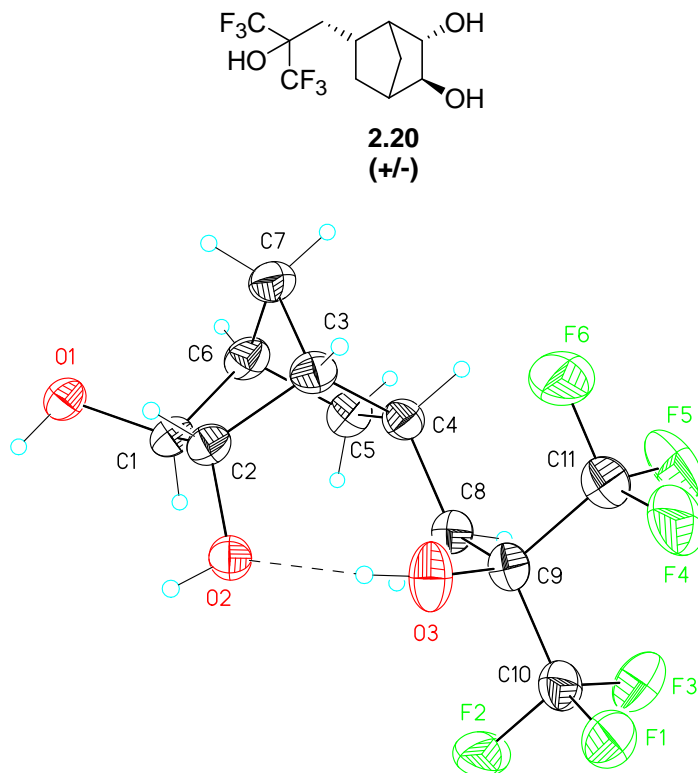
X-ray Experimental for $C_{11}H_{14}O_3F_6 - H_2O$: Crystals grew as clusters of colorless prisms by slow evaporation. The data crystal was cut from a cluster and had approximate dimensions; 0.40 x 0.27 x 0.20 mm. The data were collected on a Nonius Kappa CCD diffractometer using a graphite monochromator with MoKα radiation (λ = 0.71073Å). A total of 302 frames of data were collected using ω-scans with a scan range of 1° and a counting time of 62 seconds per frame. The data were collected at 153 K using an Oxford Cryostream low temperature device. Details of crystal data, data collection and structure refinement are listed in Table B.9. Data reduction was performed using DENZO-SMN.[290] The structure was solved by direct methods using SIR97[291] and

refined by full-matrix least-squares on F^2 with anisotropic displacement parameters for the non-H atoms using SHELXL-97.[292] The hydrogen atoms on carbon were calculated in ideal positions with isotropic displacement parameters set to 1.2xUeq of the attached atom (1.5xUeq for methyl hydrogen atoms). The hydrogen atoms bound to oxygen atoms were observed in a ΔF map and refined with isotropic displacement parameters. The function, $\Sigma w(|F_o|^2 - |F_c|^2)^2$, was minimized, where $w = 1/[(\sigma(F_o))^2 + (0.0495*P)^2 + (0.4535*P)]$ and $P = (|F_o|^2 + 2|F_c|^2)/3$. $R_w(F^2)$ refined to 0.112, with R(F) equal to 0.0431 and a goodness of fit, S, = 1.01. Definitions used for calculating R(F), $R_w(F^2)$ and the goodness of fit, S, are given below.[293] The data were corrected for secondary extinction effects. The correction takes the form: $F_{corr} = kF_c/[1 + (6(2)\text{x}10^{-6})* F_c^2 \lambda^3/(\sin2\theta)]^{0.25}$ where k is the overall scale factor. Neutral atom scattering factors and values used to calculate the linear absorption coefficient are from the International Tables for X-ray Crystallography (1992).[294] All figures were generated using SHELXTL/PC.[295] Tables of positional and thermal parameters, bond lengths and angles, torsion angles, H-bonding interactions, figures and lists of observed and calculated structure factors are located in Tables B.9 through B.10.

Table B.9: Crystal data and structure refinement for compound **2.20**.

Empirical formula	C11 H16 F6 O4
Formula weight	326.24
Temperature	293(2) K
Wavelength	0.71073 Å
Crystal system	Monoclinic
Space group	P21/c
Unit cell dimensions	a = 6.7177(2) Å α= 90°.
	b = 23.6978(6) Å β= 96.050(2)°.
	c = 8.5574(2) Å γ= 90°.

|		
Volume	1354.71(6) Å^3	
Z	4	
Density (calculated)	1.600 Mg/m^3	
Absorption coefficient	0.170 mm^{-1}	
F(000)	672	
Crystal size	0.40 x 0.27 x 0.20 mm	
Theta range for data collection	2.95 to 27.47°.	
Index ranges	-8<=h<=8, -30<=k<=30, -11<=l<=11	
Reflections collected	5684	
Independent reflections	3092 [R(int) = 0.0223]	
Completeness to theta = 27.47°	99.5 %	
Absorption correction	None	
Refinement method	Full-matrix least-squares on F^2	
Data / restraints / parameters	3092 / 0 / 211	
Goodness-of-fit on F^2	1.010	
Final R indices [I>2sigma(I)]	R1 = 0.0431, wR2 = 0.0968	
R indices (all data)	R1 = 0.0747, wR2 = 0.1115	
Extinction coefficient	$6(2)\text{x}10^{-6}$	
Largest diff. peak and hole	0.310 and -0.268 e.Å^{-3}	

Table B.10: Atomic coordinates (x 10^4) and equivalent isotropic displacement parameters (Å^2x 10^3) for compound **2.20**. U(eq) is defined as one third of the trace of the orthogonalized U^{ij} tensor.

	x	y	z	U(eq)
F1	6350(2)	5640(1)	-122(1)	47(1)
F2	9283(2)	5582(1)	1117(1)	56(1)
F3	7066(2)	4965(1)	1511(1)	49(1)
F4	3330(2)	5819(1)	1475(2)	58(1)
F5	4213(2)	5259(1)	3380(2)	63(1)

164

F6	3828(2)	6139(1)	3804(2)	63(1)
O1	12008(2)	7280(1)	7572(1)	31(1)
O2	9915(2)	6871(1)	3843(1)	29(1)
O3	6831(2)	6443(1)	2118(2)	38(1)
C1	11086(3)	6805(1)	6725(2)	28(1)
C2	9449(3)	6989(1)	5409(2)	27(1)
C3	7570(3)	6679(1)	5797(2)	30(1)
C4	7727(3)	6030(1)	5660(2)	29(1)
C5	9436(3)	5885(1)	6971(2)	34(1)
C6	9902(3)	6454(1)	7804(2)	33(1)
C7	7839(3)	6744(1)	7598(2)	36(1)
C8	8116(3)	5746(1)	4107(2)	27(1)
C9	6715(3)	5880(1)	2616(2)	28(1)
C10	7345(3)	5513(1)	1271(2)	35(1)
C11	4506(3)	5769(1)	2816(2)	39(1)
O1W	4179(2)	7221(1)	548(2)	39(1)

Figure B.6: ORTEP diagram of compound **6.16**.

6.16
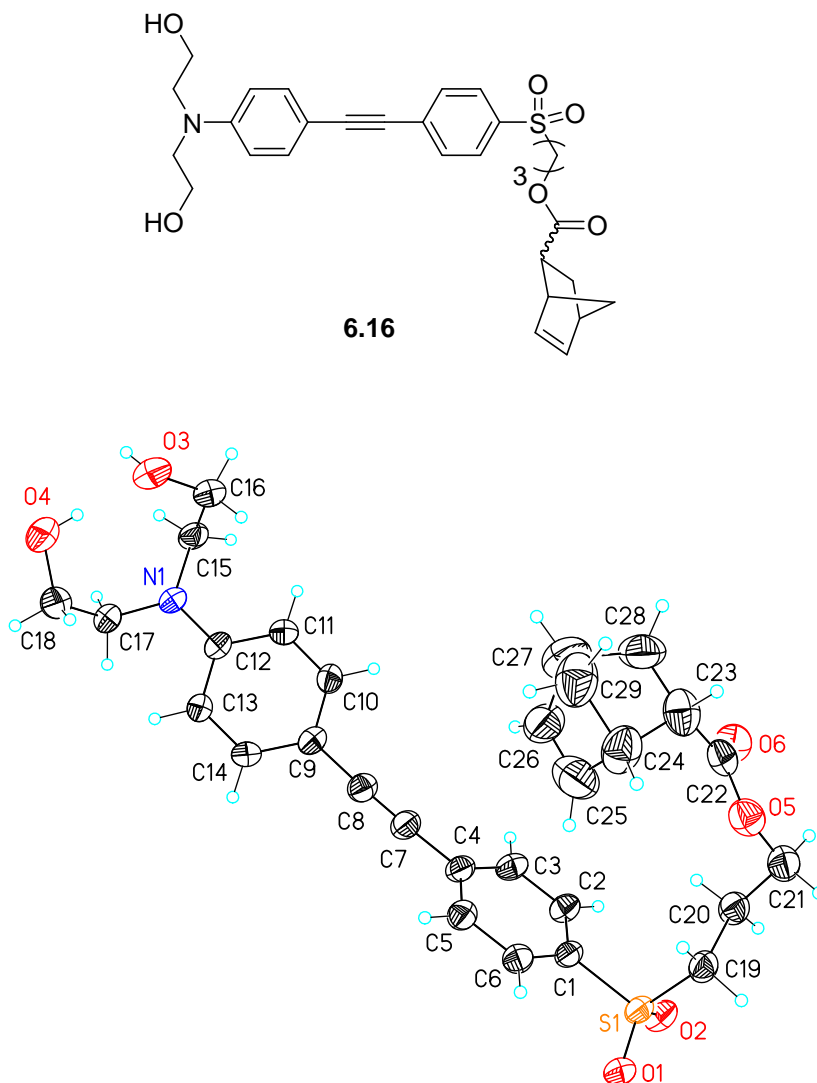
X-ray Experimental for C$_{29}$H$_{33}$NO$_6$S: Crystals grew as colorless plates by slow evaporation from DCM. The data crystal was cut from a large plate and had approximate dimensions; 0.32 x 0.29 x 0.08mm. The data were collected on a Nonius Kappa CCD diffractometer using a graphite monochromator with MoKα radiation (λ = 0.71073Å). A total of 574 frames of data were collected using ω-scans with a scan range of 0.7° and a counting time of 23 seconds per frame. The data were collected at 153 K using an

Oxford Cryostream low temperature device. Details of crystal data, data collection and structure refinement are listed in Table B.11. Data reduction were performed using DENZO-SMN.[290] The structure was solved by direct methods using SIR97[291] and refined by full-matrix least-squares on F2 with anisotropic displacement parameters for the non-H atoms using SHELXL-97.[292] The hydrogen atoms were calculated in ideal positions with isotropic displacement parameters set to 1.2xUeq of the attached atom (1.5xUeq for methyl hydrogen atoms). The function, $\Sigma w(|Fo|^2 - |Fc|^2)^2$, was minimized, where $w = 1/[(\Sigma(Fo))^2 + (0.0435*P)^2 + (2.5958*P)]$ and $P = (|Fo|^2 + 2|Fc|^2)/3$. $Rw(F^2)$ refined to 0.164, with R(F) equal to 0.0652 and a goodness of fit, S, = 1.15. Definitions used for calculating R(F), $Rw(F^2)$ and the goodness of fit, S, are given below.[293] The data were checked for secondary extinction effects but no correction was necessary. Neutral atom scattering factors and values used to calculate the linear absorption coefficient are from the International Tables for X-ray Crystallography (1992).[294] All figures were generated using SHELXTL/PC.[295] Tables of positional and thermal parameters, bond lengths and angles, torsion angles, figures and lists of observed and calculated structure factors are located in Tables B.11 through B.12.

Table B.11: Crystal data and structure refinement for **6.16**.

Empirical formula	C29 H33 N O6 S	
Formula weight	523.62	
Temperature	153(2) K	
Wavelength	0.71073 Å	
Crystal system	Monoclinic	
Space group	P21/c	
Unit cell dimensions	a = 18.7620(2) Å	$\alpha = 90°$.
	b = 6.2671(2) Å	$\beta = 108.5780(10)°$.
	c = 23.806(4) Å	$\gamma = 90°$.

Volume	2653.4(5) Å^3		
Z	4		
Density (calculated)	1.311 Mg/m^3		
Absorption coefficient	0.166 mm^{-1}		
F(000)	1112		
Crystal size	0.32 x 0.29 x 0.08 mm		
Theta range for data collection	2.42 to 27.43°.		
Index ranges	-24<=h<=24, -8<=k<=8, -30<=l<=30		
Reflections collected	11374		
Independent reflections	6034 [R(int) = 0.0454]		
Completeness to theta = 27.43°	99.6 %		
Absorption correction	None		
Refinement method	Full-matrix least-squares on F^2		
Data / restraints / parameters	6034 / 0 / 334		
Goodness-of-fit on F^2	1.153		
Final R indices [I>2sigma(I)]	R1 = 0.0652, wR2 = 0.1446		
R indices (all data)	R1 = 0.1170, wR2 = 0.1637		
Largest diff. peak and hole	1.071 and -0.393 e.Å^{-3}		

Table B.12: Atomic coordinates (x 10^4) and equivalent isotropic displacement
parameters (Å^2x 10^3) for **6.16**. U(eq) is defined as one third of the trace of
the orthogonalized U^{ij} tensor.

	x	y	z	U(eq)
S1	8912(1)	8609(1)	4868(1)	37(1)
O1	9093(1)	10851(3)	4914(1)	44(1)
O2	9277(1)	7247(3)	5365(1)	45(1)
O3	882(1)	5339(4)	2443(1)	54(1)
O4	277(1)	7807(4)	3089(1)	66(1)
O5	8348(1)	4721(3)	3125(1)	50(1)
O6	7861(1)	1673(4)	3338(1)	54(1)

168

N1	1821(1)	5940(4)	3734(1)	37(1)
C1	7931(1)	8371(5)	4729(1)	33(1)
C2	7643(2)	6496(5)	4885(1)	37(1)
C3	6876(2)	6307(5)	4780(1)	38(1)
C4	6393(2)	7989(5)	4522(1)	38(1)
C5	6692(2)	9861(5)	4371(1)	39(1)
C6	7460(2)	10054(5)	4469(1)	37(1)
C7	5599(2)	7760(5)	4416(1)	40(1)
C8	4945(2)	7490(5)	4330(1)	38(1)
C9	4150(2)	7121(5)	4196(1)	35(1)
C10	3847(2)	5159(5)	3963(1)	37(1)
C11	3080(2)	4785(5)	3798(1)	36(1)
C12	2584(1)	6348(5)	3876(1)	32(1)
C13	2895(2)	8324(5)	4111(1)	34(1)
C14	3660(2)	8686(5)	4263(1)	35(1)
C15	1513(2)	3957(5)	3436(1)	41(1)
C16	1451(2)	3939(5)	2787(1)	46(1)
C17	1338(2)	7257(5)	3970(1)	41(1)
C18	863(2)	8806(5)	3535(2)	52(1)
C19	9066(2)	7593(5)	4218(1)	39(1)
C20	9011(2)	5159(5)	4180(1)	44(1)
C21	9041(2)	4294(6)	3598(2)	52(1)
C22	7791(2)	3277(5)	3050(1)	45(1)
C23	7091(2)	3901(6)	2563(2)	60(1)
C24	6812(2)	6174(7)	2592(2)	70(1)
C25	6667(3)	6361(7)	3141(2)	83(1)
C26	6056(2)	5109(9)	3120(2)	83(1)
C27	5786(3)	4201(9)	2512(2)	95(2)
C28	6384(2)	2576(7)	2516(2)	76(1)
C29	5977(2)	5878(8)	2158(2)	82(1)

Figure B.7: ORTEP diagram of compound **A.17**.
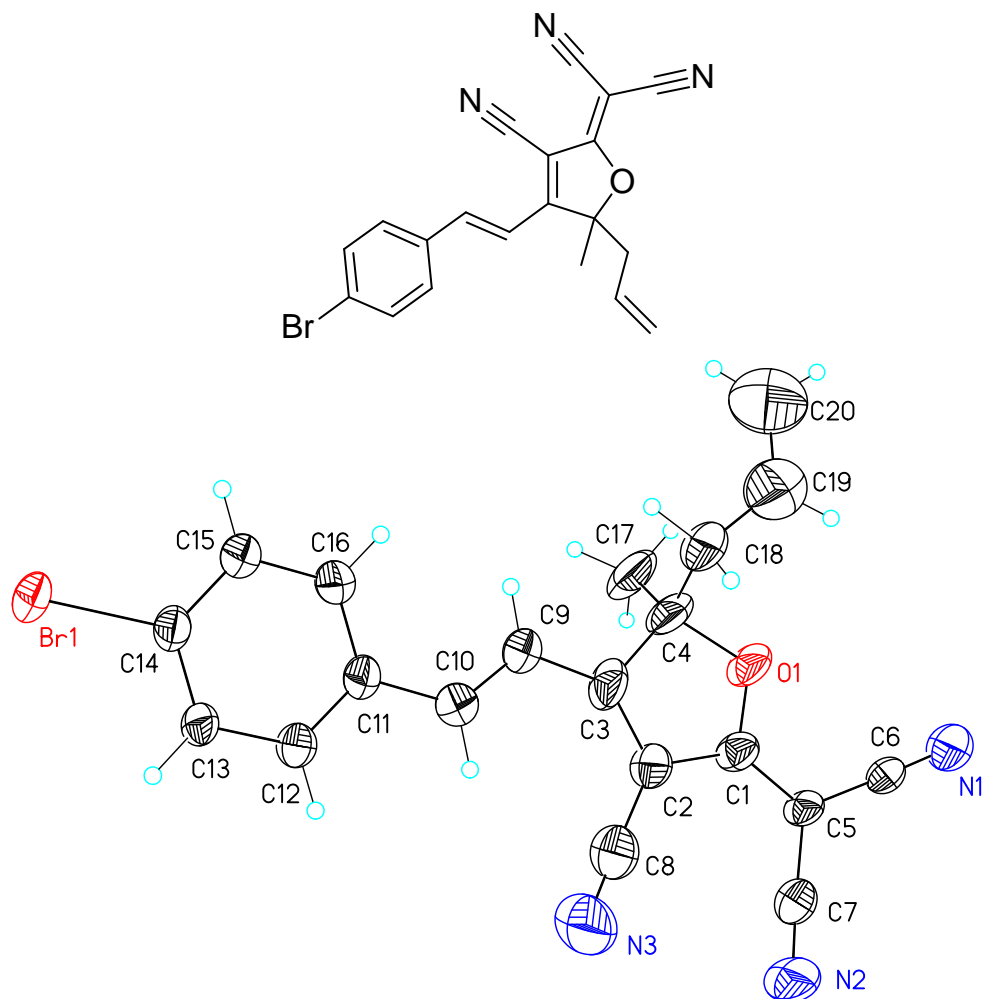
X-ray Experimental for $C_{20}H_{19}BrNO_3$: Crystals grew as very thin, yellow plates and laths by slow evaporation from ethanol. The data crystal was cut from cluster of plates and had approximate dimensions; 0.31 x 0.06 x 0.06mm. The data were collected on a Nonius Kappa CCD diffractometer using a graphite monochromator with MoKα radiation (λ = 0.71073Å). A total of 163 frames of data were collected using ω-scans with a scan range of 1.8° and a counting time of 519 seconds per frame. The data were collected at 153 K using an Oxford Cryostream low temperature device. Details of

crystal data, data collection and structure refinement are listed in Table 13. Data reduction were performed using DENZO-SMN.[290] The structure was solved by direct methods using SIR92[291] and refined by full-matrix least-squares on F^2 with anisotropic displacement parameters for the non-H atoms using SHELXL-97.[292] The hydrogen atoms were calculated in ideal positions with isotropic displacement parameters set to 1.2xUeq of the attached atom (1.5xUeq for methyl hydrogen atoms).

The crystal was twinned. The twin law was determined using ROTAX[293] to be (-1,0,-0/0,-1,0/-0.5,-0.4,0,1) about 001 reciprocal axis direction. The twin fraction refined to 0.242(5). Reflections that were partially overlapped due to the twinning were not used in the refinement. Of the 5338 reflections possible, 991 were omitted. ROTAX was used as incorporated into WinGX.[294]

The function, $\Sigma w(|Fo|^2 - |Fc|^2)^2$, was minimized, where $w = 1/[(\sigma(Fo))^2 + (0.02*P)^2]$ and $P = (|Fo|^2 + 2|Fc|^2)/3$. $Rw(F^2)$ refined to 0.164, with R(F) equal to 0.0817 and a goodness of fit, S, = 1.55. Definitions used for calculating R(F),$Rw(F^2)$ and the goodness of fit, S, are given below.[295] The data were corrected for secondary extinction effects. The correction takes the form: Fcorr = kFc/[1 + (1.4(4)x10^{-5})* Fc^2 λ^3/(sin2θ)]0.25 where k is the overall scale factor. Neutral atom scattering factors and values used to calculate the linear absorption coefficient are from the International Tables for X-ray Crystallography (1992).[296] All figures were generated using SHELXTL/PC.[297] Tables of positional and thermal parameters, bond lengths and angles, torsion angles, figures and lists of observed and calculated structure factors are located in Tables 13 through 14.

Table B.13: Crystal data and structure refinement for **A.17**.

Empirical formula   C20 H19 Br N3 O

Formula weight	397.29	
Temperature	153(2) K	
Wavelength	0.71073 Å	
Crystal system	Triclinic	
Space group	P-1	
Unit cell dimensions	a = 7.9520(5) Å	α= 80.105(3)°.
	b = 8.6850(6) Å	β= 79.511(3)°.
	c = 13.9920(12) Å	γ = 71.891(6)°.
Volume	896.22(11) Å^3	
Z	2	
Density (calculated)	1.472 Mg/m^3	
Absorption coefficient	2.306 mm^{-1}	
F(000)	406	
Crystal size	0.31 x 0.06 x 0.06 mm	
Theta range for data collection	2.49 to 27.43°.	
Index ranges	-10<=h<=10, -11<=k<=11, -18<=l<=18	
Reflections collected	4347	
Independent reflections	4347	
Completeness to theta = 27.43°	77.5 %	
Absorption correction	None	
Refinement method	Full-matrix least-squares on F^2	
Data / restraints / parameters	4347 / 425 / 303	
Goodness-of-fit on F^2	1.548	
Final R indices [I>2sigma(I)]	R1 = 0.0817, wR2 = 0.1531	
R indices (all data)	R1 = 0.1281, wR2 = 0.1638	
Extinction coefficient	1.4(4)x10^{-5}	
Largest diff. peak and hole	0.936 and -0.450 e.Å^{-3}	

Table B.14: Atomic coordinates (x 10^4) and equivalent isotropic displacement parameters (Å^2x 10^3) for **A.17**. U(eq) is defined as one third of the trace of the orthogonalized U^{ij} tensor.

	x	y	z	U(eq)
Br1	-3962(1)	11199(1)	7544(1)	49(1)
O1	1870(5)	5000(6)	1206(3)	53(1)
N1	5017(7)	2838(8)	-474(5)	66(2)
N2	7261(8)	1427(8)	2273(5)	74(2)
N3	4744(11)	3903(10)	4037(6)	105(3)
C1	3193(7)	4257(8)	1747(5)	41(2)
C2	2744(8)	4830(8)	2682(5)	43(2)
C3	1118(8)	5991(8)	2726(5)	51(2)
C4	421(8)	6155(9)	1777(6)	60(2)
C5	4659(7)	3161(7)	1338(5)	36(2)
C6	4871(8)	2950(8)	334(6)	43(2)
C7	6062(8)	2224(8)	1867(5)	48(2)
C8	3813(11)	4276(10)	3438(6)	71(2)
C9	-14(15)	7049(15)	3411(7)	51(3)
C10	375(11)	7055(12)	4270(7)	44(2)
C11	-657(13)	8126(13)	5020(7)	39(2)
C12	-117(12)	7873(11)	5904(7)	38(2)
C13	-1074(11)	8779(11)	6657(7)	35(2)
C14	-2629(16)	9966(16)	6487(7)	38(2)
C15	-3176(14)	10327(13)	5574(7)	45(2)
C16	-2187(14)	9378(15)	4846(8)	48(2)
C9A	540(30)	6650(20)	3718(18)	44(4)
C10A	-870(20)	7890(20)	3845(11)	46(3)
C11A	-1580(30)	8710(20)	4744(12)	38(3)
C12A	-1000(30)	8010(20)	5602(12)	43(3)
C13A	-1720(30)	8690(20)	6470(11)	42(3)
C14A	-3010(40)	10170(30)	6413(12)	39(3)

173

C15A	-3650(30)	10940(20)	5553(12)	42(3)
C16A	-2910(20)	10200(20)	4706(11)	43(3)
C17	-1273(8)	5536(11)	1911(6)	77(3)
C18	324(10)	7827(10)	1198(6)	68(2)
C19	-76(12)	7833(12)	210(8)	92(3)
C20	-1605(13)	8665(13)	-151(9)	115(4)

Appendix C: Experimental Procedures

FLUORINATED TRANS DIOL PROJECT EXPERIMENTALS.

General Methods and Materials:

All solvents and reagents were obtained from Aldrich and were used without further purification except where noted. Dry DCM, pyridine, toluene, and TEA were obtained by distillation over CaH_2 while THF was distilled from sodium/benzophenone. Methanol, DMF, and ether were obtained from a Glass Contour solvent delivery system. All reactions were run in oven dried glassware and under nitrogen atmosphere except where noted. All ^1H and ^{13}C NMR spectra were recorded on a Varian Unity Plus 300 or 500 MHz instrument. All chemical shifts are reported in ppm downfield from TMS using the residual protonated solvent as an internal standard (DMSO-d_6, ^1H 2.49 ppm and ^{13}C 39.5 ppm or CDCl₃, ^1H 7.26 ppm and ^{13}C 77.0 ppm). Coupling constants are expressed in Hz. HRMS (CI) was obtained on a VG analytical ZAB2-E instrument while HRMS (ESI) was obtained on an Ion Spec FT-ICR (7 Tesla) instrument. IR data was recorded on a Nicolet Avatar 360 FT-IR using either a KBr pellet or thin film on a NaCl disc. Melting points were recorded using a Mel-Temp II. Polymer molecular weights were recorded on an Agilent 1100 series GPC relative to polystyrene standards.
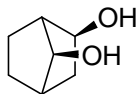
2.6 (+/-)

exo-**2**-*syn*-**7**-**Dihydroxynorbornane**[298] (**2.6**). To a round bottom flask was added 1.5 g of *exo*-norbornene oxide 100 ml of dioxane, and 100 ml of 1 M HCl (aq). The reaction mixture was stirred and heated to 90 ˚C for 16 hour. The reaction mixture was worked up by washing with dichloromethane and extracting with sodium bicarbonate (aq), and brine, and the organic fractions reduced *in vacuo*. The

crude reaction mixture was purified to remove oligomers by sublimation to yield a white amorphous solid (yield 62%). Product was a racemic mixture of (2R, 7S) and (2S, 7R) dihydroxynorbornane. mp 183-185 °C;[299] ^{1}H NMR 0.9-1.1 (m, 2H), 1.4-1.5 (m, 1H), 1.5-1.6 (m, 1H), 1.88 (m, 2H), 2.08 (d, 1H, J = 5.0 Hz), 2.18 (m, 1H), 3.84 (d, 1H, J = 4.5 Hz), 3.99 (d, 1H, J = 7.0 Hz), 4.02 (s, 1H), 4.28 (d, H, J = 4.5 Hz); ^{13}C NMR (CDCl$_3$ calibrated to 77.00): 21.3, 25.0, 39.4, 40.5, 45.8, 75.8, 80.4; LRMS (EI) m/z (%) 110 (60, M-18$^+$), 95 (35), 92 (30), 81 (100), 79 (70), 66 (90); HRMS ([M+H]$^+$ calcd. = 129.0916 found = 129.0921) FTIR ν = 3342 (br), 2958, 2875, 1083 cm^{-1}; Anal Calcd for C$_7$H$_{12}$O$_2$: C, 65.60%; H, 9.44%. Found: C, 65.20%; H, 9.47%.

2.9 (+/-)
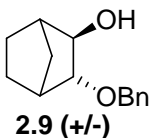
endo-**3-Benzoxybicyclo[2.2.1]heptan-*exo*-2-ol (2.9).**To a dry 500 ml round bottom flask in an ice bath were added 200 g (1.78 mol) of benzyl alcohol and a stir bar. Over 12 h 13.64 g (0.35 mol) of potassium metal was added in 1g increments and allowed to stir under a nitrogen atmosphere until the metal was fully dissolved. After all of the potassium was added, 33 g of *exo*-norbornene epoxide (0.30 mol) was added and the reaction mixture heated to 150 ˚C. The reaction mixture was allowed to stir for 20 days, at which point the reaction mixture was worked up by quenching with water, extracting with dichloromethane (3x), and organic layers combined and reduce *in vacuo*. The organic residue was then distilled under vacuum to remove the excess benzyl alcohol and the product was purified by column chromatography using 15% ethyl acetate in hexanes as eluent affording 39.4 g of a transparent oil. Yield: 30% ^{1}H NMR: 1.1-1.3 (m, 3H), 1.5-1.8 (m. 3H), 2.01 (d, 1H, br), 2.10 (d, 1H, J = 5.0 Hz), 2.48 (br s, 1H), 3.51 (m, 1H), 3.63 (m, 1H), 4.51 (dd, 2H, J = 11.4 Hz, 31.7 Hz), 7.2-7.2 (m, 5H) ^{13}C NMR: 19.6, 25.3, 33.6, 39.0, 44.4, 71.3, 80.1, 89.7, 127.5, 127.7, 128.3, 138.4 LRMS (EI) m/z (%) 110 (60, M-18$^+$), 95 (35), 92 (30),

81 (100), 66 (90); HRMS ([M+H]$^+$ calcd. = 219.1385 found = 219.1393) FTIR ν = 3388, 3031, 2957, 1454, 1126 cm^{-1}; Anal. Calcd. for C$_{14}$H$_{18}$O$_2$: C, 77.03%; H, 8.31%. Found: C, 76.77%; H, 8.42%.

2.8 (+/-)
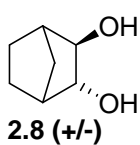
trans-**Bicyclo[2.2.1]heptan-2,3-diol (2.8).** To a 100 ml cylindrical glass sleeve was added a stirbar, 1.30 g of *endo*-3-benzoxybicyclo[2.2.1]heptan-*exo*-2-ol (**2.9**), 50 ml of 1:1 ethanol/ethyl acetate, and 40 mg of 10% Pd/C. The sleeve was placed inside a steel Parr reactor and charged with 400 psi of H$_2$. The reaction vessel was allowed to stir vigorously for 12 h, at which point the Parr reactor was depressurized, refreshed with an additional 20 mg of Pd/C, recharged to 400 psi of H$_2$, and the reaction allowed to react for an additional 12 h. The reaction vessel was then depressurized, and reaction mixture filtered through a Whatman 0.2 micron PTFE filter to remove the Pd/C catalyst. The clear solution was reduced *in vacuo* to yield the racemic product as a white amorpous solid. (yield 99%) mp 216-8 °C; ^{1}H NMR (CDCl$_3$ calibrated to 7.29) 1.2-1.4 (m, 3H), 1.5-1.8 (m, 3H), 2.11 (d, 1H, J = 6 Hz), 2.31 (s, 1H), 2.68 (br s, 2H), 3.38 (s, 1H), 3.89 (d, 1H, J = 5.2 Hz) ^{13}C NMR (CDCl$_3$ calibrated to 77.00): 19.1, 25.3, 34.0, 41.5, 44.9, 82.4, 82.9; LRMS (EI) *m/z* (%) 128 (5, M$^+$), 110 (25, M-18$^+$), 95 (50), 81 (70), 67 (100), 57 (100); HRMS ([M+H]$^+$ calcd. = 129.0916 found = 129.0911) FTIR ν = 3285 (br), 2956, 2873, 1048 cm^{-1}; Anal Calcd for C$_7$H$_{12}$O$_2$: C, 65.60%; H, 9.44%. Found: C, 65.30%; H, 9.40%.

2.2
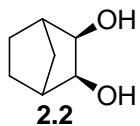
2-*exo*-3-*exo*-Bicyclo[2.2.1]heptan-diol (2.2). Prepared as reported in the literature.[300] Characterization data provided for comparison: mp 141-142 °C; ^{1}H NMR (CDCl$_3$ calibrated to 7.29) 1.07 (m, 3H), 1.49 (m, 2H), 1.76 (m, 1H), 2.13 (m, 2H), 3.15 (s, 2H), 3.67 (s, 2H) ^{13}C NMR (CDCl$_3$ calibrated to 77.00):

24.48, 31.55, 43.00, 74.76. LRMS (M$^+$ calcd. = 128 found = 128) Anal Calcd for C$_7$H$_{12}$O$_2$: C, 65.60%; H, 9.44%. Found: C, 65.56%; H, 9.48%.

2.10
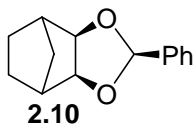
4-Phenyl-3,5-dioxatricyclo[5.2.1.0^{2,6}]decane (2.10). If the reaction was carried out at 60 °C as previously reported[301] the product isolated was a 3:1 mixture of *exo* and *endo* benzylidene isomers. However, if the reaction was carried out in an ice bath under reduced pressure, the product formed was exclusively the *exo* isomer (99% yield). ^{1}H NMR (CDCl$_3$ calibrated to 7.29) 1.0-1.2 (m, 3H), 1.4-1.6 (m, 2H), 2.43 (m, 2H), 4.03 (d, 2H), 5.55 (s, 1H), 7.3-7.4 (m, 3H), 7.5-7.6 (m, 2H); ^{13}C NMR (CDCl$_3$ calibrated to 77.00): 23.0, 31.8, 39.8, 76.6, 83.0, 102.6, 126.8, 128.4, 129.4, 129.5, 136.3. LRMS (EI) *m/z* (%) 215 (100, M-1$^+$), 187 (15), 105 (35), 91 (40), 77 (25); HRMS ([M+H]$^+$ calcd. = 217.1229 found = 217.1223) FTIR ν = 2964, 1718, 1450, 1137 cm^{-1}; Anal Calcd for C$_{14}$H$_{16}$O$_2$: C, 77.75%; H, 7.46 %. Found: C, 77.57%; H, 7.36%.

2.11
(+/-)
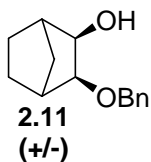
***exo*-3-Benzoxybicyclo[2.2.1]heptan-*exo*-2-ol (2.11).** To a dry 250 ml round bottom flask were added 1.60 g of **2.10** and a stirbar. The reactant was dried under vacuum for 24 h. To the dried reactant was added 45 ml of DIBAL solution (1.5 M in toluene) and the reaction mixture was allowed to stir at 80 °C under N$_2$ for 12 h. The product was purified by column chromatography using 6% ethyl acetate in hexanes as eluent affording 1.52 g of a transparent oil. Yield: 94% ^{1}H NMR: 0.9-1.0 (m, 2H), 1.0-1.1 (m, 1H), 1.4-1.5 (m. 2H), 1.77 (m, 1H), 2.15 (s, 1H), 2.25 (s, 1H), 3.37 (m, 1H), 3.43 (m, 1H), 3.68 (m, 1H), 4.58 (dd, 2H, *J* = 16 Hz, 31 Hz), 7.2-7.2 (m, 5H) ^{13}C NMR: 24.0, 24.6, 31.9, 39.5, 43.0, 72.4, 74.8, 82.0, 127.5, 127.7, 128.3, 137.7; LRMS (EI) *m/z* (%) 215 (1, M-1$^+$), 127 (45), 91 (100), 81 (90), 65 (20); HRMS

([M+H]$^+$ calcd. = 219.1385 found = 219.1385) FTIR ν = 3518, 3030, 2958, 1453, 1144, 1073 cm^{-1} ; Anal. Calcd. for $C_{14}H_{18}O_2$: C, 77.03%; H, 8.31%. Found: C, 76.94%; H, 8.34%.
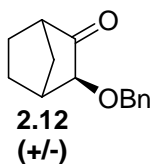
exo-**3-Benzoxybicyclo[2.2.1]heptan-2-one (2.12).** To a dry 50 ml round bottom flask were added 0.44 g (0.20 mmole) of **2.11** and a stirbar. The reactant was diluted with 50 ml of dichloromethane and 0.66 g (0.30 mmole) of PCC was added. The transparent orange reaction mixture was allowed to stir for 12 h until a dark brownish precipitate was formed. The reaction mixture was diluted with a large excess of diethyl ether, and filter through celite to yield a light greenish oil. The product could be further purified by column chromatography using 5% ethyl acetate 95% hexane as eluent to yield 0.42 g (96% yield) a transparent oil. ^{1}H NMR (CDCl$_3$ calibrated to 7.29) 1.42 (m, 2H), 1.57 (m, 2H), 1.81 (m, 2H), 2.26 (m 1H), 2.60 (d, 1H, J = 1.5 Hz), 3.28 (d, 1H, J = 1.5 Hz), 4.70 (dd, 2H, J = 1.2 Hz, 42 Hz), 7.2-7.2 (m, 5H) ^{13}C NMR (CDCl$_3$ calibrated to 77.00): 23.6, 24.4, 34.6, 40.6, 48.0, 71.8, 81.0, 127.7, 127.9, 128.4, 137.9, 215.5 ppm; LRMS (EI) *m/z* (%) 216 (1, M$^+$), 125 (10), 110 (30), 91 (100), 79 (30); HRMS [M+H]$^+$ calcd. = 217.1227 found = 217.1229) FTIR ν = 3030, 2963, 1749, 1453, 1117 cm^{-1}; Anal Calcd for $C_{14}H_{16}O_2$: C, 77.75%; H, 7.46%. Found: C, 78.11%; H, 7.54%.
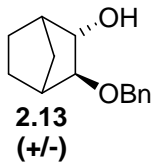
exo-**3-Benzoxybicyclo[2.2.1]heptan-2-*endo*-ol (2.13).** To a dry 50 ml round bottom flask were added 0.12 g of **2.12** and 1 ml of 1 M lithium triethylborohydride (Superhydride) in THF. The reactions mixture was allowed to stir for 24 h in an ice bath at which time GC-MS of the crude product verified the starting material had been consumed, but two isomer of the product was observed.

179

The product was purified by column chromatography using 5% ethyl acetate in hexanes as eluent affording 0.11 g of a transparent oil. Yield: 92% ^{1}H NMR: 1.1-1.3 (m, 3H), 1.5-1.6 (m, 1H), 1.6-1.8 (m. 2H), 2.08 (d, 1H, $J = 4.5$ Hz), 2.45 (m, 1H), 2.45 (br s, 1H), 3.49 (m, 1H), 3.60 (m, 1H), 4.49 (dd, 2H, $J = 12$ Hz, 37 Hz), 7.2-7.2 (m, 5H) ^{13}C NMR: 19.6, 25.3, 33.6, 39.0, 44.4, 71.3, 80.2 , 89.7, 127.5, 127.7, 128.3, 138.4 LRMS (EI) *m/z* (%) 215 (2), 127 (50), 93 (60), 91 (100), 81 (90); HRMS ([M+H][+] calcd. = 219.1385 found = 219.1383) FTIR ν = 3518, 3030, 2958, 1454, 1128 cm^{-1} ; Anal. Calcd. for $C_{14}H_{18}O_2$: C, 77.03%; H, 8.31%. Found: C, 76.89%; H, 8.41%.

2.8 (+/-)
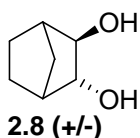
trans-**Bicyclo[2.2.1]heptan-2,3-diol (2.8).** Compound **2.8** was also prepared via procedure identical to that above, replacing **2.9** with its isomer **2.13**.

2.15 (+/-)
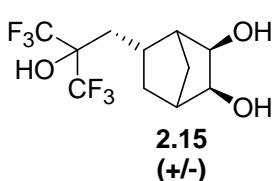
2-(*exo*-2-*exo*-3-Dihydroxybicyclo[2.2.1]heptan-5-ylmethyl)-1,1,1,3,3,3-hexafluoro-2-propan-2-ol (2.15). To a round bottom flask containing 116 g of bicyclo[2.2.1]hept-5-en-2-ylmethyl-1,1,1,3,3,3-hexafluoro-propan-2-ol were added 1350 mL of THF, 150 mL of water, and 60 g of N-morpholine oxide. The reagents were stirred until dissolved and the reaction vessel was lowered into a water bath. Then 43 mL of a 2.5 wt % solution of osmium tetroxide was added and the reaction mixture was stirred at room temperature for 12 h. The solution was reduced *in vacuo* and the aqueous mixture extracted 3 times with ethyl acetate. The organic layers were combined, reduced *in vacuo*, and purified by filtration through a plug of silica gel. The filtrate was then reduced *in vacuo*, dissolved in a minimal amount of ethyl acetate and precipitated into dichloromethane yielding 117.6 g of a slightly yellowish powder (91% yield). ^{1}H NMR (CDCl₃) 0.66, (m, 1H), 1.16 (d, 1H, J = 10.2, Hz), 1.7-1.9 (m, 3H), 2.0-2.1 (m, 2H), 2.09

(s, 1H), 2.13 (m, 1H), 3.60 (d, 1H, J = 6.0 Hz), 3.93 (d, 1H, J = 6.0 Hz); ^{13}C NMR (CDCl$_3$): 32.4, 33.9, 34.0, 34.5, 45.5, 49.9, 70.3, 75.7, 77.5 (m, J$_{C-F}$ = 28 Hz), 125.1 (dq, J$_{C-F}$ = 16.8, 287 Hz); ^{19}F NMR (CDCl$_3$) –77.5, (q, 3F, J$_{F-F}$ = 10.0 Hz), -78.7, (q, 3F, J$_{F-F}$ = 10.0 Hz); LRMS (EI) *m/z* (%) 308 (3, M$^+$), 290 (10), 272 (15), 261 (20), 248 (25), 237 (50), 95 (65), 81 (65), 67 (65), 57 (100); HRMS ([M+H]$^+$ calcd. = 309.0925 found = 309.0926); FTIR ν = 3385, 2970, 2880, 1416, 1203, 1033 cm^{-1}; Anal Calcd for C$_{11}$H$_{14}$F$_6$O$_3$: C, 42.87%; H, 4.58% F, 36.98% Found: C, 42.90%; H, 4.60%.

2.16
(+/-)
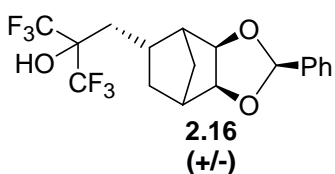
1,1,1,3,3,3-Hexafluoro-2-(4-phenyl-3,5-dioxatricyclo[5.2.1. 0^{2,6}]dec-8-ylmethyl)-propan-2-ol **(2.16).** To a round bottomed flask containing 109.3 g of **2.15** were added 200 mL of toluene, and 78 g benzaldehyde dimethoxyacetal. The reaction vessel was cooled in an ice bath to 0 °C and 7.5 g of p-toluenesulfonic acid was added, and the reaction mixture stirred under reduced pressure. After 3 h, the reaction was washed with sodium bicarbonate, and extracted with dichloromethane. The organic extracts were combined, reduced *in vacuo*, and filtered through a plug of silica gel to afford 140 g a white amorphous solid (99% yield). ^{1}H NMR (mixture of R and S isomers) 0.60, (m, 1H), 1.21 (m, 1H), 1.84 (dd, 1H, J = 8.0, 15.0 Hz), 1.9-2.0 (m, 2H), 2.03 (dd, 1H, J = 6.4, 15.0 Hz), 2.21 (m, 1H, J = 6.0 Hz), 2.42 (m, 1H J = 4.2 Hz), 2.51(d, 1H, J = 3.8 Hz), 3.22 (s, 1H), 4.06 (d, 1H J = 5.9 Hz), 4.35 (d, 1H, J = 5.8 Hz), 5.56 (s, 1H), 7.3-7.4 (m, 3H), 7.5-7.6 (m, 2H); ^{13}C NMR: 30.5, 31.7, 32.0, 33.5, 40.7, 45.0, 76.5 (m, J$_{C-F}$ = 29.0 Hz), 78.5, 82.6, 102.7, 123.1 (q, J$_{C-F}$ = 5.0, 287 Hz), 126.8, 128.4, 129.6, 136.0; ^{19}F NMR: -76.7, (q, 3F, J$_{F-F}$ = 10.2 Hz), -78.0, (q, 3F, J$_{F-F}$ = 10.2 Hz); LRMS (EI) *m/z* (%) 395 (100, M-1$^+$), 349 (10), 273 (15), 105 (80), 91 (60); HRMS ([M+H]$^+$ calcd. = 397.1222 found = 397.1238); FTIR ν = 3338, 3040, 2962, 2879, 1460, 1403, 1214, 1143,

1063 cm^{-1}; Anal Calcd for C$_{18}$H$_{18}$F$_6$O$_3$: C, 54.55%; H, 4.58% F, 28.76%. Found: C, 54.58%; H, 4.62%.
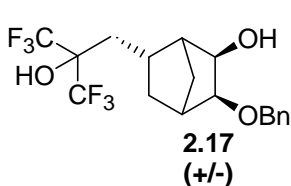
2-(*exo*-2-Benzyloxy-*exo*-3-hydroxybicyclo[2.2.1]heptan-5-ylmethyl)-1,1,1,3,3,3-hexafluoropropan-2-ol (2.17). To a round bottomed flask containing 14.0 g of **2.16** diluted in 500 mL of toluene was added 214 mL of DIBAL (1.5 M solution in toluene) dropwise. The reaction mixture stirred at room temperature for 12 h, then cooled to 0 °C and the excess DIBAL was quenched by adding 0.3 M aq solution of Rochelle's salt dropwise until evolution of gas ceased. The resulting solution was extracted twice with dichloromethane and the organic fractions combined and reduced *in vacuo*. The desired product was isolated by chromatography on silica, (eluent 20 % ethyl acetate 80% hexane) as a mixture of enantiomers (yield 91%.) ^{1}H NMR (mixture of R and S isomers) 0.50 (m, 1H), 1.18 (m, 1H), 1.76 (dd, 1H, J = 1.6, 10.4 Hz), 1.8-2.0 (m, 3H), 2.11 (m, 1H), 2.23 (d, 1H, J = 4.6 Hz), 2.35 (d, 1H, J = 2.6 Hz), 3.46 (d, 1H, J = 6.2 Hz), 3.70 (m, 1H), 4.10 (d, 1H, J = 6.2Hz), 4.54 (d, 1H, J = 11.7 Hz), 4.61 (d, 1H, J = 11.7 Hz), 6.05 (s, 1H), 7.2-7.4 (m, 5H); ^{13}C NMR: 32.1, 32.3, 33.6, 34.0, 40.8, 48.0, 70.3, 73.1, 77.1 (m, J$_{C-F}$ = 28.4 Hz), 82.3, 124.1 (q, J$_{C-F}$ = 287, 6.2 Hz), 128.2, 128.4, 129.0, 138.3; ^{19}F NMR; – 76.0, (q, 3F, J$_{F-F}$ = 10.0 Hz), -78.5, (q, 3F, J$_{F-F}$ = 10.0 Hz); LRMS (EI) *m/z* (%) 395 (2, M$^+$), 289 (45), 261 (90), 91 (100); HRMS ([M+H]$^+$ calcd. = 399.1395 found = 399.1391); FTIR ν = 3489, 3208, 3034, 2965, 2877, 1453, 1207, 1140, 1090 cm^{-1}; Anal Calcd for C$_{18}$H$_{20}$F$_6$O$_3$: C, 54.27%; H, 5.06% F, 28.62% Found: C, 54.37%; H, 5.04%.
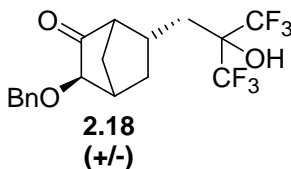
2-(*exo*-2-Benzyloxy-bicyclo[2.2.1]hept-3-on-5-ylmethyl)-1,1,1,3,3,3-hexafluoropropan-2-ol (2.18). To a round bottomed

flask containing 12.3 g of **2.17** diluted in 500 mL of dichloromethane was added 14.0 g

of pyridium chlorochromate. The reaction mixture was stirred at room temperature for

12 h, after which it was filtered through a plug of silica gel with ethyl acetate as eluent.

The solvent was removed *in vacuo* to yield 12.1 g of a lightly brownish viscous liquid

(yield 98%) ^{1}H NMR: 1.14 (m, 1H), 1.67 (m, 1H), 1.94 (m, 1H), 2.05 (m, 1H), 2.2-2.3

(m, 2H), 2.49 (m, 1H), 2.53 (m, 1H), 2.65 (m, 1H), 3.19 (s, 1H), 3.58 (d, 1H, J = 2.8Hz),

4.62 (d, 1H, J = 12Hz), 4.77 (d, 1H, J = 12Hz), 7.2-7.4 (m, 5H). ^{13}C NMR: 31.5, 32.2,

33.2, 35.7, 46.2, 49.2, 72.7, 77.1 (m, J_{C-F} = 28.4 Hz), 123.3 (q, J_{C-F} = 288, 20.0 Hz),

128.2, 128.3, 128.7, 138.4, 214.3. ^{19}F NMR: –75.2 (q, 3F, J_{F-F} = 10.0 Hz), -79.1 (q, 3F, J_{F-F}

= 10.0 Hz); LRMS (EI) *m/z* (%) 290 (15), 259 (20), 247 (15), 91 (100); HRMS ([M+H]$^+$

calcd. = 397.1221 found =397.1238) FTIR ν = 3336, 2971, 2882, 1744, 1454, 1250, 1086

cm^{-1}; Anal Calcd for $C_{18}H_{18}F_6O_3$: C, 54.55%; H, 4.58% F, 28.76% Found: C, 54.47%; H,

4.56%.

2.19
(+/-)
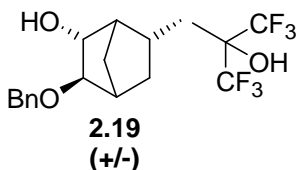
2-(*exo*-2-Benzyloxy-*endo*-3-hydroxybicyclo[2.2.1]heptan-5-ylmethyl)-1,1,1,3,3,3-hexafluoropropan-2-ol (2.19). A round bottomed flask containing 0.169 g of **2.18** was diluted in 6 mL of

THF and cooled to 0 °C. To this solution was added 1.1 mL of lithium

triethylborohydride (1 M solution in THF) and the reaction was warmed to room

temperature and stirred for 12 h. The reaction mixture was cooled to 0 °C and quenched

by addition of concentrated aqueous NaHSO$_4$. The resulting solution was extracted twice

with dichloromethane and the organic fractions combined and reduced *in vacuo*. The

product was isolated by chromatography on silica, (eluent 11% ethyl acetate 89%

hexane) as a mixture of enantiomers (yield 99%) ^{1}H NMR: 1.18 (d, 1H, J = 11 Hz), 1.20

(d, 1H, J = 11 Hz), 1.33 (m, 1H), 1.54 (m, 1H), 1.94 (dd, 1H, J = 5.5, 15 Hz), 2.02 (m,

1H), 2.25 (s, 1H), 2.37 (s, 1H), 2.47 (t, 1H, J = 13 Hz), 4.54 (d, 1H, J = 9.5 Hz), 4.90 (d,

1H, J = 9.5 Hz), 7.2-7.4 (m, 5H); ^{13}C NMR: 34.4, 38.0, 39.3, 39.5, 46.4, 50.3, 77.5, 77.6,

81.2, 82.7 (m, J_{C-F} = 28.4 Hz) 123.1 (dq, J_{C-F} = 21.3, 288 Hz), 133.4, 133.6, 134.1, 144.6.

^{19}F NMR: –73.9, (q, 3F, J_{F-F} = 10.0 Hz), -75.3, (q, 3F, J_{F-F} = 10.0 Hz).   LRMS (EI) m/z

(%) 398 (1, M$^+$), 289 (30), 261 (65), 91 (100); HRMS ([M+H]$^+$ calcd. = 399.1395 found

= 399.1407) FTIR ν = 3460, 3230, 3022, 2960, 2883, 1456, 1202, 1163, 1052 cm^{-1}; Anal

Calcd for $C_{18}H_{20}F_6O_3$: C, 54.27%; H, 5.06% F, 28.62% Found: C, 54.34%; H, 5.08%.
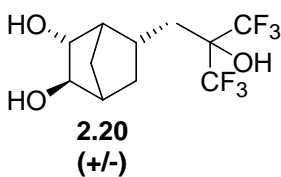
2-(*exo*-2-*endo*-3-Dihydroxybicyclo[2.2.1]heptan-5-ylmethyl)-

1,1,1,3,3,3-hexafluoropropan-2-ol   (2.20).   To   a   100   mL

cylindrical glass sleeve was added a stirbar, 1.30 g of **2.19**, 50 mL

of 1:1 ethanol/ethyl acetate, and 40 mg of 10% Pd/C. The sleeve was placed inside a

stainless steel Parr reactor and charged with 400 psi of H$_2$. The reaction vessel was stirred

vigorously for 12 h, at which point the reactor was depressurized, refreshed with an

additional 20 mg of Pd/C, recharged to 400 psi of H$_2$, and stirred for an additional 12 h.

The reaction vessel was then depressurized, and reaction mixture filtered through a

Whatman 0.2 micron PTFE filter to remove the Pd/C catalyst. The clear solution was

reduced *in vacuo* to yield the racemic product as a white amorphous solid. (yield 99%)

^{1}H NMR: 1.31 (ddt, 1H, J = 1.4, 2.2, 10.7 Hz), 1.39 (dt, 1H, J = 2.0, 10.7 Hz), 1.58 (ddd,

1H, J = 2.4, 5.8, 12.5 Hz), 1.73 (dt, 1H, J = 4.8, 11.5 Hz), 2.02 (m, 1H), 2.1-2.3 (m, 3H),

2.31 (m, 1H), 2.5 (b, 2H), 3.94 (ddd, 1H, J = 1.4, 4.4, 9.2 Hz), 4.01 (ddd, 1H, J = 1.3,

4.6, 9.0 Hz); ^{13}C NMR: 28.8, 33.5, 34.4, 35.0, 43.8, 45.7, 69.1, 72.2, 77.9 (m, J_{C-F} = 28.4

Hz) 125.1 (dq, J_{C-F} = 22.6, 288 Hz); ^{19}F NMR (CDCl$_3$) –76.1, (q, 3F, J_{F-F} = 10.4 Hz), -

80.4, (q, 3F, J_{F-F} = 10.4 Hz); LRMS (EI) m/z (%) 308 (5, M$^+$), 290 (20), 272 (25), 261

(30), 248 (40), 237 (75), 95 (75), 57 (100); HRMS ([M+H]$^+$ calcd. = 309.0925 found =

309.0912); FTIR ν = 1049, 1150, 1200, 2885, 2959, 3227, 3360 cm^{-1}; Anal Calcd for C$_{11}$H$_{14}$F$_6$O$_3$: C, 42.87%; H, 4.58% F, 36.98% Found: C, 43.17%; H, 4.56%.

2.22
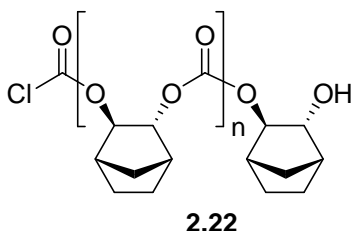
Synthesis of Polymer 2.22. To an oven dried three neck 100 ml round bottomed flask was added 0.2501 g of diol **8**. To this was added 8 ml of freshly distilled DCM and 0.325 g of freshly distilled pyridine. Then 2.560 g of a 20% phosgene in toluene solution was added dropwise over 10 min. After stirring at room temperature for 24 hrs the reaction was complete by GCMS and the mixture was evaporated to dryness to remove excess phosgene. The crude product was redissolved in 8 ml of dry DCM and 0.2500 g of diol **8** was added along with 0.325 g of pyridine. The reaction mixture was brought to reflux for a further 48 hrs before being precipitated into methanol. The precipitate was extremely fine but was able to be collected via filtration. Mw = 10 kDa, Mn = 6 kDa, PDI = 1.66.

2.24
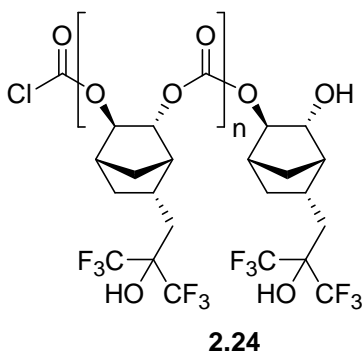
Synthesis of Polymer 2.24. To an oven dried three neck 100 ml round bottomed flask was added 0.297 g of diol **20**. To this was added 10 ml of freshly distilled DCM and 0.190 g of freshly distilled pyridine. Then 1.155 g of a 20% phosgene in toluene solution was added dropwise over 10 min. After stirring at room temperature for 24 hrs the reaction was complete by GCMS and the mixture was evaporated to dryness to remove excess phosgene. The crude product was redissolved in 10 ml of dry DCM and 0.300 g of diol **20** was then added along with 0.190 g of pyridine. The reaction mixture was brought to reflux for a further 48 hrs before being precipitated

into methanol. The precipitate was extremely fine but was able to be collected via filtration. Mw = 7 kDa, Mn = 4 kDa, PDI = 1.75.

General Methods and Materials:

All solvents and reagents were obtained from Aldrich and were used without further purification except where noted. Dry DCM, pyridine, and TEA were obtained by distillation over CaH$_2$ while THF was distilled from sodium/benzophenone. Methacryloyl chloride was fractionally distilled prior to use. All reactions were run in oven dried glassware and under nitrogen atmosphere except where noted. All ^{1}H and ^{13}C NMR spectra were recorded on a Varian Unity Plus 300 MHz instrument. All chemical shifts are reported in ppm downfield from TMS using the residual protonated solvent as an internal standard (DMSO-d_6, ^{1}H 2.49 ppm and ^{13}C 39.5 ppm or CDCl$_3$, ^{1}H 7.26 ppm and ^{13}C 77.0 ppm). Coupling constants are expressed in Hz. HRMS (CI) was obtained on a VG analytical ZAB2-E instrument while HRMS (ESI) was obtained on an Ion Spec FT-ICR (7 Tesla) instrument. IR data was recorded on a Nicolet Avatar 360 FT-IR using either a KBr pellet or thin film on a NaCl disc. Melting points were recorded using a Mel-Temp II. Melting points for most Diels-Alder adducts were not obtained as cycloreversion occurred prior to melting. Polymer molecular weights were recorded on a Agilent 1100 series GPC relative to polystyrene standards.
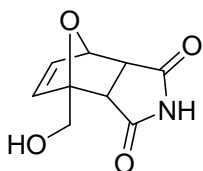
 Synthesis of 1-(hydroxymethyl)-10-oxa-4-azatricyclo [5.2.1.0^{2,6}]dec-8-ene-3,5-dione (4.4a). To a nitrogen purged flask equipped with reflux condenser was added 0.5605 g of maleimide. 8 mL of 3:1 EtOAc/diethyl ether was added along with 0.566 g of freshly distilled furfuryl alcohol. The reaction was stirred at 65 °C for 18 hours and cooled slowly. Product precipitated out

187

of solution as a colorless solid and was collected by vacuum filtration and washed with two portions of cold diethyl ether. The product was found to be 100% *exo* form by ^{1}H NMR (yield 93%). Upon scale up of this reaction it was found that a 40:60 ratio of *endo*/*exo* isomers was obtained. Conversion to 100% *exo* product was achieved by refluxing the product in benzene for 24 hrs followed by cooling, vacuum filtration, and washing with two portions of cold diethyl ether. ^{1}H NMR (300 Mhz, DMSO-d$_6$) δ 11.143 (s, 1H), 6.481 (m, 2H), 5.047 (d, $J = 1.2$ Hz, 1H), 4.924 (t, $J = 6$ Hz, 1H), 4.010 (dd, $J = 6, 6$ Hz, 1H), 3.701 (dd, $J = 12.3, 5.4$ Hz, 1H), 2.977 (d, $J = 6.6$ Hz, 1H), 2.789 (d, $J = 6.3$ Hz, 1H); ^{13}C NMR (DMSO-d$_6$) δ 177.7, 176.4, 138.1, 136.5, 91.7, 80.2, 58.9, 51.3, 49.1; HRMS ([M+H]$^+$ calcd. = 196.0610, found = 196.0613). IR (KBr) ν = 3429, 3343, 3297, 3237, 3071, 2925, 1765, 1719, 1348, 1188 cm^{-1}.
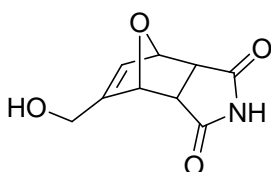
Synthesis of 8-(hydroxymethyl)-10-oxa-4-azatricyclo[5.2.1.0^{2,6}] dec-8-ene-3,5-dione (4.4b). To a nitrogen purged flask equipped with reflux condenser was added 3.385 g of maleimide. A 2:1 mixture of EtOAc/diethyl ether (36 mL) was added along with 3.42 g of 3-hydroxymethyl furan. The reaction was stirred at 65 °C for 18 hours and cooled slowly. The product preciptitated out of solution as colorless solid and was then collected by vacuum filtration and washed with two portions of cold diethyl ether. The product was found to be 100% *exo* form by ^{1}H NMR (yield 90%). Upon scale up of this reaction it was found that a 30:70 ratio of *endo*/*exo* isomers were obtained. Conversion to 100% *exo* product was achieved by refluxing the product in benzene for 24 hrs followed by cooling, vacuum filtration, and washing with two portions of cold diethyl ether. ^{1}H NMR (300 Mhz, DMSO-d$_6$) δ 11.124 (s, 1H), 6.158 (q, $J = 1.5$ Hz, 1H), 5.053 (s, 1H), 4.992 (br, 1H), 4.129 (m, 2H), 2.902 (q, $J = 6.3$ Hz, 2H); ^{13}C NMR (DMSO-d$_6$) δ 178.0,

177.9, 151.6, 128.7, 81.0, 80.8, 56.5, 50.0, 48.2; HRMS ([M+H]$^+$ calcd. = 196.0610, found = 196.0605). IR (KBr) ν = 3456, 3197, 3071, 2925, 2866, 2773, 1772, 1699, 1354 cm^{-1}.
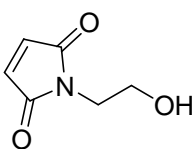
Synthesis of 1-(2-hydroxyethyl)-1*H*-pyrrole-2,5-dione (4.5). To a 100 ml round bottom flask with stir bar and open air condenser was added 4.419 g of **4.16** and 50 mL of toluene. The reaction was brought to reflux for 7 hours. The mixture was hot filtered and the product crystallized from solution upon cooling. The colorless solid was collected via vacuum filtration (yield 92%). ^{1}H NMR (300 Mhz, DMSO-d$_6$) δ 6.999(s, 2H), 4.774 (br, 1H) 3.442 (br, 4H); ^{13}C NMR (DMSO-d$_6$) δ 171.1, 164.5, 57.9, 39.9; HRMS ([M+H]$^+$ calcd = 142.0504 found = 142.0503); IR (KBr) ν = 3363.54, 2919.34, 2853.04, 2355.80, 1706.08, 1407.73, 1162.43 cm^{-1}.
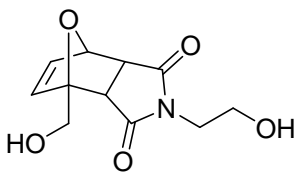
Synthesis of 1-(hydroxymethyl)-10-oxatricyclo[5.2.1.0^{2,6}]dec-8-ene-3,5-dione-2-aminoethanol (4.7a). To a 100 ml round bottom flask with magnetic stir bar and reflux condenser was added 1.301 g of maleimide **4.5**, 20 mL of benzene, and 0.8 mL of freshly distilled furfuryl alcohol. The reaction was refluxed for 24 hours. The product precipitated out of the reaction mixture overnight. The mixture was cooled to room temperature and the products was collected via vacuum filtration, and washed with diethyl ether to produce a colorless solid (yield 86%). Scale up of this procedure often gave a mixture of *endo* and *exo* isomers. This could be avoided through elongated reaction times of up to 48 hrs. ^{1}H NMR (300 Mhz, DMSO-d$_6$) δ 6.508 (br, 2H) 5.061 (s, 1H) 4.931 (t, *J* = 5.7 Hz, 1H) 4.757 (t, *J* = 5.7 Hz, 1H) 4.020 (dd, *J* = 12.6, 6 Hz, 2H),

3.671 (dd, *J* = 12.6, 5.4 Hz, 1H), 3.395 (br, 4H) 3.027 (d, *J* = 6.3 Hz, 1H) 2.864 (d, *J* = 6.3 Hz, 1H); ^{13}C NMR (DMSO-d$_6$) δ 176.4, 174.9, 138.1, 136.5, 91.6, 80.2, 58.9, 57.3, 49.9, 47.8, 40.5; HRMS ([M+H]$^+$ calcd = 240.0872 found = 240.0872); IR (KBr) ν = 3423.20, 3078.45, 2919.34, 1692.82, 1407.73, 1182.32, 1029.83 cm^{-1}.
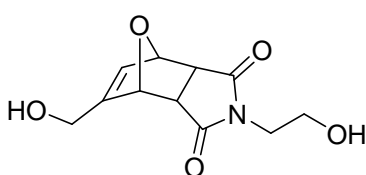
Synthesis of 8-(hydroxymethyl)-10-oxatricyclo[5.2.1.0^{2,6}] dec-8-ene-3,5-dione-2-aminoethanol (4.7b). To a 100 ml round bottom flask with magnetic stir bar and reflux condenser was added 1.301 g of maleimide **4.5**, 20 mL of benzene, and 0.8 mL of freshly distilled furfuryl alcohol. The reaction was refluxed for 24 hours. The product precipitated out of the reaction mixture overnight. The mixture was cooled to room temperature and the product was collected via vacuum filtration, and washed with diethyl ether to produce a colorless solid (yield 90%). Scale up of this procedure often gave a mixture of *endo* and *exo* isomers. This could be avoided through elongated reaction times of up to 48 hrs. ^{1}H NMR (300 Mhz, DMSO-d$_6$) δ 6.178 (d, *J* = 9 Hz, 1H) 5.060 (s, 1H) 5.010 (m, 2H) 4.762 (t, *J* = 3.6 Hz, 1H) 4.150 (m, 2H), 3.401 (br, 4H), 2.974 (dd, *J* = 5.1, 12.9 Hz, 2H); ^{13}C NMR (DMSO-d$_6$) δ 176.7, 176.6, 151.7, 128.7, 81.0, 80.8, 57.3, 56.6, 48.7, 46.9, 40.7; HRMS ([M+H]$^+$ calcd = 240.0872 found = 240.0872); IR (KBr) ν = 3423.20, 3078.45, 2919.34, 1692.82, 1407.73, 1182.32, 1029.83 cm^{-1}.
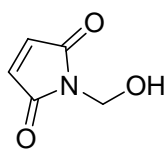
Synthesis of 1-Hydroxymethyl-pyrrole-2,5-dione (4.9). To a 50 mL round bottom flask with magnetic stir bar was added 0.999 g of maleimide. The flask was submerged in an oil bath at 30 °C and 0.850 g of 37 wt% formaldehyde in water was added to the flask. Slowly, 0.08 mL of 1*M* NaOH was added

to the mixture until the solid maleimide dissolved into solution and within 2 minutes product began to precipitate. Upon standing at room temp for 2 hours solid was filtered off and washed with cold water. The crude product was recrystalized from ethyl acetate yielding a colorless solid (yield 60%). ^{1}H NMR (300 Mhz, DMSO-d$_6$) δ 7.056 (s, 2H), 6.263 (t, J = 6.9 Hz, 1H), 4.766 (d, J = 6.9 Hz, 2H); ^{13}C NMR (DMSO-d$_6$) δ 170.6, 134.9, 59.6; HRMS ([M+H]$^+$ calcd. = 128.0348 found = 128.0349); IR (KBr) ν = 3458, 3165, 3093, 2970, 1774, 1703, 1618, 1583 cm^{-1}.
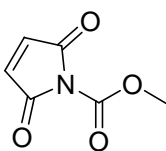
Synthesis of methyl 2,5-dioxo-2,5-dihydro-1*H*-pyrrole-1-carboxylate (4.11). To a flame-dried 100 ml round bottom flask with magnetic stir bar was added 10.066 g of maleimide and 325 mL of EtOAc (shaken over MgSO$_4$ and filtered). The flask was submerged in an ice bath then 11.5 mL of N-methylmorpholine, and 8 mL of methyl chloroformate were added drop wise via syringe. The reaction mixture was stirred in the ice bath for 40 min and then washed with water and brine. The organic layer was dried over MgSO$_4$ and solvent was removed via rotary evaporation to produce a pink colored solid. The product was recrystallized from 9:1 ether to THF to produce a colorless crystalline solid (yield 45.3%). ^{1}H NMR (300 Mhz, DMSO-d$_6$) δ 7.165(s, 2H), 3.823 (s, 3H); ^{13}C NMR (DMSO-d$_6$) δ 166.410, 147.926, 135.764, 53.687. HRMS ([M+H]$^+$ calcd = 156.0297 found = 156.0299). IR (KBr) ν = 3244, 3184, 3085, 3018, 2587, 1765, 1712, 1520, 1440, 1341, 1261, 1208 cm^{-1}
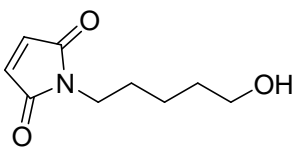
Synthesis of 1-(5-hydroxypentyl)-1*H*-pyrrole-2,5-dione (4.12). To a 100 mL round bottom flask with magnetic stir bar was placed 65 mL of a saturated Na$_2$CO$_3$ solution and 1.4 mL of 5-aminopentanol. The reaction vessel was submerged into an ice bath and 2.008 g of

maleimide **4.11** was added portion wise with continuous stirring. The reaction was stirred in an ice bath for 30 minutes and then stirred at room temperature for 40 min. The reaction mixture was extracted three times with 75 mL of $CHCl_3$. The combined organic layers were then dried with $MgSO_4$ and rotary evaporated to produce a white crystalline solid. The product was collected via vacuum filtration and washed with minimal amounts of cold $CHCl_3$ (yield 65.1%). ^{1}H NMR (300 Mhz, DMSO-d_6) δ 6.998(s, 2H) 4.339 (t, J = 5.1 Hz, 1H) 3.346 (m, 5H) 1.413(m, 4H) 1.206(m, 2H) ; ^{13}C NMR (DMSO-d_6) δ 171.1, 134.4, 60.4, 37.1, 31.9, 27.8, 22.7; HRMS ([M+H]$^+$ calcd = 184.0974 found = 184.0969); IR (KBr) ν = 3244.20, 3098.34, 2932.60, 2859.67, 1706.08, 1414.36 cm^{-1}.
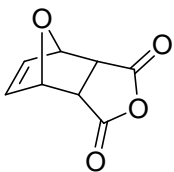
Synthesis of 4,10-dioxatricyclo[5.2.1.0^{2,6}]dec-8-ene-3,5-dione (4.15). To a flame dried 500 mL round bottom flask with magnetic stir bar was added 40.009 g of maleic anhydride, 200 mL of benzene, and 30 mL of furan. The reaction was stirred at room temperature under nitrogen atmosphere for 24 hours. The product precipitated out of solution and was collected via vacuum filtration and washed with diethyl ether (100% *exo*) (yield 93.3%). ^{1}H NMR (300 Mhz, DMSO-d_6) δ 6.566 (s, 2H), 5.334 (s, 2H) 3.296 (s, 2H); 13C NMR (DMSO-d_6) δ 171.5, 136.8, 81.6, 49.1; HRMS ([M+H]$^+$ calcd = 167.0344 found = 167.0344). IR (KBr) ν = 3091, 3032, 2998, 1858, 1785, 1215 cm^{-1}
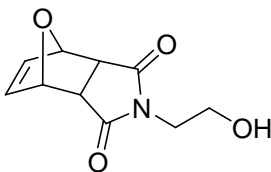
Synthesis of 4-(2-Hydroxy-ethyl)-10-oxa-4-aza-tricyclo [5.2.1.0^{2,6}]dec-8-ene-3,5-dione (4.16). To a flame dried 100 mL 3 neck round bottom flask with magnetic stir bar and reflux condenser was added 10.008 g of compound **4.15**. Next, 20 mL of

192

dry methanol and 3.680 g of ethanolamine were added quickly. The solution turned dark orange and all of the starting material went into solution. The mixture was stirred at room temperature for 30 minutes and then refluxed for 24 hours. The flask was cooled to room temperature, and after 2 hours product began to crystallize. The product was stored in the freezer overnight and the precipitate was collected by vacuum filtration. The volume of the filtrate was then reduced by rotary evaporation and a second crop of crystals were collected (yield 59%). ^{1}H NMR (300 Mhz, DMSO-d$_6$) δ 6.535 (s, 2H), 5.108 (s, 2H), 3.402 (s, 4H), 2.912 (s, 2H); ^{13}C NMR (DMSO-d$_6$) δ 176.5, 136.5, 80.3, 57.3, 47.1, 40.6; HRMS ([M+H]$^+$ calcd. = 210.0766 found = 210.0770); IR (KBr) ν = 3480, 3097, 2971, 2932, 2894, 1769, 1686 cm^{-1}.
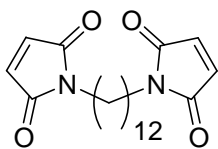
Synthesis of 1,12-Bis-N,N(maleimido)dodecane (4.17a). To a flame dried 250 mL round bottom flask with magnetic stir bar was added 4.899 g of maleic anhydride, 15 mL of dry DMF, and 4.999 g of 1,12 diaminododecane and the mixture was brought to 75 °C. After 24 hours, 30 mL of acetic anhydride, 3 mL of triethylamine, and 0.300 g of Ni(OAc)$_2$•4H$_2$0 were added in one portion to the reaction. The reaction temperature was then raised to 85 °C. The reaction immediately turned dark green, then dark brown within 1 hour. After 24 hours the temperature was lowered to 40 °C and the reaction volume was doubled with water and the mixture was stirred for a further 24 hours. The solvent and water were removed by rotary evaporation and the residue was redissolved in DCM. This mixture was then shaken with 150 mL of silica gel in a separatory funnel and filtered. The solvent was then removed via rotary evaporation. The solid product was then dissolved in minimal amounts of DCM and purified via flash chromatography on a silica gel plug. The solvent was then removed by rotary evaporation to produce the product as a colorless solid. The

193

product was recrystalized from 50:50 ethyl acetate/hexanes (yield 75%). ^{1}H NMR (300 Mhz, CDCl$_3$ with TMS set to δ = 0.00) δ 6.684 (s, 4H), 3.504 (t, J = 7.2 Hz, 4H), 1.58 (m, 4H), 1.238 (m, 16H); ^{13}C NMR (CDCl$_3$) δ 170.9, 134.0, 37.9, 29.43, 29.4, 29.1, 28.5, 26.7; HRMS ([M+H]$^+$ calcd. = 361.2127 found = 361.2127); IR (KBr) ν = 3107, 3088, 2912, 2847, 1696 cm^{-1}.
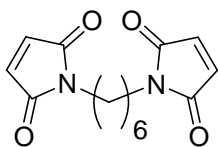
Synthesis of 1,6-Bis-N,N(maleimido)hexane (4.17b). To a flame dried 250 mL round bottom flask with magnetic stir bar was added 16.876 g of maleic anhydride and 50 mL of dry DMF. Hexamethylenediamine (13 mL) was added dropwise to the solution and the mixture was brought to 75 °C. After 24 hours, 40 mL of acetic anhydride, 6 mL of triethylamine, and 0.245 g of Ni(OAc)$_2$•4H$_2$O tetrahydrate were added in one portion to the reaction. The reaction temperature was then raised to 85 °C. The reaction immediately turned dark green, then dark brown within 1 hour. After 24 hours the temperature was lowered to 40 °C and the reaction volume was doubled with water and stirred for a further 24 hours. The solvent and water were removed by rotary evaporation and the residue was redissolved in DCM. This mixture was then shaken with 150 mL of silica gel in a separatory funnel and filtered. The solvent was then removed via rotary evaporation. The solid product was then dissolved in minimal amounts of DCM and purified via flash chromatography on a silica gel plug. The solvent was then removed by rotary evaporation to produce the product as a colorless solid. The product was recrystalized from 50:50 ethyl acetate/hexanes (yield 51%). ^{1}H NMR (300 Mhz, DMSO-d$_6$) δ 6.987 (s, 4H), 3.350 (t, J = 7.2 Hz, 4H), 1.440 (m, 4H), 1.184 (m, 4H); ^{13}C NMR (DMSO-d$_6$) δ 171.1, 134.4, 36.9, 27.8, 25.5; HRMS ([M+H]$^+$ calcd. = 277.1188 found = 277.1188). IR (KBr) ν = 3100, 2950, 1700, 1410, 1130 cm^{-1}
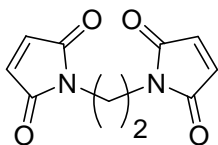
Synthesis of 1,2-Bis-N,N(maleimido)ethane (4.17c). To a flame dried 100 mL round bottom flask with magnetic stir bar was added 5.002 g of maleic anhydride and 15 mL of dry DMF. Ethylenediamine (1.544 g) was added dropwise to the solution and the mixture was brought to 75 °C. After 24 hours 30 mL of acetic anhydride, 3 mL of triethylamine, and 0.342 g of Ni(OAc)$_2$•4H$_2$0 were added in one portion to the reaction. The reaction temperature was then raised to 85 °C. The reaction immediately turned dark green, then dark brown within 1 hour. After 24 hours the temperature was lowered to 40 °C and the reaction volume was doubled with water and stirred for a further 24 hours. The solvent and water were removed by rotary evaporation and the residue was redissolved in DCM. This mixture was then shaken with 150 mL of silica gel in a separatory funnel and filtered. The solvent was then removed via rotary evaporation. The solid product was then dissolved in minimal amounts of DCM and purified via flash chromatography on a silica gel plug. The solvent was then removed by rotary evaporation to produce the product as a colorless solid. The product was recrystalized from 50:50 ethyl acetate/hexanes (yield 20.8%). ^{1}H NMR (300 Mhz, DMSO-d$_6$) δ 7.00 (s, 4H), 3.545 (s, 4H); ^{13}C NMR (DMSO-d$_6$) δ 170.8, 134.6, 35.8; HRMS ([M+H]$^+$ calcd. = 221.0562 found = 221.0562). IR (KBr) ν = 3100, 2960, 1700, 1410, 1130 cm^{-1}
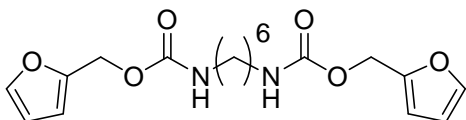
Synthesis of 1,6-Hexamethylene-bis(2-furanyl methylcarbamate) (4.18). To a flame dried 3 necked round bottom flask with magnetic stir bar and condenser was added 50 mL of dry THF, 0.330 g of freshly distilled furfuryl alcohol,

and 1.033 g of diisocyanatohexane. The reaction mixture was refluxed for 24 hours. The Reaction flask was removed from the oil bath and upon cooling, product crystallized out of solution. The solution was maintained at 4 °C overnight and crystals were collected via vacuum filtration yielding a colorless solid (yield 76%). ^{1}H NMR (300 Mhz, DMSO-d$_6$) δ 7.693 (d, J = 1.8 Hz, 2H), 6.432 (m, 4H), 4.933 (s, 4H), 2.940 (q, J = 6.6 Hz, 4H), 1.347 (m, 4H), 1.204 (m, 4H); ^{13}C NMR (DMSO-d$_6$) δ 155.7, 150.3, 143.3, 110.6, 110.1, 57.2, 30.7, 29.3, 25.9; HRMS ([M+H]$^+$ calcd. = 365.1713 found = 365.1709). IR (KBr) ν = 3124, 3045, 2939, 2859, 1686, 1533, 1334, 1261 cm^{-1}
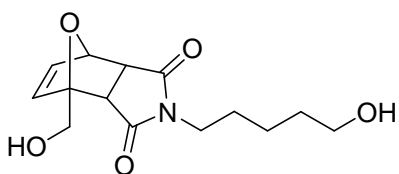
Synthesis of 1-(hydroxymethyl)-10-oxatricyclo [5.2.1.0^{2,6}]dec-8-ene-3,5-dione - 5-aminopentan-1-ol (4.19). To a 25 mL round bottom flask with magnetic stir bar and reflux condenser was added 0.500 g of compound **4.12**, 10 mL of benzene, and 2.6 mL of freshly distilled furfuryl alcohol. The reaction was refluxed for 48 hours. The reaction mixture was rotavapped down to produce an amorphous resin. The crude product was purified via column chromatography using 25% acetone in DCM yielding a colorless solid. The product was determined by NMR to be 40/60 *endo/exo* ratio (yield 64%). A pure sample of *exo* product was obtained from extended reaction times of up to 10 days at 70 °C. ^{1}H NMR (300 Mhz, DMSO-d$_6$) (*exo* compound only) δ 6.508 (m, 2H), 5.066 (s, 1H), 4.950 (t, J = 6 Hz, 1H), 4.335 (t, J = 5.1 Hz, 1H), 4.019 (dd, J = 12.6, 6 Hz, 1H), 3.663 (dd, J = 12.5, 5.4 Hz, 1H), 3.308 (m, 4H), 3.016 (d, J = 6.3 Hz, 1H), 2.852 (d, J = 6.3 Hz, 1H), 1.381 (m, 4H), 1.191 (m, 2H); ^{13}C NMR (DMSO-d$_6$) (*exo* compound only) δ 176.4, 174.9, 138.1, 136.4, 91.6, 80.2, 60.4, 59.0, 49.8, 47.7, 37.8, 31.8, 26.9, 22.5; HRMS ([M+H]$^+$

calcd = 282.1341 found = 282.1340). IR (KBr) ν = 3383, 3098, 2932, 2866, 1765, 1692, 1440, 1401, 1354 cm^{-1}
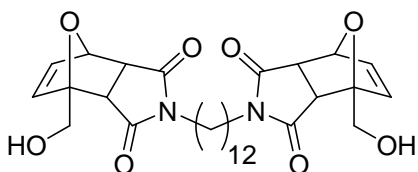
Synthesis of bisadduct 4.20a. To a 50 ml round bottom flask equipped with magnetic stir bar and reflux condenser was added 0.498 g of dodecylbismaleimide **4.17a**, 20 mL of benzene, and 0.25 mL of freshly distilled furfuryl alcohol. The reaction was refluxed for 48 hours. The reaction mixture was reduced and then purified via column chromatography using 20% acetone in DCM as eluent to yield a colorless solid (yield 72%). ^{1}H NMR (300 Mhz, DMSO-d$_6$) δ 6.507 (t, J = 6 Hz, 4H), 5.059 (s, 2H), 4.948 (t, J = 5.4 Hz, 2H), 4.015 (dd, J = 12.45, 5.7 Hz, 4H), 3.655 (dd, J = 12.6, 4.5 Hz, 4H), 3.325 (br, 8H), 3.01 (d, J= 6.6, 2H), 2.849 (d, J= 6.6, 2H), 1.402 (br, 8H), 1.193 (br, 8H); ^{13}C NMR (DMSO-d$_6$) δ 176.4, 174.9, 138.1, 136.4, 91.6, 80.2, 58.9, 49.8, 47.7, 37.7, 28.9, 28.8, 28.4, 26.9, 25.9; HRMS ([M+H]$^+$ calcd = 557.2860 found = 557.2857); IR (KBr) ν = 3356.91, 3191.16, 2919.34, 2846.41, 1692.82, 1646.41 cm^{-1}.
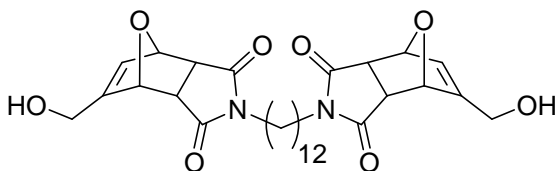
Synthesis of bisadduct 4.20b. To a flame dried 100 mL round bottom flask with magnetic stir bar was added 0.320 g of compound **4.17a**, 5 mL of dry toluene, and 0.200 g of 3-furanmethanol. The reaction mixture was heated to 90 °C for 2 hours and then held at 70 °C for 24 hours under a nitrogen atmosphere. The flask was removed from the oil bath and precipitates formed. The precipitate was a colorless amorphous solid and excess solvent was decanted. The solid was washed with ether to remove impurities and a colorless powder was collected via vacuum filtration (yield 52%). ^{1}H

NMR (300 Mhz, DMSO-d$_6$) δ 6.172 (s, 2H), 5.052 (s, 2H), 4.991 (s, 2H), 4.146 (s, 4H), 3.304 (t, J = 6.9 Hz, 4H), 2.958 (m, 4H), 1.405 (m, 4H), 1.190 (m, 16H); ^{13}C NMR (DMSO-d$_6$) δ 176.7, 176.5, 151.7, 128.7, 81.0, 80.8, 56.5, 48.6, 46.9, 37.8, 28.9, 28.4, 27.0, 25.9; IR (KBr) ν = 3449, 2925, 2853, 1771, 1698 cm^{-1}.
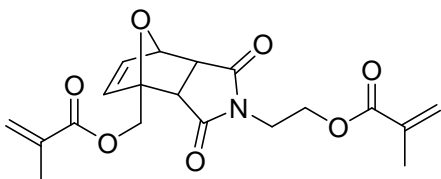
Synthesis of {4-[2-(acryloyloxy)ethyl]-3,5-dioxo-10 -oxa-4-azatricyclo[5.2.1.0^{2,6}]dec-8-en-1-yl} methyl acrylate (4.21a). To a flame dried 100 ml round bottom flask equipped with a magnetic stir bar was added 0.9431 g of **4.7a**. The apparatus was evacuated and backfilled with nitrogen atmosphere three times before 20 mL of dry DCM and 1.5 mL of freshly distilled TEA were added. To this mixture, 0.800 mL of freshly distilled methacryloyl chloride was added drop wise via syringe. The reaction was stirred overnight in an ice bath shielded from light. The reaction mixture was extracted with aqueous NH$_4$Cl, H$_2$0, and Brine. The organic layer was dried over MgSO$_4$, filtered, and 50 μL of a 1 mg/mL solution of p-methoxy phenol in toluene was added as a radical inhibitor and then reduced *in vacuo* (yield 80%). ^{1}H NMR (300 Mhz, DMSO-d$_6$) δ 6.583 (m, 1H), 6.465 (d, J = 5.7 Hz, 1H) 6.358-5.871 (m, 6H) 5.120 (d, J = 1.5 Hz, 1H) 4.833 (d, J = 12.9 Hz, 1H), 4.385 (d, J = 12.9 Hz, 1H), 4.181 (m, 2H), 3.660 (m, 2H), 3.106 (d, J = 6.3 Hz, 2H), 3.033 (d, J = 6.3 Hz, 2H); ^{13}C NMR (DMSO-d$_6$) δ 176.0, 174.7, 165.1, 165.0, 137.3, 136.8, 132.2, 131.8, 128.2, 127.8, 88.8, 80.5, 61.5, 60.5, 49.7, 48.3, 37.1; HRMS ([M+H]$^+$ calcd = 348.1083 found = 348.1082); IR (KBr) ν = 3091, 2952, 2252, 1770, 1716, 1631, 1405, 1332, 1266, 1180, 1067, 982 cm^{-1}.
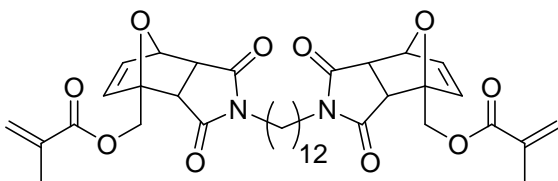
Synthesis of 4.22a. To a flame dried 100 ml round bottom flask equipped with a magnetic stir bar was added 0.500 g of **4.21a**. The apparatus was evacuated and backfilled with nitrogen atmosphere three times before 20 mL of dry DCM and 3 mL of freshly distilled TEA were added. To this mixture, 0.435 mL of freshly distilled methacryloyl chloride was added drop wise via syringe. The reaction was stirred overnight in an ice bath shielded from light. The reaction mixture was extracted with aqueous NH_4Cl, H_2O, and Brine. The organic layer was dried over $MgSO_4$, filtered, and 50 μL of a 1 mg/mL solution of p-methoxy phenol in toluene was added as a radical inhibitor and then reduced *in vacuo* (yield 60%). ^1H NMR (400 Mhz, CDCl$_3$) δ 6.385 (d, J = 5.2 Hz, 2H), 6.272 (d, J = 5.2 Hz, 2H), 5.909 (s, 2H), 5.393 (s, 2H), 5.041 (s, 2H), 4.746 (d, J = 12.4 Hz, 1H), 4.301 (d, J = 12.4 Hz, 2H), 3.239 (t, J = 7.6 Hz, 4H), 2.786 (dd, J = 6.4, 26.4 Hz, 4H), 1.731 (s, 6H), 1.325 (bs, 4H), 1.028 (bs, 16H); ^{13}C NMR (CDCl$_3$) δ 175.3, 173.8, 166.1, 136.9, 136.5, 135.3, 125.6, 88.9, 80.5, 61.2, 49.3, 47.8, 38.3, 30.3, 28.9, 28.8, 28.5, 26.9, 26.1, 17.7; HRMS ([M+H]$^+$ calcd = 693.3385 found = 693.3382); IR (KBr) ν = 3060, 2986, 2928, 2854, 1770, 1704, 1405, 1363, 1219, 1165, 986, 737 cm^{-1}.

NLO Project Experimental

General Methods and Materials:

All solvents and reagents were obtained from Aldrich and were used without further purification except where noted. 5-Norbornene-2-carboxylic acid chloride was synthesized according to literature.[302] Dry DCM, pyridine, and TEA were obtained by distillation over CaH_2 while THF was distilled from sodium/benzophenone. Methacryloyl chloride was fractionally distilled prior to use. All reactions were run in oven dried glassware and under nitrogen atmosphere except where noted. All ^1H and ^{13}C NMR spectra were recorded on a Varian Unity Plus 300 MHz instrument. All chemical shifts are reported in ppm downfield from TMS using the residual protonated solvent as an internal standard (DMSO-d_6, ^1H 2.49 ppm and ^{13}C 39.5 ppm or $CDCl_3$, ^1H 7.26 ppm and ^{13}C 77.0 ppm). Coupling constants are expressed in Hz. HRMS (CI) was obtained on a VG analytical ZAB2-E instrument while HRMS (ESI) was obtained on an Ion Spec FT-ICR (7 Tesla) instrument. IR data was recorded on a Nicolet Avatar 360 FT-IR using either a KBr pellet or thin film on a NaCl disc. Melting points were recorded using a Mel-Temp II. Polymer molecular weights were recorded on a Agilent 1100 series GPC relative to polystyrene standards. Glass transition temperatures were recorded on a TA Q100 DSC and TGA data was recorded on a TA Q500 TGA.
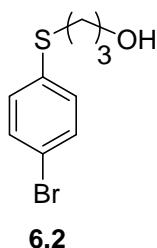
Synthesis of 3-[(4-bromophenyl)thio]propan-1-ol (6.2). A 100 mL round bottom flask with reflux condenser and magnetic stir bar was charged with NaH (1.70 g, 60% in mineral oil, 42.5 mmol) and THF (30 mL). *p*-Bromothiophenol (**6.1**) (8.03 g, 42.5 mmol) was added to a separate 50 mL

round bottom flask and was dissolved in THF (15 mL). The thiol solution was added to the suspension of NaH dropwise over a period of 20 min and stirred for an additional 30 min at room temperature. 3-Bromopropanol (3.71 mL, 42.5 mmol) was placed into a separate 25 mL round bottom flask followed by THF (5 mL). The bromopropanol solution was added to the 100 mL flask dropwise, after which the reaction mixture was heated to reflux for 1 h. The mixture was cooled to room temperature and quenched with water. The aqueous layer was extracted three times with ether, and the organic layers were combined, washed with 1 M KOH, water, brine, then dried over MgSO$_4$, filtered, and concentrated to give **6.2** as colorless viscous oil (10.3 g, 94%). ^{1}H NMR (DMSO-d_6): δ 1.69 (p, J = 6.6 Hz, 2H), 2.99 (t, J = 7.5 Hz, 2H), 3.48 (q, J = 5.4 Hz, 2H), 4.57 (t, J = 5.4 Hz, 1H), 7.23 (d, J = 6.3 Hz, 2H), 7.46 (d, J = 8.7 Hz, 2H); ^{13}C NMR (DMSO-d_6): δ 136.29, 131.73, 129.53, 118.16, 59.15, 31.71, 28.60; HRMS [M+H]$^+$ calcd. = 246.9792 found = 246.9797; FTIR ν = 3340 (br), 2920, 2869, 1467, 1382, 1091, 1071, 1001, 811 cm^{-1}.
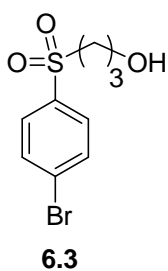
Synthesis of 3-[(4-bromophenyl)sulfonyl]propan-1-ol (6.3). Compound **6.2** (10.36 g, 41.9 mmol) was placed in a 250 mL round bottom flask equipped with reflux condenser and magnetic stir bar. Hydrogen peroxide (50 mL, 30 wt% in water) was added followed by glacial acetic acid (100 mL). The reaction mixture was stirred at room temperature for 1 h and then heated to 90 ^{o}C for 10 h. The reaction was cooled and extracted with three portions of ether. The organic fractions were combined and washed with 1 M KOH until basic, then washed with brine, dried over MgSO$_4$, filtered, and concentrated to yield a mixture of the free alcohol and acylated product (8.85 g). The mixture was placed in a 250 mL flask with condenser, charged with MeOH (75 mL) and NaOH (2.6 g, 65 mmol). The reaction

mixture was heated to 70 $^{\circ}$C for 4 h and then cooled to room temperature. The reaction was quenched with 1 *M* HCl and extracted with ether. The organic layers were combined and washed with sat. NaHCO$_3$ until basic, water, and brine, then dried over MgSO$_4$, filtered, and concentrated to give **6.3** as a white solid (5.6 g, 65%). mp 64-66 °C; ^{1}H NMR (DMSO-d_6): δ 1.65 (m, 2H), 3.1 (m, 2H), 3.39 (q, *J* = 5.4-6.3 Hz, 2H), 4.63 (t, *J* = 5.4 Hz, 1H), 7.85 (m, 4H); ^{13}C NMR (DMSO-d_6): δ 25.89, 52.01, 58.60, 127.94, 129.76, 132.56, 138.20; HRMS [M+H]$^+$ calcd. = 277.9613 found = 277.9612; FTIR ν = 3514 (br), 3083, 2951, 2920, 2869, 1572, 1394, 1312, 1273, 1137, 1067, 1005 cm^{-1}.
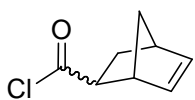
Synthesis of bicyclo[2.2.1]hept-5-ene-2-carbonyl chloride. THF (100 mL) was added to an oven dried 250 mL round bottom flask under a nitrogen atmosphere. Norbornene carboxylic acid 4 (6.5 mL, 57.2 mmol) and a catalytic amount of dry DMF was then added. The flask was cooled in an ice bath and oxalyl chloride (5.48 mL, 62.9 mmol) was added dropwise. After stirring for three hours at 0 °C, the solution was concentrated *in vacuo* and the resulting concentrate was distilled (10 mmHg, 59 °C) to give 5 as a clear liquid. (6.5 g, yield 78%); ^{1}H NMR (CDCl$_3$): δ 1.50 (m, 2H), 1.95 (m, 2H), 2.98 (s, 1H), 3.43 (m, 2H), 6.12 (m, 1H), 6.24 (m, 1H); ^{13}C NMR (CDCl$_3$): δ 30.01, 42.82, 48.16, 56.36, 131.54, 134.82, 138.98, 174.98; For complete characterization see Ref 302.

6.4
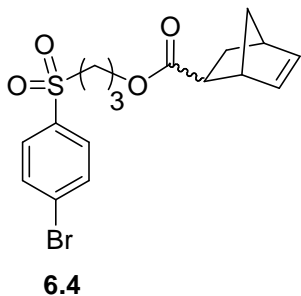
Synthesis of 3-[(4-bromophenyl)sulfonyl]propylbicycle [2.2.1]hept-5-ene-2-carboxylate (6.4). A 250 mL round bottom was charged with sulfone **6.3** (4.993 g, 17.9 mmol) and THF (90 mL). Pyridine (3 mL, 35.8 mmol) was added and the flask was immersed in an ice bath followed by dropwise addition of 5-

norbornene-2-carboxylic acid chloride (3.5 mL, 22.4 mmol) over a period of 15 min. After addition, the reaction was warmed to room temperature and stirred for a further 14 h. The reaction was diluted with DCM and washed with 1 *M* HCl until the washings were acidic. The organic extracts were washed with sat. $NaHCO_3$, water, and brine, then dried over $MgSO_4$, filtered and concentrated to give a reddish brown oil. Flash chromatography of the residue using 2% Acetone in DCM as eluent yielded a mixture of *endo* and *exo* **6.4** as white solid (63%). mp 64-67 °C; ^{1}H NMR (DMSO-d_6): δ 1.27 (m, 2H), 1.82 (m, 4H), 2.92 (m, 3H), 3.39 (m, 2H), 3.99 (m, 2H), 5.80 (m, 1H), 6.15 (m, 1H), 7.88 (m, 4H); ^{13}C NMR (CDCl₃): δ 175.8, 174.3, 138.0, 137.9, 137.7, 132.7, 131.9, 129.6, 129.2, 61.8, 61.5, 53.2, 49.6, 46.5, 46.2, 45.6, 43.1, 42.9, 42.4, 41.5, 30.3, 29.1, 22.5; HRMS [M+H][+] calcd. = 399.0266 found =399.027; FTIR ν = 3084, 3060, 2975, 2870, 1728, 1577, 1394, 1313, 1274, 1169, 1150 cm^{-1}.
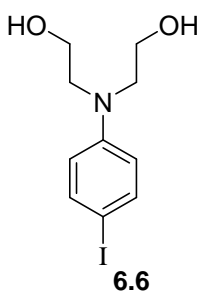
Synthesis of 2,2'-[(4-iodophenyl)imino]diethanol (6.6). Compound **6.5** (10.00 g, 55.18 mmol) and dilute HCl (1 M, 55 mL)was added to a 250 mL round bottom flask with magnetic stir bar. ICl (8.96 g, 55.18 mmol) was added to HCl (90 mL, 6 N), cooled in an ice bath and then added to the reaction flask in one portion with stirring. The reaction mixture turned dark red immediately and after 2 h, 1 M $Na_2S_2O_3$ was added slowly until the solution became colorless. The reaction mixture was added dropwise to a saturated solution of $NaHCO_3$ and the product precipitated out as an off white solid. The solid was filtered off, washed with cold water, and dried *in vacuo* to produce **6.6** as an white solid (83%). mp 82-84 °C; ^{1}H NMR (DMSO-d_6): δ 3.36 (t, *J* = 6 Hz, 4H), 3.49 (t, *J* = 6 Hz, 4H), 4.74 (bs, 2H), 6.51 (d, *J* = 9 Hz, 2H), 7.36 (d, *J* = 9 Hz, 2H); ^{13}C NMR (DMSO-d_6):

δ 147.6, 137.1, 114.1, 75.5, 57.9, 53.1; HRMS [M+H]$^+$ calcd. = 308.0142 found = 308.0143; FTIR ν = 3254 (br), 2944, 2862, 1580, 1491, 1351, 1192, 1060, 812 cm^{-1}.
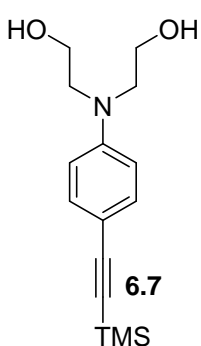
Synthesis of 2,2'-[(4-(trimethylsilyl)ethynylphenyl)imino]diethanol (6.7). Compound **6.6** (1.00 g, 3.256mmol) was added to a round bottom flask with stir bar containing PdCl$_2$(PPh$_3$)$_2$ (0.230 g, 0.325 mmol) and CuI (31 mg, 0.166 mmol). THF (30 mL) was added along with ethynyltrimethylsilane (TMSA) (1.12 mL, 8.14 mmol) and TEA (4.54 mL, 32.56 mmol). The reaction mixture was degassed by three freeze-pump-thaw cycles and was stirred for 30 min. before heating to 60 °C for 15 h. The crude mixture was reduced *in vacuo* and passed through a plug of celite and silica gel before concentrating and purification via flash column chromatography with 15% acetone in DCM as eluent, yielding **6.7** as a faint yellow solid (97%). mp 98-100 °C; ^{1}H NMR (DMSO-d_6): δ 0.18 (s, 9H), 3.41 (t, J = 5.7 Hz, 4H), 3.50 (t, J = 5.4 Hz, 4H), 4.76 (t, J = 5.4 Hz, 2H), 6.62 (d, J = 8.7 Hz, 2H), 7.20 (d, J = 9 Hz, 2H); ^{13}C NMR (DMSO-d_6): δ 148.23, 132.80, 111.07, 107.66, 107.09, 90.65, 57.97, 53.04, 0.23; HRMS [M+H]$^+$ calcd. = 278.1576 found = 278.1579; FTIR ν = 3243 (br), 3138, 2955, 2874, 2140, 1604, 1518, 1355, 1184, 1068, 1002, 847 cm^{-1}.
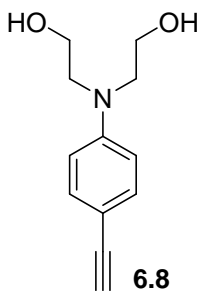
Synthesis of 2,2'-[(4-ethynylphenyl)imino]diethanol (6.8). Compound **6.7** (0.936 g, 3.37 mmol) was added to a 50 mL round bottom flask with magnetic stir bar. MeOH (20 mL) and K$_2$CO$_3$ (1.502 g, 10.12 mmol) were added and the reaction mixture was stirred at room temperature for 2 h. The crude reaction mixture was reduced *in vacuo* and purified by passing through a plug of silica gel using 1:5 acetone/DCM yielding **6.8** as a faint yellow

solid (97%). mp 119-121 °C; ^{1}H NMR (DMSO-d_6): δ 3.41 (t, J = 6 Hz, 4H), 3.50 (t, J = 5.7 Hz, 4H), 3.82 (s, 1H), 4.76 (t, J = 5.4 Hz, 2H), 6.63 (d, J = 9 Hz, 2H), 7.21 (d, J = 9 Hz, 2H); ^{13}C NMR (DMSO-d_6): δ 148.15, 132.76, 111.11, 107.16, 84.84, 77.79, 57.97, 53.03; HRMS [M+H]$^+$ calcd. = 206.1181 found = 206.1186; FTIR ν = 3285 (br), 2928, 2882, 2093, 1612, 1511, 1355, 1060, 1041, 823 cm^{-1}.
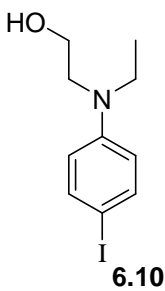
Synthesis of 2-[ethyl(4-iodophenyl)amino]ethanol (6.10). Compound **6.9** (4.00 g, 24.2 mmol) was added to dioxane (180 mL) and pyridine (180mL) in a 500 mL round bottom flask with magnetic stir bar. The reaction mixture was cooled to 0 °C and I$_2$ (9.23 g, 36.2 mmol) was added in one portion. The reaction was maintained at 0 °C for one hour then warmed to room temperature for a further hour. Additional I$_2$ (3.07 g, 12 mmol) was added and stirred for an additional hour. The reaction mixture was washed with 1 M Na$_2$S$_2$O$_3$ until the brown color dissipated and was the extracted with DCM. The crude product was purified via column chromatography using DCM as eluent to afford pure **6.10** as a white solid. (5.527 g, yield 78%) mp 50-52 °C; ^{1}H NMR (DMSO-d_6): δ 1.03 (t, J = 6.9 Hz, 3H), 3.30 (m, 4H), 3.50 (q, J = 6Hz, 2H), 4.70 (t, J = 5.4Hz, 1H), 6.49 (d, J = 8.7Hz, 2H), 7.36 (d, J = 9Hz, 2H); ^{13}C NMR (Solvent): δ 147.3, 137.2, 114.0, 75.3, 58.2, 51.9, 44.5, 11.7; HRMS ([M+H]$^+$ calcd. = 291.0120 found = 291.0120) FTIR ν = 3304, 3215, 2920, 2866, 1499, 1588, 1355, 1266, 1184, 1064, 796 cm^{-1}.
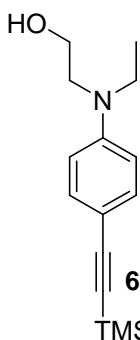
Synthesis of 2-[ethyl(4-(trimethylsilyl)ethynylphenyl)amino]ethanol (6.11). A dry 100 mL round bottom flask was equipped with a magnetic stir bar and condenser, and was charged with compound **6.10** (0.521 g, 1.79 mmol), $PdCl_2(PPh_3)_2$ (125.6 mg, 0.179 mmol), and copper (I) iodide (17 mg, 0.0894 mmol). The flask was placed under nitrogen and THF (25 mL) was added followed by ethynyltrimethylsilane (0.623 mL, 4.49 mmol) and diisopropylamine (2.5 mL, 1.79 mmol) in one portion. The reaction was degassed by three freeze-pump-thaw cycles and was stirred at room temperature for 30 min. and was then heated to 70 °C for 14 h. After cooling to room temperature, the reaction mixture was concentrated *in vacuo* and passed through a short silica gel/celite plug with 2% acetone in DCM to recover the product **6.11** as a yellow liquid. (yield 97%); ^1H NMR ($CDCl_3$): δ 0.23 (s, 9H), 1.15 (t, J = 5.4 Hz, 3H), 3.41 (t, J = 5.1 Hz, 2H), 3.46 (t, J = 4.8 Hz, 2H), 3.78 (t, J = 4.5 Hz, 2H), 6.63 (d, J = 6.6 Hz, 2H), 7.31 (d, J = 6.6 Hz, 2H); ^{13}C NMR ($CDCl_3$): δ 148.05, 133.31, 111.71, 109.98, 106.29, 91.26, 60.16, 52.23, 45.47, 21.03, 11.82, 0.17; HRMS ($[M+H]^+$ calcd. = 261.1549 found = 261.1547) FTIR ν = 3386, 3040, 2959, 2893, 2147, 1603, 1514, 1401, 1359, 1242, 1188, 1044, 862 cm^{-1}.
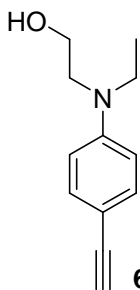
Synthesis of 2-[ethyl(4-ethynylphenyl)amino]ethanol (6.12). Compound **6.11** (0.102 g, 0.39 mmol) was added to a 25 mL round bottom flask with magnetic stir bar under a nitrogen atmosphere. THF (5 mL) was added along with one drop of water. TBAF (0.6 mL, 1 M in THF, 0.6 mmol) was added and stirred at room temperature overnight. The reaction mixture was diluted with 1:1 hex/EtOAc and washed with water, brine and dried with $MgSO_4$. The solvent was removed *in vacuo* and was purified via silica gel plug

206

using DCM as eluent to produce compound **6.12** as a faint yellow solid. (yield 95%) mp 50-53 °C; ^{1}H NMR (DMSO-d_6): δ 1.05 (t, J = 6.9 Hz, 3H), 3.36 (m, 4H), 3.51 (q, J = 5.7 Hz, 2H), 3.81 (s, 1H), 4.72 (t, J = 5.4 Hz, 1H), 6.61 (d, J = 6.9 Hz, 2H), 7.22 (d, J = 6.9, 2H); ^{13}C NMR (DMSO-d_6): δ 147.84, 132.83, 111.03, 107.01, 84.88, 77.68, 58.21, 51.88, 44.56, 11.83; HRMS ([M+H]$^{+}$ calcd. = 190.1232 found = 190.1236) FTIR ν = 3254, 2963, 2897, 2093, 1883, 1611, 1510, 1401, 1172, 1009, 819, 536 cm^{-1}.

6.13
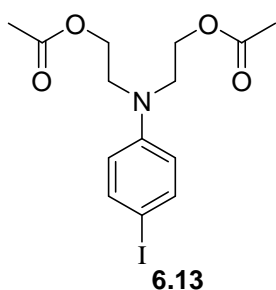
Synthesis of [(4-iodophenyl)imino]diethane-2,1-diyl diacetate (6.13). Compound **6.6** (1.03 g, 3.3 mmol) was added to a dry 250 mL round bottom flask under a nitrogen atmosphere. A catalytic amount of DMAP was then added followed by pyridine (66 mL) and acetic anhydride (15 mL, 163 mmol). The reaction mixture was stirred for 12 h at room temperature and then concentrated *in vacuo*. The product was isolated by silica gel chromatography using 25% Ethyl acetate in Hexanes as eluent yielding **6.13** as a viscous clear liquid. (yield 82%) ^{1}H NMR (DMSO-d_6): δ 1.97 (s, 6H,CH$_3$), 3.55 (t, J = 6.0 Hz, 4H), 4.11 (t, J = 5.9 Hz, 4H), 6.61 (d, J = 9.3 Hz, 2H), 7.41 (d, J = 8.7 Hz, 2H); ^{13}C NMR (DMSO-d_6): δ 170.37, 146.96, 137.32, 114.46, 77.11, 60.82, 48.82, 20.65; HRMS ([M+H]$^{+}$ calcd. = 392.0355 found = 392.0359) FTIR ν = 3071, 2959, 2893, 1871, 1735, 1584, 1499, 1378, 1234, 1048, 803 cm^{-1}.

6.14

TMS
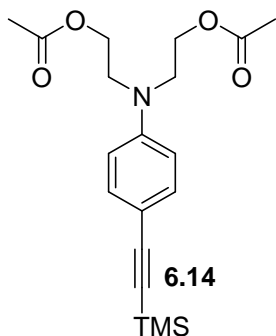
Synthesis of [(4-(trimethylsilyl)ethynylphenyl)imino]diethane-2,1-diyl diacetate (6.14). A dry 100 mL round bottom with magnetic stir bar was charged with PdCl$_2$(PPh$_3$)$_2$ (170 mg, 0.237 mmol) and Copper (I) Iodide (34 mg, 0.119 mmol) and placed under a nitrogen atmosphere. THF (30 mL) was added followed

by **6.13** (0.929 g, 2.37 mmol) dissolved in THF (10 mL) and TMS-Acetylene (0.822 mL, 5.94 mmol). Diisopropylamine (3.3 mL, 2.37 mmol) was added in one portion and the mixture was degassed by three freeze-pump-thaw cycles and was stirred at room temperature for 30 min.. The reaction was then heated to 60 °C for 12 h, after which it was concentrated *in vacuo* and passed through a plug of silica gel and celite using 5% Acetone in DCM as eluent. The mixture was concentrated and purified by flash chromatography using DCM as the eluent yielding **6.14** as a faint viscous yellow liquid. (yield 98%) ^{1}H NMR (DMSO-d_6): δ .018 (s, 9H), 1.97 (s, 6H), 3.61 (t, J = 5.6 Hz, 4H), 4.13 (t, J = 5.9 Hz, 4H), 6.72 (d, J = 10.8 Hz, 2H), 7.22 (d, J = 9 Hz, 2H) ; ^{13}C NMR (DMSO-d_6): δ 170.34, 147.61, 132.84, 111.48, 108.88, 106.65, 91.02, 660.91, 48.67, 20.61, 0.15; HRMS ([M+H]$^+$ calcd. = 362.1782 found = 362.1788) FTIR ν = 3048, 2959, 2897, 2147, 1743, 1600, 1514, 1382, 1238, 1048, 850, 757 cm^{-1}.
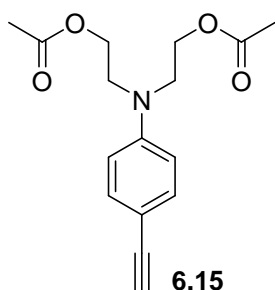
Synthesis of [(4-ethynylphenyl)imino]diethane-2,1-diyl diacetate (6.15). Compound **6.14** (0.44 g, 1.3 mmol) was added to a 50 mL round bottom flask followed by THF (20 mL) and 3 drops of water. TBAF (2 mL, 1 M in THF, 2 mmol) was added in one portion and the reaction mixture was stirred at room temperature for 10 h. The reaction was stopped by diluting the mixture with 50:50 ethyl acetate:ether and then washing with water and brine. The organic layer was dried over MgSO$_4$, filtered, concentrated, and then flashed on silica gel with 25% Ethyl acetate in hexanes to yield **6.15** as a viscous yellow oil. (yield 60%); ^{1}H NMR (DMSO-d_6): δ 1.97 (s, 6H, CH$_3$), 3.60 (t, J = 6 Hz, 4H), 3.86 (s, 1H, CH), 4.13 (t, J = 6.15 Hz, 4H), 6.74 (d, J = 9 Hz, 2H), 7.25 (d, J = 8.7 Hz, 2H); ^{13}C NMR (CDCl$_3$): δ 170.89, 147.36, 133.50, 111.47, 109.69, 84.30, 75.10, 61.14, 49.45, 20.82; HRMS

([M+H]$^+$ calcd. = 290.1396 found = 290.1392) FTIR ν = 3281, 3048, 2955, 2892, 2096, 1739, 1603, 1517, 1378, 1234, 1043, 822 cm^{-1}.

6.16
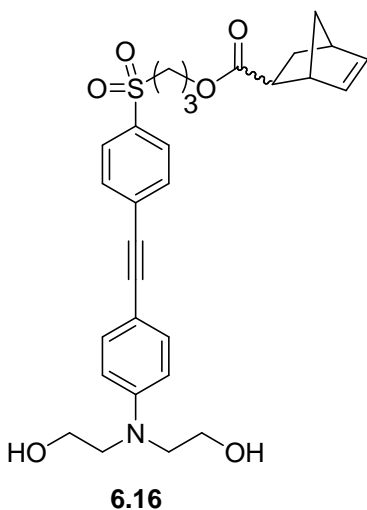
Synthesis of Tolane 6.16. Alkyne **6.8** (0.137 g, 0.662 mmol), PdCl$_2$(PPh$_3$)$_2$ (47 mg, 0.066 mmol), and of CuI (7 mg, 0.033 mmol) were added to a 25 mL round bottom flask with magnetic stir bar. The flask was maintained under N$_2$ atmosphere and compound **6.4** (0.238 g, 0.596 mmol) dissolved in THF (10 mL) was added. Diisopropylamine (1 mL) was added and the reaction was degassed by three freeze-pump-thaw cycles and was stirred at room temperature for 40 min. before being brought to 60 °C for 15 h. The crude reaction mixture was reduced in *vacuo* and passed through a celite and silica gel plug before column purification using 15% acetone in DCM as eluent to produce **6.16** as a yellow solid (82%). mp 56-59 °C (compound is extremely hygroscopic and mp determination was difficult); *endo*-norbornyl isomer: ^{1}H NMR (DMSO-d_6): δ 1.18-1.30 (m, 3H), 1.77-1.86 (m, 3H), 2.83 (s, 1H), 2.97 (dt, *J* = 4.2, 9.3 Hz, 1H), 3.09 (s, 1H), 3.34-3.420 (m, 2H), 3.46 (t, *J* = 5.1 Hz, 4H), 3.534 (t, *J* = 5.7 Hz, 4H), 3.97 (t, *J* = 6.3 Hz, 2H), 4.79 (t, *J* = 5.4 Hz, 2H), 5.80 (dd, *J* = 2.7, 5.4 Hz, 1H), 6.13 (dd, *J* = 2.7, 5.4 Hz, 1H), 6.72 (d, *J* = 9 Hz, 2H), 7.36 (d, *J* = 8.7 Hz, 2H), 7.71 (d, *J* = 8.7 Hz, 2H), 7.87 (d, *J* = 8.4 Hz, 2H); ^{13}C NMR (DMSO-d_6): δ 173.57, 148.74, 137.65, 136.97, 132.99, 132.28, 131.44, 129.05, 128.06, 111.34, 106.51, 95.46, 86.16, 61.53, 57.99, 53.04, 51.63, 49.09, 45.13, 42.45, 41.92, 28.66, 22.22; HRMS [M+H]$^+$ calcd. = 523.2029 found = 523.2023; FTIR ν = 3379 (br), 3052, 2963, 2866, 2198, 1720, 1603, 1584, 1522, 1130 cm^{-1}.

6.17
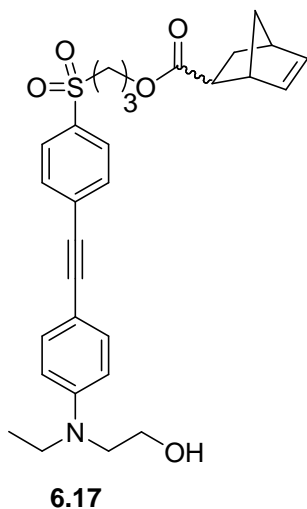
Synthesis of Tolane 6.17. Alkyne **6.12** (1.392 g, 7.355 mmol), PdCl$_2$(PPh$_3$)$_2$ (516 mg, 0.736 mmol), and CuI (70 mg, 0.368 mmol) were added to an oven dried 250 mL round bottom flask with magnetic stir bar. The flask was maintained under N$_2$ atmosphere and compound **6.4** (2.878 g, 7.21 mmol) dissolved in THF (150 mL) was added. Diisopropylamine (10.31 mL, 73.552 mmol) was added and the reaction was degassed by three freeze-pump-thaw cycles and was stirred at room temperature for 40 min. before being brought to 50 °C for 15 h.

The crude reaction mixture was reduced in vacuo and passed through celite and a silica gel plug before column purification using 2% acetone in DCM as eluent to produce **6.17** as a viscous yellow oil. (yield 52%); ^{1}H NMR (Solvent): δ 1.180 (t, J = 5.4 Hz, 3H), 1.262 (d, J = 6 Hz, 1H), 1.335-1.381 (m, 1H), 1.416-1.462 (m, 1H), 1.835-1.914 (m, 1H), 1.988-2.204 (m, 3H), 2.888-2.931 (m, 2H), 3.156 (p, J = 6 Hz, 2H), 3.458 (q, J = 5.1 Hz, 2H), 3.506 (t, J = 5.1 Hz, 2H), 3.806 (t, J = 5.1 Hz, 1H), 4.054-4.174 (m, 1H), 5.839-5.860 (m, 1H), 6.099-6.187 (m, 1H), 6.693 (d, J = 6.6 Hz, 2H), 7.385 (d, J = 6.6 Hz, 2H), 7.638 (d, J = 9 Hz, 2H), 7.825 (d, J = 9 Hz, 2H); ^{13}C NMR (Solvent): δ 174.4, 170.8, 148.5, 137.9, 136.4, 133.3, 132.0, 131.7, 130.4, 127.9, 111.6, 108.3, 86.1, 61.6, 59.9, 53.2, 52.1, 49.6, 46.5, 45.7, 45.4, 43.1, 42.4, 29.1, 22.5, 11.8; HRMS ([M+H]$^+$ calcd. = 508.2155 found = 508.2158) FTIR ν = 3514 (br), 3060, 2970, 2873, 2205, 1728, 1584, 1522, 1401, 1312, 1188, 912, 734 cm^{-1}.
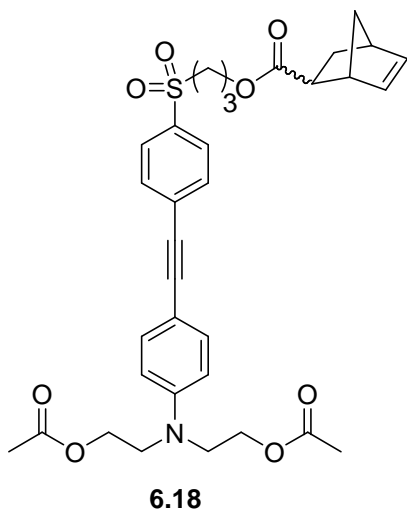
Synthesis of Tolane 6.18. Alkyne **6.15** (0.458 g, 1.58 mmol), PdCl$_2$(PPh$_3$)$_2$ (121 mg, 0.170 mmol), and CuI (16 mg, 0.086 mmol) were added to an oven dried 100 mL round bottom flask with magnetic stir bar. The flask was maintained under N$_2$ atmosphere and compound **6.4** (0.691 g, 1.73 mmol) dissolved in THF (20 mL) was added. Diisopropylamine (2.43 mL, 17.3 mmol) was added and the reaction was degassed by three freeze-pump-thaw cycles and was stirred at room temperature for 40 min. before being brought to 50 °C for 15 h. The crude reaction mixture was reduced in vacuo and passed through celite and a silica gel plug before column purification using 2% acetone in DCM as eluent to produce **6.18** as a viscous yellow oil. (yield 52%); ^{1}H NMR (DMSO-d_6): δ 1.18-1.32 (m, 3H), 1.77-1.86 (m, 3H), 1.97 (s, 6H) 2.83 (s, 1H), 2.97 (dt, J = 4.2, 9 Hz, 1H), 3.08 (s, 1H), 3.34-3.420 (m, 2H), 3.65 (t, J = 5.1 Hz, 5H), 3.98 (t, J = 6 Hz, 2H), 4.16 (q, J = 5.4 Hz, 5H), 5.81 (dd, J = 2.7, 5.4 Hz, 1H), 6.13 (dd, J = 3, 5.7 Hz, 1H), 6.82 (d, J = 6 Hz, 2H), 7.37 (d, J = 8.7 Hz, 2H), 7.72 (d, J = 8.7 Hz, 2H), 7.88 (d, J = 8.4 Hz, 2H); ^{13}C NMR (DMSO-d_6): δ 173.56, 170.37, 148.11, 137.64, 137.16, 133.05, 132.27, 131.56, 128.88, 128.06, 111.74, 107.79, 94.92, 86.30, 61.52, 60.91, 51.63, 49.08, 48.74, 45.12, 42.45, 41.92, 41.03, 28.65, 22.21, 20.63; HRMS ([M+H]$^+$ calcd. = 608.2325 found = 608.2313) FTIR ν = 3056, 2966, 2209, 1735, 1603, 1588, 1522, 1363, 1234, 1126, 1052, 819, 733, 710 cm^{-1}.

6.19
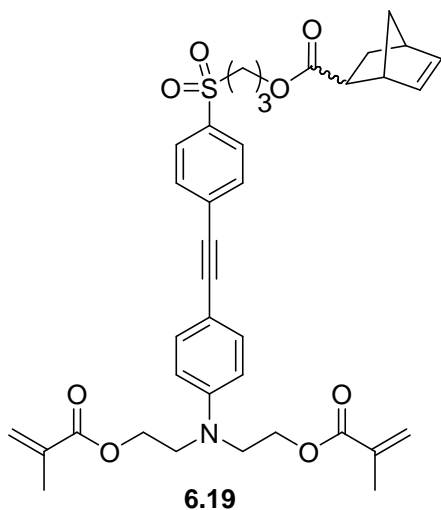
Synthesis of Bismethacrylate Tolane 6.19. Compound **6.16** (0.503 g, 0.96 mmol) and DMAP (0.0137g, 0.096 mmol) were placed in a 100 mL round bottom flask with magnetic stir bar. DCM (5 mL), TEA (0.54 mL, 3.84 mmol) were added followed by methacryloyl chloride (0.281 mL, 2.90 mmoles). The reaction mixture was stirred at 0 °C for 1 h and then stirred at room temp for a further 10 h. The reaction was diluted with DCM, washed with water, brine, and then dried over $MgSO_4$, filtered, and concentrated. The crude mix was purified via flash column chromatography using 1% acetone in DCM as eluent to yield **6.19** as a viscous yellow oil (46%). ^{1}H NMR (DMSO-d_6): δ δ 1.18-1.30 (m, 3H), 1.77-1.86 (m, 3H), 2.1 (s, 3H), 2.83 (s, 1H), 2.97 (dt, J = 4.2, 9.3 Hz, 1H), 3.09 (s, 1H), 3.30-3.41 (m, 2H), 3.738 (t, J = 5.4 Hz, 4H), 3.97 (t, J = 5.4 Hz, 2H), 4.263 (t, J = 5.4 Hz, 4H), 5.66 (t, J = 1.8 Hz, 1H), 5.98 (bs, 1H), 6.87 (d, J = 8.7 Hz, 2H), 7.38 (d, J = 9 Hz, 2H), 7.72 (d, J = 8.4 Hz, 2H), 7.88 (d, J = 8.7 Hz, 2H); HRMS [M+H]$^+$ calcd. = 660.2631 found = 660.2631.

6.20
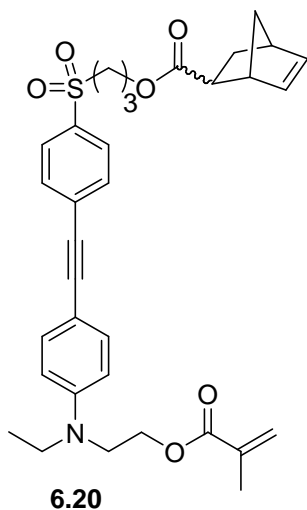
Synthesis of Monomethacrylate Tolane 6.20. Compound **6.17** (4.261 g, 8.4 mmol) and DMAP (0.0137 g, 0.096 mmol) were placed in a 250 mL round bottom flask with magnetic stir bar. DCM (200 mL), TEA (4.7 mL, 33.55 mmol) were added followed by methacryloyl chloride (1.60 mL, 16.78 mmoles). The reaction mixture was stirred at 0 °C for 1 h and then stirred at room temp for a further 10 h. The reaction was diluted with DCM, washed with water, brine, and then dried over MgSO$_4$, filtered, and concentrated. The crude mix was purified via flash column chromatography using 1% acetone in DCM as eluent to yield **6.20** as a viscous yellow oil (72%). ^{1}H NMR (CDCl$_3$): δ 7.797 (d, J = 8.4 Hz, 2H), 7.595 (d, J = 8.4 Hz, 2H), 7.352 (d, J = 8.7 Hz, 2H), 6.655 (d, J = 8.7 Hz, 2H), 6.111 (m, 1H), 6.046 (s, 1H), 5.804 (m, 1H), 5.534 (s, 1H), 4.265 (t, J = 6 Hz, 2H), 4.059 (m, 2H), 3.592 (t, J = 6.6 Hz, 2H), 3.406 (q, J = 6.6 Hz, 2H), 3.120 (m, 3H), 2.847 (m, 2H), 2.042-1.790 (m, 3H), 1.883 (s, 3H), 1.447-1.198 (m, 3H), 1.144 (t, J = 6.9 Hz, 3H); ^{13}C NMR (CDCl$_3$): δ 175.7, 174.1, 167.1, 147.9, 137.9, 137.7, 136.5, 135.8, 135.4, 133.2, 131.9, 131.5, 130.2, 127.8, 125.8, 111.3, 108.3, 95.4, 85.9, 61.7, 61.6, 61.5, 53.3, 53.1, 49.4, 48.3, 46.4, 46.1, 45.5, 44.9, 42.9, 42.7, 42.3, 41.4, 30.7, 30.2, 28.9, 22.4, 18.1, 11.9; HRMS [M+H]$^+$ calcd. = 576.2420 found = 576.2405. FTIR ν = 3060, 2974, 2873, 2205, 2166, 1716, 1607, 1588, 1512, 1448, 1161, 1083, 819, 733 cm^{-1}.

6.21
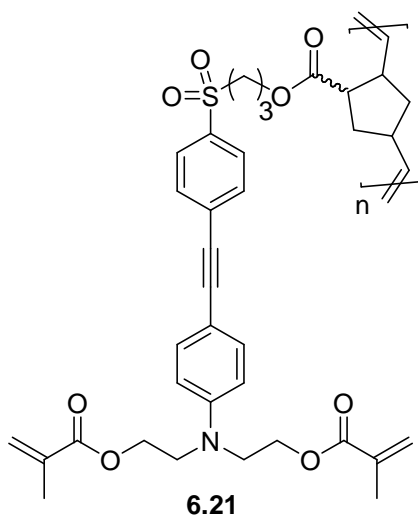
Synthesis of Biscross-Linkable Polymer 6.21. To a 500 mL round bottom flask was added Grubbs II catalyst (34 mg, 0.0397 mmoles), which was then cooled in an ice bath. To a separate 500 mL flask was added bismethacrylate tolane **6.19** (2.509 g, 3.974 mmoles) and DCM (265 mL). The monomer solution was degassed via three freeze-pump-thaw cycles and was then transferred via canula to the flask containing catalyst. The reaction was monitored by removing aliquats and the reaction determined to be complete after 13 h. Excess ethyl vinyl ether was added, then concentrated, then dissolved into THF and precipitated into cold hexanes to yield **6.21** as an light yellow powder (85%). Mn = 59 kDa; PDI = 1.9; ^{1}H NMR (DMSO-d_6): δ 1.78 (bs), 3.33 (bs), 3.69 (bs), 3.95 (bs), 4.22 (bs), 5.32 (bt), 5.59 (bs), 5.94 (bs), 6.81 (bs), 7.32 (bs), 7.64 (bs), 7.81 (bs).

6.22
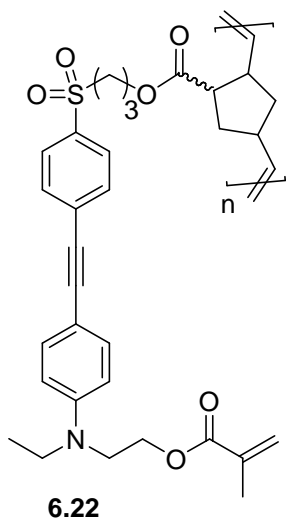
Synthesis of Monocross-Linkable Polymer 6.22. To a 500 mL round bottom flask was added Grubbs II catalyst (78 mg, 0.0920 mmoles), which was then cooled in an ice bath. To a separate 500 mL flask was added bismethacrylate tolane **6.20** (5.30 g, 9.20 mmoles) and DCM (400 mL). The monomer solution was degassed via three freeze-pump-thaw cycles and was then transferred via canula to the flask containing catalyst. The reaction was monitored by removing aliquats and the reaction

determined to be complete after 13 h. Excess ethyl vinyl ether was added, then concentrated, then dissolved into THF and precipitated into cold hexanes to yield **6.22** as an light yellow powder (85%). Mn = 52 kDa; PDI = 1.62
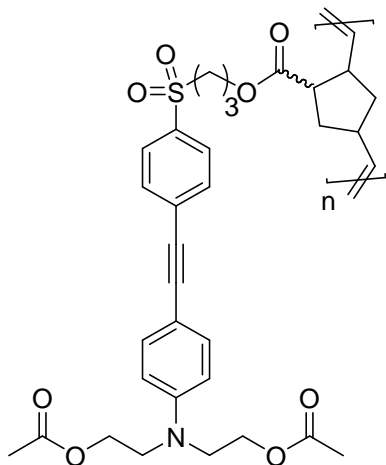
6.23

Synthesis of Noncross-Linkable Polymer 6.23. To a 500 mL round bottom flask was added Grubbs II catalyst (53 mg, 0.062 mmoles), which was then cooled in an ice bath. To a separate 500 mL flask was added bismethacrylate tolane **6.18** (3.788 g, 6.539 mmoles) and DCM (400 mL). The monomer solution was degassed via three freeze-pump-thaw cycles and was then transferred via canula to the flask containing catalyst. The reaction was monitored by removing aliquats and the reaction determined to be complete after 13 h. Excess ethyl vinyl ether was added, then concentrated, then dissolved into THF and precipitated into cold hexanes to yield **6.23** as an light yellow powder (85%). Mn = 33 kDa; PDI = 1.59.

Appendix D: Academic Genealogy

C. Grant Willson
PhD U.C. Berkeley, 1973

Henry Rapoport
PhD MIT, 1943

Avery A. Morton
PhD MIT, 1924

James F. Norris
PhD Johns Hopkins, 1895

Ira Remsen
Göttingen, 1870

Wilhelm R. Fittig
PhD Göttingen, 1858

Heinrich Limpricht
PhD Göttingen, 1850

217

Friedrich Wohler
Heidelber, 1823

Friedrich was co-advised by:

Jons Jakob Berzelius
MD Uppsala, 1802

Leopold Gmelin
Göttingen, 1810

Johann Afzelius
MS Uppsala, Sweden 1776

Joseph Jacquin
MD Vienna, 1788

Tobern Olof Bergman
Uppsala, 1758

Nicolas Joseph Jacquin
Leiden, ~1752

Bengt Fermer Laurent
Uppsala ~1751
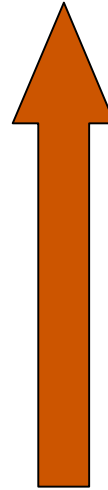
Theodor Gronovius II
MD Leiden ~1750

Samuel Klingenstierna
LLB Uppsala 1717

Johannes F. Gronovius II
Leiden 1715

Anders Gabriel Duhre
LLB Uppsala ~1739

Petrus Elvius
MA Uppsala 1688

Petrus Hoffvenius
MD Leiden 1660

Johannes Antonides van der Linden
MD Franker 1630

Menelaus Winsemius
MD Leiden 1613

Petrus Pauw
MD Rostock 1587

Henricus Brucaeus
College Royal, Paris ~1550

Petrus Ramus
MA Paris 1536

References

[1] Knauer, K., *Great Inventions: Geniuses and Gizmos: Innovations in Our Time,* Time Inc.: New York, **2003**.

[2] Malone, M. S., *The Microprocessor: A Biography*, Springer: New York, **1995**.

[3] See http://www.computerhistory.org/timeline/?year=1946

[4] See http://en.wikipedia.org/wiki/File:ENIAC_Penn2.jpg

[5] Shockley W., *IEEE Trans. Elec. Devices,* **1976**, *7*, 597.

[6] Turley, J., *The Essential Guide to Semiconductors,* Prentice Hall: New Jersey, **2003**.

[7] Bardeen J.; Brattain W., *Phys. Rev.*, **1948**, *74*, 230.

[8] Brattain W.; Bardeen J., *Phys. Rev.*, **1948**, *74*, 231.

[9] See www.nobelprize.org.

[10] See http://www.computerhistory.org/timeline/?year=1947

[11] Reid T., *The Chip: How Two Americans Invented the Microchip and Launched a Revolution*, Simon and Schuster, New York, **1984**.

[12] See http://www.ti.com/corp/docs/kilbyctr/downloadphotos.shtml

[13] Thompson L.; Willson C.; Bowden M., *Introduction to Microlithography*, 2nd edition, American Chemical Society, Washington DC, **1994**.

[14] Moreau, W. M., *Semiconductor Lithography: Principles, Practices, and Materials.* Plenum Press: New York, **1998**.

[15] See http://en.wikipedia.org/wiki/File:Intel_4004.jpg

[16] Moore, G. E., *Electronics Magazine*, April 19, **1965**.

[17] Peercy, P. S., *Nature,* **2000,** *406*, 1023.

[18] See http://www.intel.com/museum/archives/history_docs/moore.htm

[19] Jaeger, R., *Introduction to Microelectronic Fabrication,* Addison-Wesley Publishing, Reading, Mass., **1993**.

[20] See http://en.wikipedia.org/wiki/File:N-channel_enhancement-type_MOSFET.JPG

[21] Wolf, S.; Tauber, R. N., *Silicon Processing for the VLSI Era: Volume 1: Process Technology.* Lattice Press: Sunset Beach, **1986**.

[22] http://www.asml.com/asml/show.do?ctx=427

[23] Chambers, C. R., Dissertation, The University of Texas at Austin, 2005.

[24] Gernsheim, H.; Gernsheim, A., *The History of Photography: From the Camera Obscura to the Beginnings of the Modern Era*, McGraw Hill. New York. **1969**.

[25] Marignier, J. L., *Aspha1t as the Worlds First Photopolymer Revisiting the Invention of Photography* in *Processes in Photopolymers*. Chapman and Hall: New York, N.Y. **1995**.

[26] Willson, C. G.; Dammel, R. A.; Reiser, A. *Proceedings of SPIE-The International Society for Optical Engineering,* **1997**, 3048, 28.

[27] Gernsheim, H.; Gernsheim, A., *The Photographic Journal.* Section A., **1952**, 118.

[28] See http://en.wikipedia.org/wiki/File:View_from_the_Window_at_Le_Gras,_Joseph_Nic%C3%A9phore_Ni%C3%A9pce.jpg

[29] See http://en.wikipedia.org/wiki/File:Georges_d%27Amboise.jpg

[30] Becquerel, A., *Compte. Rend.*, **1840**, *10*, 469.

[31] Jorgensen, J. G.; Bruno, M. H., *The Sensitivity of Bichromated Coatings*, Lithographic Technical Foundation. New York, N.Y., **1954**.

[32] See http://en.wikipedia.org/wiki/File:William_Henry_Fox_Talbot,_by_John_Moffat,_1864.jpg

[33] See http://en.wikipedia.org/wiki/File:William_Fox_Talbot_1853.jpg

[34] Stobbe, H.; Lehfeldt, A., *Ber.,* **1925**, *58*, 2415.

[35] Reichmanis, E.; Thompson, L., *Chem. Rev.*, **1989**, *89*, 1273.

[36] Wolff, L., *Liebig's Ann. Chem.* **1902**, *325*, 129:and **1912**, *394*, 23.

[37] Schroeter, G., *Ber. Dtsch. Chem. Ges.*, **1909**, *42*, 2346.

[38] Suss, O., Liebigs Ann Chem. **1944**, *556*, 65.

[39] While this story is nice and has been documented in literature, the actual names of the father and son have eluded those who have sought them. Regardless, it is well described with the words of Dante Alighieri: Si non é vero, é ben trovato" (if it is not true, it has been well invented).

[40] Azoplate Corp., U.S. Patent 2,766,118, **1956**.

[41] Moreau, W. M.; Schmidt, R. R., *Abstracts of Papers 138th Electrochemical Society Meeting: Electrochemical Society:* Pennington, NJ, **1970,** Extended Abstract 187.

[42] Ito, H; Willson, C. G.; Frechet, J. M. J., *Digest of Technical Papers, SPIE Symposium on VLSI Technology*, **1982**, 6.

[43] Willson, C. G.; Ito, H.; Frechet, J. M. J.; Tessier, T. G.; Houlihan, F. M., *J. Electrochem. Soc.*, **1986**, *133*, 181.

[44] Heath, W. H., Dissertation, The University of Texas at Austin, 2006.

[45] Smith, G. H.; Bonham, J. A., U.S. Patent 3,779,778, **1973**.

[46] Crivello, J. V.; Lam, J. H., *J. Polym. Sci.: Polym. Chem. Ed.*, **1979**, *17*, 977.

[47] Frechet, J. M. J.; Eichler, E.; Ito, H.; Willson, C. G., *Polymer,* **1983**, *24*, 995.

[48] Umbach; Broers, A. N.; Koch, R.; Willson, C. G.; Laibowitz, R. B., *IBM J. Res. Dev.*, **1988**, *32*, 454.

[49] MacDonald, S. A.; Hinsberg, W. D.; Wendt, H. R.; Clecak, N. J.; Willson, C. G.; Snyder, C. D., *Chem. Mater.*, **1993**, *5*, 348.

[50] Hinsberg, W. D.; MacDonald, S. A.; Clecak, N. J.; Snyder, C. D.; Ito, H., *Proceedings of SPIE-The International Society for Optical Engineering,* **1993**, *1925*, 43.

[51] Ito, H.; England, W. P.; Clecak, N. J.; Bryta, G.; Lee, H.; Yoon, D. Y.; Sooriakumaran, R.; Hinsberg, W. D., *Proceedings of SPIE-The International Society for Optical Engineering,* **1992***, 1925*, 65.

[52] Kunz, R. R.; Allen, R. D.; Hinsberg, W. D.; Wallraff, G. M., *Proceedings of SPIE-The International Society for Optical Engineering,* **1993**, *1925*, 167.

[53] Takechi, S.; Kaimoto, Y.; Nozaki, K.; Abe, N., *J. Photopolym. Sci. Tech.*, **1992**, *5*, 439.

[54] Kaimoto, Y.; Nozaki, K.; Takechi, S.; Abe, N., *Proceedings of SPIE-The International Society for Optical Engineering,* **1992**, *1672*, 66.

[55] Wallraff, G. M.; Allen, R. D.; Hinsberg, W. D.; Willson, C. G.; Simpson, L. L.; Webber, S. E.; Sturtevant, J. L., *J. Imag. Sci. Tech.,* **1992**, *36*, 468.

[56] Ito, H., *Adv. Polym. Sci.*, **2005**, *172*, 37.

[57] Allen, R. D.; Sooriyakumaran, R.; Optiz, J.; Wallraff, G. M.; Breyta, G.; DiPietro, R. A.; Hofer, D. C.; Kunz, R. R.; Okoroanyanwu, U.; Willson, C. G., *J. Photo. Poly. Sci. Tech.*, **1996**, *9*, 465.

[58] Kunz, R.; Palmateer, S.; Forte, A.; Allen, R.; Wallraff, G.; DiPietro, R.; Hofer, D., *Proceedings of SPIE-The International Society for Optical Engineering,* **1996**, *2724*, 365.

[59] Wallow, T. I.; Houlihan, F. M.; Nalamasu, O.; Chandross, E. A.; Neenan, T., Reichmanis, E., *Proc. SPIE*, **1996**, *2724*, 355.

[60] Hennis, A. D.; Polley, J. D.; Long, G. S.; Sen, A.; Yandulov, D.; Lipian, J.; Benedikt, G. M.; Rhodes, L. F., *Organometallics*, **2001**, *20*, 2802.

[61] Lipian, J.; Mimna, R. A.; Fondran, J. C.; Yandulov, D.; Shick, R. A.; Goodall, B. L.; Rhodes, L. F.; Huffman, J. C., *Macromolecules,* **2002**, *35*, 8969.

[62] Benedikt, G. M.; Elce, E.; Goodall, B. L.; Kalamarides, H. A.; McIntosh, L. H. III; Rhodes, L. F.; Selvy, K. T.; Andes, C.; Oyler, K.; Sen, A., *Macromolecules*, **2002**, *35*, 8978.

[63] Grayson, S. M.; Long, B. K.; Kusomoto, S.; Osborn, B. P.; Callahan, R. P.; Chambers, C. R.; Willson, C. G. *J. Org. Chem.,* **2006**, *71*, 341-344.

[64] Levinson, H. J. Principles of Microlithography, 2nd ed.; SPIE Press: Bellingham, WA, 2005.

[65] Saunders, D. P.; Connor, E. F.; Grubbs, R. H.; Hung, R. J.; Osborn, B. P.; Chiba, T.; MacDonald, S. A.; Willson, C. G.; Conley, W. *Macromolecules*, **2003**, *36*, 1534.

[66] Barnes, D. A.; Benedikt, G. M.; Goodall, B. L.; Huang, S. S.; Kalamarides, H. A.; Lenhard, S.; McIntosh, L. H.; Selvy, K. T.; Shick, R. A.; Rhodes, L. F. *Macromolecules* **2003**, *36*, 2623.

[67] Benedikt, G. M.; Elce, E.; Goodall, B. L.; Kalamarides, H. A.; McIntosh, L. H.; Rhodes, L. F.; Selvy, K. T.; Andes, C.; Oyler, K.; Sen, A. *Macromolecules* **2002**, *35*, 8978.

[68] Lipian, J.; Mimna, R. A.; Fondran, J. C.; Yandulov, D.; Shick, R. A.; Goodall, B. L.; Rhodes, L. F.; Huffman, J. C. *Macromolecules* **2002**, *35*, 8969.

225

[69] Mathew, J. P.; Reinmuth, A.; Melia, J.; Swords, N.; Risse, W. *Macromolecules* **1996**, *29*, 2755.

[70] Kunz, R. R.; Bloomstein, T. M.; Hardy, D. E.; Goodman, R. B.; Downs, D. K.; Curtin, J. E. *Proc. SPIE* **1999**, *3678*, 13.

[71] Trinque, B. C.; Chambers, C. R.; Osborn, Br. P.; Callahan, R.P.; Lee, G. S.; Kusumoto, S.; Sanders, D. P.; Grubbs, R. H. Conley, W. E.; Willson, C. G. *J. Fluorine Chem.* **2003**, *122*, 17.

[72] Tran, H. V.; Hung, R. J.; Chiba, T.; Yamada, S.; Mrozek, T.; Hsieh, Y.-T.; Chambers, C. R.; Osborn, B. P.; Trinque, B. C.; Pinnow, M. J.; Sanders, D. P.; Connor, E. F.; Grubbs, R. H.; Conley, W.; MacDonald, S. A.; Willson, C. G. *J. Photopolym. Sci. Technol.* **2001**, *14*, 669.

[73] Heyns, K.; Rudiger, G.; Paulsen, H. *Chem. Ber*. **1972**, *105*, 1019; Taylor, J. E. *Synthesis* **1985**, 1142.

[74] Kwart, H.; Vosburgh, W. G. *J. Am. Chem. Soc.* **1954***, 76*, 5400.

[75] Walborsky, H. M.; Loncrini, D. F. *J. Am. Chem. Soc.* **1954***, 76*, 5396.

[76] Crandall, J. K. *J. Org. Chem..* **1964***, 29*, 2830.

[77] Shealy, Y. F.; Clayton, J. D. *J. Am. Chem. Soc.* **1969**, *91*, 3075.

[78] Tenaglia, A.; Terranova, E.; Waegell, B. *Tetrahedron Lett.* **1990**, *31*, 1157.

[79] Kotsuki, H.; Kataoka, M.; Nishizawa, H. *Tetrahedron Lett.* **1993**, *34*, 4031.

[80] Brown, H. C.; Kawakami, J. H.; Liu, K. T. *J. Am. Chem. Soc.* **1973***, 95*, 2209.

[81] Löwenhielm, P.; Claesson, H.; Hult, A. *Macromol. Chem. Phys.* **2004**, *205*, 1489.

[82] Shibasaki, Y.; Sanda, F.; Endo, T. *Macromolecules* **2000**, *33*, 3630.

[83] Kricheldorf, H. R.; Jenssen, J. *J. Macromol. Sci. Chem*. **1989**, *A26*, 631.

[84] McDonald, R. N; Tabor, T. E. *J. Org. Chem*. **1968**, *33*, 2934.

[85] Takano, S.; Akiyama, M.; Sato, S.; Ogasawara, K. *Chem. Lett*. **1983**, 1593.

[86] Schreiber, S. L.; Wang, Z.; Schulte, G. *Tetrahedron Lett*. **1988**, *29*, 4085.

[87] Takano, S.; Kurotaki, A.; Sekiguchi, Y.; Satoh, S.; Hirama, M; Ogasawara, K. *Synthesis* **1986**, 811.

[88] Osborn, B. P.; Callahan, R. P.; Chiba, T.; Trinque, B. C.; Brodsky, C. J.; Hung, R. J.; Tran, H. V., Yamachika, M.; Chambers, Jr., C. R.; Pinnow, M. J.; Long, B. K.; Willson, C. G.; Sanders, D. P.; Grubbs, R. H.; Zhan, C. G.; Matsuzawa., N. N.; Dixon, D. A.; Miller, D. A.; Conley, W. E., 2008, In preparation

[89] Long, B. K.; Keitz, B. K.; Willson, C. G., *J. Mat. Chem.,* **2007**, *17*, 3575.

[90] Gates, B. D.; Xu, Q.; Stewart, M.; Ryan, D.; Willson, C. G.; Whitesides, G. M., *Chem. Rev.*, **2005**, *105*, 1171.

[91] Chou, S. Y.; Krauss, P. R.; Renstrom, P. J., *Appl. Phys. Lett*., **1995**, *67*, 3114.

[92] Chou, S. Y.; Krauss, P. R.; Renstrom, P. J., *J. Vac. Sci. Technol., B*, **1996**, *14*, 4129.

[93] Austin, M. D.; Ge, H.; Wu, W.; Li, M.; Yu, Z.; Wasserman, D.; Lyon, S. A.; Chou, S. Y., *Appl. Phys. Lett*., **2004**, *84*, 5299.

[94] Austin, M. D.; Zhang, W.; Ge, H.; Wasserman, D.; Lyon, S. A.; Chou, S. Y., *Nanotechnology*, **2005**, *16*, 1058.

[95] Stewart, M.; Johnson, S.; Sreenivasan, S. V.; Resnick, D.; Willson, C. G., *J. Microlithogr., Microfabr., Microsyst*., **2005**, *4*, 1.

[96] Colburn, M.; Johnson, S.; Stewart, M.; Damle, S.; Bailey, T.; Choi, B.; Wedlake, M.; Michaelson, T.; Sreenivasan, S. V.; Ekerdt, J.; Willson, C. G., *Proc. SPIE-Int. Soc. Opt. Eng*., **1999**, *3676*, 379.

[97] Hua, F.; Sun, Y.; Gaur, A.; Meiti, M. A.; Bilhaunt, L.; Rotkina, L.; Wang, J.; Geil, P.; Shim, M.; Rogers, J. A., *Nano Lett*., **2004**, *4*, 2467.

[98] http://www.itrs.net/Links/2006Update/FinalToPost/08_Lithography2006Update.pdf.

[99] Kim, E. K.; Stacey, N. A.; Smith, B. J.; Dickey, M. D.; Johnson, S. C.; Trinque, B. C.; Willson, C. G., J. *Vac. Sci. Technol., B*, **2004**, *22*, 131.

[100] Resnick, D. J.; Sreenivassan, S. V.; Willson, C. G., *Mater. Today*, **2005**, *8*, 34.

[101] Dickey, M. D.; Willson, C. G., *AIChE J*., **2006**, *52*, 778.

[102] Dickey, M. D.; Burns, R. L.; Kim, E. K.; Johnson, S. C.; Stacey, N. A.; Willson, C. G., *AIChE J*., **2005**, *51*, 2547.

[103] Odian, G., *Principles of Polymerization*, John Wiley & Sons, Inc., Hoboken, New Jersey, USA, 4th ed., **2004**, ch. 3, pp. 255–263.

[104] Kim, E. K.; Stewart, M. D.; Wu, K.; Palmieri, F. L.; Dickey, M. D.; Ekerdt, J. G.; Willson, C. G., *J. Vac. Sci. Technol., B*, **2005**, *23*, 2967.

[105] Kim, E. K.; Willson, C. G., *Microelectron. Eng.*, **2006**, *83*, 213.

[106] Ito, H.; Houle, F. A.; Hart, M. W.; DiPietro, R. A., *Proc. SPIE Int. Soc. Opt. Eng.*, **2006**, *6153*, 61531A–1.

[107] Schmid, G. M.; Stewart, M. D.; Wetzel, J.; Palmieri, F.; Hao, J.; Nishimura, Y.; Jen, K.; Kim, E. K.; Resnick, D. J.; Liddle, J. A.; Willson, C. G., *J. Vac. Sci. Technol., B*, **2006**, *24*, 1283.

[108] Hao, J.; Palmieri, F.; Stewart, M. D.; Nishimura, Y.; Chao, H. L.; Collins, A.; Willson, C. G., *Polym. Prepr.*, **2006**, *47*, 1158.

[109] Morgen, M.; Ryan, E. T.; Zhao, J. H.; Hu, C.; Cho, T. H.; Ho, P. S., *Annu. Rev. Mater. Sci.*, **2000**, *30*, 645.

[110] Hedrick, J. L.; Miller, R. D.; Hawker, C. J.; Carter, K. R.; Volksen, W.; Yoon, D. Y.; Trollsas, M., *Adv. Mater.*, **1999**, *10*, 1049.

[111] Stewart, M. D.; Wetzel, J. T.; Schmid, G. M.; Palmieri, F.; Thompson, E.; Kim, E. K.; Wang, D.; Sotoodeh, K.; Jen, K.; Johnson, S. C.; Hao, J.; Dickey, M. D.; Nishimura, Y.; Laine, R. M.; Resnick, D. J.; Willson, C. G., *Proc. SPIE-Int. Soc. Opt. Eng.*, **2005**, *5751*, 210.

[112] Odian, G., in *Principles of Polymerization*, John Wiley & Sons, Inc., Hoboken, New Jersey, USA, 4th Edition, **2004**, ch. 9, pp. 731–732.

[113] Levine, A. W.; Fech, Jr., J. *J. Org. Chem.*, **1972**, *37*, 1500.

[114] Heath, W. H.; Palmieri, F.; Adams, J. R.; Long, B. K.; Chute, J.; Holcombe, T.; Zieren, S.; Truitt, M. J.; White, J. L.; Willson, C. G., *Macromolecules*, **2008,** *41*, 719.

[115] Chen, X.; Wudl, F.; Mal, A. K.; Shen, H.; Nutt, S. R., *Macromolecules*, **2003**, *36*, 1802.

[116] Chen, X.; Dam, M. A.; Ono, K.; Mal, A.; Shen, H.; Nutt, S. R.; Sheran, K.; Wudl, F., *Science*, **2002**, *295*, 1698.

[117] Liu, Y. L.; Hsieh, C. Y., *J. Polym. Sci., Part A: Polym. Chem.*, **2005**, *44*, 905.

[118] Szalai, M. L.; McGrath, D. V.; Wheeler, D. R.; Zifer, T.; McElhanon, J. R., *Macromolecules*, **2007**, *40*, 818.

[119] Gheneim, R.; Perez-Berumen, C.; Gandini, A., *Macromolecules*, **2002**, *35*, 7246.

[120] Imai, Y.; Itoh, H.; Naka, K.; Chujo, Y., *Macromolecules*, **2000**, *33*, 4343.

[121] McElhanon, J. R.; Zifer, T.; Kline, S. R.; Wheeler, D. R.; Loy, D. A.; Jamison, G. M.; Long, T. M.; Rahimian, K.; Simmons, B. A., *Langmuir*, **2005**, *21*, 3259.

[122] Montague, M. F.; Hawker, C. J., *Chem. Mater*., **2007**, *19*, 526.

[123] Ogino, K.; Chen, J. S.; Ober, C. K., *Chem. Mater*., **1998**, *10*, 3833.

[124] Kilian, L.; Wang, Z. H.; Long, T. E., *J. Polym. Sci., Part A: Polym. Chem*., **2003**, *41*, 3083.

[125] De Clercq, R. R.; Goethals, E. J., *Macromolecules*, **1992**, *25*, 1109.

[126] Ruckenstein, E.; Zhang, H., *Macromolecules*, **1999**, *32*, 3979.

[127] Themistou, E.; Patrickios, C. S., *Macromolecules*, **2006**, *39*, 73.

[128] Lorette, N. B.; Howard, W. L., *J. Org. Chem*., **1960**, *25*, 521.

[129] Jain, R.; Standley, S. M.; Frechet, J. M. J., *Macromolecules*, **2007**, *40*, 452.

[130] Jen, K.; Palmieri, F.; Chao, B.; Lin, M.; Hao, J.; Owens, J.; Sotoodeh, K.; Cheung, R.; Willson, C. G., *Proc. SPIE-Int. Soc. Opt. Eng*., **2007**, *6517*, 65170K.

[131] Bailey, T.; Choi, B. J.; Colburn, M.; Meissl, M.; Shaya, S.; Ekerdt, J. G.; Sreenivasan, S. V.; Willson, C. G., *J. Vac. Sci. Tech.*, B, **2000**, *18*, 3572-3577.

[132] Wu, K.; Kim, E. K.; Ekerdt, J. G.; Willson, C. G., Abstracts of Papers, 229th ACS National Meeting, San Diego, CA, United States, March 13-17, **2005**, COLL-573.

[133] Odian, G., in Principles of Polymerization, John Wiley & Sons, Inc., Hoboken, New Jersey, USA, 4th Edition, **2004**, ch. 9, pp. 731–732.

[134] See Kurt Alder's Nobel Lecture at http://nobelprize.org/nobel_prizes/chemistry/laureates/1950/alder-lecture.html.

[135] Chen, X; Dam, M. A.; Ono, K.; Mal, A.; Shen, H.; Nutt, S. R.; Sheran, K.; Wudl, F. *Science* **2002**, *295*, 1698.

[136] Chen, X; Wudl, F.; Mal, A.; Shen, H.; Nutt, S. R., *Macromolecules* **2003**, *36*, 1802.

[137] Gousse, C.; Gandini, A.; Hodge, P., *Macromolecules,* **1998**, *31*, 314.

[138] Imai, Y.; Itoh, H.; Naka, K.; Chujo, Y., *Macromolecules*, **2000**, *33*, 4343.

[139] Szalai, M.; McGrath, D.; Wheeler, D.; Zifer, T.; McElhanon, J., *Macromolecules*, **2007**, *40*, 818.

[140] Liu, Y.; Hsieh, C., *J. Poly. Sci., A.*, **2006**, *44*, 905.

[141] McElhanon, J.; Russick, E.; Wheeler, D.; Loy, D.; Aubert, J., *J. Appl. Poly. Sci.*, **2002**, *85*, 1496.

[142] Pelter, A.; Singaram, B., *J. Chem. Soc. Perkin Trans. I*, **1983**, *7*, 1383.

[143] Conley, N. R.; Hung, R. J.; Willson, C. G., *J. Org. Chem.* **2005**, *70*, 4553-4555.

[144] Tawney, P. O.; Snyder, R. H.; Conger, R. P.; Leibbrand, K. A.; Stiteler, C. H.; Williams, A. R., *J. Org. Chem.*, **1961**, *26*, 15-21.

[145] Keller, O.; Rudinger, *J. Helv. Chim. Acta,* **1975**, *58*, 5331.

[146] Keller, K.; Guo, J.; Punna, S.; Finn, M., *Tett. Lett.*, **2005**, *46*, 1181.

[147] Long, B. K.; Keitz, B. K.; Willson, C. G., *J. Mater. Chem.*, **2007**, *17*, 3575.

[148] Heath, W. H.; Palmieri, F.; Adams, J. R.; Long, B. K.; Chute, J.; Holcombe, T.; Zieren, S.; Truitt, M. J.; White, J. L.; Willson, C. G., *Macromolecules*, **2008**, *41*, 719.

[149] Chujo, Y.; Sada, K.; Saegusa, T., *Macromolecules*, **1990**, *23*, 2636.

[150] Pontrello, J. K.; Allen, M. J.; Underbakke, E. S.; Kiessling, L. L., *J. Amer. Chem. Soc.*, **2005**, *127*, 14536.

[151] Palmieri, F., Doctoral Dissertation, University of Texas at Austin, Austin, **2008**.

[152] Cho, M.; Choi, D.; Sullivan, P.; Akelaitis, A.; Dalton, L., *Prog. Poly. Sci.*, **2008**, *33*, 1013.

[153] Franken, P. A.; Hill, A. E.; Peters, C. W.; Weinreich, G., *Phys. Rev. Lett*, **1961**, *7*, 118.

[154] Meredith, G.; VanDusen, J.; Williams, D., *Macromolecules,* **1982**, *15*, 1385.

[155] Garito, A.; Singer, K., *Laser Focus,* **1982**, *80*, 59.

[156] Prasad, P. N.; Williams, D. J., *Introduction to Nonlinear Optical Effects in Molecules and Polymers*, John Wiley and Sons, Inc.: New York, **1991**.

[157] Thakur, M.; Xu, J.; Bhowmik, A.; Zhou, L., *Appl. Phys. Lett.*, **1999**, *74*, 635.

[158] Pan, F.; McCallion, K.; Chiappetta, M., *Appl. Phys. Lett.*, **1999**, *74*, 492.

[159] Meier, U.; Bösch, M.; Bosshard, C.; Pan, F.; Günter, P., *J. Appl. Phys.*, **1998**, *83*, 3486.

[160] Sohma, S.; Takahashi, H.; Taniuchi, T.; Ito, H., *Chem. Phys.*, **1999**, *245*, 359.

[161] Wang, W.; Chen, D.; Fetterman, H.; Shi, Y.; Steier, W.; Dalton, L., *Appl. Phys. Lett.*, **1995**, *67*, 1806.

[162] He, G. S.; Liu, S. H., Physics of Nonlinear Optics, World Scientific Publishing, Singapore, **1999**.

[163] Chandra, M.; Krishna, M.; Mimata, H.; Kawamata, T.; Nakamura, T.; Radhakrishnan, T., *Adv. Mater.*, **2005**, *17*, 1937.

[164] Burland, D.; Miller, R.; Walsh, C., *Chem. Rev.*, **1994**, *94*, 31.

[165] Dalton, L. R.; Harper, A. W.; Ghosn, R.; Steier, W. H.; Ziari, M,; Fetterman, H. R., *Chem. Mater.*, **1995**, *7*, 1060–81.

[166] Dalton, L., Nonlinear Optical Polymeric Materials: *From Chromophore Design to Commercial Applications*, Springer-Verlag, Berlin/Heidelberg, **2002**.

[167] Eich, M.; Looser, H.; Yoon, D.; Tweig, R.; Bjorklund, G.; Baumert, J., *J. Opt. Soc. Am., B*, **1989**, *6*, 1590.

[168] Kajzar, F.; Lee, K-S.; Jen, A., *Polymeric Materials and their Orientation Techniques for Second-Order Nonlinear Optics, Advances in Polymer Science*, Vol. 161, Springer-Verlag, Berlin/Heidelberg, **2003**.

[169] Clays, K.; Persoons, A., *Phys. Rev. Lett.*, **1991**, *66*, 2980.

[170] Verbiest, T.; Clays, K.; Samyn, C.; Wolff, J.; Reinhoudt, D.; Persoons, A., *J. Am. Chem. Soc.*, **1994**, *116*, 9320.

[171] Stadler, S.; Bourhill, G.; Bräuchle, C., *J. Phys. Chem.*, **1996**, *100*, 6927.

[172] Flipse, M. C.; de Jonge, R.; Woudenberg, R. H.; Marsman, A. W.; van Walree, C.A.; Jenneskens, L. W., *Chem. Phys. Lett.*, **1966**, *245*, 297–303.

[173] Noordman, O. F. J.; van Hulst, N. F., *Chem. Phys. Lett.*, **1996**, *253*, 145.

[174] Levine, B.; Bethea, C., *J. Chem. Phys.*, **1975**, *63*, 2666.

[175] Jen, A.; Rao, V.; Drost, K.; Cai, Y.; Mininni, R.; Kenney, J., *Proc. SPIE*, **1994**, *2143*, 30–40.

[176] Serbutoviez, C.; Bosshard, C.; Knöepfie, G.; Wyss, P.; Prêtre, P.; Günter, P.; Schenk, K.; Solari, E.; Chapuis, G., *Chem. Mater.*, **1995**, *7*, 1198.

[177] Blanchard-Desce, M.; Alain, V.; Midrier, L.; Wortmann, R.; Lebus, S.; Glania, C.; Kraemer, P.; Fort, A.; Muller, J.; Barzoukas, M., *J. Photochem. Photobiol., A*, **1997**, *105*, 115.

[178] Boshard, C.; Sutter, K.; Prêtre, P.; Hulliger, J.; Flörsheimer, M.; Kaatz, P., *Organic nonlinear optical materials, Advances in nonlinear optics series,* vol. 1, Basel: Gordon & Breach; **1995**.

[179] Dentan, V.; Lévy, Y.; Dumont, M.; Robin, P.; Chastaing, E., *Opt. Commun.*, **1989**, *69*, 379–83.

[180] Lu, J.; Yin, J.; Deng, X.; Shen, Q.; Cao, Z., *Opt. Mater.*, **2004**, *25*, 17–25.

[181] Chang, H.; Ha, N.; Kim, A.; Lim, J.; Park, B.; Park, E., *Opt. Mater.*, **2002**, *21*, 413.

[182] Teng, C.; Man, H., *Appl. Phys. Lett.*, **1990**, *56*, 1734.

[183] Michelotti, F.; Nicolao, G.; Tesi, F.; Bertolotti, M., *Chem. Phys.*, **1999**, *245*, 311.

[184] Lévy, Y.; Dumont, M.; Chastaing, E.; Robin, P.; Chollet, P.; Gadret, G., *Mol. Cryst. Liq. Cryst. Sci. Technol., Sect. B, Nonlinear Optics*, **1993**, *4*, 1–19.

[185] Lévy, Y., *Mol. Cryst. Liq. Cryst. Sci. Technol., Sect. B, Nonlinear Optics*, **1993**, *5*, 371.

[186] Ziari, M.; Kalluri, S.; Garner, S.; Steier, W.; Liang, Z.; Dalton, L.; et al., *Proc. SPIE*, **1995**, *2527*, 218.

[187] Kalluri, S.; Garner, S.; Ziari, M.; Steier, W.; Shi, Y.; Dalton, L., *Appl. Phys. Lett.*, **1996**, *69*, 275.

[188] Ma, H.; Liu, S.; Luo, J.; Suresh, S.; Liu, L.; Kang, S.; Haller, M.; Sassa, T.; Dalton, L.; Jen, A., *Adv. Funct. Mater.*, **2002**, *12*, 565–574.

[189] Pauley, M.; Wang, C., *Chem. Phys. Lett*. **1997**, *280*, 544.

[190] Spraul, B.; Suresh, S.; Sassa, T.; Ángeles Herranz, M.; Echegoyen, L.; Wada, T.; et al., *Tetrahedron Lett.*, **2004**, *45*, 3253.

[191] Suresh, S.; Zengin, H.; Spraul, B.; Sassa, T.; Wada, T.; Smith, Jr., D., *Tetrahedron Lett.*, **2005**, *46*, 3913.

[192] Kuo, W.; Hsiue, G.; Jeng, R., *Macromolecules*, **2001**, *34*, 2373.

[193] Kanis, D.; Ratner, M.; Marks, T., *Chem. Rev.,* **1994**, *94*, 195–242.

[194] Cheng, L.; Tam, W.; Marder, S.; Stiegman, A.; Rikken, G.; Spangler, C., *J. Phys. Chem.*, **1991**, *95*, 10643.

[195] Marder, S.; Gorman, C.; Tiemann, B.; Cheng, L., *J. Am. Chem. Soc*., **1993**, *115*, 3006.

[196] Marder, S.; Cheng, L.; Tiemann, B.; Friedli, A.; Blanchard-Desce, M.; Perry, J.; et al., *Science*, **1994**, *263*, 511.

[197] Staub, K.; Levina, G.; Barlow, S.; Kowalczyk, T.; Lackritz, H.; Barzoukas, M.; et al., *J. Mater. Chem.*, **2003**, *13*, 825.

[198] Reynolds, G.; Drexhage, K., *J. Org. Chem.*, **1977**, *42*, 885.

[199] Kopainsky, B.; Kaiser, W.; Drexhage, K., *Opt. Commun.*, **1980**, *32*, 451.

[200] Kopainsky, B.; Qiu, P.; Kaiser, W.; Sens, B.; Drexhage, K., *Appl. Phys., B*, **1982**, *29*, 15.

[201] Shu, Y.; Gong, Z.; Shu, C.; Breitung, E.; McMahon, R.; Lee, G.; et al., *Chem. Mater*., **1999**, *11*, 1628.

[202] Raimundo, J.; Blanchard, P.; Ledoux-Rak, I.; Hierle, R.; Michaux, L.; Roncali, J., *Chem. Commun.*, **2000**, *17*, 1597.

[203] Jen, A.; Ma, H.; Wu, X.; Wu, J.; Liu, S.; Herguth, P.; et al., *Mol. Cryst. Liq. Cryst. Sci. Technol., Sec. B, Nonlinear Opt.*, **1999**, *22*, 9.

[204] Lee, I.; Seo, H.; Chung, Y., *Organometallics*, **1999**, *18*, 1091.

[205] Jeffery, T.; Ferber, B., *Tetrahedron Lett*., **2002**, *44*, 193.

[206] Brooker, L.; Craig, A.; Heseltine, D.; Jenkins, P.; Lincoln, L., J. *Am. Chem. Soc.*, **1965**, *87*, 2443.

[207] Melikian, G.; Rouessac, F.; Alexandre, C., *Synth. Commun.*, **1995**, *25*, 3045.

[208] Zhang, C.; Wang, C.; Dalton, L.; Zhang, H.; Steier, W., *Macromolecules*, **2001**, *34*, 253.

[209] Liao, Y.; Eichinger, B.; Firestone, K.; Haller, M.; Luo, J.; Kaminsky, W.; et al., *J. Am. Chem. Soc.*, **2005**, *127*, 2758.

[210] Cheng, Y.; Luo, J.; Hau, S.; Bale, D.; Kim, T.; Shi, Z.; et al., *Chem. Mater.*, **2007**, *19*, 1154.

[211] He, M.; Leslie, T.; Sinicropi, J., *Chem. Mater.*, **2002**, *14*, 4662.

[212] Liu, S.; Haller, M.; Ma, H.; Dalton, L.; Jang, S.; Jen, A., *Adv. Mater.*, **2003**, *15*, 603.

[213] Carboni, R., USP 3,013,013, **1961**.

[214] Hu, Z.; Fort, A.; Barzoukas, M.; Jen, A.; Barlow, S.; Marder, S., *J. Phys. Chem., B*, **2004**, *108*, 8626.

[215] Ahlheim, M.; Barzoukas, M.; Bedworth, P.; Blanchard-Desce, M.; Fort, A.; Hu, Z.; et al., *Science*, **1996**, *271*, 335.

[216] Meredith, G.; VanDusen, J.; Williams, D. *Macromolecules* **1982**, *15*, 1385.

[217] Dalton, L., *Nonlinear Optical Polymeric Materials: From Chromophore Design to Commercial Applications*, Springer-Verlag, Berlin/Heidelberg, **2002**.

[218] Dalton, L.; Harper, A.; Wu, B.; Ghosn, R.; Laquindanum, J.; Liang, Z.; Hubbel, A.; Xu, C., *Adv. Mater.*, **1995**, *7*, 519.

[219] Boyd, G.; Francis, C.; Trend, J.; Ender, D., *J. Opt. Soc. Am., B*, **1991**, *8*, 887.

[220] Levenson, R.; Liang, J.; Toussaere, E.; Carenco, A.; Zyss, J., *Proc. SPIE,* **1991**, *1560*, 251.

[221] Hampsch, H. L.; Yang, J.; Wong, G. K.; Torkelson, J. M., *Polym. Commun.,* **1989**, *30*, 40.

[222] Hampsch, H.; Yang, J.; Wong, *G.;* Torkelson, J., *Macromolecules*, **1998**, *21*, 526.

[223] Chen, T.; Jen, A.; Cai, Y., *Macromolecules*, **1996**, *29*, 535.

[224] Saadeh, H.; Wang, L.; Yu, L., *Macromolecules*, **2000**, *33*, 1570.

[225] Singer, K.; Kuzyk, M.; Holland, W.; Sohn, J.; Lalama, S.; Comizzoli, R.; Katz, H.; Schilling, M., *Appl. Phys. Lett*., **1988**, *53*, 1800.

[226] Mitchell, M.; Mulvaney, J.; Hall, H., Jr.;Willand, C.; Hampsch, H.; Williams, D., *Poly. Bull.*, **1992**, *28*, 381.

[227] Becker, M.; Sapochak, L.; Ghosen, R.; Xu, C.; Dalton, L.; Shi, Y.; Steier, W.; Jen, A., *Chem. Mater*., **1994**, *6*, 104.

[228] Morgan, R. J., *Advances in Polymer Science,* Springer-Verlag, Berlin, **1985**, p 72.

[229] Oleinik, G. F., *Advances in Polymer Science,* Springer-Verlag, Berlin, **1986**, p 80.

[230] Hood, K., *Comprehensive Polymer Science: The Synthesis, Characterization and Applications of Polymers,* Pergamon Press, Oxford, **1989**, Chapter 37, p 5.

[231] Eich, M.; Bjorklund, G. C.; Yoon, D. Y., *Polym. Adv. Technol*., **1990**, *1*, 189.

[232] Hubbard, M. A.; Marks, T. J.; Lin, W.; Wong. G. K., *Chem. Mater.,* **1992**, *4*, 965.

[233] Eich, M.; Reck, B.; Yoon, D.; Willson, C. G.; Bjorklund, G., *J. App. Phys*., **1989**, *66*, 3241.

[234] Xu, C.; Wu, B.; Dalton, L. R.; Ramon, P. M.; Shi, Y.; Steier, W. H., *Macromolecules,* **1992**, *25*, 6716.

[235] Chen, M.; Dalton, L. R.; Xu, L. P.; Shi, X. Q.; Steier, W. H., *Macromolecules,* **1992**, *25*, 4032.

[236] Shi, Y.; Steier, W. H.; Chen, M.; Yu, L.; Dalton, L. R., *Appl. Phys. Lett.,* **1992**, *60,* 2577.

[237] Yu, L.; Chan, W.; Bao, Z., *Macromolecules,* **1992**, *25*, 5609.

[238] Yu, L.; Chan, W.; Dikshit, S.; Bao, Z., *Appl. Phys. Lett.,* **1992**, *60*, 1655.

[239] Lon, J. T.; Hubbard, M. A.; Marks, T. J.; Lin, W.; Wong, G. K., *Chem. Mater.,* **1992**, *4*, 1148.

[240] Zhang, C.; Wang, C.; Dalton, L.; Zhang, H.; Steier, W., *Macromolecules*, **2001**, *34*, 253.

[241] Haller, M.; Luo, J.; Li, H.; Kim, T.; Liao, Y.; Robinson, B.; Dalton, L.; Jen, A., *Macromolecules*, **2004**, *37*, 688.

[242] Robello, D.; Willand, C.; Scozzafava, M.; Ullman, A.; Williams, D., *Materials for Nonlinear Optics. Chemical Perspectives, ACS symposium Series 455*, American Chemical Society, Washington, DC, **1991**, p. 279.

[243] Hayashi, A.; Goto, Y.; Nakayama, M.; Sato, H.; Watanabe, T.; Miyata, S., *Macromolecules*, **1992**, *25*, 5094.

[244] Matauda, H.; Okada, S.; Minami, N.; Nakanishi, H.; Kamaimoto, Y.; Hashidate, S.; Nagasaki, Y.; Kato, M., *Nonlinear Optics: Fundamentals, Materials and Devices*, Elsevier Science Publishers, Holland, **1992**, p 195.

[245] Chenzeng, X.; Wu, B.; Dalton, L. R.; Shi, Y.; Ranon, P. M.; Steier, W. H. *Macromolecules*, **1992**, *25*, 6714.

[246] Betterton, K.; Ebert, M.; Haeussling, L.; Lux, M. G.; Twieg, R. J.; Willson, C. G.; Yoon, D.; Burns, E. G.; Grubbs, R., *Poly. Mater. Sci. Eng.*, **1992**, *66*, 312-13.

[247] Long, B. K.; Keitz, B. K.; Webb, R. C.; Willson, C. G., *POLY Preprints*, 235th ACS National Meeting, New Orleans, LA, **2008**, 49, 264.

[248] Zhang, C.; Wang, C.; Yang, J.; Dalton, L. R.; Sun, G.; Zhang, H.; Steier, W. H. *Macromolecules* **2001**, *34*, 235-243.

[249] Xu, C.; Wu, B.; Todorova, O.; Dalton, L. R.; Shi, Y.; Ranon, P. M.; Steier, W. H. *Macromolecules*, **1993**, *26*, 5303.

[250] Xu, C.; Wu, B.; Dalton, L. R.; Shi, Y.; Ranon, P. M.; Steier, W. H. *Macromolecules*, **1992**, *25*, 6714.

[251] Long, B. K.; Keitz, B. K.; Webb, R. C.; Willson, C. G., *POLY Preprints*, 235th ACS National Meeting, New Orleans, LA, **2008**, *49*, 264.

[252] Schwab, P.; France, M. B.; Ziller, J. W.; Grubbs, R. H. *Angew. Chem. Int. Ed. Engl.* **1995**, *34*, 2039.

[253] Scholl, M.; Ding, S.; Lee, C. W.; Grubbs, R. H. *Org. Lett.* **1999**, *1*, 953.

[254] Love, J. A.; Morgan, J. P.; Trnka, T. M.; Grubbs, R. H. *Angew. Chem., Int. Ed.* **2002**, *41*, 4035-4037.

[255] Schrock, R. R.; Murdzek, J. S.; Bazan, G. C.; Robbins, J.; DiMare, M.; O'Regan, M. *J. Am. Chem. Soc.* **1990**, *112*, 3875.

[256] Godt, A.; Frechet, J. M. J.; Beecher, J. E.; Willand, C. S. *Macromol. Chem. Phys*. **1995**, *196*, 133-47.

[257] Nguyen, P.; Lesley, G.; Marder, T. B.; Ledoux, I.; Zyss, J. *Chem. Mater*. **1997**, *9*, 406-408.

[258] Ulman, A.; Willand, C. S.; Kohler, W.; Robello, D. R.; Williams, D. J.; Handley, L. *J. Am. Chem. Soc.* **1990**, *112*, 7083-90.

[259] Marder, S. R.; Perry, J. W. *Science* **1994**, *263*, 1706-1707.

[260] Thayumanavan, S.; Mendez, J.; Marder, S. R. *J. Org. Chem.* **1999**, *64*, 4289-4297.

[261] Li, Z.; Li, Z.; Di, C.; Zhu, Z.; Li, Q.; Zeng, Q.; Zhang, K.; Liu, Y.; Ye, C.; Qin, J. *Macromolecules* **2006**, *39*, 6951-6961.

[262] Cheng, Y.; Luo, J.; Hau, S.; Bale, D. H.; Kim, T.; Shi, Z.; Lao, D. B.; Tucker, N. M.; Tian, Y.; Dalton, L. R.; Reid, P. J.; Jen, A. K.-Y. *Chem. Mater.* **2007**, *19*, 1154-1163.

[263] Bielawski, C. W.; Grubbs, R. H., *Macromolecules* **2001**, *34*, 8838.

[264] Private communication with Prof. Robert H. Grubbs, California Institute of Technology.

[265] Matos, J.; Lima-Neto, B., *J. Mol. Cat., A*, **2006**, *259*, 286.

[266] Pavlinec, J.; Moszner, N., J. Appl. Poly. Sci., 2003, 89, 579.

[267] Burget, D.; Mallein, C.; Fouassier, J. P., Polymer, 2003, 44, 7671.

[268] Jakubiak, J.; Allonas, X.; Fouassier, J. P.; Sionkowska, A.; Andrzejewska, E.; Linden, L. A.; Rabek, J. F., Polymer, 2003, 44, 5219.

[269] Chen, Y. C.; Ferracane, J. L.; Prahl, S. A., Proc. SPIE, 2005, 5771, 256.

[270] Wu, G.; Nie, J., J. Photochem. Photobio. A, 2006, 183, 154.

[271] Tarle, Z.; Meniga, A.; Knezevic, A.; Sutalo, J.; Ristic, M.; Pichler, G., J. Oral Rehab., 2002, 29, 662.

[272] Rigoli, I. C.; Riga, A. T.; Cavalheiro, C. C. S.; Neumann, M. G.; Cavalheiro, E. T. G., J. Appl. Poly. Sci., 2008, 107, 187.

[273] Burland, D. M.; Miller, R. D.; Walsh, C. A., *Chem. Rev.* **1994**, *94*, 31.

[274] Herman, W. N.; Hayden, L. M., *J. Opt. Soc. Am., B*, **1995**, *12*, 416.

[275] Hoyle, C., University of Southern Mississippi (private communication).

[276] Bowman, C., University of Colorado at Boulder (private communication).

[277] Hu, Z. Y.; Fort, A.; Barzoukas, M.; Jen, A. K. Y.; Barlow, S.; Marder, S. R., *J. Phys. Chem. B*, **2004**, *108*, 8626.

[278] He, M.; Leslie, T. M.; Sinicropi, J. A., *Chem. Mater*., **2002**, *14*, 2393.

[279] Jang, S. H.; Luo, J.; Tucker, N. M.; Leclercq, A.; Zojer, E.; Haller, M. A.; Kim, T. D.; Kang, J. W.; Firestone, K.; Bale, D.; Lao, D.; Benedict, J. B.; Cohen, D.; Kaminsky, W.; Kahr, B.; Bredas, J. L.; Reid, P.; Dalton, L. R.; Jen, A. K.-Y., *Chem. Mater*., **2006**, *18*, 2982.

[280] Bello, K. A.; Cheng, L.; Griffiths, J., *J. Chem. Soc. Perkin Trans. II*, **1987**, 815.

[281] Sun, S. S.; Zhang, C.; Dalton, L. R., *Chem. Mater*., **1996**, *8*, 2539.

[282] Norman, M. H.; Kelley, J. L.; Hollingsworth, E. B., *J. Med. Chem*., **1993**, *36*, 3417.

[283] Buckle, D. R.; Morgan, N. J.; Ross, J. W.; Smith, H.; Spicer, B. A., *J. Med. Chem*., **1973**, *16*, 1334.

[284] Luo, J.; Liu, S.; Haller, M.; Liu, L.; Ma, H.; Jen, A. K. Y., *Adv. Mater*., **2002**, *14,* 1763.

[285] Luo, J.; Haller, M.; Li, H.; Kim, T. D.; Jen, A. K. Y., *Adv. Mater*., **2003**, *15*, 1635.

[286] Nair, V.; Jayan, C. N., *Tetrahedron Lett*., **2000**, *41*, 1091.

[287] Nair, V.; Jayan, C. N.; Ros, S., *Tetrahedron*, **2001**, *57,* 9453.

[288] Melikian, G.; Rouessac, F. P.; Alexandre, C., *Synth. Comm*., **1995**, *25*, 3045.

[289] Kondoh, A.; Yorimitsu, H.; Oshima, K., *Tetrahedron*, **2006**, *62*, 2357.

[290] DENZO-SMN. (**1997**). Z. Otwinowski and W. Minor, Methods in Enzymology, 276: Macromolecular Crystallography, part A, 307 – 326, C. W. Carter, Jr. and R. M. Sweets, Editors, Academic Press.

[291] SIR97. (**1999**). A program for crystal structure solution. Altomare A., Burla M.C., Camalli M., Cascarano G.L., Giacovazzo C. , Guagliardi A., Moliterni A.G.G., Polidori G.,Spagna R. J. Appl. Cryst. 32, 115-119.

[292] Sheldrick, G. M. (**1994**). SHELXL97. Program for the Refinement of Crystal Structures. University of Gottingen, Germany.

[293] Rw(F2) = {Σw(|Fo|2 - |Fc|2)2/Σw(|Fo|)4}1/2 where w is the weight given each reflection. R(F) = Σ(|Fo| - |Fc|)/Σ|Fo|} for reflections with Fo > 4(Σ(Fo)). S = [Σw(|Fo|2 - |Fc|2)2/(n - p)]1/2, where n is the number of reflections and p is the number of refined parameters.

[294] International Tables for X-ray Crystallography (**1992**). Vol. C, Tables 4.2.6.8 and 6.1.1.4, A. J. C. Wilson, editor, Boston: Kluwer Academic Press.

[295] Sheldrick, G. M. (**1994**). SHELXTL/PC (Version 5.03). Siemens Analytical X-ray Instruments, Inc., Madison, Wisconsin, USA.

[296] International Tables for X-ray Crystallography (1992). Vol. C, Tables 4.2.6.8 and 6.1.1.4, A. J. C. Wilson, editor, Boston: Kluwer Academic Press.

[297] Sheldrick, G. M. (1994). SHELXTL/PC (Version 5.03). Siemens Analytical X-ray Instruments, Inc., Madison, Wisconsin, USA.

[298] Kwart, H.; Vosburgh, W. G. J. Am. Chem. Soc. 1954, 76, 5400.

[299] Crandall, J. K. J. Org. Chem.. 1964, 29, 2830.

[300] Shealy, Y. F.; Clayton, J. D. J. Am. Chem. Soc. 1969, 91, 3075.

[301] Bazbouz, A.; Christol, H.; Coste, J.; Plenat, F. Bull. Soc. Chim. Fr. 1978, 5-6, II, 305.

[302] Stille, J. R.; Santarsiero, B. D.; Grubbs, R. H. *J. Org. Chem.* 1990, *55*, 843.

Vita

Brian Keith Long, son of Raymond and Sherry Long, was born June 25, 1981 in Ellijay, Georgia. He graduated from Gilmer High School in Ellijay, Georgia in 1999 and then enrolled at North Georgia College and State University in Dahlonega, Georgia in the fall of 1999. While at NGCSU, Brian met Cecilia Trotter, whom he married in April of 2004 in Dacula, Georgia. Brian received his Bachelor of Science degree in Chemistry in the fall of 2003 and entered the graduate program at The University of Texas at Austin in July of 2004 under the guidance of Professor C. Grant Willson.

Permanent address: 1880 Crowe Rd., Dacula, GA 30019

This dissertation was typed by the author.